Dynamic analysis of multiple liquid-storage tanks

Von der Fakultät für Bauingenieurwesen
der Rheinisch-Westfälischen Technischen Hochschule Aachen
zur Erlangung des akademischen Grades eines Doktors der Ingenieurwissenschaften
genehmigte Dissertation

vorgelegt von

Konstantinos Mykoniou

aus Thessaloniki (Griechenland)

Berichter: Universitätsprofessor Dr.-Ing. habil. Sven Klinkel
Universitätsprofessor Dr.-Ing. habil. Carsten Könke

Tag der mündlichen Prüfung: 12. Dezember 2014

Veröffentlicht als Heft 04 (2015) in der Schriftenreihe
des Lehrstuhls für Baustatik und Baudynamik
der RWTH Aachen

Herausgeber:

Universitätsprofessor Dr.-Ing. habil. Sven Klinkel

Organisation und Verwaltung:

Rheinisch-Westfälische Technische Hochschule Aachen
Fakultät für Bauingenieurwesen
Lehrstuhl für Baustatik und Baudynamik
Mies-van-der-Rohe-Str. 1
52074 Aachen

Telefon: +49 241 80 25088
Telefax: +49 241 80 22303
E-mail: sekretariat@lbb.rwth-aachen.de

D 82 (Diss. RWTH Aachen University, 2015)

ISSN 1437-0840
ISBN 978-3-946090-03-8

...I have swam through libraries and sailed through oceans;

Herman Melville, Moby-Dick, Chapter XXXII

Preface

The present work was developed in the years 2010-2014, while I was working as a research assistant at the Chair of Structural Analysis and Dynamics at RWTH Aachen University and accepted by the University's Department of Civil Engineering as a dissertation. The research reported here was supported by the German Research Foundation DFG within the framework of a project on "Complex soil-structure interaction issues" (Ref.-Nr. GZ566-ME72511-1).

Firstly, I would like to thank Prof. Dr.-Ing. Konstantin Meskouris for having given me the opportunity to carry out this work with so much freedom for my own ideas. He created the appropriate framework conditions in the initial stage of this project that paved the way for progress in my study at the time of his retirement. I gratefully acknowledge Prof. Dr.-Ing. habil. Sven Klinkel for his supervision halfway through this project. His endeavor to search for novelty upgraded the standards I had set in research. I would also like to convey my appreciation to Prof. Gao Lin and his research team for my beneficial and pleasant stay in Dalian, China. My gratitude goes also to Prof. Dr.-Ing. habil. Carsten Könke for his interest in my work and for accepting the role of my co-adviser. The contribution of Prof. Dr.-Ing. Martin Ziegler as Chairman of the Examination Committee is greatly appreciated.

I would also like to extend my gratitude to Dr.-Ing. Christoph Butenweg for his pertinent remarks during our numerous, long discussions. His faith in me when efforts lacked tangible results is highly appreciated. The cooperation with Dr.-Ing. Britta Holtschoppen led to further development of a computer program used in this work, for which I am grateful. Many thanks go in particular to my colleagues Dr.-Ing. Francesca Taddei for her ''non mollare'' attitude, as well as to M. Sc. Lin Chen for having shared together several evenings at the office. Both of them supported me in every possible way and provided me a lifeline in those moments when I was bumping along rutty tracks. Not forgetting the secretarial staff of the Chair, I also thank Rita Gau-Crump and Marlies Schewe for their helpfulness and professionalism.

I owe my deepest gratitude to Prof. Dr.-Ing. Anastasios Sextos. Without him neither this work would have been initiated nor completed, since every single sentence in this thesis was written with a view to partially reciprocating his trust in me.

My special thanks go to my former companions in Aretzstraße and my friend Panagiotis Grigoriadis. Lastly, I would like to thank my family. The sight of my father constantly bending absorbed over his own books was engraved on my mind, and years after made the labor on this work a familiar experience. The unconditional love of my mother and her continuous encouragement gave me tons of confidence. My sister's support whenever I needed it made things run smoothly.

Aachen, September 2015 *Konstantinos Mykoniou*

Abstract

The seismic analysis of liquid-storage tanks proceeds ordinarily on the basis of neglecting the dynamic interaction with adjacent tanks, although they are frequently arranged next to each other, for instance in tank farms. In this work, a study on the dynamic behavior of tanks is therefore carried out, which takes into account group interaction effects.

To this aim, a refined substructure technique in the frequency domain is developed, which permits consideration of the interaction effects among adjacent containers through the supporting deformable soil medium. The tank-liquid systems are represented by means of mechanical models, whereas discrete springs and dashpots stand for the soil beneath the foundations. The properties assigned to the models for the superstructures result from a semi-analytical method for the dynamic analysis of circular, cylindrical shells, which takes into account both coupled free surface-shell vibrations and liquid's compressibility. The coefficients for the dynamic impedance functions of the foundations are obtained with the aid of a coupled FEM-BEM formulation, which incorporates the solution of a three-dimensional wave propagation problem for the soil medium into the surface foundations equation of motion.

The proposed model is employed to assess the responses of adjacent tanks for harmonic and seismic excitations over wide range of tank proportions and soil conditions. The influence of the number, spatial arrangement of the containers and their distance on the overall system's behavior is addressed. The results indicate that the cross-interaction effects can substantially alter the impulsive components of response of each individual element in a tank farm. The degree of this impact is primarily controlled by the tank proportions and the proximity of the predominant natural frequencies of the shell-liquid-soil systems and the input seismic motion. The group effects should not a priori disregarded, unless the tanks are founded on shallow soil deposit overlying very stiff material or bedrock.

With a focus on issues concerning engineering practice, a simplified seismic design process is proposed for the determination of the hydrodynamic pressures exerted on liquid-storage tanks in fixed-base conditions. A guideline for preliminary evaluation of group effects for general, dynamic structure-soil-structure interaction problems is also provided.

Zusammenfassung

Die seismische Analyse flüssigkeitsgefüllter Tankbauwerke erfolgt üblicherweise ohne die Berücksichtigung von Effekten aus der dynamischen Interaktion mit benachbarten Tankbauwerken, obwohl diese beispielsweise in Tanklagern häufig eng nebeneinander in Gruppen angeordnet sind. In der vorliegenden Arbeit soll deshalb das dynamische Verhalten von Tankbauwerken unter Berücksichtigung der Gruppeninteraktionen untersucht werden.

Dazu wird eine verfeinerte Substrukturtechnik im Frequenzbereich entwickelt, welche die Berücksichtigung der Interaktionseffekte entlang benachbarter flüssigkeitsgefüllter Tanks durch das tragende, verformbare Bodenmedium erlaubt. Die Tank-Flüssigkeitssysteme werden durch mechanische Modelle dargestellt, wobei diskrete Federn und Dämpfer den Boden unter den Fundamenten abbilden. Die den Modellen der Superstruktur zugeordneten Eigenschaften resultieren aus den Ergebnissen einer halb-analytischen Berechnungsmethode für die dynamische Analyse flüssigkeitsgefüllter, kreisförmiger, Zylinderschalen. Dabei werden sowohl die Kopplung der Schwingung der freien Fluidoberfläche und der Schalenschwingung als auch die Kompressibilität der Flüssigkeit berücksichtigt. Die Koeffizienten der dynamischen Impedanzfunktionen für die Fundamente werden mit Hilfe einer gekoppelten FEM-BEM Formulierung erlangt, welche die Lösung des Problems dreidimensionaler Wellenausbreitung im Bodenmedium in die Bewegungsgleichung der Oberflächenfundamente integriert.

Mit Hilfe des vorgeschlagenen Modells wird die dynamische Antwort benachbarter Tanks für harmonische und seismische Bodenanregungen über eine große Bandbreite von Tankgeometrien und Bodenbedingungen ermittelt. Der Einfluss der Anzahl und der räumlichen Anordnung der Tanks sowie deren Abstand auf das Gesamtsystemverhalten wird untersucht. Die Ergebnisse deuten an, dass die Wechselwirkungseffekte die impulsiven Komponenten der Antwort jedes einzelnen Elementes in einer Tankanlage wesentlich verändern können. Der Grad dieser Auswirkung wird hauptsächlich von den Tankgeometrien sowie dem Abstand der dominanten Schwingungsfrequenzen der Schale-Flüssigkeit-Boden Systeme und der seismischen Bodenbewegung kontrolliert. Es zeigt sich, dass die Gruppeneffekte bei der Tankbemessung nicht a priori außer Betracht gelassen werden dürfen, sofern die Tanks nicht auf einem flachen Sediment gegründet, welches Felsgestein oder starres Material überlagert.

Für die baupraktische Bemessung von Tankbauwerken wird aus den Erkenntnissen der Arbeit ein vereinfachter seismischer Nachweis zur Berechnung der hydrodynamischen Druckverteilungen auf starr gelagerte Tankschalen vorgeschlagen. Ebenfalls wird eine Berechnungshilfe für eine überschlägige Bewertung der Gruppeneffekte der allgemeinen, dynamischen Bauwerk-Boden-Bauwerk Interaktion hergeleitet.

Σύνοψη

Η σεισμική ανάλυση δεξαμενών αποθήκευσης υγρών πραγματοποιείται κατά κανόνα χωρίς να λαμβάνει υπόψη τη δυναμική αλληλεπίδραση με παρακείμενες δεξαμενές, μολονότι συχνά διατάσσονται αναμεταξύ τους σε μικρές αποστάσεις ως συγκροτήματα. Στην παρούσα εργασία, η δυναμική συμπεριφορά δεξαμενών ερευνάται λαμβάνοντας υπόψη τις δυναμικές αμοιβαίες επιδράσεις τους.

Για αυτόν το σκοπό, μια προσαρμοσμένη μέθοδος αποσύζευξης αναπτύσσεται στο πεδίο των συχνοτήτων, η οποία επιτρέπει τη συνεκτίμηση της αλληλεπίδρασης γειτονικών δεξαμενών διαμέσου του υποκείμενου εδάφους. Τα υποσυστήματα των κατασκευών με το περιέχοντα υγρά προσομοιώνονται ως μηχανικά ισοδύναμα, ενώ ελατήρια και αποσβεστήρες αντικαθιστούν το υπέδαφος στο οποίο εδράζονται οι θεμελιώσεις. Τα χαρακτηριστικά των μοντέλων για τις ανωδομές προσδιορίζονται με βάση μια ημι-αναλυτική δυναμική ανάλυση κυκλικών, κυλινδρικών κελυφών που περιέχουν υγρό. Αυτή λαμβάνει υπόψη τις συζευγμένες ταλαντώσεις του κελύφους και του υγρού στην ελεύθερη επιφάνεια καθώς και τη συμπιεστότητα του τελευταίου. Οι τιμές των συντελεστών δυναμικής δυσκαμψίας για τις θεμελιώσεις υπολογίζονται κατόπιν εφαρμογής μιας συνδυαστικής μεθόδου πεπερασμένων και συνοριακών στοιχείων, η οποία ενσωματώνει τη λύση του προβλήματος της τρισδιάστατης διάδοσης κυμάτων στο χώρο του υπεδάφους στην εξίσωση κίνησης των επιφανειακών θεμελιώσεων.

Το προτεινόμενο μοντέλο χρησιμοποιείται για τον προσδιορισμό των αποκρίσεων γειτονικών δεξαμενών που υπόκεινται σε αρμονικές και σεισμικές διεγέρσεις για ένα ευρύ φάσμα διαστάσεων των ανωδομών και εδαφικών συνθηκών. Η επιρροή του αριθμού, της χωρικής διάταξης των δεξαμενών καθώς και της απόστασής τους στη συνολική συμπεριφορά του συστήματος διερευνάται. Τα αποτελέσματα καταδεικνύουν ότι τα φαινόμενα διεπίδρασης μπορεί να διαφοροποιήσουν σημαντικά την ωστική συνιστώσα της απόκρισης κάθε στοιχείου μιας εγκατάστασης δεξαμενών. Ο βαθμός της επιρροής καθορίζεται από τη γεωμετρία των δεξαμενών και την εγγύτητα μεταξύ των δεσπόζουσων φυσικών ιδιοσυχνοτήτων των συστημάτων κελύφους-υγρού-εδάφους και του σεισμικού κραδασμού. Οι επιπτώσεις της αλληλεπίδρασης δεν είναι a priori αμελητέες, εκτός και αν οι δεξαμενές εδράζονται σε επιφανειακή εδαφική στρώση μικρού πάχους υπερκείμενης δύσκαμπτου υλικού ή βραχώδους υποβάθρου.

Με επίκεντρο τον αντισεισμικό σχεδιασμό δεξαμενών αποθήκευσης υγρών στην πράξη, προτείνεται μια απλοποιημένη διαδικασία για τον υπολογισμό των υδροδυναμικών πιέσεων σε δεξαμενές πακτωμένες στο έδαφος. Επίσης, παρέχονται οδηγίες για μια προκαταρκτική αξιολόγηση της σπουδαιότητας της γενικότερης, δυναμικής αλληλεπίδρασης κατασκευής-εδάφους-κατασκευής.

Contents

Notation

Cylindrical shell

r, θ, z	Cylindrical coordinates
x, y, z	Cartesian coordinates
H	Height
R	Radius
h	Thickness
E	Young's modulus
ν	Poisson's ratio
ρ	Mass density
u_r, u_θ, u_z	Wall displacements
$\mathbf{N}^s$	Shape functions
$\mathbf{q}_w^s, \mathbf{q}_d^s$	Vectors of total degrees of freedom on the liquid-covered and remain wall surface respectively
$\mathbf{K}_s$	Stiffness matrix
$\mathbf{M}_s$	Mass matrix
$\mathbf{M}_A$	Added impulsive mass matrix
$\rho_{1,1}$	Added mass density for the 1st circumferential and axial mode

Liquid

r, θ, z	Cylindrical coordinates
H_L	Filling height
ρ_L	Mass density
c_L	Speed of sound
φ	Velocity potential
p	Pressure
m_L	Total mass
f	Free-surface displacement
$\mathbf{N}^f$	Shape functions for the free-surface displacements

$\mathbf{q}^f$	Vector of total degrees of freedom on the free-surface
$\mathbf{K}_L$	Stiffness matrix
$\mathbf{M}_C$	Added sloshing mass matrix

Container-liquid system

$\mathbf{M}_B,\ \mathbf{M}_C$	Coupled added mass matrices
$\omega_{m,n}$	Natural circular frequency for the mth circumfential and nth axial mode of the tank-liquid system
m_{HR}	Portion of liquid mass attached to the rigid tank wall under horizontal excitation
h_{HRW}, h_{HRP}	Height at which the mass m_{HR} must be concentrated to yield the actual bending moment at the tank base due to the wall and base pressure respectively
$m_{SL,n}$	Portion of liquid mass associated with the nth sloshing mode
$h_{SLW,n}, h_{SLP,n}$	Heights at which the mass $m_{SL,n}$ must be concentrated to yield the actual bending moment at the tank base due to the wall and base pressure respectively
$m_{1,n}, m_{0,n}$	Modal mass of the tank-liquid system for the 1st and 0th circumferential mode, nth axial mode
$M_{1,n}, \Delta M_{1,n}, MM_{1,n}$	Bending moments at the tank base due to the wall, base and total pressure respectively for the 1st circumferential and nth axial mode of the tank-liquid system
$h_{1,n}, \Delta h_{1,n}, h'_{1,n}$	Heights at which the mass $m_{1,n}$ must be concentrated to yield $M_{1,n}, \Delta M_{1,n}, MM_{1,n}$ respectively
$Q_{1,n}, Q_{0,n}$	Base shear corresponding to the 1st and 0th circumferential, nth axial mode of the tank-liquid system
$\boldsymbol{\psi}_{1,n}, \boldsymbol{\psi}_{0,n}$	Eigenmode vector for the 1st and 0th circumferential, nth axial mode of the tank-liquid system
$\Gamma_{1,n}, \Gamma_{0,n}$	Participation factor for the 1st and 0th circumferential, nth axial mode of the tank-liquid system
$\xi_{1,n}, \xi_{0,n}$	Damping ratio for the 1st and 0th circumferential mode, nth axial mode of the tank-liquid system
$\ddot{X}_g, \ddot{Z}_g$	Free-field ground acceleration in x and z direction
$\bar{S}_{a,SL,n}$	Pseudoacceleration corresponding to the nth sloshing mode
$\bar{S}_{a,x,n}, \bar{S}_{a,z,n}$	Pseudoacceleration corresponding to nth axial mode of the tank-liquid system for the horizontal and vertical component of ground motion respectively

$S_{a,SL,n}, S_{a,x,n}, S_{a,z,n}$	Maximum absolute (spectral) values of the corresponding pseudoacceleration

Soil

r, θ, z	Cylindrical coordinates
x, y, z	Cartesian coordinates
κ	Wavenumber
$\widetilde{\mathbf{w}}$, $\widetilde{\mathbf{W}}$	Displacement vectors in frequency-wavenumber domain
$\mathbf{w}$	Surface displacement vector
$\widetilde{\mathbf{p}}$, $\widetilde{\mathbf{P}}$	Load vectors in frequency-wavenumber domain
$\mathbf{p}$	Surface point load vector
$\widetilde{\mathbf{G}}$	Stiffness matrix
$\mathbf{G}$	Green's functions matrix in cylindrical coordinates
U_{ij}	Green's functions in direction i due to unit load in direction j in Cartesian coordinates
μ	Shear modulus
V_s, V_p	S- and P-wave velocity
ρ_s	Mass density
λ	Lamé constant
ν_s	Poisson's ratio
ξ_s	Damping ratio
d	Layer's thickness
$\mathbf{v}$	Displacement vector for all finite element nodes at the interface of the foundations
$\mathbf{q}$	Contact stresses for all finite element nodes at the interface of the foundations

Foundation

x, y, z	Cartesian coordinates
R	Radius
$m_F,\ I_F$	Mass and mass moment of inertia

$\mathbf{u}^m$	Displacement vector for the mth foundation
$\mathbf{V}^m$	Vector of external forces for the mth foundation
$\mathbf{Q}^m$	Vector of interaction forces for the mth foundation
$\mathbf{S}^m$	Dynamic stiffness matrix for the mth foundation

Foundations-soil system

$\mathbf{K}^{mp}$	Impedance matrix associated with generalized forces at the base of the mth foundation and generalized displacements along the principal axes of the base of the pth foundation
K_{ij}	Impedance function associated with generalized forces at the base of the foundation in direction i and generalized displacements in direction j
D	Distance between the foundations
$\mathbf{S}_{\text{soil}}$	Subgrade stiffness with respect to the finite element nodes at the interface of the foundations

Multiple liquid-storage tanks

x_1, x_2, x_3	Cartesian coordinate system
$m_{R,n}$	Modal mass of the tank-liquid system under base rocking for the nth axial mode
I_0^B	Mass moment of inertia about a horizontal centroidal axis for the part of the liquid that is considered to move together with the rocking base
$T_{1,n}$, $T_{0,n}$	Transfer functions corresponding to the 1st and 0th circumferential, nth axial mode of the tank-liquid system for a prescribed foundation motion
$T_{SL,n}$	Transfer function corresponding to the nth sloshing mode for a prescribed foundation motion
$AF_{k,n}^{IMP.}$, $AF_{k,n}^{SL.}$	Transfer functions corresponding to the nth impulsive and sloshing mode respectively in direction k for a prescribed surface ground motion
FS_k	Transfer function of the ground free surface to the displacement excitation at the soil-rock interface in direction k.

Other symbols

$\mathrm{i} = \sqrt{-1}$	Imaginary unit
t	Time
Ω	Excitation's frequency
$a_o = \frac{\Omega R}{V_s}, r_o = \frac{r \Omega}{V_s}$	Normalized frequency
I_m, K_m	Modified Bessel functions of order m, first and second kind respectively
J_m, Y_m	Bessel functions of order m, first and second kind respectively
$\bar{\lambda}_n$	nth root of Bessel function of first kind and order m
$\dot{(\,)} = \frac{\partial}{\partial t}$	Time derivative
$P' = \frac{\partial P}{\partial r}, Z' = \frac{\partial Z}{\partial z}, \Theta' = \frac{\partial \Theta}{\partial \theta}$	Derivatives with respect to the position coordinates

1 Introduction

1.1 Motivation

Liquid storage tanks are significant elements of liquid fuel lifeline transmission and distribution systems and should be designed to endure the earthquakes to which they may be subjected. Their value exceeds by far the economic worth associated with their construction, installation and contents.

The field of analysis of seismic loaded, aboveground, liquid-storage tanks has become an area of research since the middle of the 20th century and received a significant boost in the ensuing decades due to the vast increase in the number of storage systems installed which was accompanied, after some severe earthquake damages, with the recognition of an insufficient state of knowledge of the vibrating behavior of those systems. Therefore, the discipline broadened remarkably and gave rise to myriad publications that strengthened the knowledge of an adequate design of storage tanks. Indeed, the fundamental findings by Housner (1957) allowed one to estimate the dynamic loads of rigid tanks resting on rigid foundations; nowadays the accumulated experience and the available high-performance computational resources permit the study of the problem as a structure-liquid-soil interaction phenomenon.

Nevertheless, past research focused exclusively on the seismic performance of isolated tanks during strong ground motion. Numerous investigations, which considered complex aspects of their dynamic response, such as large amplitude nonlinear sloshing, buckling of the tank wall and contact separation between tank base and soil, neglected the influence of the subsoil interaction with adjacent tanks due to seismic loads. In reality, tanks appear in industry in groups, building complex systems which include filling/discharging bays, piping networks, pump groups etc. In some cases, those tank farms spread out over several miles (Figure 1.1), such as the Cushing tank farm in Oklahoma, U.S.A, one of the world's largest oil storage facilities (Figure 1.2). The center to center distance between the tanks, which so far is regulated according to fire-extinguishing aspects (accessibility, possibility of inserting water walls, etc.), can be small enough to raise the question: is it possible, in case of a tank farm constructed on deformable soil, the vibration behavior of each tank subjected to incident wavefield to be mutually affected by the adjacent containers dynamic response?

Research work conducted on the investigation of the dynamic foundation-soil-foundation interaction indicated considerable effects with respect to subgrade dynamic coupling of close-spaced foundations due to interplay of wavefields propagating between them. Additionally, the fact that large capacity liquid containers are massive structures calls for an examination of their -through the soil coupled-

dynamic response in zones of high seismic activity and soft local site conditions. The realization that the arrangement of the tanks in space may have a notable influence on their seismic behavior demands a systematic effort in quantifying the relative impact of the parameters involved in the problem. The outcome of this study may contribute to a future prescription of regulations, based on economic design, with which end users, equipment manufacturers, automation and management technology suppliers must comply.

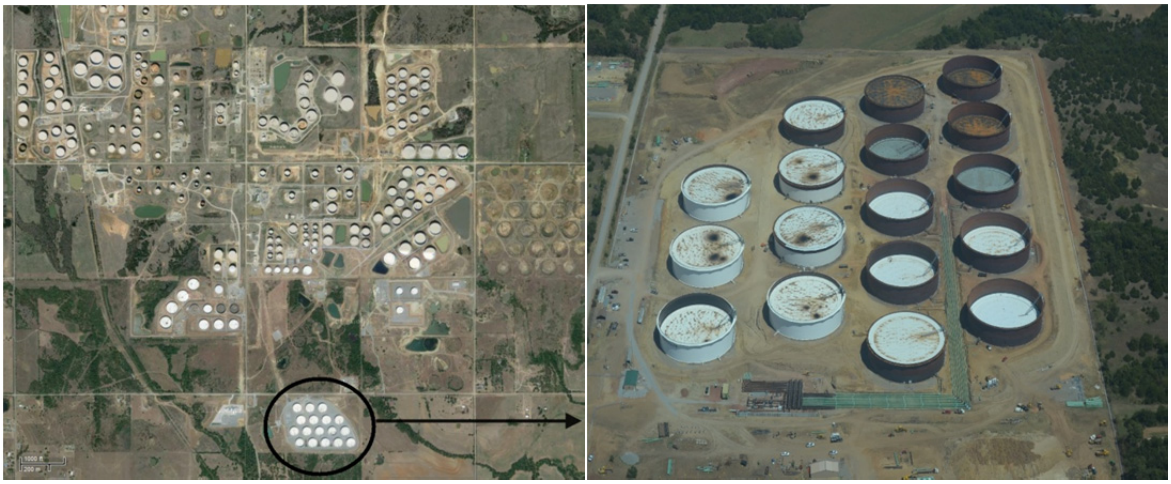

Figure 1.1: Cushing tank farm in Oklahoma, U.S.A.

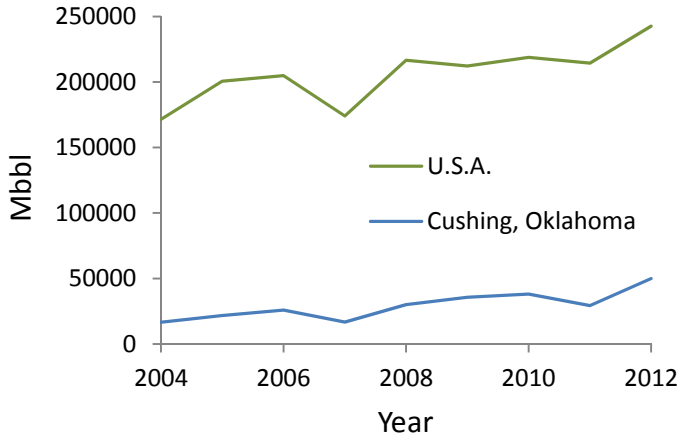

Figure 1.2: Crude Oil Stocks at Tank Farms & Pipelines in thousand barrels, Mbbl (U.S. EIA).

1.2 Statement of problem

The dynamic interaction of adjacent liquid-storage tanks under ground motion belongs to an interdisciplinary field of study, which resides at the intersection of earthquake and geotechnical engineering, soil and structural dynamics, hydrodynamics, computational mechanics and other distinct technical subfields. In order to gain insight into the nature of the phenomena associated with this

subject, it is initially convenient to split the original field of interest into two parts: the structure-soil-structure interaction (SSSI) and the fluid-structure interaction (FSI). However, these parts do not compose the original problem in a cumulative manner; likewise one could simple add two vectors together to determine the resultant vector. On the contrary, a dynamic reciprocal relationship is present between all the components involved in the system, namely the containers, the enclosed liquids, the foundations and the soil underneath. Nevertheless, this subdivision coincides with the current state of the art and suits conceptually to the proposed framework for the analysis, which is based on the substructure technique. The underlying principles of the available methods for the investigation of the -through the soil- interaction of nearby tanks are also summarized.

1.2.1 Structure-soil-structure interaction

During earthquake shaking, seismic waves are transmitted through the soil from the fault rupture to the structures lying on the surface of the soil or embedded in it. The wave motion of the soil excites the structures and generates inertial forces which in turn modify the input motion. To describe these phenomena the well-established term Soil-Structure-Interaction (SSI) is used. It is commonly approved that the SSI effects are negligible for very firm or rigid subgrade materials. Each structure at the site can accordingly be analyzed individually for a prescribed seismic load. On the contrary, for soft soils the interaction effects can no longer be disregarded. A substantial part of the vibrational energy of an elastically supported structure may be dissipated into the supporting medium by geometrical spreading of the waves (radiation damping) and by hysteretic action in the soil itself (material damping).

The SSI analysis is inherently associated with additional complications apart from those emanating from conventional earthquake engineering. This is primarily attributed to the fact that a wave propagation problem in an unbounded medium has to be solved. The complexity becomes more pronounced if one considers the soil as a semi-infinite medium whose properties are not homogeneous either in the horizontal direction or along the depth (Figure 1.3). The presence of discontinuities inside the medium generated by boundaries of soil layers, within the properties remain relatively constant, imposes changes in the propagation wave in form of refractions and reflections at their interfaces, see Achenbach (1984). Another physical event that has to be addressed is that the material of the subgrade may exhibit nonlinear behavior under strong ground motion, especially in the vicinity of the structures, which fact alters the magnitude of the dynamic soil effects. A comprehensive description of the SSI effects is provided by Wolf (1985).

In reality, the group of structures and the soil behave as a single continuum. Each structure diffracts the incident wave propagating in the soil and produces a secondary wavefield which influences the adjacent structures, which in turn cause responses to the former ones. Thus the ‘‘through the soil

coupling'' between nearby constructions may be conceived as an additional wave source which modifies locally the seismic excitation. Structure-Soil-Structure-Interaction (SSSI) analysis is essential for the determination of the response of structures built in small separation distances. Nevertheless, the seismic design provisions do not provide guidelines on carrying out such analysis. In fact, the research on this interdisciplinary field remains at initial stage and the studies conducted in the past are primarily restricted to foundations, excluding the superstructures. Systematic efforts on estimating the dynamic cross-interaction effects of multiple structures have been made only for nuclear power plants. An extensive review of the studies on SSSI is provided by Menglin et al. (2011). More recently, the focus of research activity extended to consider global city effects on dense building areas submitted to seismic waves (Kham et al., 2006). Weighty simplifications for both building and soil models are still inevitable in those types of analyses and thus the reached conclusions may not correspond to the real seismic conditions. Although the advances achieved the last decades in the field of SSI analysis provide sophisticated mathematical models for the investigation of SSSI effects, a complete representation of the seismic environment turns out to be a formidable challenge. Even the examination of idealized situations regarding the structural response and the subsoil configuration requires computationally expensive solutions. Thus, an exhaustive study of the problem taking into account all the parameters involved in the problem is inexpedient; besides, the greatest uncertainties arise from the source mechanism and the temporal and spatial variations of the ground motion. Bearing in mind that an exact deterministic solution is impossible, it is preferable to use simplified models which allow capturing the essential features of the system's dynamic behavior and estimate the degree of interaction between the adjacent structures. Elaborate models should be realized afterwards, in case the initial analysis should point out pronounced structure-soil-structure effects.

1.2.1.1 Basic methods of analysis

Two methods are generally available for the solution of this type of wave propagation problem: the direct and subsuctructure method (Figure 1.4). The latter is adopted in the present study.

Direct method

The soil around the (embedded) structures is taken into account by enforcing an artificial boundary condition at a certain distance from the structure-soil interface and the total system is analyzed in an one-stage concept. To ensure that no energy is emitted from infinity towards the structure-soil interface, an extended part of the soil is modeled as a finite system with certain demands of discretization (Lysmer and Kuhlemeyer, 1969), resulting usually to a cumbersome system of a large number of degrees of freedom especially if three-dimensional wave propagation is investigated. Therefore, a variety of absorbing boundaries have been developed for discrete models of infinite

media. The most common among them are the viscous boundaries, the paraxial boundaries and the perfectly-matched layer (Kausel, 1998; 1992). On the other hand, the direct method is suitable for irregular geometrical features and material nonlinearities of the soil, which may account for the response of structures founded on a soft site (Kausel et al., 1976). To the direct methods belongs also the modeling of the soil with infinite elements, a refinement of the Finite Element Method (FEM) with element shape functions that extend to infinity (Beer and Watson, 1989).

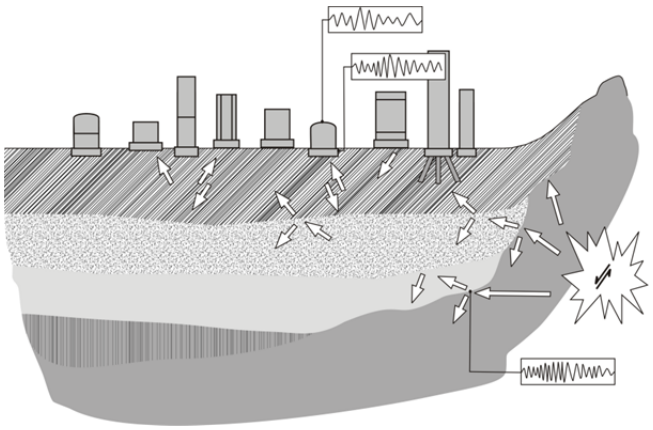

Figure 1.3: Structures-unbounded soil medium excited by a seismic source: Representative dynamic problem.

Substructure method

In this method, the soil and the structures are analyzed individually and rigorous boundary conditions are enforced at the surface which encloses the structures (interaction horizon) in order to take into account the unbounded soil exterior to this boundary. Those conditions are derived from the governing differential equation of motion for the unbounded media, which is converted into an equivalent boundary integral statement. The latter in a discretized form is the cornerstone of the Boundary Element Method (BEM). Prerequisite for the implementation of this method is the existence of solutions to the wave propagation problem, known as fundamental solutions. These are analytic or semi-analytic expressions of the response anywhere in the soil, elicited by a dynamic load source at some arbitrary location. The substructure technique enables the investigation of the SSI effects by employing different methods for the two subsystems. Thus, in a large number of studies reported, coupled BEM and FEM formulations were developed in order to profit from the advantages of each of the two basic approaches (Zienkiewicz et al., 1977; Beskos and Maier, 2003). The FEM has been used to depict the bounded structures, since it facilitates the modeling of geometric or material nonlinearities, as well as anisotropic materials. On the contrary, the BEM has been primarily applied to the dynamic modeling of the unbounded medium, since computational time is significantly saved due to reduction in the spatial dimensionality. The scaled boundary finite-element method, a novel

semi-analytical technique for solving unbounded domains, possesses also this advantage (Song and Wolf, 1997), yet dispenses with the requirement of fundamental solutions.

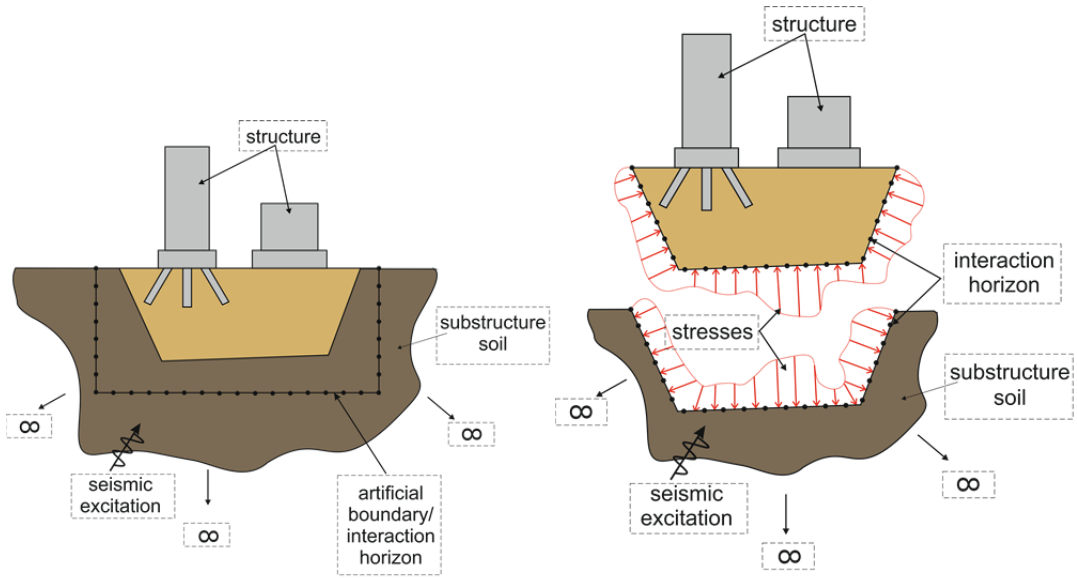

Figure 1.4: Dynamic model of unbounded medium-structures-interaction analysis based on the direct method (left) and substructure method (right).

1.2.2 Fluid-structure interaction

The assessment of the dynamic response of liquid-storage tanks subjected to ground motion is a special subfield of earthquake engineering. The specialty of those structures may be traced in the pressures exerted by the liquid on the tank during ground shaking. The hydrodynamic pressures differ in intensity and distribution from those corresponding to a state of static equilibrium and may significantly affect its performance. The pressures and the resultant stresses of tanks anchored on a non-deformable medium depend on the characteristics of the seismic motion, the properties of the contained liquid and the flexibility of the container (Veletsos, 1984). The latter introduces the necessity to solve a fluid-structure interaction problem since the magnitude and distribution of the pressures and the associated tank forces are strongly influenced by the wall stiffness of the container.

For design purposes, the hydrodynamic effects of an anchored tank can be evaluated as the sum of two separate parts (Haroun and Housner, 1981): an impulsive part, which represents the action of the portion of the liquid which move in unison with the tank and a convective part, which represents the action of the portion of the liquid that experiences sloshing motion. The former corresponds to low-frequency oscillations whereas the latter corresponds to high-frequency oscillations. Nevertheless, there is always certain coupling between the liquid surface fluctuations and the structural deformations (Amabili et al., 1996; Lakis and Neagu, 1997).

Analytic studies and post-earthquake observations have manifested that the hydrodynamic impulsive forces induced by seismic ground motion in flexible tanks may be appreciably higher than those in rigid tanks of the same dimensions (Yang, 1976). Therefore, the interaction between the liquid and the elastic container should be taken into account in the seismic design of flexible tanks. Regarding linear elastic responses, this fact calls for a solution to an eigenvalue problem prior to the computation of the associated hydrodynamic pressures. The integration of the latter in conjunction with the seismic motion results to the design tank forces and moments applied to the tank and the foundation.

In practice, liquid-storage tanks are not always fully anchored at their base. Unanchored or partially anchored tanks tend to uplift during high-intensity ground shaking and respond in a highly nonlinear fashion. Base uplifting alters completely the characteristics of the system in terms of flexibility and energy dissipation capacity. Under these circumstances, phenomena such as buckling of the tank wall caused by large axial stresses, material yielding, plastic rotation of the plate and large amplitude nonlinear sloshing may arise (Peek, 1986; Malhotra, 1997). In this case, numerical methods are indispensable tools for the investigation of these nonlinear mechanisms.

1.2.2.1 Basic methods of analysis

The available procedures for the assessment of the dynamic response of liquid-storage tanks may be classified according to the treatment of the coupled response of the structure and liquid (Figure 1.5). Accordingly, we distinguish two approaches: the added mass formulation and finite element formulations for the fluid. The former is used in the present study.

Added mass formulation

In this approach, the governing equations of the fluid flow are used to transform the pressures applied to the structure in an equivalent virtual mass added on the structural model. Analytical solutions or finite element modelling are used for the computation of the structural stiffness whereas the body of fluid is solved using FEM or BEM formulations (Haroun, 1980; Lay, 1993). In the context of fluid-structure interaction, this procedure is highly desirable since it reduces the spatial dimensionality of the problem by one: the three-dimensional governing partial differential equations for the fluid flow are transformed into the wall-surface integral equations. The sloshing motion may be included in the analysis if the free-surface integral equations are incorporated in the equations of motion (Amabili, 2000). Unfortunately, the added mass concept can not replicate the actual physical behavior of liquid-storage tanks when the latter exhibit nonlinear behavior. For this case, finite element formulations are proven to be appropriate.

Finite element formulations for the fluid

The methods for the development of fluid elements can be categorized into the following three basic approaches: Eulerian, Lagrangian and Arbitrary Largange Eulerian (ALE) formulation (Brüggemann, 2002; Ozdemir et al., 2010). In the Lagrangian approach, the behaviour of the fluid is expressed in terms of the displacements at the finite element node points. Hence, compatibility and equilibrium are automatically satisfied at the node along the interfaces between the fluid and structure. In Lagrangian algorithms, each individual node of the computational mesh follows the associated material particle during motion. In the Eulerian approach, the behavior of the fluid is formulated in terms of a pressure potential. The computational mesh is fixed and the continuum moves with respect to the grid. In the ALE description, the nodes of the computational mesh may move with the continuum in normal Lagrangian fashion or be held fixed in Eulerian manner or follow one arbitrarily specified path. It is beyond the scope of this study to outline the drawbacks and merits of each method. Generally, the suitable solver is the one that can capture the complexities of interest related to the tank response in a stable and precise way.

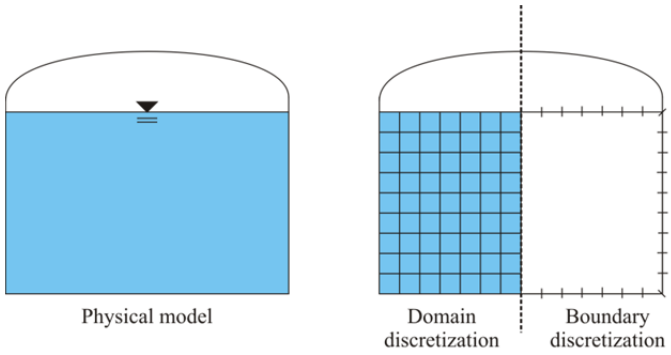

Figure 1.5: Discretization techniques for fluid-structure interaction problems.

1.3 Solution outline

The solution proposal for the analysis of the dynamic interaction of adjacent liquid storage tanks is based on a substructure concept. The procedure can be summarized in the following three steps:

In the first step, the continuous system of nearby tanks is divided in the subsystems liquid-tank and foundations-soil.

In the second step, each of the subsystems will be analyzed individually. The eigenvalue problem of the liquid-tank subsystem is solved taking into account the free-surface fluctuations and the compressibility of the fluid. The results of a modal expansion analysis are used to represent each of the superstructures as series of independent Single Degree Of Freedom (SDOF) systems.

Subsequently, the frequency-dependent force-displacement relationships, known as impedance functions, are computed with the aid of a coupled FEM-BEM formulation for a group of adjacent rigid circular foundations. Accordingly, the soil is represented by springs and dashpots coeffiecients, which reproduce its dynamic stiffness and radiation (as well as material) damping respectively.

In the third step, the two subsystems are coupled together. By establishing the equilibrium of moments and forces around each foundation, the harmonic foundation motion of each tank under horizontal or vertical ground excitation is determined. The response of each tank for every mode of vibration is obtained afterwards. The superposition of each modal contribution furnishes the total response of the tanks in the frequency domain. The response to an arbitrary transient excitation can be then obtained by recourse to Fourier analysis and synthesis techniques.

The solution scheme is illustrated in Figure 1.6.

1.4 Thesis roadmap

This work is divided in four chapters which are organized on a self-contained level and may be read independently from each other. Despite the author's intention to present this study without excessive theoretical prerequisites for engineering dynamics, frequent reference to past works was proven inevitable in order to stay focused on the objective.

In the first section of *Chapter 2*, the free vibration of aboveground circular cylindrical containers, which enclose incompressible liquids in an arbitrary filling ratio, is addressed. The proposed semi-analytical method is validated by available solutions in the literature. Results of a numerical investigation concerning particular case studies are discussed. In the second section of the chapter, attention is shifted to the response of liquid-storage tanks subjected to seismic loads. The solutions for the fluid flow are firstly presented. Subsequently, the equations of motion in each excitation's direction are derived. The solution to the forced vibration problem is used as reference point in an inspection of the adequacy of the design procedure provided in the current standard provisions. Representative examples clarify some aspects of the dynamic response that may be encountered in practice. In the last part of the chapter, a proposal for a simplified design process is introduced, which enables the calculation of hydrodynamic pressures exerted on clamped-free liquid-storage tanks due to ground motion.

Chapter 3 deals with the dynamic interaction of multiple circular foundations through the soil. First, the wave propagation problem for the soil medium is solved in the frequency domain with the aid of the Stiffness Matrix Method and Thin Layer Method. The solutions, known as Green's functions, are employed successively to formulate the boundary integral equations at the soil-foundations interfaces. After discretizing spatially the boundaries of the domain, the so-called Boundary Element Method (BEM) is coupled with the Finite Element Method (FEM); the latter is used to model the foundations.

A set of numerical investigations with respect to the number and spatial arrangement of externally loaded foundations are conducted. Two idealized soil profiles are taken into account. On the basis of the determined force-displacement relationships (dynamic impedance functions), the remaining part of the chapter is dedicated to a recommendation of a guideline for preliminary estimation of structure-soil-structure interaction effects.

Chapter 4 can be regarded as hybrid, since it constitutes the resultant of the methodology established in the previous two chapters. After a review of the conventional concept of substructure method for single structures, the equations governing the dynamic behavior of multiple tanks on halfspace are derived by means of a refined substructure formulation in the frequency domain. Critical responses are afterwards evaluated for harmonic ground excitations in several benchmark problems and the relative importance of the parameters included in the analyses is elucidated. Both impulsive and sloshing actions of the liquid are investigated and noteworthy phenomena are discussed. Eventually, the transient response to seismic excitation is exemplarily assessed.

At last, conclusions are drawn and an outlook on future work is given in *Chapter 5*.

<table>
<tr><td colspan="4">System under study:
Multiple liquid-storage tanks
on halfspace soil medium
 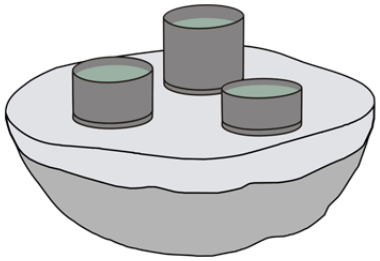 </td></tr>
<tr><td colspan="2">Analysis step</td><td colspan="2">Technique description</td></tr>
<tr><td>1</td><td>Separation of the system</td><td>Substructure: Tank-liquid</td><td>Substructure: Soil-foundations</td></tr>
<tr><td rowspan="5">2</td><td>Analysis type</td><td>Interaction of container and liquid
(Chapter 2)</td><td>Foundation-soil-foundation interaction
(Chapter 3)</td></tr>
<tr><td>Physical model</td><td>Tank wall-liquid continuum
 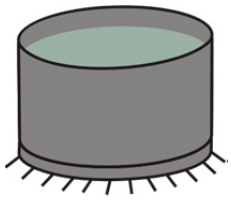 </td><td>Soil-foundations continuum
 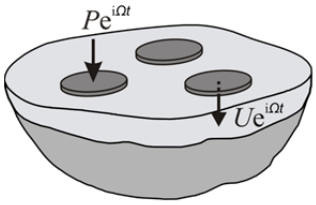 </td></tr>
<tr><td>Method</td><td>Modal analysis-FEM
 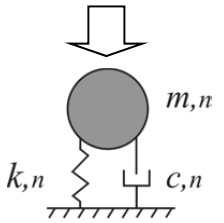 </td><td>coupled FEM-BEM
 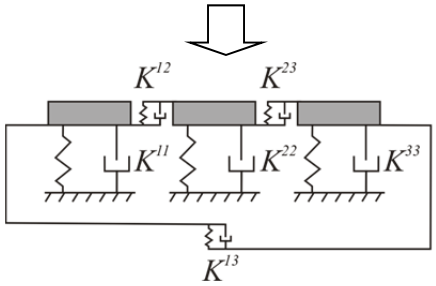 </td></tr>
<tr><td>Results</td><td>Uncoupled SDOFs</td><td>Frequency-dependent springs-dashpots</td></tr>
<tr><td rowspan="3">3</td><td>Coupling of substructures</td><td colspan="2">Dynamic interaction of adjacent liquid-storage tanks
(Chapter 4)</td></tr>
<tr><td>Method</td><td>D’Alembert equations for dynamic equilibrium</td><td rowspan="2"> 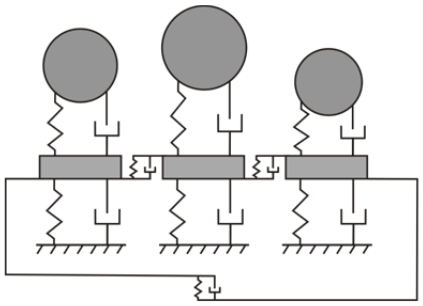 </td></tr>
<tr><td>Results</td><td>Harmonic response of containers</td></tr>
</table>

Figure 1.6: Outline of substructure-based solution proposal -refinement of past works on single liquid-storage tanks (Tang, 1986; Veletsos and Tang, 1990; 1992, Habenberger, 2001).

2 Interaction of container and liquid

2.1 Eigenvalue problem for cylindrical shells partially filled with compressible liquid

2.1.1 State of the art report

According to a well-established concept, the hydrodynamic effects of a structure coupled with quiescent fluid can be evaluated as the sum of two parts: an impulsive part, which represents the action of the portion of the liquid which moves in unison with the structure and a convective part, which represents the action of the portion of the liquid that experiences sloshing motion. Mathematically this distinction leads to different boundary conditions which are fulfilled for the fluid flow. In case of containers, commonly constructed as thin cylindrical shells, the dynamic interaction between sloshing waves and shell vibrations is traditionally neglected. Thus, the response is evaluated as a superposition of two uncoupled solutions that take into account: a) the liquid-shell system and b) the free surface gravity waves of a rigid cylinder. Case a) is associated with the unknown radial amplitudes of a flexible container with a bottom regarded as rigid. This indicates the necessity to solve a fluid-structure interaction problem. Case b) is associated with the sloshing natural frequencies of the fluid which can be determined in closed form.

The assessment of the mode shapes corresponding to the impulsive motion has motivated systematic research efforts over the last decades, especially for liquid-storage tanks. Early studies (Veletsos and Yang, 1977; Fischer, 1979) considered the tank-fluid system as a single degree of freedom system and the deflection configuration of the tank at any time was considered as prescribed. The work of Yang (1976), who considered the displacements of the tank as linear combinations of the natural vibration of a cantilever beam and solved the problem by making use of Lagrange's equations, highlighted the significance of container flexibility. More recently, the eigenvalue problem of the liquid-filled circular cylinder was formulated analytically by Habenberger (2001) as an integral equation with the influence functions of the statically loaded empty shell.

Numerical techniques such as the Finite Element Method (FEM) have been also employed for the solution of the eigenvalue problem. The majority of them are founded on the added-mass concept: the shell is considered ‘‘dry’’ and the inertial influence of the liquid interacting with the structure is taken into account by virtually equating the hydrodynamic force to the equivalent acceleration force on the

structure. Among those studies, Haroun and Tayel (1985), Lakis and Sinno (1992), Amabili (1996) and Virella et al. (2006) are noteworthy, where the free vibration of a liquid-filled cylinder was derived in closed form.

In all the above-mentioned studies, the coupling of the sloshing and impulsive modes was excluded due to the fact that the significant liquid sloshing modes and the combined liquid-elastic cylinder vibrational modes have well-separated frequency ranges. Refinement of this classical procedure considers the effect of free surface fluctuation on the structural deformation and vice versa. Closed form formulations based on energy and variational principles can been derived as long as the system is solved as a whole, that means when the vibrational amplitudes include both the surface and the structure generalized coordinates or degrees of freedom. In other words, the boundary condition on the free surface is inserted in the governing equation of motion and an eigenvalue problem of enlarged dimension is solved. Representative examples of such treatment of the problem can be found in the literature by Haroun (1980), Gonçalves and Ramos (1996) and Amabili et al. (1996). A rigorous finite element technique, which makes use of fluid elements, has been recently employed by Moslemi and Kianoush (2012). Numerical techniques that take into account the influence of the liquid-surface fluctuation on the wall deformations by means of an added-mass matrix of the separated structure region, have been developed by Cho and Song (2001) and Cho et al. (2001). In this case, the fluid mass matrix becomes frequency dependent and an iterative scheme is essential for the calculation of the eigenfrequencies.

In all the above-mentioned studies, the liquid was assumed incompressible, mainly for the reason that the speed of sound for many liquid petrochemical fuels is relatively high. Therefore, the hydrodynamic pressure field was described by the Laplace equation emanating from the continuity and Euler momentum equations. The number of studies which involve the effect of liquid compressibility is limited. Kumar (1981) and Cho et al. (2002) investigated the axisymmetric free vibrations of tanks. It was reported that the compressible case shows slightly lower natural frequencies for slender tanks in comparison with the incompressible case. Free-surface effects were excluded from their analyses. Jeong and Kim (1998) demonstrated that the decreased coupled frequencies appear only for lower circumferential wave numbers. Although they focused on clamped-clamped cylinders bounded by top and bottom rigid plates, a relaxation of their assumption to comprise a free top surface indicated that the maximum deviation of bounded and unbounded compressible fluid occurs for the first circumferential wave number. In this study, we aim to assess the response of a liquid-shell system with a free surface at the top side of the compressible fluid region. The expression for the liquid velocity potential is obtained as a sum of two partial solutions which satisfy the Helmholtz equation and the appropriate boundary conditions.

With the aid of the presented formulation, the dynamic characteristics of partially-filled cylindrical tanks subjected to any variationally admissible set of boundary conditions and for any circumferential wavenumber $m \geq 1$ can be determined.

2.1.2 System considered and assumptions

The system investigated is shown in Figure 2.1. It is a thin-walled circular cylindrical shell of length H, radius R, and uniform thickness h. The shell is assumed to be made of an elastic material with Young's modulus E, Poisson's ratio ν and mass density ρ. The bottom of the shell is regarded as flat and rigid. The tank is filled to a height H_L with a non-viscous, irrotational and compressible liquid of mass density ρ_L. Using the cylindrical coordinate system $\mathbf{x}=\{r,\theta,z\}^{\mathrm{T}}$, we denote the displacement vector of a point on the shell middle surface by $\mathbf{u}^s=\{u_r,u_\theta,u_z\}^{\mathrm{T}}$, the free surface displacement measured from the liquid free surface by f and the liquid velocity by $\mathbf{v}=\{v_r,v_\theta,v_z\}^{\mathrm{T}}$. It is also assumed that the effect of internal static pressure on the container's free vibration is negligible.

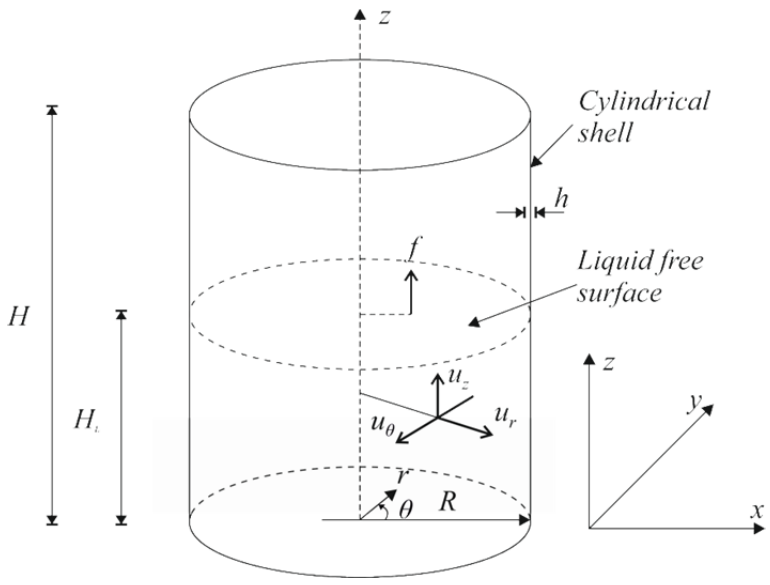

Figure 2.1: System under investigation and coordinate system.

2.1.3 Equations governing the liquid motion

2.1.3.1 Velocity potential and boundary conditions

The velocity potential ($\nabla\varphi=\mathbf{v}$) of an irrotational flow of a compressible inviscid liquid satisfies the equation:

$$\nabla^2\varphi - \frac{1}{c_L^2}\frac{\partial^2\varphi}{\partial t^2} = 0 \text{ in } \Omega_L \tag{2.1}$$

where the speed of the sound is defined by $c_L = \sqrt{K/\rho_L}$ in which K stands for the bulk modulus and t indicates time. Eq. (2.1) is an elliptic partial differential equation that can be derived by considering the continuity equation and the momentum conservation law for a frictionless fluid (Sommerfeld, 1994). Small amplitude waves are assumed, where second order terms in the perturbations are neglected. For harmonically oscillating motions:

$$\varphi(r,z,\theta,t) = \Phi(r,z,\theta)\mathrm{e}^{\mathrm{i}\omega t} \tag{2.2}$$

where i is the imaginary unit and ω is the natural circular frequency of vibration. With the aid of Eq. (2.2), Eq. (2.1) becomes the Helmholtz equation:

$$\nabla^2\Phi + \frac{\omega^2}{c_L^2}\Phi = 0$$

$$\frac{\partial^2\Phi}{\partial r^2} + \frac{1}{\mathrm{r}}\frac{\partial\Phi}{\partial r} + \frac{\partial^2\Phi}{\partial z^2} + \frac{1}{\mathrm{r}^2}\frac{\partial^2\Phi}{\partial\theta^2} + \frac{\omega^2}{c_L^2}\Phi = 0 \tag{2.3}$$

The following boundary conditions have to be satisfied:

$$\left.\frac{\partial\varphi}{\partial z}\right|_{z=0} = 0 \tag{2.4}$$

$$\left.\frac{\partial\varphi}{\partial r}\right|_{r=R} = \dot{u}_r(z,\theta,t) \tag{2.5}$$

$$\left.\left(\frac{\partial\varphi}{\partial z} - \dot{f}(r,\theta,t)\right)\right|_{z=H_L} = 0 \tag{2.6}$$

$$\left.\left(\rho_L\, g\, f(r,\theta,t) + \rho_L\frac{\partial\varphi}{\partial t}\right)\right|_{z=H_L} = 0 \tag{2.7}$$

The dot superscript denotes differentiation with respect to time and g the acceleration of gravity. Due to the linearity of the problem the solution can be decomposed in two partial solutions:

$$\varphi = \varphi_1 + \varphi_2 \tag{2.8}$$

where φ_1 represents the velocity potential of a cylinder with flexible wall, rigid flat bottom, and undisturbed surface whereas φ_2 represents the velocity potential of a cylinder with rigid wall and flat bottom and free liquid surface. The velocity potential φ_1 must satisfy the following boundary conditions:

$$\left.\frac{\partial\varphi_1}{\partial z}\right|_{z=0} = 0, \quad \left.\frac{\partial\varphi_1}{\partial r}\right|_{r=R} = \dot{u}_r(z,\theta,t), \quad \left.\frac{\partial\varphi_1}{\partial z}\right|_{z=H_L} = 0 \tag{2.9a-c}$$

The velocity potential φ_2 must satisfy the following boundary conditions:

$$\left.\frac{\partial\varphi_2}{\partial z}\right|_{z=0} = 0, \quad \left.\frac{\partial\varphi_2}{\partial r}\right|_{r=R} = 0, \quad \left.\left(\frac{\partial\varphi_2}{\partial z} - \dot{f}(r,\theta,t)\right)\right|_{z=H_L} = 0 \tag{2.10a-c}$$

Solution for potential φ_1

We attempt a solution of Eq. (2.3) using separation between the position coordinates:

$$\Phi_1(r,z,\theta) = P(r)Z(z)\Theta(\theta) \quad \text{or} \quad \Phi_1 = PZ\Theta \tag{2.11}$$

Substituting Eq. (2.11) into Eq. (2.3) and dividing by $PZ\Theta$ yields:

$$\frac{P''}{P} + \frac{1}{r}\frac{P'}{P} + \frac{Z''}{Z} + \frac{1}{r^2}\frac{\Theta''}{\Theta} + \frac{\omega^2}{c_L^2} = 0 \tag{2.12}$$

where the prime superscript denotes differentiation with respect to one of the three position coordinates. Since r, θ and z are independent variables, the separation constants κ and β can be introduced:

$$\frac{P''}{P} + \frac{1}{r}\frac{P'}{P} + \frac{1}{r^2}\frac{\Theta''}{\Theta} + \frac{\omega^2}{c_L^2} = -\frac{Z''}{Z} = \kappa \tag{2.13}$$

$$r^2\frac{P''}{P} + r\frac{P'}{P} + r^2\frac{\omega^2}{c_L^2} - r^2\kappa = -\frac{\Theta''}{\Theta} = \beta \tag{2.14}$$

Eq. (2.13) together with the boundary conditions in Eq. (2.9a) $Z'|_{z=0} = 0$ and Eq. (2.9c) $Z'|_{z=H_L} = 0$ denote a regular Sturm-Liouville problem, thus only non-negative eigenvalues κ exist. We examine the two distinct cases:

Case (a): $\kappa = a^2 \neq 0$

The solution has the following form:

$$Z = A_1\cos(az) + A_2\sin(az) \tag{2.15}$$

The boundary condition in Eq. (2.9a) gives us $A_2 = 0$. Application of the boundary condition in Eq. (2.9c) furnishes the non-trivial solution:

$$a_i = \frac{\pi\, i}{H_L}, i = 1,2,..,k \tag{2.16}$$

Case (b): $\kappa = 0$

The solution has the following form:

$$Z = A_1 + A_2 z \tag{2.17}$$

Due to the boundary conditions in Eq. (2.9a) and Eq. (2.9c) we get $A_2 = 0$. Obviously the general solution is given as:

$$Z = A\cos\left(\frac{\pi\, i}{H_L}z\right), i = 0,1,2,..,k \tag{2.18}$$

Eq. (2.14) together with the periodicity conditions $\Theta(-\pi) = \Theta(\pi)$ and $\Theta'(-\pi) = \Theta'(\pi)$, which ensure that the solution is single valued and continuous, represent also a regular Sturm-Liouville

problem, thus only non-negative eigenvalues $\beta = m^2$ exist. Working out the equations analogously to the function Z results to the general solution:

$$\Theta = B_1 \cos(m\theta) + B_2 \sin(m\theta), m = 1,2,..,k \tag{2.19}$$

Multiplication of Eq. (2.14) with P yields, after rearrangement, the following ordinary differential equation:

$$r^2 P'' + rP' - P\left[r^2\left(a_i^2 - \frac{\omega^2}{c_L^2}\right) + m^2\right] = 0 \tag{2.20}$$

The general solution of Eq. (2.20) is (Hildebrand, 1962):

$$P = C\, I_m\left(r\sqrt{a_i^2 - \frac{\omega^2}{c_L^2}}\right) + D\, K_m\left(r\sqrt{a_i^2 - \frac{\omega^2}{c_L^2}}\right) \tag{2.21}$$

where I_m and K_m are the modified Bessel functions of order m, first and second kind respectively and C and D are constants. By setting $\bar{a}_i = \sqrt{a_i^2 - \frac{\omega^2}{c_L^2}}$ and satisfying the requirement that Φ and thus P are finite at $r = 0$, Eq. (2.21) is given as follows:

$$P = C\, I_m(r\bar{a}_i) \tag{2.22}$$

If we make use of the boundary condition of Eq. (2.9b): $P'|_{r=R}\, Z\Theta\, e^{i\omega t} = \dot{u}_r(z,\theta,t)$ and expand the radial velocity in Fourier series we get by application of the superposition principle $B_1 = 1$ and $B_2 = 0$, thus:

$$\Theta = \sum_{m=1}^{\infty} \cos(m\theta) \tag{2.23}$$

and Eq. (2.9b) is written as:

$$\sum_{i=0}^{\infty} (AC)_{mi}\, I_m'(R\bar{a}_i)\ \bar{a}_i \cos(a_i z)\, e^{i\omega t} = \dot{u}_r(z,t) \tag{2.24}$$

The unknown constants $(AC)_{mi}$ can be determined if we employ the orthogonality relations of the cosine functions:

$$\int_0^H \cos(a_i z)\cos(a_s z)\, dz = \begin{cases} H/2, & i = s \neq 0 \\ H, & i = s = 0 \\ 0, & i \neq s \end{cases} \tag{2.25}$$

by multiplying both sides of Eq. (2.24) by $\cos(a_s z)$, $s = 0,1,2,..,k$, and integrate from 0 to H_L. Application of the superposition principle and use of Eq. (2.2) and (2.11) yields the solution for the potential:

$$\varphi_1 = \sum_{m=1}^{\infty}\left[(AC)_{m0}\, I_m(r\bar{a}_0) + \sum_{i=1}^{\infty}(AC)_{mi}\, I_m(r\bar{a}_i)\ \cos(a_i z)\right]\cos(m\theta) \tag{2.26}$$

where:

$$(AC)_{m0} = \frac{\int_0^{H_L} \dot{u}_r(z,t)\,\mathrm{dz}}{H_L\, I'_m(R\bar{a}_0)\bar{a}_0} \tag{2.27}$$

$$(AC)_{mi} = \frac{2\int_0^{H_L} \dot{u}_r(z,t)\cos(a_i z)\mathrm{dz}}{H_L\, I'_m(R\bar{a}_i)\,\bar{a}_i}, i = 1,2,..,k \tag{2.28}$$

Solution for potential φ_2

Again, we use the method of separation of variables according to:

$$\Phi_2(r,z,\theta) = P(r)Z(z)\Theta(\theta) \quad \text{or} \quad \Phi_2 = PZ\Theta \tag{2.29}$$

If we apply the boundary condition in Eq. (2.10c) and expand the free surface velocity in Fourier series, the variable Θ can be determined from Eq. (2.23). Regarding non-trivial solutions, the requirement to satisfy the boundary condition in Eq. (2.10b) leads necessarily to a separation constant κ with negative sign for a differential equation of the form given by Eq. (2.13) on the condition that $\kappa > \omega^2/c_L^2$. Then we can write:

$$\frac{Z''}{Z} = \frac{\lambda^2}{R^2} \tag{2.30}$$

with λ being a constant and the solution is obtained in the following form:

$$Z = A_1\cosh\left(\frac{\lambda}{R}z\right) + A_2\sinh\left(\frac{\lambda}{R}z\right) \tag{2.31}$$

Due to the boundary condition in Eq. (2.10a): $Z'|_{z=0} = 0$ we have $A_2 = 0$. With a similar manipulation followed for Φ_1, one can readily obtain the following equation:

$$r^2P'' + rP' + P\left[r^2\left(\frac{\lambda^2}{R^2} + \frac{\omega^2}{c_L^2}\right) - m^2\right] = 0 \tag{2.32}$$

The general solution of Eq. (2.32) is:

$$P = C\,J_m\left(r\sqrt{\frac{\lambda^2}{R^2} + \frac{\omega^2}{c_L^2}}\right) + D\,Y_m\left(r\sqrt{\frac{\lambda^2}{R^2} + \frac{\omega^2}{c_L^2}}\right) \tag{2.33}$$

where J_m and Y_m are the Bessel functions of order m, first and second kind respectively. Since Y_m is singular at $r = 0$, only the first part of the above expression must be kept. We set $\bar{\lambda} = \bar{\lambda}_n = R\sqrt{\frac{\lambda_n^2}{R^2} + \frac{\omega^2}{c_L^2}}$ and observe that Eq. (2.10b) implies:

$$J'_m(\bar{\lambda}_n) = 0 \tag{2.34}$$

thus, $\bar{\lambda}_n$ becomes the roots of Eq. (2.34). The constant λ_n is determined for all cases as:

$$\lambda_n = \mp\sqrt{\left|\bar{\lambda}_n^2 - \frac{\omega^2}{c_L^2}R^2\right|} \tag{2.35}$$

The boundary condition in Eq. (2.10c) results to:

$$\left(PZ'|_{z=H_L} \right) \mathrm{e}^{\mathrm{i}\omega t} = \dot{f}(r,t) \tag{2.36}$$

By plugging the functions Z and P into Eq. (2.36) and using the superposition principle we get:

$$\sum_{n=1}^{\infty} (AC)_{mn} J_m\left(\frac{r}{R}\bar{\lambda}_n\right) \sinh\left(\frac{\lambda_n H_L}{R}\right) \frac{\lambda_n}{R} \mathrm{e}^{\mathrm{i}\omega t} = \dot{f}(r,t) \tag{2.37}$$

On the condition that $J'_m(a_n) = 0$, if the two sides of Eq. (2.37) are multiplied by $J_m\left(\frac{r}{R}\bar{\lambda}_s\right), s = 1,2,..,k$ and then integrated from 0 to R, all but one term on the left side cancel due to the orthogonality properties of Bessel functions (Abramowitz and Stegun, 1972):

$$\int_0^1 t\, J_\nu(a_m t)\, J_\nu(a_n\, t)\mathrm{dt} = \begin{cases} \dfrac{a_n^2 - \nu^2}{2a_n^2}[J_\nu(a_n)]^2, & m = n \\ 0, & m \neq n \end{cases} \tag{2.38}$$

and the constants $(AC)_{mn}$ can be determined. Appropriate algebraic manipulation and the combination of the functions Z, Θ and P yields the final solution for the potential φ_2 expressed as:

$$\varphi_2 = \sum_{m=1}^{\infty} \sum_{n=1}^{\infty} (AC)_{mn} J_m\left(\frac{r}{R}\bar{\lambda}_n\right) \cosh\left(\frac{\lambda_n z}{R}\right) \cos(m\theta) \tag{2.39}$$

where:

$$(AC)_{mn} = \frac{2\bar{\lambda}_n^2 \int_0^R \dot{f} \frac{r}{R} J_m\left(\frac{r}{R}\bar{\lambda}_n\right) \mathrm{d}r}{(\bar{\lambda}_n^2 - m^2)\left[J_m(\bar{\lambda}_n)\right]^2 \sinh\left(\frac{\lambda_n H_L}{R}\right) \lambda_n} \tag{2.40}$$

2.1.3.2 Integro-differential equations for the flow

With the obtained solutions for the potential, the remaining free surface boundary condition Eq. (2.7) should be considered. Substitution of Eq. (2.26) and Eq. (2.39) into Eq. (2.7) yields:

$$\rho_L \sum_{m=1}^{\infty} \left[\sum_{n=1}^{\infty} \left(\dot{AC}\right)_{mn} J_m\left(\frac{r}{R}\bar{\lambda}_n\right) \cosh\left(\frac{\lambda_n H_L}{R}\right) + \left(\dot{AC}\right)_{m0} I_m(r\bar{a}_0) + \sum_{i=1}^{\infty} \left(\dot{AC}\right)_{mi} I_m(r\bar{a}_i)\, \cos(a_i H_L) + g\, f(r,t) \right] \cos(m\theta) = 0 \tag{2.41}$$

In order to establish an integral equilibrium equation, we make use of the principle of virtual displacements. For an arbitrary virtual displacement $\delta \mathrm{f} \cos(m\theta)$ corresponding to the imposed boundary conditions the total virtual work must be zero over the free surface. Therefore, for each circumferential wave number it follows:

$$\rho_L \int_0^R \int_0^{2\pi} \left[\sum_{n=1}^{\infty} \left(\dot{AC}\right)_{mn} J_m\left(\frac{r}{R}\bar{\lambda}_n\right) \cosh\left(\frac{\lambda_n H_L}{R}\right) + \left(\dot{AC}\right)_{m0} I_m(r\bar{a}_0) + \sum_{i=1}^{\infty} \left(\dot{AC}\right)_{mi} I_m(r\bar{a}_i)\ \cos(a_i H_L) + g\, f(r,t) \right] \cos^2(m\theta)\ \delta \mathrm{f}\, \mathrm{d}\theta\, r \mathrm{dr} = 0 \tag{2.42}$$

The variation of the total pressure can be determined from the Bernoulli equation:

$$p(r,z,\theta,t) = \rho_L\, g\, (H_L - z) - \rho_L \frac{\partial \varphi}{\partial t} \tag{2.43}$$

Thus, the total hydrodynamic pressure exerted on the wall of the cylinder is given by:

$$p_d(R,z,t) = -\rho_L \left. \frac{\partial[\varphi_1 + \varphi_2]}{\partial t} \right|_{r=R} \tag{2.44}$$

By plugging Eq. (2.26) and Eq. (2.39) into Eq. (2.44) we get:

$$p_d = -\rho_L \left[\sum_{i=1}^{\infty} \left(\dot{AC}\right)_{mi} I_m(R\bar{a}_i)\ \cos(a_i z) + \left(\dot{AC}\right)_{m0} I_m(R\bar{a}_0) + \sum_{n=1}^{\infty} \left(\dot{AC}\right)_{mn} J_m(\bar{\lambda}_n) \cosh\left(\frac{\lambda_n z}{R}\right) \right] \cos(m\theta) \tag{2.45}$$

The virtual work done by the pressure through an arbitrary virtual displacement $\delta \mathrm{u}_r \cos(m\theta)$ is expressed by:

$$\delta \mathrm{W} = \int_0^{H_L} \int_0^{2\pi} p_d(R,z,t)\ \delta \mathrm{u}_r\ \cos(m\theta) R\ \mathrm{d}\theta \mathrm{dz} \tag{2.46}$$

and thus:

$$\delta \mathrm{W} = -\rho_L \int_0^{H_L} \int_0^{2\pi} \left[\sum_{i=1}^{\infty} \left(\dot{AC}\right)_{mi} I_m(R\bar{a}_i)\ \cos(a_i z) + \left(\dot{AC}\right)_{m0} I_m(R\bar{a}_0) + \sum_{n=1}^{\infty} \left(\dot{AC}\right)_{mn} J_m(\bar{\lambda}_n) \cosh\left(\frac{\lambda_n z}{R}\right) \right] \cos^2(m\theta)\ \delta \mathrm{u}_r\ R\ \mathrm{d}\theta \mathrm{dz} \tag{2.47}$$

2.1.4 Equations governing the shell motion

2.1.4.1 Basic theory

The behavior of the thin elastic shell is described on the basis of the Love's first approximation theory. The latter is based on the following Kirchhoff-Love postulates:

1. The thickness is small compared to the radius of curvature.
2. The transverse normal stress may be neglected.
3. A normal to the reference surface before deformation remains straight and normal to the deformed reference surface and suffers no extensions.

Novozhilov's consistent consideration of the strain terms in the potential energy expression is adopted (Novozhilov, 1964; Haroun, 1980). The employed kinematic relations allow for both membrane (stretching) and bending strains. The material is regarded as homogeneous, isotropic with respect to the reference surface and linear elastic; hence, it obeys the generalization of Hooke's law.

2.1.4.2 Computation of kinetic and strain energies

The potential energy U stored in the shell can be computed by integrating the strain energy density over the surface:

$$U = \frac{1}{2}\int_0^H \int_0^{2\pi} \boldsymbol{\varepsilon}^{\mathrm{T}}\, \boldsymbol{\sigma}\; R\mathrm{d}\theta\mathrm{d}z \tag{2.48}$$

where $\boldsymbol{\varepsilon}$ is the strain vector and $\boldsymbol{\sigma}$ the vector of the bending and membrane force resultants. In terms of the displacement vector, $\mathbf{u}^s$ Eq. (2.48) is written in the form:

$$U = \frac{1}{2}\int_0^H \int_0^{2\pi} (\mathbf{B}\,\mathbf{u}^s)^{\mathrm{T}}\mathbf{D}\,(\mathbf{B}\,\mathbf{u}^s)\; R\mathrm{d}\theta\mathrm{d}z \tag{2.49}$$

where $\mathbf{B}$ is the differential operator matrix that relates the displacement vector $\mathbf{u}^s$ with the strain vector $\boldsymbol{\varepsilon}$ and $\mathbf{D}$ is the rigidity matrix. The kinetic energy of the shell is computed through integration of the kinetic density of the surface:

$$T = \frac{1}{2}\int_0^H \int_0^{2\pi} h\,\rho\left(\dot{u}_r^2 + \dot{u}_\theta^2 + \dot{u}_z^2\right)\; R\mathrm{d}\theta\mathrm{d}z \tag{2.50}$$

In terms of the velocity vector $\dot{\mathbf{u}}^s$ Eq. (2.50) is written in the form:

$$T = \frac{1}{2}\int_0^H \int_0^{2\pi} \dot{\mathbf{u}}^{s\mathrm{T}}\, h\,\rho\,\dot{\mathbf{u}}^s\; R\mathrm{d}\theta\mathrm{d}z \tag{2.51}$$

2.1.5 Coupled matrix equations of motion

The selected finite element formulation is a cylindrical frustum, thus geometrically modeling of the structure in the circumferential direction is avoided. The displacements within the element have to be uniquely determined by the nodal displacements and the position, and maintain slope and displacement continuity. Due to the strain-displacement relations the displacements u_θ and u_z can be of $\mathrm{C_o}$ type, while u_r should be of $\mathrm{C_1}$ type (Zienkiewicz and Taylor, 2000). Therefore, we choose linear interpolation functions for u_θ and u_z and cubic Hermitian polynomials for u_r. In order to encompass the coupling with the sloshing modes, the free surface is divided into homocentric circular elements.

The continuous free surface displacements can be expressed as linear function of the surface nodal values. The same interpolation functions were used by Haroun (1980). Figure 2.2 shows the discretization scheme adopted for the system.

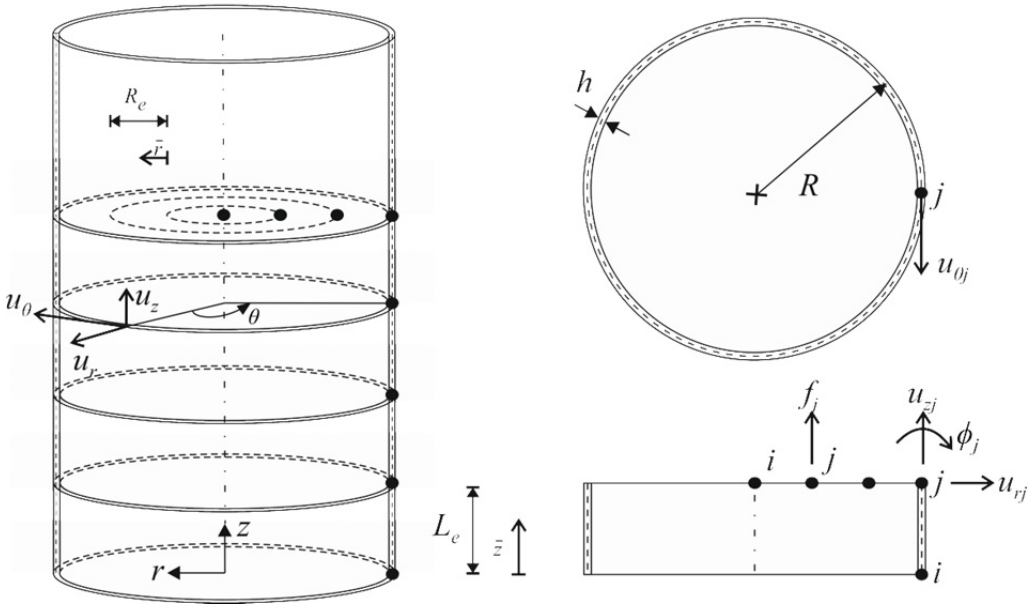

Figure 2.2: Discretization of the system.

Accordingly, the displacements of the system $\mathbf{u}$ for each circumferential wave number m are expressed in terms of the generalized nodal displacements as follows:

$$\mathbf{u} = \mathbf{G}\,\mathbf{N}\,\mathbf{u}_e \tag{2.52}$$

where $\mathbf{u} = \{f, u_r, u_\theta, u_z\}^{\mathrm{T}}$ and $\mathbf{u}_e = \left\{\mathbf{u}_e^f, \mathbf{u}_e^s\right\}^{\mathrm{T}} = \{f_i, f_j, u_{ri}, u_{\theta i}, u_{zi}, \varphi_i, u_{rj}, u_{\theta j}, u_{zj}, \varphi_j\}^{\mathrm{T}}$. The matrix of the interpolation functions $\mathbf{N}$ is defined as:

$$\mathbf{N} = \begin{bmatrix} \mathbf{N}^f & \mathbf{0} \\ \mathbf{0} & \mathbf{N}^s \end{bmatrix} \tag{2.53}$$

where $\mathbf{N}^f$ contains the shape functions for the free-surface displacements:

$$\mathbf{N}^f = \begin{bmatrix} N_i^f & N_j^f \end{bmatrix} \tag{2.54}$$

and $\mathbf{N}^s$ contains the shape functions for the wall displacements:

$$\mathbf{N}^s = \begin{bmatrix} \mathbf{N}_r \\ \mathbf{N}_\theta \\ \mathbf{N}_z \end{bmatrix} = \begin{bmatrix} N_{ri} & 0 & 0 & N_{\varphi i} & N_{rj} & 0 & 0 & N_{\varphi j} \\ 0 & N_{\theta i} & 0 & 0 & 0 & N_{\theta j} & 0 & 0 \\ 0 & 0 & N_{zi} & 0 & 0 & 0 & N_{zj} & 0 \end{bmatrix} \tag{2.55}$$

The matrix $\mathbf{G}$ is defined as:

$$\mathbf{G} = \begin{bmatrix} \mathbf{G}^f & \mathbf{0} \\ \mathbf{0} & \mathbf{G}^s \end{bmatrix} = \begin{bmatrix} \cos(m\theta) & 0 & 0 & 0 \\ 0 & \cos(m\theta) & 0 & 0 \\ 0 & 0 & \sin(m\theta) & 0 \\ 0 & 0 & 0 & \cos(m\theta) \end{bmatrix} \tag{2.56}$$

where $\mathbf{G}^f$ and $\mathbf{G}^s$ are 1x1 and 3x3 matrices respectively. The expressions for the interpolation functions are given in Appendix A. By plugging Eq. (2.52) into Eq. (2.49) the element strain energy is straightforwardly expressed by means of the stiffness matrix of the shell $\mathbf{K}_s$:

$$U = \frac{1}{2}\sum_{e=1}^{\mathrm{EZ}} \mathbf{u}_e^{s\mathrm{T}}\, \mathbf{K}_e\, \mathbf{u}_e^s = \frac{1}{2}\mathbf{q}^{s\mathrm{T}}\mathbf{K}_s\mathbf{q}^s \tag{2.57}$$

where $\mathbf{K}_s = \sum_{e=1}^{\mathrm{EZ}} \mathbf{K}_e$, $\mathbf{K}_e = \pi R \int_0^{L_e} \mathbf{P}^{\mathrm{T}}\mathbf{D}_e\mathbf{P}\ \mathrm{d}\bar{z}$ and $\mathbf{P} = \mathbf{B}\,\mathbf{G}^s\,\mathbf{N}^s$. The total number of shell elements is EZ and $\mathbf{q}^s$ denotes the assemblage of all the structural degrees of freedom: $\mathbf{q}^s = \sum_{e=1}^{\mathrm{EZ}} \mathbf{u}_e^s$.The consistent mass matrix $\mathbf{M}_s$ of the shell is obtained by inserting Eq. (2.52) into Eq. (2.51):

$$T = \frac{1}{2}\sum_{e=1}^{\mathrm{EZ}} \dot{\mathbf{u}}_e^{s\mathrm{T}}\, \mathbf{M}_e\, \dot{\mathbf{u}}_e^s = \frac{1}{2}\dot{\mathbf{q}}^{s\mathrm{T}}\, \mathbf{M}_s\, \dot{\mathbf{q}}^s \tag{2.58}$$

where $\mathbf{M}_s = \sum_{e=1}^{\mathrm{EZ}} \mathbf{M}_e$ and $\mathbf{M}_e = \pi\, R\, h\, \rho_e \int_0^{L_e} \mathbf{N}^{s\mathrm{T}}\mathbf{N}^s\ \mathrm{d}\bar{z}$. Eq. (2.47) can be written in the form:

$$\begin{aligned} \delta W = &-\sum_{i=1}^{\infty} A_{im} \int_0^{H_L} \ddot{u}_r(z,t)\cos(a_i z)\mathrm{d}z \int_0^{H_L} \delta u_r \cos(a_i z)\mathrm{d}z - A_{0m}\int_0^{H_L} \ddot{u}_r(z,t)\ \mathrm{d}z \int_0^{H_L} \delta u_r\ \mathrm{d}z \\ &-\sum_{n=1}^{\infty} B_{nm} \int_0^{R} \ddot{f}(r,t) r\, J_m\left(\frac{r}{R}\bar{\lambda}_n\right)\mathrm{d}r \int_0^{H_L} \delta u_r \cosh\left(\frac{\lambda_n z}{R}\right)\mathrm{d}z \end{aligned} \tag{2.59}$$

where A_{im}, A_{0m} and B_{nm} are given in Appendix A. With the aid of the interpolation functions Eq. (2.59) can be constructed in matrix form:

$$\begin{aligned} \delta W = -\sum_{k=1}^{\mathrm{EZL}} \Bigg[&\sum_{i=1}^{\infty}\sum_{e=1}^{\mathrm{EZL}} A_{im}(\,\delta\mathbf{u}_e^s\,\mathbf{T}_{ie})^{\mathrm{T}}\,\mathbf{T}_{ik}\,\ddot{\mathbf{u}}_k^s + \sum_{e=1}^{\mathrm{EZL}} A_{0m}\,(\delta\mathbf{u}_e^s\,\mathbf{T}_{0e})^{\mathrm{T}}\,\mathbf{T}_{0k}\,\ddot{\mathbf{u}}_k^s \\ &+\sum_{n=1}^{\infty}\sum_{e=1}^{\mathrm{ERL}} B_{nm}\,(\delta\mathbf{u}_k^s\,\mathbf{Y}_{nk})^{\mathrm{T}}\,\mathbf{Z}_{nme}\,\ddot{\mathbf{u}}_e^f \Bigg] \end{aligned} \tag{2.60}$$

where ERL and EZL are the total number of elements on the free-surface and along the liquid-covered wall respectively. The vectors $\mathbf{T}, \mathbf{Y}$ and $\mathbf{Z}$ that appear in Eq. (2.60) are given in Appendix A. Finally the expression for the virtual work can be further condensed in the following form:

$$\delta W = -\begin{Bmatrix} \delta\mathbf{q}_w^s \\ \delta\mathbf{q}_d^s \end{Bmatrix}^{\mathrm{T}} \begin{bmatrix} \mathbf{M}_{Aw} & \mathbf{0} \\ \mathbf{0} & \mathbf{0} \end{bmatrix} \begin{Bmatrix} \ddot{\mathbf{q}}_w^s \\ \ddot{\mathbf{q}}_d^s \end{Bmatrix} - \begin{Bmatrix} \delta\mathbf{q}_w^s \\ \delta\mathbf{q}_d^s \end{Bmatrix}^{\mathrm{T}} \begin{bmatrix} \mathbf{M}_{Bw} \\ \mathbf{0} \end{bmatrix} \ddot{\mathbf{q}}^f \tag{2.61}$$

and for the sake of brevity Eq. (2.61) is written as:

$$\delta W = -\delta\mathbf{q}^{s\mathrm{T}}\,\mathbf{M}_A\,\ddot{\mathbf{q}}^s - \delta\mathbf{q}^{s\mathrm{T}}\,\mathbf{M}_B\,\ddot{\mathbf{q}}^f \tag{2.62}$$

where the assemblage of all the free-surface degrees of freedom $\mathbf{q}^f$ is given by: $\mathbf{q}^f = \sum_{e=1}^{\mathrm{ERL}} \mathbf{u}_e^f$, whereas the vectors $\mathbf{q}_w^s = \sum_{e=1}^{\mathrm{EZL}} \mathbf{u}_e^s$ and $\mathbf{q}_d^s = \sum_{e=1}^{\mathrm{EZ-EZL}} \mathbf{u}_e^s$ stand for the total structural degrees of

freedom on the liquid-covered and remaining area respectively. The system examined is conservative, thus the first matrix equation of motion can be deduced from Hamilton's principle:

$$\delta \int_{t_1}^{t_2} (T - U + W)\mathrm{dt} = 0 \tag{2.63}$$

where δ is a variational operator taken during the specified time interval. Substituting Eq. (2.57), (2.58) and (2.62) into (2.63) yields:

$$\int_{t_1}^{t_2} (\,\delta\dot{\mathbf{q}}^{s\mathrm{T}}\,\mathbf{M}_s\,\dot{\mathbf{q}}^s - \delta\mathbf{q}^{s\mathrm{T}}\,\mathbf{K}_s\,\mathbf{q}^s - \delta\mathbf{q}^{s\mathrm{T}}\,\mathbf{M}_A\,\ddot{\mathbf{q}}^s - \delta\mathbf{q}^{s\mathrm{T}}\,\mathbf{M}_B\,\ddot{\mathbf{q}}^f)\mathrm{dt} = \mathbf{0} \tag{2.64}$$

The integration by parts in time of the first term of Eq. (2.64) leads to the first governing matrix equation of the free undamped vibration of the liquid-filled cylinder since the time-boundary term vanishes according to the application conditions of Hamilton's principle:

$$\mathbf{K}_s\,\mathbf{q}^s + \mathbf{M}_s\,\ddot{\mathbf{q}}^s + \mathbf{M}_A\ddot{\mathbf{q}}^s + \mathbf{M}_B\,\ddot{\mathbf{q}}^f = \mathbf{0} \tag{2.65}$$

The last term of Eq. (2.65) incorporates the coupling of the free surface fluctuations with the structural deformations. The second governing matrix equation is derived by Eq. (2.42). It is expedient to write the latter in the following form:

$$\begin{aligned}\sum_{n=1}^{\infty} C_{nm} \int_0^R \ddot{f}(r,t) r\, J_m\left(\frac{r}{R}\bar{\lambda}_n\right)\mathrm{dr} \int_0^R \delta\mathrm{f}\, r\, J_m\left(\frac{r}{R}\bar{\lambda}_n\right)\mathrm{dr} + D_{0m}\int_0^{H_L} \ddot{u}_r(z,t)\,\mathrm{dz}\int_0^R \delta\mathrm{f}\, r\, I_m(r\bar{a}_0)\mathrm{dr}\\ + \sum_{i=1}^{\infty} D_{im}\int_0^{H_L} \ddot{u}_r(z,t)\cos(a_i z)\mathrm{dz}\int_0^R \delta\mathrm{f}\, r\, I_m(r\bar{a}_i)\mathrm{dr} + \rho_L\pi\, g\int_0^R \delta\mathrm{f}\, f\, r\,\mathrm{dr} = 0\end{aligned} \tag{2.66}$$

where C_{nm} and D_{im} are provided in Appendix A. By carrying out the same discretization scheme as before Eq. (2.66) is written as:

$$\begin{aligned}\sum_{k=1}^{\mathrm{ERL}}\Bigg[\sum_{n=1}^{\infty}\sum_{e=1}^{\mathrm{ERL}} C_{nm}\left(\delta\mathbf{u}_e^f\,\mathbf{Z}_{nme}\right)^{\mathrm{T}}\mathbf{Z}_{nmk}\ddot{\mathbf{u}}_k^f + \sum_{e=1}^{\mathrm{EZL}} D_{0m}\left(\delta\mathbf{u}_k^f\,\mathbf{L}_{0mk}\right)^{\mathrm{T}}\mathbf{T}_{0e}\ddot{\mathbf{u}}_e^s\\ + \sum_{i=1}^{\infty}\sum_{e=1}^{\mathrm{EZL}} D_{im}\left(\delta\mathbf{u}_k^f\,\mathbf{L}_{imk}\right)^{\mathrm{T}}\mathbf{T}_{ie}\,\ddot{\mathbf{u}}_e^s\Bigg] + \sum_{e=1}^{\mathrm{ERL}}\delta\mathbf{u}_e^{f\,\mathrm{T}}\mathbf{V}_e\mathbf{u}_e^f = \mathbf{0}\end{aligned} \tag{2.67}$$

The vectors and matrices that appear in Eq. (2.67) are given in Appendix A. Finally Eq. (2.67) can be further condensed in the following form:

$$\delta\mathbf{q}^{f\,\mathrm{T}}\mathbf{M}_C\,\ddot{\mathbf{q}}^f + \delta\mathbf{q}^{f\,\mathrm{T}}[\mathbf{M}_{Dw}\quad\mathbf{0}]\begin{Bmatrix}\ddot{\mathbf{q}}_w^s\\ \ddot{\mathbf{q}}_d^s\end{Bmatrix} + \delta\mathbf{q}^{f\,\mathrm{T}}\mathbf{K}_L\,\mathbf{q}^f = \mathbf{0} \tag{2.68}$$

Since $\delta\mathbf{q}^f$ is arbitrary Eq. (2.68) can be satisfied if and only if we set:

$$\mathbf{M}_C\,\ddot{\mathbf{q}}^f + \mathbf{M}_D\,\ddot{\mathbf{q}}^s + \mathbf{K}_L\,\mathbf{q}^f = \mathbf{0} \tag{2.69}$$

By combining Eq. (2.69) and Eq. (2.65) the undamped free vibration equation of the system is obtained as:

$$\begin{bmatrix} \mathbf{K}_S & \mathbf{0} \\ \mathbf{0} & \mathbf{K}_L \end{bmatrix} \begin{Bmatrix} \mathbf{q}^S \\ \mathbf{q}^f \end{Bmatrix} + \begin{bmatrix} \mathbf{M}_S + \mathbf{M}_A & \mathbf{M}_B \\ \mathbf{M}_D & \mathbf{M}_C \end{bmatrix} \begin{Bmatrix} \ddot{\mathbf{q}}^S \\ \ddot{\mathbf{q}}^f \end{Bmatrix} = \mathbf{0} \tag{2.70}$$

with $\mathbf{M}_B$=$\mathbf{M}_C$. In symbolic vector-tensor notation, Eq. (2.70) is written as:

$$\mathbf{K}\,\mathbf{q} + \mathbf{M}\,\ddot{\mathbf{q}} = \mathbf{0} \tag{2.71}$$

In order to solve the eigenvalue problem we introduce a harmonic motion for every generalized degree of freedom by means of: $\mathbf{q}(\mathbf{x}, t) = \mathbf{q}(\mathbf{x})\cos(\omega t)$. For a non-trivial solution of Eq. (2.71) the determinant of the matrix $\mathbf{K} - \omega^2\mathbf{M}$ should vanish, thus we enforce that:

$$\det[\mathbf{K} - \omega^2\mathbf{M}] = \mathbf{0} \tag{2.72}$$

The mass and stiffness matrices are symmetric and positive definite. The stiffness matrix $\mathbf{K}$ is a band matrix whereas the mass matrix $\mathbf{M}$ is a partially dense matrix. Consideration of the kinematic boundary conditions corresponds to deletion of appropriate rows and columns of Eq. (2.72) reducing the order of the matrix equation. Eq. (2.72) finally yields N solutions $\omega_i^2, i = 1,2,..,N$, where $N = 4\mathrm{EZ} + \mathrm{ERL} + 5 - B$ corresponding to N eigenvectors and B imposed kinematic boundary conditions. Computational time can be saved by calculating only one of the matrices $\mathbf{M}_B$ and $\mathbf{M}_D$. In order to prove the symmetry of the mass matrix we apply Green's second identity for two scalar functions such as Φ_1 and Φ_2 that satisfy the Helmholtz equation (Amabili, 2000):

$$\iint_{\partial\Omega_L} (\Phi_2 \nabla\Phi_1 - \Phi_1 \nabla\Phi_2)\,\mathrm{dA} = \iiint_{\Omega_L} (\Phi_2 \nabla^2\Phi_1 - \Phi_1 \nabla^2\Phi_2)\mathrm{d}\Omega_L = 0 \tag{2.73}$$

If we split the surface integral of Eq. (2.73) into the intervals defined by the free-surface, wall and bottom areas and consider the boundary conditions the following relationship is obtained:

$$\iint_{A^w} \Phi_2 \frac{\partial\Phi_1}{\partial r}\,\mathrm{dA}^w = \iint_{Af} \Phi_1 \frac{\partial\Phi_2}{\partial z}\,\mathrm{dA}^f \tag{2.74}$$

The straightforward evaluation of the determinant presumes a priori assessment of the natural frequencies since the mass matrix remains implicit frequency-dependent due to the liquid's compressibility. Therefore, an iterative scheme should be employed: we assume an initial frequency of very small value ω_i^k and the eigenvalue problem is solved resulting to a new frequency ω_i^{k+1}, which is used for an improved assumption of the next iteration step. The iteration process is continued until two successive frequencies are the same within a preset tolerance.

The developed formulations have been implemented in a computer program with the aid of the commercial mathematical software ©MAPLE (2013). The shell stiffness matrix has been computed by using ©ANSYS (2013a). It should be noted that the integrals that appear in the derivation of the solution are evaluated analytically. Therefore, the accuracy of the solution depends exclusively on the

number of elements included in the analysis, the number of terms considered for the series expanded to infinite and the tolerance inserted in the iterative incremental scheme. For our study, we set $\left|\omega_i^k - \omega_i^{k-1}\right|/\omega_i^k \leq 0.001$, where k represents the iteration step.

2.1.6 Convergence and validation of the method

In order to ensure the accuracy of the solution, the convergence behavior is initially addressed. The first three lowest natural frequencies of a fully-filled clamped-free circular cylinder are calculated by conducting axisymmetric modal analyses ($m = 0$) with finite elements varying from 10 to 40 and compared with the analytical solution derived by Cho et al. (2002) using Novozhilov's thin shell theory and disregarding the free surface fluctuations. The exclusion of the free surface effects ($\varphi_2 = 0$) is related with constant pressure at the free surface and can be assumed zero. In this case, the following boundary conditions must be considered:

$$\left.\frac{\partial \varphi_1}{\partial z}\right|_{z=0} = 0, \quad \left.\frac{\partial \varphi_1}{\partial r}\right|_{r=R} = \dot{u}_r(z,t), \qquad \rho_L \left.\frac{\partial \varphi_1}{\partial t}\right|_{z=H_L} = 0 \tag{2.75a-c}$$

which yield the following solution for the potential φ_1:

$$\varphi_1(r,z,t) = 2\sum_{i=1}^{\infty} \frac{I_0(r\bar{a}_i)\cos(a_i z)}{H_L\, I_1(R\bar{a}_i)\, \bar{a}_i} \int_0^{H_L} \dot{u}_r(z,t)\, \cos(a_i z)\mathrm{dz} \tag{2.76}$$

where $a_i = \pi(2\,i - 1)/(2\,H_L)$. Subsequently, we solve a matrix equation of the form given in Eq. (2.65) with the last term omitted. The geometrical data and physical properties for the steel cylinders examined are: $R = 20$ m, $h = 0.0283$ m, $E = 21.5 \text{ x } 10^7$ kPa, $\nu = 0.3$, $\rho_L = 1000$ kg/m^3, $\rho = 7850$ kg/m^3, $c_L = 1410$ m/s. The results presented in Table 2.1 show that the solution converges rapidly as the number of shell elements increases to the exact solution of the differential equations that govern the response of the mathematical model. A coarse mesh with 10 elements suffices to calculate the first natural frequency with a divergence of less than 1% from the exact solution for the case of an incompressible liquid. As expected, for higher eigenmodes and slender cylinders more elements should be included to achieve high accuracy. A discretization with 40 elements furnishes natural frequencies, which are almost equal to the theoretical results for all modes and slenderness ratios. Therefore, all the succeeding results presented in this study are obtained by using 40 elements along the height. The values of Table 2.1 also indicate that the present results agree quite well with the exact solution when the compressibility of the liquid is taken into account.

To verify the present methodology when the effect of the free surface waves is taken into account, a simply supported, circular cylindrical shell partially filled with a sloshing incompressible liquid and with a rigid flat bottom is analyzed. The results are compared with those obtained by Amabili (2000) who made use of the Rayleigh-Ritz method and Flügge's shell theory. The following dimensions and

material properties are taken: $H = 3.5\text{m}$, $H_L = 2.35$ m, $R = 1$ m, $h = 0.1$ mm, $E = 20.6 \text{ x } 10^7$ kPa, $\nu = 0.3$, $\rho_L = 1000\ \text{kg/m}^3$, $\rho = 7850\ \text{kg/m}^3$. The free surface is divided into 40 elements and modes with $m = 6$ nodal diameters are investigated. The solution for an incompressible liquid is obtained if the velocity potential φ is substituted with: $\bar{\varphi} = \lim_{c_L \to \infty} \varphi$. In this case, the sloshing frequencies for a rigid cylinder are computed by using the formula:

$$\omega_{SL,n}^2 = \frac{\lambda_n\, g}{R} \tanh\left(\frac{\lambda_n H_L}{R}\right) \tag{2.77}$$

which emanates from the solution for the potential φ_2 if we substitute the boundary condition of Eq. (2.10c) with the free vibration condition:

$$\frac{\partial^2 \varphi_2}{\partial t^2} + g \frac{\partial \varphi_2}{\partial z}\bigg|_{z=H_L} = 0 \tag{2.78}$$

The natural frequencies listed in Table 2.2 are in good agreement with the reported ones.

2.1.7 Numerical investigation

Several cases of cylinders which are allowed to undergo free vibration are examined. All the clamped-free systems under study have the following properties in common: $E = 21.0 \text{ x } 10^7$ kPa, $\nu = 0.3$, $\rho_L = 1000\ \text{kg/m}^3$, $\rho = 7850\ \text{kg/m}^3$. The containers have in the most general case a free surface and are partially or fully filled with a compressible liquid. Initially, it is useful to focus solely on the effect of the surface elevation of the liquid. Preliminary investigations indicated that we may distinguish two cases in which the free-surface fluctuations have a considerable influence on the dynamic characteristics of the system.

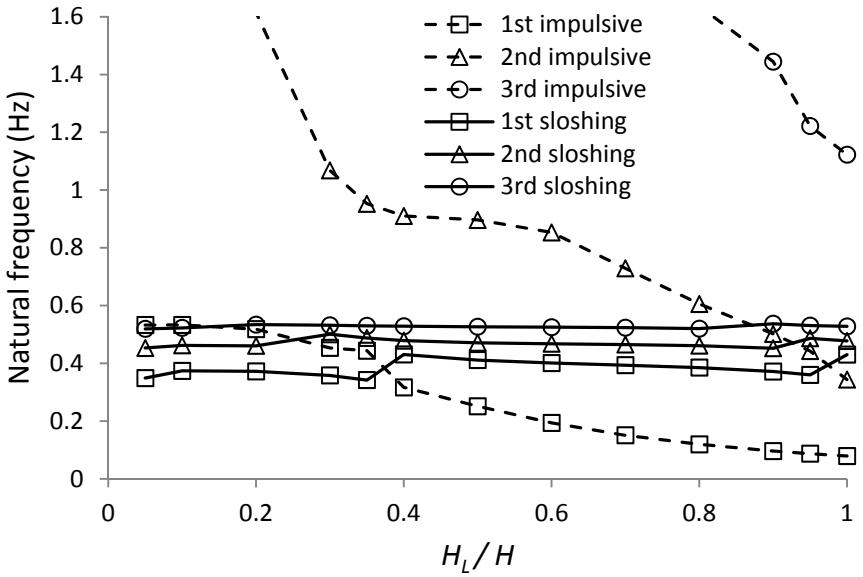

Figure 2.3: Natural frequencies versus the filling ratio of cylinder with free surface, 7th circumferential mode.

The first case refers to a state in which a cross-interaction between the sloshing and impulsive motion occurs. In the low frequency range and for higher circumferential modes, the free surface and the surrounding wall may experience free oscillations with convergent natural frequencies. Characteristic example is a cylinder with the following properties: $h = 6\text{x}\,10^{-3}\text{m}$, $R = 15\text{m}$, $H = 45\text{m}$, $c_L = \infty$. In a diagram of natural frequencies as a function of the filling ratio H_L/H, such as that shown in Figure 2.3 for $m = 7$, this ultimate state for the two -otherwise distinct- vibrations is represented by an abrupt change in the curvatures of the coupled modes combined with an exchange of their natural frequencies, if we conceptually interpolate the curves around the intersection point. Similar phenomena are revealed also for graphs depicting the coupled natural frequencies of systems for various circumferential modes (Figure 2.4). Nevertheless, for low natural frequencies remoted from this ‘‘crossroad’’, the coupling of the shell with the sloshing modes is weak. The second case is related to the great amount of energy produced by the free-surface motion when specific conditions concerning the geometric and physical properties of the container are satisfied. Specifically, for small values of the ratios H/R and R/h the impulsive modes are notably affected by the sloshing oscillations. When the height of the cylinder decreases towards the radius, the free-surface becomes larger compared to the surrounding lateral wall. On the other hand, the considerable kinetic energy related to the distributed inertia force of thicker wall systems emphasizes the influence of the free surface’s kinetic energy on the wall motion.

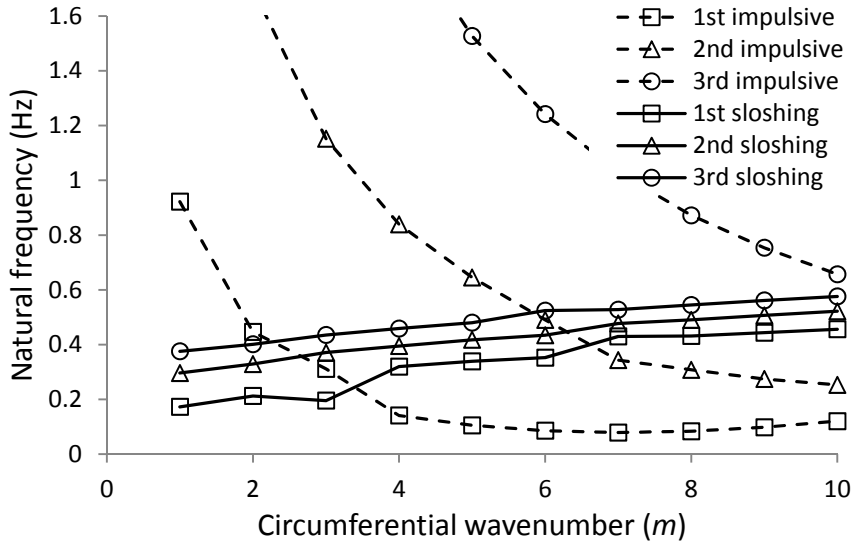

Figure 2.4: Natural frequencies versus circumferential wavenumber of cylinder with free surface, $H_L/H = 1$.

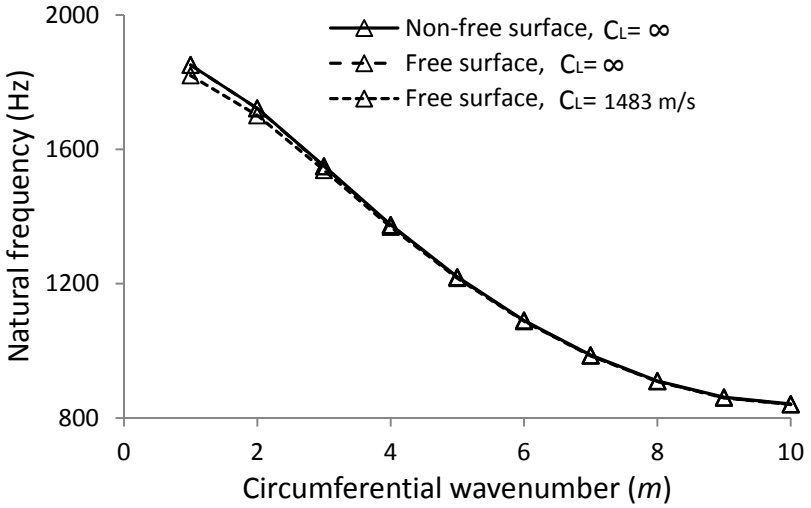

Figure 2.5: Natural frequencies versus the circumferential wavenumber of cylinder with free surface, $H_L/H = 1$, 1st axial mode.

Next, a shell ascribed with the following properties is investigated: $h = 10^{-3}$m, $R = 0.2$m, $H = 0.06$m. Figures 2.5, 2.6 and 2.7 show that the natural frequencies associated with the wall vibrations are generally reduced due to existence of an incompressible liquid free-surface. The coupling effects are more pronounced for higher axial modes and lower values of the circumferential modes. The same figures also illustrate the changes of the impulsive natural frequencies, if a finite value of the sound velocity in the liquid is considered. The compressibility effect acts cumulatively to the free-surface effect resulting to a further reduction of the natural frequencies for higher axial modes. Lowering of the liquid's sound speed leads to reduction of the liquid stiffness due to diminution of the bulk modulus of elasticity and consequently intensifies the effect of liquid's mass resulting in decreased frequencies for the system (Jeong and Kim, 1998).

The influence of the compressibility on the impulsive natural frequencies in absence of free-surface is illustrated in Figure 2.8, in which the results of two cylinders with different slenderness ratios ($h = 10^{-3}$m, $R = 0.2$m, $H/R = 0.3, 3$, $m = 1$) are presented as a function of the filling ratio H_L/H. One may observe that consideration of compressibility reduces the natural frequencies once there is a little fluid in the slender shell. However, the phenomenon becomes notable only for fully-filled containers and relatively high values of the sound velocity.

Table 2.1: Natural frequencies for different number of finite elements, clamped-free case of a fully-filled cylinder without surface effects, 0th circumferential mode (in parentheses the relative % difference from analytical solution given by Cho et al., 2002).

Incompressible liquid (Hz)									
Mode	1			2			3		
Number of elements	*H/R*								
	0.5	1	2	0.5	1	2	0.5	1	2
10	7.356(0.35)	4.431(0.54)	2.382(0.77)	13.308(1.58)	8.966(0.33)	5.239(10.48)	17.278(3.77)	11.542(1.44)	6.410(20.15)
16	7.338(0.11)	4.417(0.22)	2.391(0.44)	13.187(0.66)	9.044(0.54)	5.812 (0.70)	16.929(1.67)	11.862(1.29)	7.828 (2.49)
20	7.335(0.07)	4.413(0.12)	2.385(0.19)	13.154(0.41)	9.028(0.36)	5.789 (0.49)	16.829(1.07)	11.822(0.95)	7.741 (3.57)
25	7.332(0.03)	4.411(0.07)	2.385(0.18)	13.133(0.25)	9.034(0.43)	5.853 (0.01)	16.764(0.68)	11.849(1.18)	8.012 (0.20)
32	7.332(0.03)	4.411(0.07)	2.384(0.13)	13.118(0.13)	9.018(0.25)	5.861 (0.14)	16.718(0.40)	11.796(0.73)	8.053 (0.31)
40	7.331(0.01)	4.408(0.01)	2.382(0.06)	13.109(0.07)	8.999(0.04)	5.857 (0.07)	16.691(0.25)	11.734(0.20)	8.044 (0.20)
Compressible liquid (Hz)									
40	7.237(0.01)	4.302(0.01)	2.305(0.05)	13.061(0.06)	8.928(0.03)	5.761 (0.07)	16.658(0.25)	11.682(0.20)	7.968 (0.19)

Table 2.2: Natural frequencies of a simple supported partially-filled cylinder, 6th circumferential mode (comparison with results of Amabili, 2000).

	Coupled system				Surface waves neglected		Rigid wall	
	Impulsive modes		Sloshing modes		Impulsive modes		Sloshing modes	
Mode	Present study	Amabili	Present study	Amabili	Present study	Amabili	Present study	Amabili
1	1.515	1.482	1.234	1.243	1.394	1.361	1.365	1.365
2	6.382	6.297	1.722	1.715	6.360	6.285	1.707	1.708
3	14.398	14.350	1.951	1.950	14.391	14.350	1.947	1.948
4	22.957	23.790	2.153	2.153	22.956	23.780	2.151	2.152

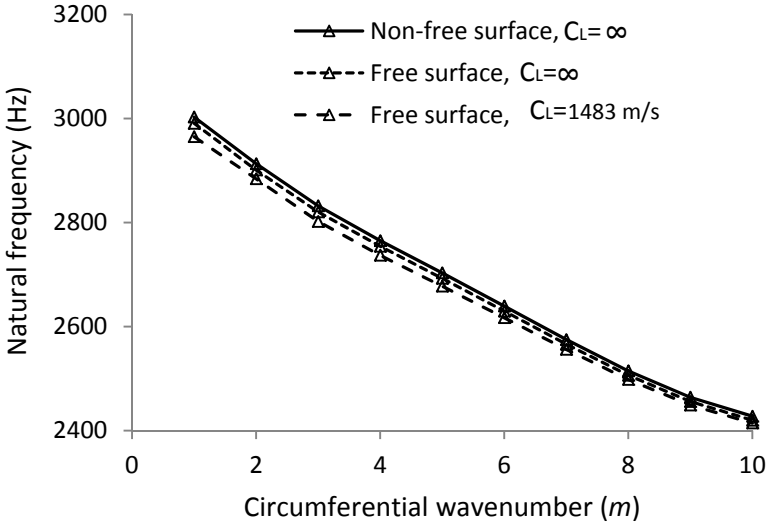

Figure 2.6: Natural frequencies versus the circumferential wavenumber of cylinder with free surface, $H_L/H = 1$, 2nd axial mode.

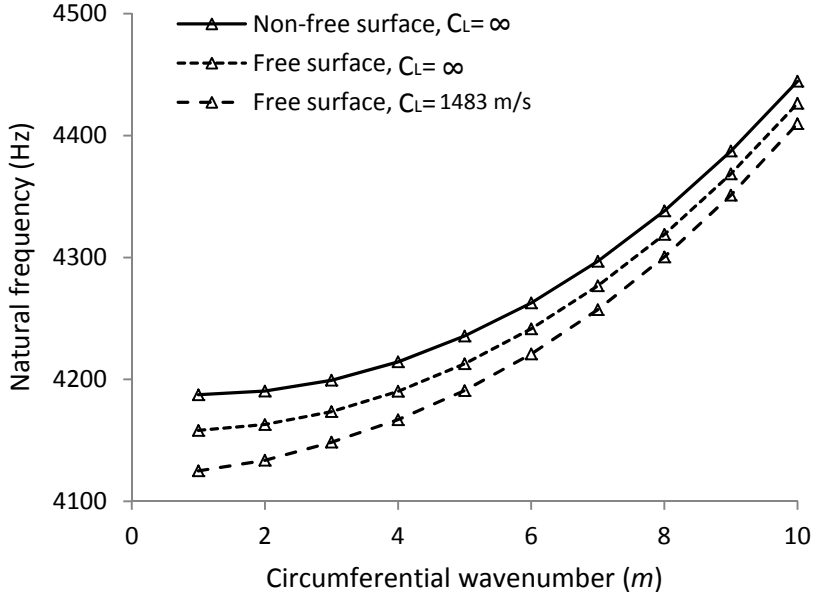

Figure 2.7: Natural frequencies versus the circumferential wavenumber of cylinder with free surface, $H_L/H = 1$, 3rd axial mode.

The first three sloshing and impulsive mode shapes in a shell section along x-axis of a half-filled container with incompressible liquid ($h = 10^{-3}$m, $R = 0.2$m, $H/R = 3$, $H_L/H = 0.5$, $m = 1$) and different boundary conditions are shown in Figure 2.9 and Figure 2.10.

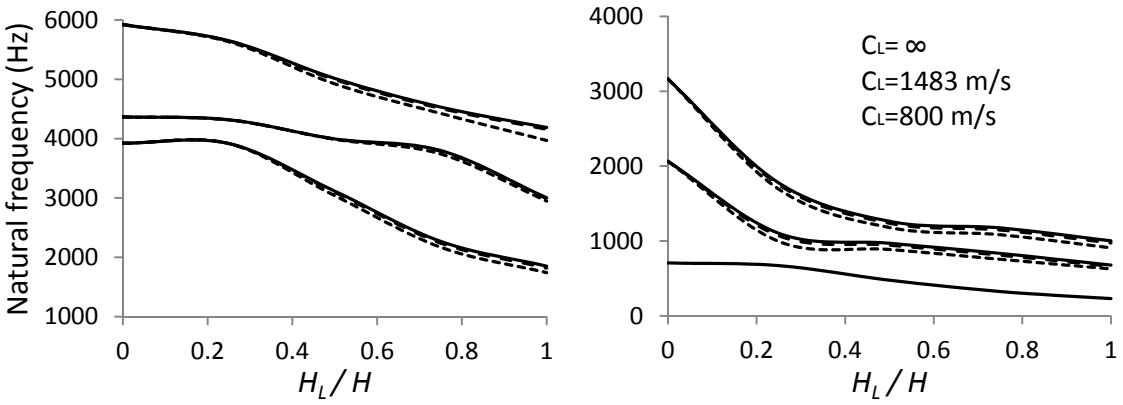

Figure 2.8: Natural frequencies versus the filling ratio of cylinder in absence of free surface, 1st circumferential mode (left: $H/R = 0.3$, right: $H/R = 3$).

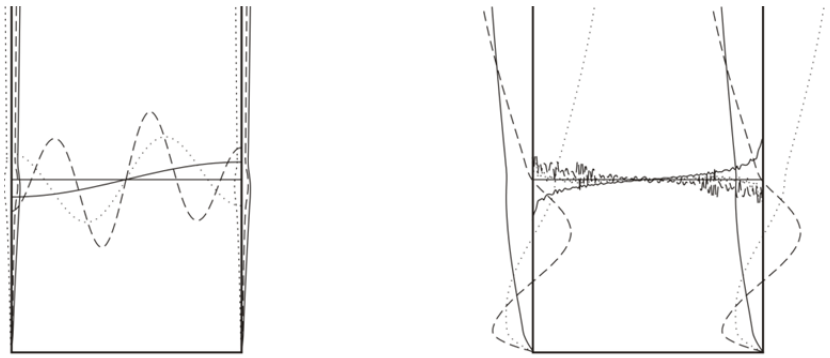

Figure 2.9: Mode shapes of the first three sloshing (left) and impulsive (right) modes of a clamped-free half-filled cylinder.

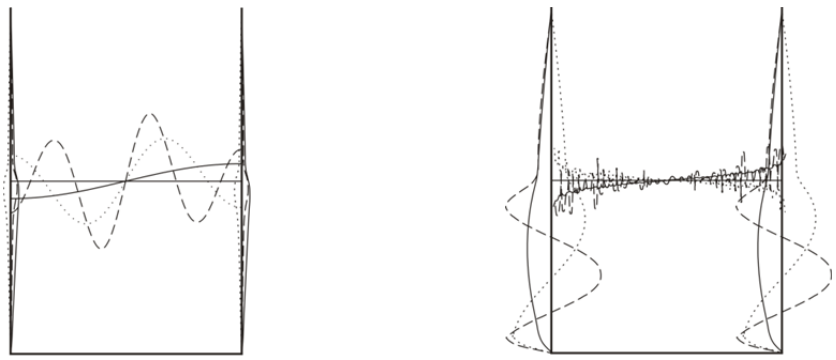

Figure 2.10: Mode shapes of the first three sloshing (left) and impulsive (right) modes of a simply supported half-filled cylinder.

2.2 Seismic analysis of liquid-storage tanks

In this section, the influence of liquid's compressibility on the free vibrational characteristics of the liquid-tank systems is disregarded. Thus, it is assumed that the sound travels through the enclosed liquid with infinite velocity. In addition, the dynamic interaction between sloshing fluctuations and shell vibrations is considered negligible. The frequency range and circumferential wavenumbers under investigation provide adequate ground for this assumption. Therefore, the free surface gravity waves are considered as if the tank wall was rigid and the response of the liquid-shell system is examined independently. Under these assumptions, the procedure followed regarding the assessment of the response to ground motion, is similar with the process proposed by Haroun (1980), Tang (1986) and Habenberger (2001). However, comprehensive numerical data for systems in fixed base condition is presented in order to: (a) Provide the parameters which set up a model for the tank-liquid system used in the dynamic analysis of adjacent containers. (b) Examine the accuracy of the method proposed in the current standard provisions EC8 (2006) for the seismic design of liquid-storage tanks. (c) Establish the theoretical background of a simplified seismic design procedure for cylindrical -anchored to non-deformable medium- tanks. Only vibration modes for circumferential wavenumber $m = 1$ are investigated for the case of horizontal ground motion, whereas only vibration modes for circumferential wavenumber $m = 0$ are investigated for the case of vertical ground motion. This is related to the fact that perfect circular shells are examined and for the analyses conducted it is presumed that the tank does not exhibit any material or geometry nonlinearity. In general linear analysis, vibration modes with $m \geq 2$ are not excited since they are related with small participation factors 0. The reader is referred to an extensive overview of the research results regarding the nonlinear vibration behavior and the instability region of oval-type vibration in the work of Amabili (2003) and Maekawa (2012).

2.2.1 Equations governing the liquid motion

For an irrotational flow the potential function φ of an incompressible ($c_L = \infty$), non-viscous fluid satisfies the Laplace equation:

$$\frac{\partial^2 \varphi}{\partial r^2} + \frac{1}{r}\frac{\partial \varphi}{\partial r} + \frac{\partial^2 \varphi}{\partial z^2} + \frac{1}{r^2}\frac{\partial^2 \varphi}{\partial \theta^2} = 0 \tag{2.79}$$

2.2.1.1 Horizontal excitation

The following boundary conditions have to be satisfied:

$$\left.\frac{\partial \varphi}{\partial z}\right|_{z=0} = 0 \tag{2.80}$$

$$\left.\frac{\partial \varphi}{\partial r}\right|_{r=R} = \dot{u}_r(z,\theta,t) + \dot{X}_g(\theta,t) \tag{2.81}$$

$$\left.\left(\frac{\partial^2 \varphi}{\partial t^2} + g\frac{\partial \varphi}{\partial z}\right)\right|_{z=H_L} = 0 \tag{2.82}$$

It is convenient to express the solution of Eq. (2.80) as the sum of three parts:

$$\varphi = \varphi_1 + \varphi_2 + \varphi_3 \tag{2.83}$$

The first part of Eq. (2.83) represents the potential due to ground velocity $\dot{X}_g(\theta,t)$ (impulsive rigid solution), the second part represents the potential due to sloshing (convective solution) and the third part represents the potential due to relative wall velocity $\dot{u}_r(z,\theta,t)$ (impulsive flexible solution). Every term of Eq. (2.83) must satisfy two homogeneous and one non-homogeneous boundary condition, resulting in the following three sets:

$$\varphi_1: \quad \left.\frac{\partial \varphi_1}{\partial z}\right|_{z=0} = 0, \quad \left.\frac{\partial \varphi_1}{\partial r}\right|_{r=R} = \dot{X}_g(\theta,t), \quad \rho_L \left.\frac{\partial \varphi_1}{\partial t}\right|_{z=H_L} = 0 \tag{2.84}$$

$$\varphi_2: \quad \left.\frac{\partial \varphi_2}{\partial z}\right|_{z=0} = 0, \quad \left.\frac{\partial \varphi_2}{\partial r}\right|_{r=R} = 0, \quad \left.\left(\frac{\partial^2 \varphi_2}{\partial t^2} + g\frac{\partial \varphi_2}{\partial z} + g\frac{\partial \varphi_1}{\partial z}\right)\right|_{z=H_L} = 0 \tag{2.85}$$

$$\varphi_3: \quad \left.\frac{\partial \varphi_3}{\partial z}\right|_{z=0} = 0, \quad \left.\frac{\partial \varphi_3}{\partial r}\right|_{r=R} = \dot{u}_r(z,\theta,t), \quad \rho_L \left.\frac{\partial \varphi_3}{\partial t}\right|_{z=H_L} = 0 \tag{2.86}$$

Solution for potential φ_1

The solution of Eq. (2.79) with the boundary conditions defined in Eq. (2.84) is given by Habenberger (2001):

$$\varphi_1(r,z,\theta,t) = 2\sum_{i=1}^{\infty} \frac{(-1)^{i+1}\, I_1(a_i\, r)}{H_L\, {a_i}^2\, {I_1}'(a_i\, R)} \cos(a_i\, z)\cos(\theta)\, \dot{X}_g(t) \tag{2.87}$$

where $a_i = \pi(2\,i-1)/(2\,H_L)$. The linearized Bernoulli equation for the pressure furnishes the impulsive hydrodynamic pressure distribution as follows:

$$p_{HR}(r,z,\theta,t) = \bar{p}_{HR}(r,z)\, R\, \rho_L\, \cos(\theta)\, \ddot{X}_g(t) \tag{2.88}$$

where:

$$\bar{p}_{HR}(r,z) = -2\rho_L \sum_{i=1}^{\infty} \frac{(-1)^{i+1}\, I_1(a_i\, r)}{R\, H_L\, {a_i}^2\, {I_1}'(a_i\, R)} \cos(a_i\, z) \tag{2.89}$$

The normalized pressure distributions $\bar{p}_{HR}$ along the tank wall and base are depicted in Figure 2.11 for various slenderness ratios. The impulsive component of the liquid mass m_{HR} that moves synchronously with the rigid tank wall is given by Habenberger (2001):

$$\frac{m_{HR}}{m_L} = 2\sum_{i=1}^{\infty} \frac{(-1)^{i+1}\, I_1(a_i\, R)}{{H_L}^2\, R\, {a_i}^3 I_1'(a_i\, R)} \sin(a_i\, H_L) \tag{2.90}$$

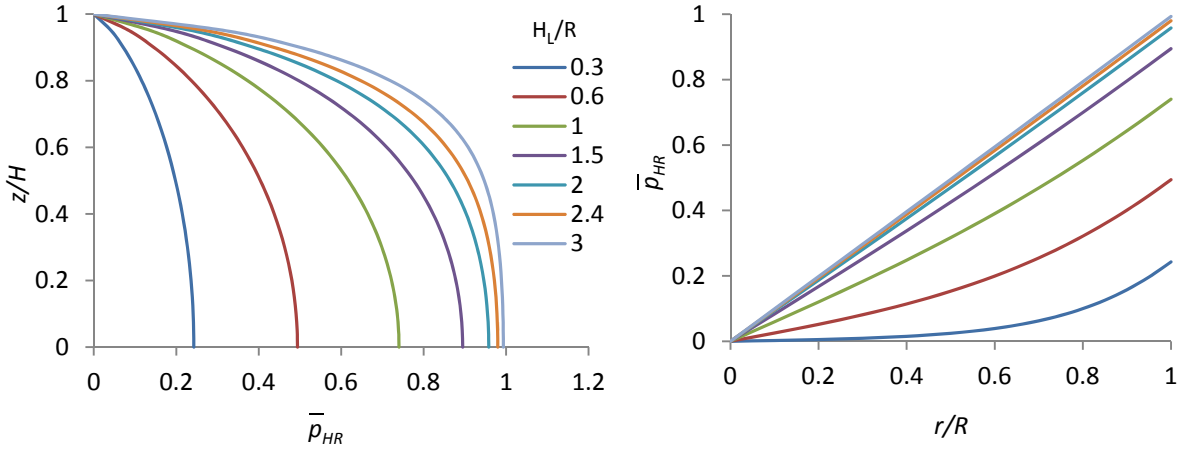

Figure 2.11: Impulsive pressure distribution along the wall (left) and over the base (right) in rigid tanks.

The height h_{HRW}, at which the impulsive component of the base shear must be applied to yield the actual value of the bending moment induced on a section of the tank immediately above the base, is calculated according to:

$$\frac{m_{HR}\, h_{HRW}}{m_L\, H_L} = 2\sum_{i=1}^{\infty} \frac{(-1)^{i+1} I_1(a_i\, R)}{{H_L}^3\, R\, {a_i}^4\, I_1'(a_i\, R)} (a_i\, H_L \sin(a_i\, H_L) + \cos(a_i\, H_L) - 1) \tag{2.91}$$

The height h_{HRP}, at which the impulsive component of the base shear must be applied to yield the actual value of the bending moment induced on the tank base, is calculated according to:

$$\frac{m_{HR}\, h_{HRP}}{m_L\, H_L} = 2\sum_{i=1}^{\infty} \frac{(-1)^{i+1}\, I_2(a_i\, R)}{{H_L}^3 {a_i}^3\, I_1'(a_i\, R)} \tag{2.92}$$

The above quantities for different slenderness ratios are presented in Figure 2.12.

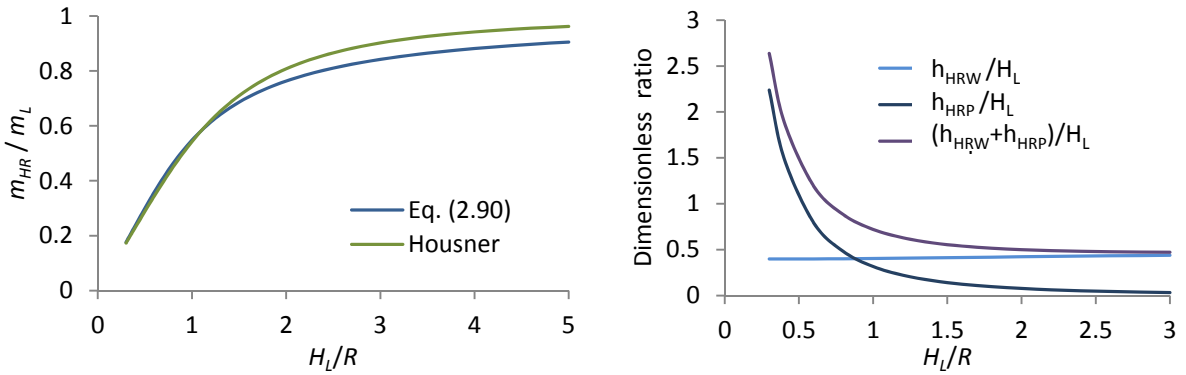

Figure 2.12: Impulsive mass (left) and equivalent heights for the overturning moments (right) in rigid tanks.

Solution for potential φ_2

The solution of Eq. (2.79) with the boundary conditions defined in Eq. (2.85) is given by Yang (1976):

$$p_{SL,n}(r,z,\theta,t) = \rho_L R\, \bar{p}_{SL,n}(r,z)\cos(\theta)\bar{S}_{a,SL,n}(t) \tag{2.93}$$

where:

$$\bar{p}_{SL,n}(r,z) = \sum_{n=1}^{\infty} \frac{2}{\lambda_n^2 - 1} \frac{J_1\left(\lambda_n \frac{r}{R}\right)}{J_1(\lambda_n)} \frac{\cosh\left(\lambda_n \frac{z}{R}\right)}{\cosh\left(\lambda_n \frac{H_L}{R}\right)} \tag{2.94}$$

and $\bar{S}_{a,SL,n}(t)$ is the pseudoacceleration of a single degree of freedom system with circular natural frequency given by Eq. (2.77). The normalized pressure distributions $\bar{p}_{SL,1}$ along the tank wall and base are depicted in Figure 2.13 for various slenderness ratios.

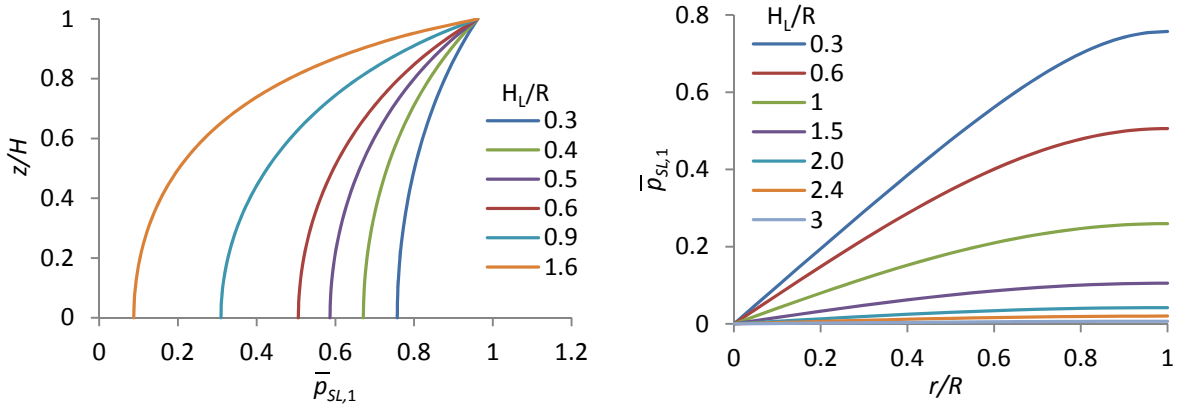

Figure 2.13: Convective pressure distribution along the wall (left) and over the base (right) in rigid tanks.

The mass of the liquid associated with the nth sloshing mode of vibration is given by:

$$\frac{m_{SL,n}}{m_L} = \sum_{n=1}^{\infty} \frac{2\,R}{(\lambda_n^2 - 1)\,\lambda_n\,H_L} \tanh\left(\lambda_n \frac{H_L}{R}\right) \tag{2.95}$$

The height $h_{SLW,n}$, at which the nth term of the convective component of the base shear must be applied to yield the actual value of the bending moment induced on a section of the tank immediately above the base, is calculated according to:

$$\frac{h_{SLW,n}}{H_L} = 1 - \frac{R}{\lambda_n\,H_L} \tanh\left(\frac{\lambda_n H_L}{2\,R}\right) \tag{2.96}$$

The height $h_{SLP,n}$, at which the nth term of the convective component of the base shear must be applied to yield the actual value of the bending moment induced on the tank base, is calculated according to:

$$\frac{h_{SLP,n}}{H_L} = \frac{1}{\lambda_n \frac{H_L}{R} \sinh\left(\lambda_n \frac{H_L}{R}\right)} \tag{2.97}$$

The above quantities for different slenderness ratios are presented in Figure 2.14.

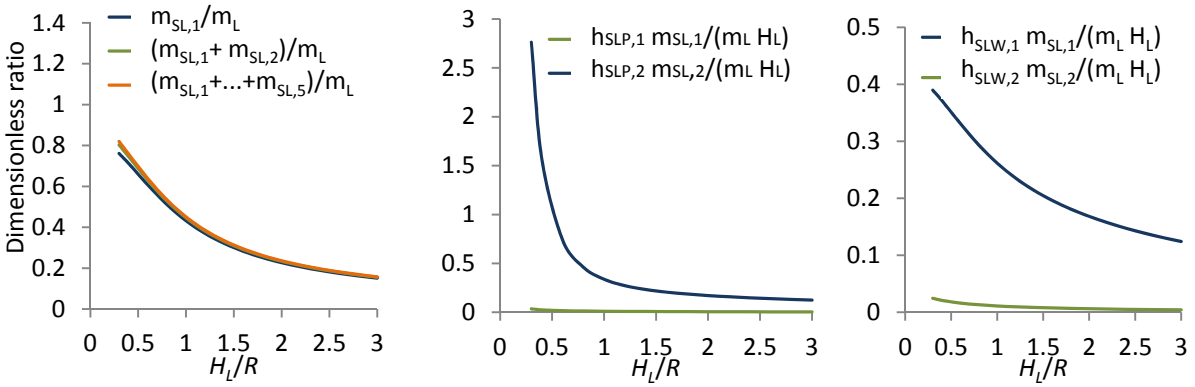

Figure 2.14: Sloshing modal quantities: (a) masses $m_{SL,n}$, (b) heights $h_{SLW,n}$, (c) heights $h_{SLP,n}$.

Solution for potential φ_3

The solution of Eq. (2.79) with the boundary conditions defined in Eq. (2.86) is given by:

$$\varphi_3(r,z,\theta,t) = 2\sum_{i=1}^{\infty} \frac{I_1(ra_i)}{H_L\, I_1'(Ra_i)\, a_i} \int_0^{H_L} \dot{u}_r(z,t)\cos(a_i z)\mathrm{dz}\ \cos(a_i z)\cos(\theta) \tag{2.98}$$

The pressure induced due to the impulsive effects is obtained by the following expression:

$$p_{HF}(r,z,\theta,t) = -2\rho_L \sum_{i=1}^{\infty} \frac{I_1(ra_i)}{H_L\, I_1'(Ra_i)\, a_i} \int_0^{H_L} \ddot{u}_r(z,t)\cos(a_i z)\mathrm{dz}\ \cos(a_i z)\cos(\theta) \tag{2.99}$$

2.2.1.2 Vertical excitation

The following boundary conditions have to be satisfied:

$$\left.\frac{\partial\varphi}{\partial z}\right|_{z=0} = \dot{Z}_g(t) \tag{2.100}$$

$$\left.\frac{\partial\varphi}{\partial r}\right|_{r=R} = \dot{u}_r(z,t) \tag{2.101}$$

$$\rho_L \left.\frac{\partial\varphi}{\partial t}\right|_{z=H_L} = 0 \tag{2.102}$$

The solution to Eq. (2.79) is given by the following expression:

$$\varphi(r,z,t) = 2\sum_{i=1}^{\infty} \frac{I_0(ra_i)\cos(a_i z)}{H_L\, I_1(Ra_i)\, a_i} \int_0^{H_L} \dot{u}_r(z,t)\cos(a_i z)\mathrm{dz}\ + (z-H_L)\dot{Z}_g(t) \tag{2.103}$$

The first term in Eq. (2.103) defines the flow field in a tank with flexible wall, whereas the second term stands for the flow field in a tank with rigid wall. The pressure function is given by:

$$p_V(r,z,t) = -2\rho_L \sum_{i=1}^{\infty} \frac{I_0(ra_i)\cos(a_i z)}{H_L\, I_1(Ra_i)\, a_i} \int_0^{H_L} \ddot{u}_r(z,t)\, \cos(a_i z)\mathrm{d}z \; - \rho_L (z - H_L)\ddot{Z}_g(t) \tag{2.104}$$

2.2.2 Response to ground motion-Effective earthquake forces

2.2.2.1 Horizontal excitation

The external forces acting on the tank due to a horizontal excitation $\ddot{X}_g(t)$ include the distributed inertia force of the shell and the hydrodynamic pressures applied on the tank wall regarded as rigid. In order to establish the matrix differential equation of motion, the virtual work δW_H done by the aforementioned forces for an arbitrary virtual displacement $\delta\mathbf{u}^s$ is evaluated. This work is equal to:

$$\delta W_H = -\int_0^H \int_0^{2\pi} \rho_s\, h\, \ddot{X}_g^r(t)\delta u_r \cos(\theta) R\, \mathrm{d}\theta\mathrm{d}z - \int_0^H \int_0^{2\pi} \rho_s\, h\, \ddot{X}_g^\theta(t)\delta u_\theta \sin(\theta) R\, \mathrm{d}\theta\mathrm{d}z + \int_0^{H_L} \int_0^{2\pi} p_{HR}(R,z,\theta,t)\, \delta u_r \cos(\theta) R\, \mathrm{d}\theta\mathrm{d}z \tag{2.105}$$

where $\ddot{X}_g^r$ and $\ddot{X}_g^\theta$ are the ground accelerations in cylindrical coordinates. Substitution of Eq. (2.88) in Eq. (2.105) and integration over the circumference yields:

$$\delta W_H = -\left[\rho_s\, h\, \pi\, R \int_0^H (\delta u_r - \delta u_\theta)\, \mathrm{d}z + \sum_{i=1}^{\infty} E_{i1} \int_0^{H_L} \delta u_r \cos(a_i z)\mathrm{d}z\right] \ddot{X}_g(t) \tag{2.106}$$

where E_{i1} is given in Appendix A. The discretized form of Eq. (2.106) is written as follows:

$$\delta W_H = -\left[\rho_s\, h\, \pi\, R \sum_{e=1}^{EZ} (\, \delta\mathbf{u}_e^s\, \mathbf{X}_e)^{\mathrm{T}} + \sum_{i=1}^{\infty} \sum_{e=1}^{EZL} E_{i1} (\, \delta\mathbf{u}_e^s\, \mathbf{T}_{ie})^{\mathrm{T}}\right] \ddot{X}_g(t) \tag{2.107}$$

where $\mathbf{X}_e$ and $\mathbf{T}_{ie}$ are vectors given in Appendix A. In vectorial form we can write:

$$\delta W_H = -\left[\begin{Bmatrix}\delta\mathbf{q}_w^s \\ \delta\mathbf{q}_d^s\end{Bmatrix}^{\mathrm{T}} \begin{Bmatrix}\mathbf{F}_{w1}^1 \\ \mathbf{F}_d^1\end{Bmatrix} + \begin{Bmatrix}\delta\mathbf{q}_w^s \\ \delta\mathbf{q}_d^s\end{Bmatrix}^{\mathrm{T}} \begin{Bmatrix}\mathbf{F}_{w2}^1 \\ \mathbf{0}\end{Bmatrix}\right] \ddot{X}_g(t) = -\delta\mathbf{q}^{s\mathrm{T}} \mathbf{F}_1\, \ddot{X}_g(t) \tag{2.108}$$

2.2.2.2 Vertical excitation

The virtual work δW_V done by the external forces acting on the tank due to a vertical excitation $\ddot{Z}_g(t)$ is equal to:

$$\delta W_V = -\int_0^H \int_0^{2\pi} \rho_s\, h\, \ddot{Z}_g(t)\delta u_z\, R\, \mathrm{d}\theta\mathrm{d}z + \int_0^{H_L} \int_0^{2\pi} p_{VR}(z,t)\, \delta u_r\, R\, \mathrm{d}\theta\mathrm{d}z \tag{2.109}$$

where p_{VR} stands for the pressure exerted in a rigid tank. Substitution of the second term of Eq. (2.104) in Eq. (2.109) and integration over the circumference yields:

$$\delta W_V = -2\,\pi\,R\left[\rho_s\,h\sum_{e=1}^{EZ}(\,\delta\mathbf{u}_e^s\,\mathbf{Q}_e)^{\mathrm{T}} + \rho_L H_L\sum_{e=1}^{EZL}(\,\delta\mathbf{u}_e^s\,\mathbf{J}_e)^{\mathrm{T}}\right]\ddot{Z}_g(t) \tag{2.110}$$

where $\mathbf{Q}_e$ and $\mathbf{J}_e$ are vectors given in Appendix A. The vectorial form of Eq. (2.110) is:

$$\delta W_V = -\left[\begin{Bmatrix}\delta\mathbf{q}_w^s\\ \delta\mathbf{q}_d^s\end{Bmatrix}^{\mathrm{T}}\begin{Bmatrix}\mathbf{F}_{w1}^0\\ \mathbf{F}_d^0\end{Bmatrix} + \begin{Bmatrix}\delta\mathbf{q}_w^s\\ \delta\mathbf{q}_d^s\end{Bmatrix}^{\mathrm{T}}\begin{Bmatrix}\mathbf{F}_{w2}^0\\ \mathbf{0}\end{Bmatrix}\right]\ddot{Z}_g(t) = -\delta\mathbf{q}^{s\,\mathrm{T}}\mathbf{F}_0\,\ddot{Z}_g(t) \tag{2.111}$$

2.2.2.3 Modal expansion

Application of Hamilton's principle in Eq. (2.63) furnishes two independent matrix equations of motion for the forced vibration of the tank-liquid system:

$$\mathbf{M}_0\,\ddot{\mathbf{q}}_0 + \mathbf{K}_0\,\mathbf{q}_0 = -\mathbf{F}_0\,\ddot{Z}_g \tag{2.112}$$

$$\mathbf{M}_1\,\ddot{\mathbf{q}}_1 + \mathbf{K}_1\,\mathbf{q}_1 = -\mathbf{F}_1\,\ddot{X}_g \tag{2.113}$$

The determination of the natural frequencies and eigenmodes of the tank-liquid system provides the option to transform Eq. (2.112) and (2.113) into two sets of uncoupled equations in modal coordinates. Hence, a simultaneous solution of coupled differential equations of motion can be skipped. The modal expansion of the generalized displacements $\mathbf{q}$ results to a set of N independent equations in modal coordinates $\eta_{m,n}(t), m = 0{,}1$ as unknowns. These equations, including the system's damping, are written as:

$$\ddot{\eta}_{0,n} + 2\,\xi_{0,n}\,\omega_{1,n}\,\dot{\eta}_{0,n} + \omega_{0,n}^2\,\eta_{0,n} = -\Gamma_{0,n}\,\ddot{Z}_g \tag{2.114}$$

$$\ddot{\eta}_{1,n} + 2\,\xi_{1,n}\,\omega_{1,n}\,\dot{\eta}_{1,n} + \omega_{1,n}^2\,\eta_{1,n} = -\Gamma_{1,n}\,\ddot{X}_g \tag{2.115}$$

where $\xi_{0,n}$ and $\xi_{1,n}$ are the damping ratios of each mode n corresponding to the horizontal and vertical excitation respectively. The quantities $\Gamma_{0,n}$ and $\Gamma_{1,n}$ are the modal participation factors of the mode n corresponding to the horizontal and vertical excitation respectively. The latter depend on how each mode is normalized and can be computed according to the following expression:

$$\Gamma_{m,n} = \frac{\boldsymbol{\psi}_{m,n}^{\mathrm{T}}\mathbf{F}_m}{\boldsymbol{\psi}_{m,n}^{\mathrm{T}}\,\mathbf{M}_m\,\boldsymbol{\psi}_{m,n}} \tag{2.116}$$

where $\boldsymbol{\psi}_{m,n}$ is the eigenmode vector. Combing the response contributions of all modes the total response is given:

$$\mathbf{q}_0 = \sum_{n=1}^{N}\Gamma_{0,n}\boldsymbol{\psi}_{0,n}\,\bar{S}_{a,z,n}^{abs.}(t) \tag{2.117}$$

$$\mathbf{q}_1 = \sum_{n=1}^{N}\Gamma_{1,n}\boldsymbol{\psi}_{1,n}\,\bar{S}_{a,x,n}^{abs.}(t) \tag{2.118}$$

where $\bar{S}_{a,z,n}^{abs.}(t)$ and $\bar{S}_{a,x,n}^{abs.}(t)$ represent the vertical and horizontal absolute pseudoacceleration responses respectively, associated with the nth mode of the system's vibration. The pressures induced by the impulsive effects of the flexible walls of the tank due to contribution of mode n during vertical and horizontal ground shaking can be obtained by inserting the nth summand of Eq. (2.117) and Eq. (2.118) into the first term of Eq. (2.104) and into Eq. (2.99) respectively. They are associated with relative values for the acceleration:

$$p_{0,n}(r,z,t) = \rho_L H_L \ \bar{p}_{0,n}(r,z)\, \bar{S}_{a,z,n}^{rel.}(t) \tag{2.119}$$

$$p_{1,n}(r,z,\theta,t) = \rho_L R \ \bar{p}_{1,n}(r,z)\, \bar{S}_{a,x,n}^{rel.}(t)\cos(\theta) \tag{2.120}$$

where:

$$\bar{p}_{0,n}(r,z,t) = 2\sum_{i=1}^{\infty} \frac{I_0(ra_i)}{H_L^2\, I_1(Ra_i)\, a_i} \int_0^{H_L} \psi_{r0,n}(\mathrm{z})\, \cos(a_i z)\mathrm{dz}\, \cos(a_i z)\, \Gamma_{0,n} \tag{2.121}$$

$$\bar{p}_{1,n}(r,z,\theta,t) = 2\sum_{i=1}^{\infty} \frac{I_1(ra_i)}{R\, H_L\, I_1'(Ra_i)\, a_i} \int_0^{H_L} \psi_{r1,n}\, \cos(a_i z)\mathrm{dz}\ \cos(a_i z)\, \Gamma_{1,n} \tag{2.122}$$

The normalized pressure distribution along the tank wall associated with the fundamental axial mode and 0th circumferential mode for typical fully filled steel tanks is shown in Figure 2.15. It is evident that the formula proposed in EC8 (2006) overestimates the pressure distribution of slender tanks. The influence of the tanks thickness on the wall pressure distribution is depicted in Figure 2.16. It can be stated that the pressure distribution of typical thin-walled steel tanks is practically independent of the wall thickness. The natural circular frequencies $\omega_{0,1}$ for different proportions of tanks are presented in Figure 2.17 by means of the dimensionless factor $C_{0,n}$ according to:

$$\omega_{0,n} = \frac{C_{0,n}}{R}\sqrt{\frac{E}{\rho}} \tag{2.123}$$

The normalized wall pressure distribution associated with higher axial modes and 0th circumferential mode for a typical fully filled steel tank is presented in Figure 2.18. It can be observed that the pressure amplitudes of higher axial eigenmodes are minor compared with the corresponding ones associated with the first mode. The normalized pressure distribution along the tank wall associated with the fundamental axial mode and 1st circumferential mode for typical fully filled steel tanks is shown in Figure 2.19.

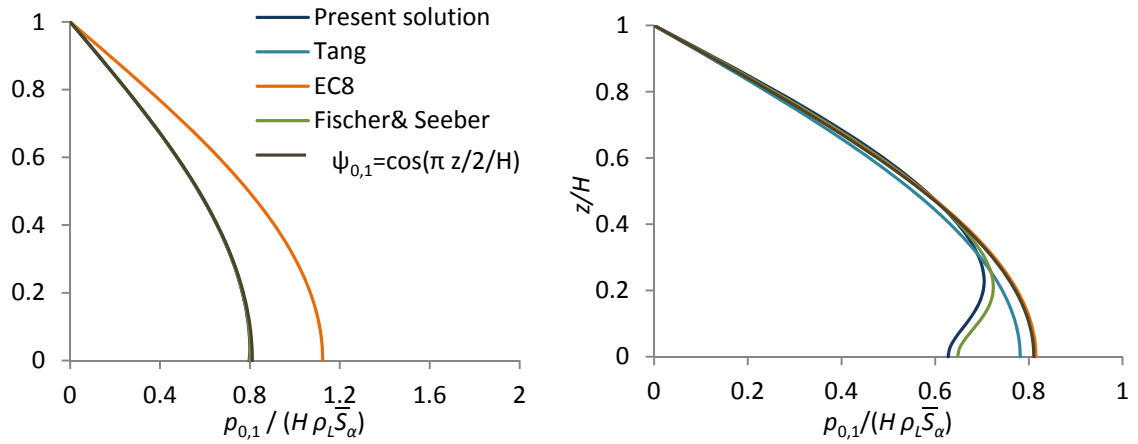

Figure 2.15: Wall pressure distribution, 0th circumferential mode and 1st axial mode, $H/R = 3, R/h = 1000$ (left) and $H/R = 0.3, R/h = 1000$ (right).

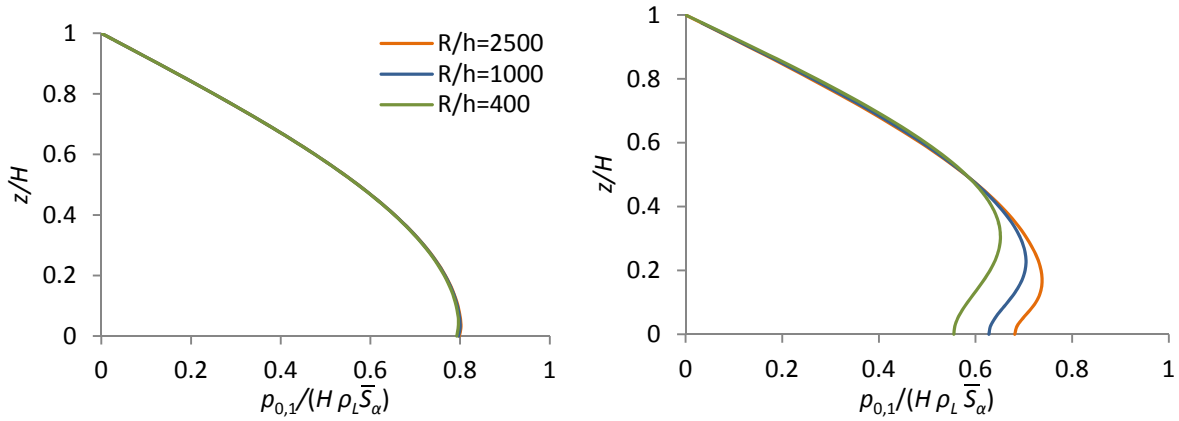

Figure 2.16: Wall pressure distribution, 0th circumferential mode and 1st axial mode, $H/R = 3$ (left) and $H/R = 0.3$ (right).

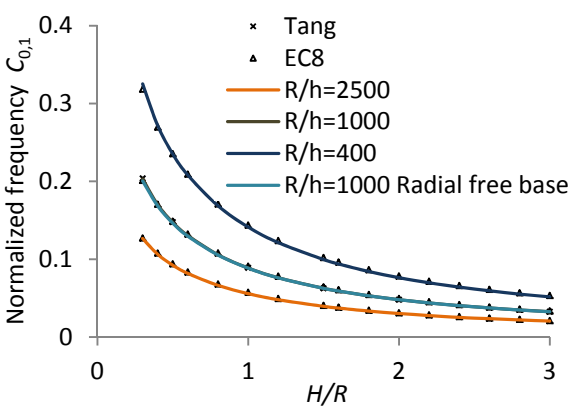

Figure 2.17: Dimensionless frequency factor $C_{0,1}$, 0th circumferential mode and 1st axial mode.

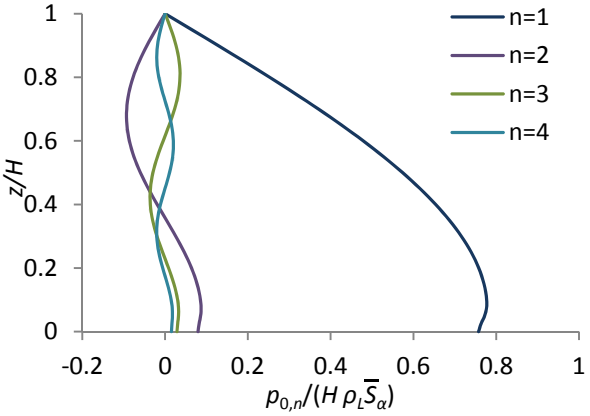

Figure 2.18: Wall pressure distribution, 0th circumferential and nth axial mode, $H/R = 3$, $R/h = 1000$.

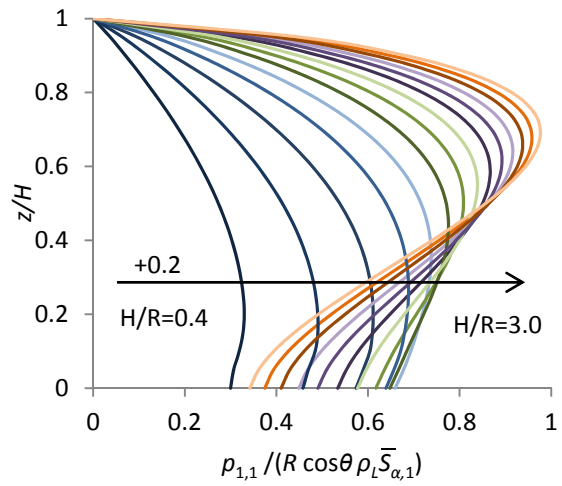

Figure 2.19: Wall pressure distribution, $R/h = 1000$, 1st circumferential and axial mode.

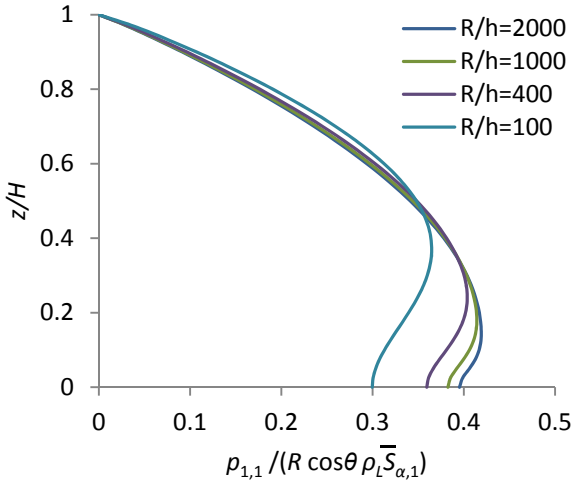

Figure 2.20: Wall pressure distribution, $H/R = 0.5$, 1st circumferential and axial mode.

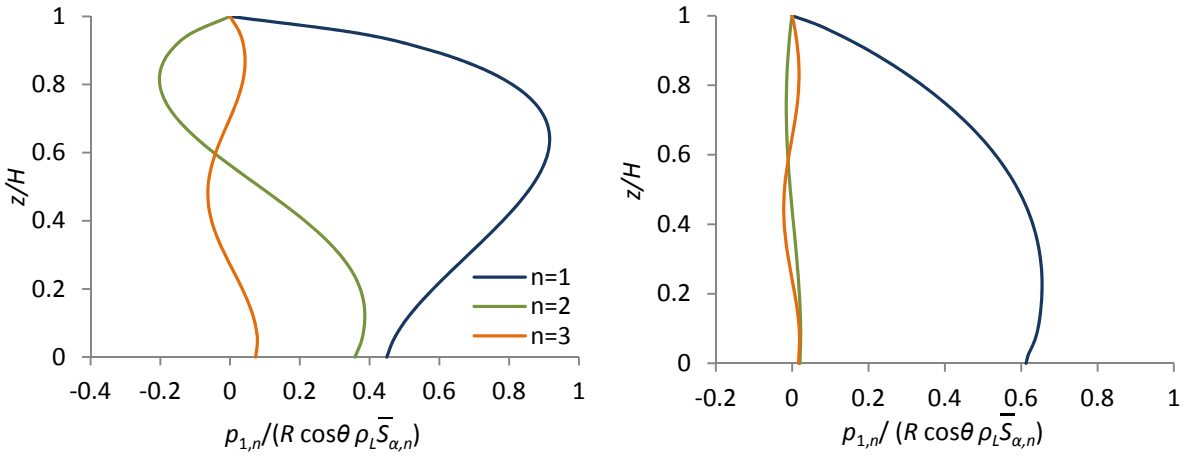

Figure 2.21: Wall pressure distribution, 1st circumferential mode, *n*th axial mode, $H/R = 2.4$, $R/h = 1000$ (left) and $H/R = 0.9, R/h = 1000$ (right).

The influence of the tanks thickness on the wall pressure distribution is depicted in Figure 2.20. Similarly to the 0th circumferential mode, the wall thickness effect becomes significant only for concrete tanks ($R/h < 400$). The contribution of higher axial eigenmodes to the tank response in terms of wall pressure distribution is depicted in Figure 2.21. Contrary to the 0th circumferential mode, the beam-like higher modes contribute considerably to the overall response of slender tanks. The natural circular frequencies $\omega_{1,n}$ for different proportions of tanks are presented in Figure 2.22 by means of the dimensionless factor $C_{1,n}$ according to:

$$\omega_{1,n} = \frac{C_{1,n}}{H}\sqrt{\frac{E}{\rho}} \tag{2.124}$$

2.2.3 Effective modal mass and modal heights

2.2.3.1 Horizontal excitation

The main aim of the dynamic analysis of liquid-filled tanks is the evaluation of the base shear and moments induced by the ground motion. The component of the instantaneous value of the base shear for the nth natural mode of the tank-liquid system $Q_{1,n}$ consists of three parts: The first due to the hydrodynamic pressure exerted on the tank as if that was rigid. The second due to the hydrodynamic pressure corresponding to the nth natural mode of the flexible wall-liquid system. The third due to the inertia force of the tank wall. It is calculated according to the following expression:

$$Q_{1,n}(t) = \int_0^{H_L}\int_0^{2\pi} \left[p_{HR}(R,z,\theta,t) + p_{1,n}(R,z,\theta,t)\right]\cos(\theta)R \, \mathrm{d}\theta\mathrm{d}z + \int_0^{H}\int_0^{2\pi} \rho_s \, h\left[\, \ddot{u}_{r,n}(z,t,\theta)\cos(\theta) - \ddot{u}_{\theta,n}(z,t,\theta)\, \sin(\theta)\right] R \, \mathrm{d}\theta\mathrm{d}z \tag{2.125}$$

By neglecting the inertia force of the tank wall, which is admissible for typical steel tanks, Eq. (2.125) can be written as:

$$Q_{1,n}(t) \; = m_{HR}\ddot{X}_g(t) \; + m_{1,n}\bar{S}^{rel.}_{a,x,n}(t) \tag{2.126}$$

where $m_{1,n}$ represents the nth modal mass of the tank-liquid system for the 1st circumferential mode. Values of $m_{1,n}$ as function of the slenderness ratio are shown in Figure 2.23a. Combing the response contributions of all modes, as Eq. (2.118) implies, the total base shear due to the impulsive effects is given by:

$$Q_H(t) = \sum_{n=1}^{N} m_{1,n}\bar{S}^{abs.}_{a,x,n}(t) \tag{2.127}$$

since the portion of the liquid mass rigidly attached to the tank m_{HR} is equal to the sum of all modal masses which move in unison with the tank wall. The hydrodynamic moment $M_{1,n}(t)$ for the nth natural mode and the total $M_H(t)$ induced on a section of the tank immediately above the base can be determined from the following formulas:

$$M_{1,n}(t) = \int_0^{H_L}\int_0^{2\pi} p_{1,n}(R,z,\theta,t)\; z\, \cos(\theta)R \, \mathrm{d}\theta\mathrm{d}z \tag{2.128}$$

$$M_H(t) = \sum_{n=1}^{N} m_{1,n}\, h_{1,n}\, \bar{S}^{abs.}_{a,x,n}(t) \tag{2.129}$$

where $h_{1,n}$ stands for the height at which the nth modal mass of the 1st circumferential mode must be lumped to yield the moment $M_{1,n}$.

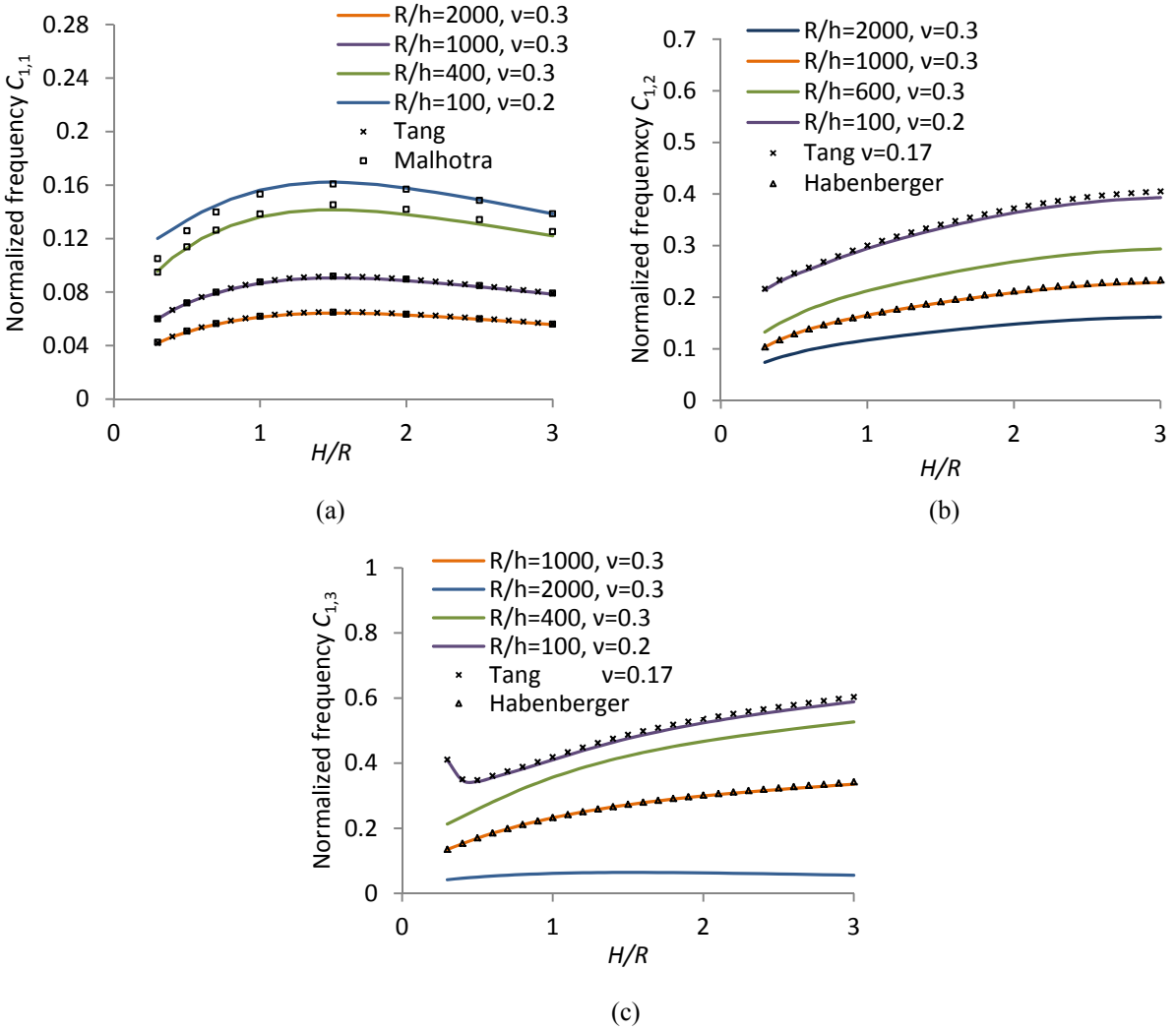

Figure 2.22: Dimensionless frequency factor $C_{1,n}$, 1st circumferential mode, (a) 1st axial mode, (b) 2nd axial mode, (c) 3rd axial mode.

This moment in conjunction with ordinary beam theory is used to evaluate the axial stresses at the base of the tank wall. Values of $h_{1,n}$ as function of the slenderness ratio are shown in Figure 2.23c. The moment $\Delta M_{1,n}(\mathrm{t})$ corresponding to the nth natural mode and the total $\Delta M_H(\mathrm{t})$ induced on the tank base by the pressure can be calculated according to:

$$\Delta M_{1,n}(t) = \int_0^{2\pi}\int_0^{R} p_{1,n}(r, z=0, \theta, t)\, r^2 \cos(\theta)\, \mathrm{dr d\theta} \tag{2.130}$$

$$\Delta M_H(\mathrm{t}) = \sum_{n=1}^{N} m_{1,n}\, \Delta h_{1,n}\, \bar{S}^{abs.}_{a,x,n}(t) \tag{2.131}$$

where $\Delta h_{1,n}$ stands for the height at which the nth modal mass of the 1st circumferential mode must be lumped to yield the moment $\Delta M_{1,n}$. The total moment used for the design of the foundation is given by:

$$MM_H(t) = \sum_{n=1}^{N} m_{1,n}\, h'_{1,n}\, \bar{S}^{abs.}_{a,x,n}(t) = M_H(\mathrm{t}) + \Delta M_H(\mathrm{t}) \tag{2.132}$$

where $h'_{1,n}$ stands for the height at which the nth modal mass of the 1st circumferential mode must be lumped to yield the moment $MM_{1,n} = M_{1,n} + \Delta M_{1,n}$. Values of $h'_{1,n}$ as function of the slenderness ratio are shown in Figure 2.23d.

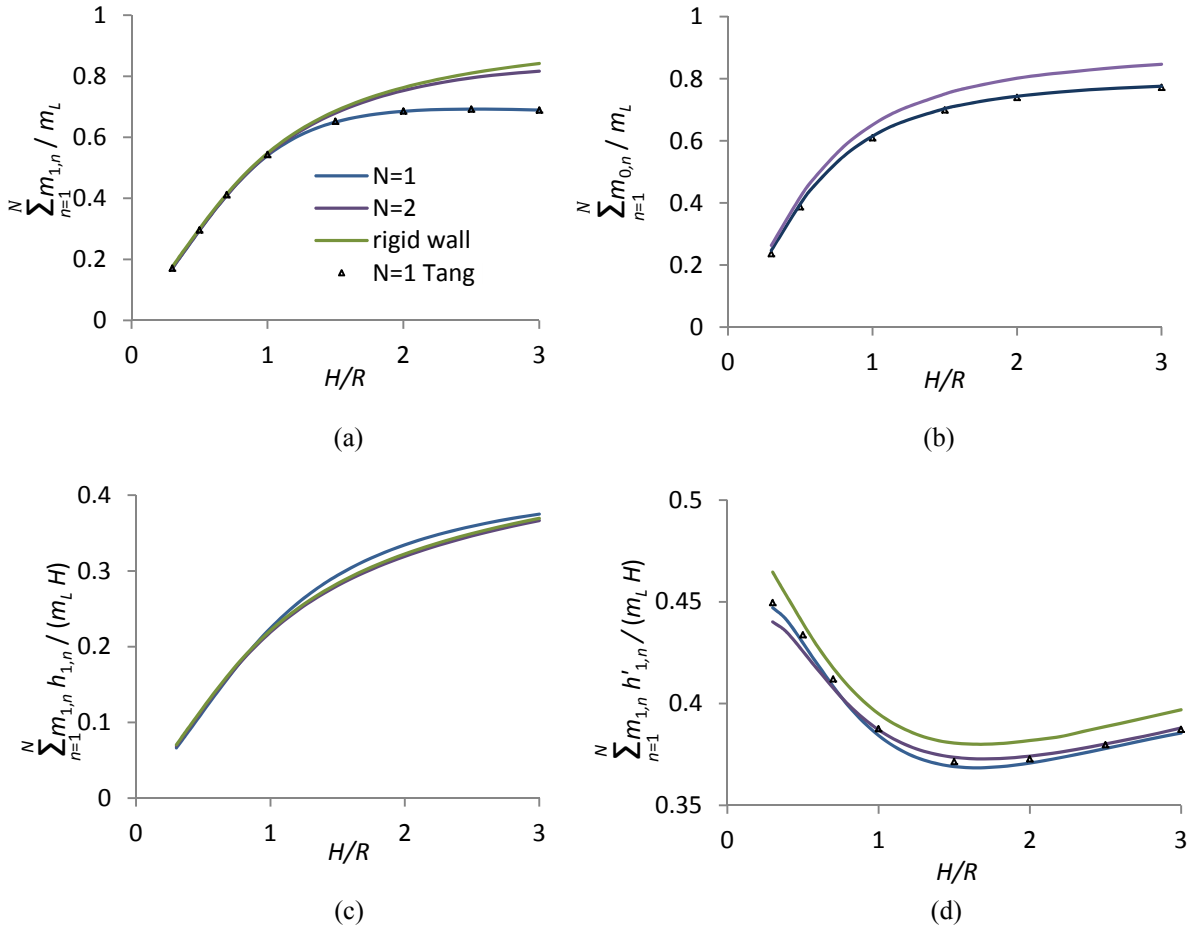

Figure 2.23: (a) Normalized modal masses, 1st circumferential mode, (b) normalized modal masses, 0th circumferential mode, (c) normalized equivalent heights for moments above the tank base, (d) normalized equivalent heights for moments induced on the tank base.

2.2.3.2 Vertical excitation

Since the vertical excitation produces axisymmetric vibration, no moments are generated on the base of the tank. Disregarding the inertia force of the tank wall, the component of the instantaneous value of the base shear for the nth natural mode of the tank-liquid system $Q_{0,n}$ is given by:

$$Q_{0,n}(t) = \int_0^R \int_0^{2\pi} \left[p_{VR}(z=0,t) + p_{0,n}(r,z=0,t)\right] r \, \mathrm{d}\theta \mathrm{d}r \tag{2.133}$$

or equivalently:

$$Q_{0,n}(t) = m_L \ddot{Z}_g(t) + m_{0,n} \bar{S}^{rel.}_{a,z,n}(t) \tag{2.134}$$

where $m_{0,n}$ represents the nth modal mass of the tank-liquid system for the 0th circumferential mode. Values of $m_{0,n}$ as function of the slenderness ratio are shown in Figure 2.23b. Taking into account the contribution of all modes, we obtain the total base shear:

$$Q_V(\mathrm{t}) = m_{VR}\ddot{Z}_g(t) + \sum_{n=1}^{N} m_{0,n}\bar{S}_{a,z,n}^{abs.}(t) \tag{2.135}$$

where $m_{VR} = m_L - \sum_{n=1}^{N} m_{0,n}$.

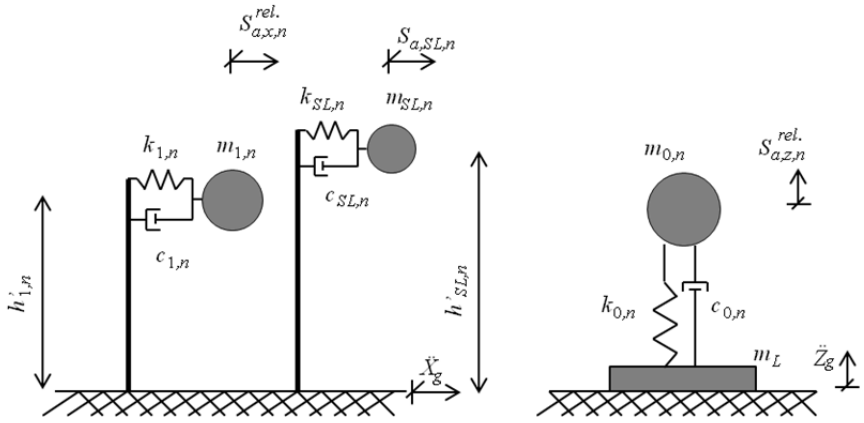

Figure 2.24: Models for rigidly supported tanks, horizontal excitation (left), vertical excitation (right).

Having derived the equations for the computation of shear forces and moments in each direction of excitation, a visual perception of the modal masses for the sloshing and wall-liquid motions comes out naturally (Figure 2.24). The affinity of these models with those used for the analysis of conventional buildings in structural dynamics is evident. By inspection, one may confirm that the tank-liquid models presented in Figure 2.24 correspond to the equations of motion expressed from Eq. (2.114) and (2.115).

2.2.4 Design provisions according to EC8

2.2.4.1 Iteration scheme for the antisymmetric vibration

The iteration scheme for the determination of the fundamental eigenmode and corresponding pressures exerted on cylindrical above-ground liquid storage tanks for the antisymmetric vibration ($m = 1$) was first proposed by Fischer and Rammerstorfer (1982) and was included in the current standard provisions-EC8 (2006). The method consists of an initial assumption of the first radial eigenmode, which is used to estimate the normalized dynamic impulsive pressure, the latter being subsequently transformed to an equivalent density distributed over the height of the shell. This density, together with the material density of the shell, is ascribed to the “dry” shell and the eigenvalue problem is

solved resulting to a new eigenmode, which is used for an improved assumption of the deformation figure. The iteration process is continued until two successive radial eigenmodes are practically the same. In our study, we use the convergence criterion defined by:

$$\frac{1}{\mathrm{EZL}}\sum_{k=1}^{\mathrm{EZL}}\left|\psi_{r1,1}^{i}(z_k)-\psi_{r1,1}^{i-1}(z_k)\right| \le \delta_{converg.} \tag{2.136}$$

where $\psi_{r1,1}^{i}(z_k)$ is the normalized first radial eigenmode at the iteration step *i,* at height z_k. In all analyses we set $\delta_{converg.} = 0.001$. The following equations for the assessment of the additional mass matrix should be regarded as part of an arbitrary iteration step *i*. This matrix stands for the effect of the impulsive fluid pressure activated by the relative shell motion associated with the first antisymmetric mode. All analyses are conducted for a fully filled tanks, namely $H = H_L$.

The resultant of the pressure distribution per unit length in the axial direction is obtained by:

$$R_{1,1}(z,t) = \int_0^{2\pi} p_{1,1}(R,z,\theta,t)\cos(\theta)\,R\,\mathrm{d}\theta \tag{2.137}$$

The first modal radial acceleration maximum value is:

$$\ddot{u}_{r1,1}(z,t) = \psi_{r1,1}(z)\,\Gamma_{1,1}\,\bar{S}_{a,x,1}^{rel.}(t) \tag{2.138}$$

The mass that is attached to the shell at height *z* experiences the same acceleration as the shell itself is determined by:

$$m_{1,1}(\mathrm{z}) = \frac{R_{1,1}(z,t)}{\ddot{u}_{r1,1}(z,t)} = \frac{\pi\,R^2\,\rho_L\,\bar{p}_{1,1}(R,z)}{\psi_{r1,1}(z)\,\Gamma_{1,1}} \tag{2.139}$$

Accordingly, every element of the finite model of the shell which belongs to the liquid-covered area is attributed with a virtual additional mass density $\rho_{1,1_e}(z)$, which can be expressed as:

$$\rho_{1,1_e}(z) = \frac{R\,\rho_L\left[\bar{p}_{1,1}(R,z_k)+\bar{p}_{1,1}\left(R,z_j\right)\right]}{2\,h\,\left[\psi_{r1,1}(z_k)+\psi_{r1,1}\left(z_j\right)\right]\Gamma_{1,1}} \tag{2.140}$$

in which the quantities in brackets represent nodal values. The kinetic energy associated with the virtual density $\rho_{1,1}$ is given by:

$$T = \frac{1}{2}\int_0^{H_L}\int_0^{2\pi} \dot{\mathbf{u}}^{s\mathrm{T}}\,\rho_{1,1}\,h\,\dot{\mathbf{u}}^{s}\;R\mathrm{d}\theta\mathrm{d}z \tag{2.141}$$

The additional element consistent mass matrix $\mathbf{M}_A$ is obtained by inserting Eq. (2.140) into the discretized form of Eq. (2.141):

$$T = \frac{1}{2}\sum_{e=1}^{\mathrm{EZL}} \dot{\mathbf{u}}_e^{s\mathrm{T}}\,\mathbf{M}_e^{w}\,\dot{\mathbf{u}}_e^{s} = \frac{1}{2}\dot{\mathbf{q}}^{s\mathrm{T}}\,\mathbf{M}_A\,\dot{\mathbf{q}}^{s} \tag{2.142}$$

where $\mathbf{M}_A = \sum_{e=1}^{\mathrm{EZL}}\mathbf{M}_e^{w}$ and $\mathbf{M}_e^{w} = \pi\,R\,h\,\rho_{1,1_e}\int_{\mathbf{0}}^{L_e}\mathbf{N}^{s\mathrm{T}}\mathbf{N}^{s}\,\mathrm{d}\bar{z}$. Finally, the following undamped free vibration equation of the system is solved:

$$\mathbf{K}_s\,\mathbf{q}^s + \mathbf{M}_s\,\ddot{\mathbf{q}}^s + \mathbf{M}_A\ddot{\mathbf{q}}^s = \mathbf{0} \tag{2.143}$$

It is evident from Eq. (2.140) that large values of the virtual density appear near the tank base for fixed-base conditions (Figure 2.25a). However, the solution of Eq. (2.143) shows that the singularity does not affect the convergence of the iteration process in case of slender tanks. On the contrary, within the frame of the iteration routine, the free vibration of broad steel tanks becomes a formidable problem, since in that case the centroid of the total mass moves towards the base and the singularity becomes dominant leading to unstable iterative steps and finally loss of convergence (Figure 2.26). This incident becomes more pronounced as the thickness ratio R/h increases due to the fact that the influence of the additional virtual density prevails against the material density. Referring to thin walled tanks, the free vibration problem cannot be generally solved if the ratio H/R is less than two; only lower values of the thickness ratio, e.g. $R/h = 800$ assure the solution for cases with smaller slenderness ratios, e.g. $H/R = 1.6$. This drawback diminishes the practicability of this method if no remedies are employed.

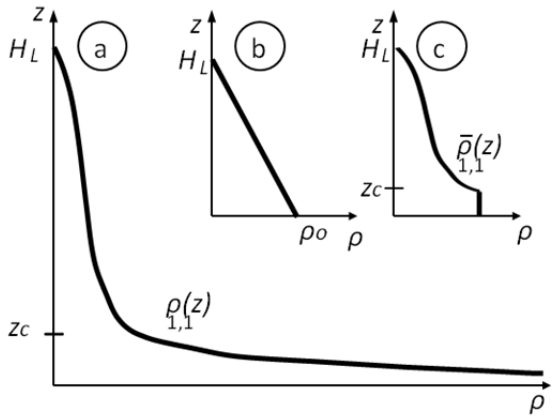

Figure 2.25: (a) Representative density distribution obtained by the iterative procedure. (b) Linear density distribution of the truncated mass according to Rayleigh's quotient. (c) Truncation of the singular density part.

2.2.4.2 Rayleigh's quotient for the coupled shell-liquid vibration

Aiming to compensate with this singularity, which has no physical meaning, the Rayleigh's quotient for the coupled shell-liquid vibration is employed. The concept is based on keeping constant the virtual mass $\rho_{1,1}$ below a specific heigt z_c (Figure 2.25c) during the iteration and distributing the cutted off portion of the mass linearly along the height of the shell (Figure 2.25b). In order to eliminate the arbirtrariness of this manipulation, the Rayleigh's quotient between the initial and the modified dynamic system is enforced to be equal and therefore the linear distributed added mass can be determined. The development of this method, assuming however that the shell is behaving as a slender

beam, was proposed by Rammerstorfer et al. (1988). In what follows, the formulation for the coupled fluid-structure vibration is derived and some novel observations are made regarding the applicability of the method for broad tanks. The implementation presented herein do not contain the approximations made by Mykoniou and Holtschoppen (2013).

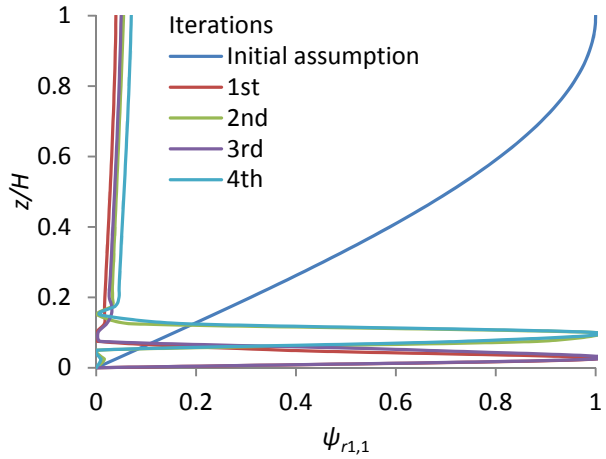

Figure 2.26: Radial eigenmodes of the iterative procedure, $H/R = 1.4$, $R/h = 1500$.

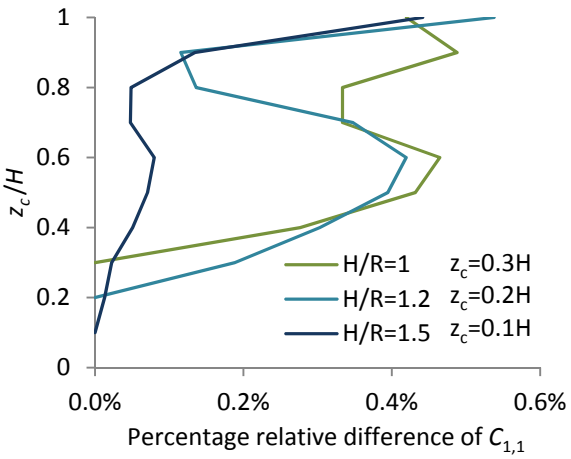

Figure 2.27: Variation of $C_{1,1}$ with z_c with respect to reference $C_{1,1}$ obtained by a minimum z_c, $H/R = 1.5$, $R/h = 1500$.

By using the orthogonality relations of wet modes obtained by Zhu (1991) and neglecting free surface waves, the Rayleigh's quotient for the coupled free vibration of a inviscid, irrotational, incompressible liquid and the cylindrical shell is formulated as follows (Zhu, 1994):

$$\omega^2 = \frac{\int_0^H \int_0^{2\pi} \mathbf{u}^s \mathbf{L}(\mathbf{u}^s) \; R\mathrm{d}\theta\mathrm{d}z}{\int_0^H \int_0^{2\pi} \mathbf{u}^{s\mathrm{T}} \, h \, \rho \, \mathbf{u}^s \; R\mathrm{d}\theta\mathrm{d}z + \rho_L \int_0^{H_L} \int_0^{2\pi} \varphi_d \frac{\partial \varphi_d}{\partial r} \; R\mathrm{d}\theta\mathrm{d}z} \tag{2.144}$$

where φ_d is the deformation potential related to the velocity potential φ by: $\varphi = \mathrm{i}\omega\varphi_d \mathrm{e}^{\mathrm{i}\omega t}$ and $\mathbf{L}$ is a differential operator described by Amabili (2000). The boundary conditions correspond to those given in Eq. (2.86). In Eq. (2.144) the first term in the numerator is twice the maximum potential energy of the structure, while the first term in the denominator stands for the kinetic energy of the structure. It is evident that the second term in the denominator of Eq. (2.144) equals twice the kinetic energy of the fluid neglecting the free surface waves, which is evaluated in Eq. (2.142).

After cutting off the density up to a dimesionless height z_c and distributing the still unknown density ρ_o linearly along the height, the Rayleigh's quotient is formulated as follows:

$$\omega^2 = \frac{\int_0^H \int_0^{2\pi} \mathbf{u}^s \mathbf{L}(\mathbf{u}^s) \; R\mathrm{d}\theta\mathrm{d}z}{\int_0^H \int_0^{2\pi} \mathbf{u}^{s\mathrm{T}} \, h \, \rho \, \mathbf{u}^s \; R\mathrm{d}\theta\mathrm{d}z + \int_0^{H_L} \int_0^{2\pi} \mathbf{u}^{s\mathrm{T}} \, h \, \left[\bar{\rho}_{1,1} + \rho_o (H_L - z)\right] \mathbf{u}^s \; R\mathrm{d}\theta\mathrm{d}z} \tag{2.145}$$

where $\bar{\rho}_{1,1} = \bar{\rho}_{1,1}(z)$ stands for the remaining virtual density after the truncation. By equating Eq. (2.144) and (2.145) and splitting the integrals at height z_c, the following equation for the density ρ_o is obtained after algebraic manipulation:

$$\rho_o = \frac{\int_0^{z_c} \Delta\rho_{1,1}(z)\left[\psi_{r1,1}(z)\right]^2 \mathrm{dz}}{\int_0^{H_L}\left[\psi_{r1,1}(z)\right]^2 (H_L - z)\mathrm{dz}} \tag{2.146}$$

where $\Delta\rho_{1,1}(z)$ stands for the truncated portion of the density. The outline of the above procedure is shown in Figure 2.28.

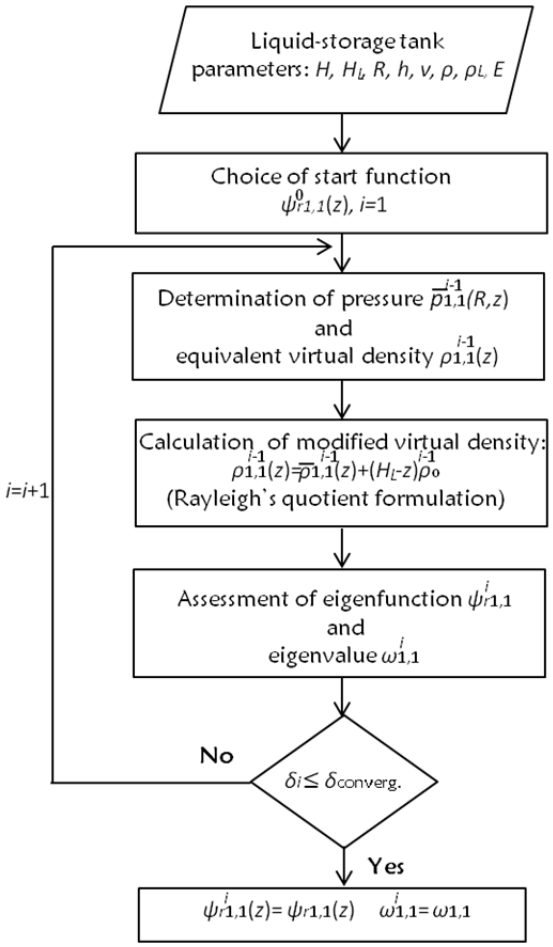

Figure 2.28: Outline scheme for the modified iteration routine.

In this study, a minimum height z_c was chosen exclusively on the basis of the criterion of convergence for the iterative procedure. This is believed to be justified as it furnishes greater values of z_c as the slenderness of the tank decreases: in this case, the singularity spreads out over a greater relative height of the liquid-covered wall due to the gradual shift to the bottom of the maximum value of deflection, especially for higher values of the ratio R/h. However, the effect of the selected values of z_c on the fundamental eigenfrequency is found to be minor as it can be seen in Figure 2.27, where the relative difference of the normalized frequency $C_{1,1}$ for different heights z_c with respect to $C_{1,1}$ for the chosen z_c is depicted. This fact indicates the accuracy of this approach. It has to be mentioned, that for broad

tanks convergence can be only ensured by sufficiently large values of z_c, which leads to spurious eigenmodes, since the distribution of the virtual mass tends to be necessarily linear along the height, a fact that violates the validity of Eq. (2.140). This approach reaches its limits for the investigated cases bounded by the ratios $H/R \leq 0.6$ and $R/h \geq 800$. Within them convergence cannot be reached independent of the choice of z_c.

In Figure 2.29 the dimensionless frequency coefficient $C_{1,1}$ is shown for various proportions of steel tanks. As it can be observed, the iteration scheme furnishes precise results for slenderness ratios $H/R \geq 3$. As the radius of the container increases towards its height, the computed fundamental eigenfrequencies progressively diverge from the corresponding values obtained with the aid of the closed-form procedure described in section 2.1. The discrepancies are also noticeable for those cases that do not include the virtual density transform according to the Rayleigh's quotient formula. For example, the relative difference of the normalized frequency $C_{1,1}$ between the two methods is 9.5% for a tank with $H/R = 1.8$ and $R/h = 1500$. Therefore, the observed deviations should not be primarily attributed to the approximation inserted in the problem by cutting off the virtual density at the lower part of the model.

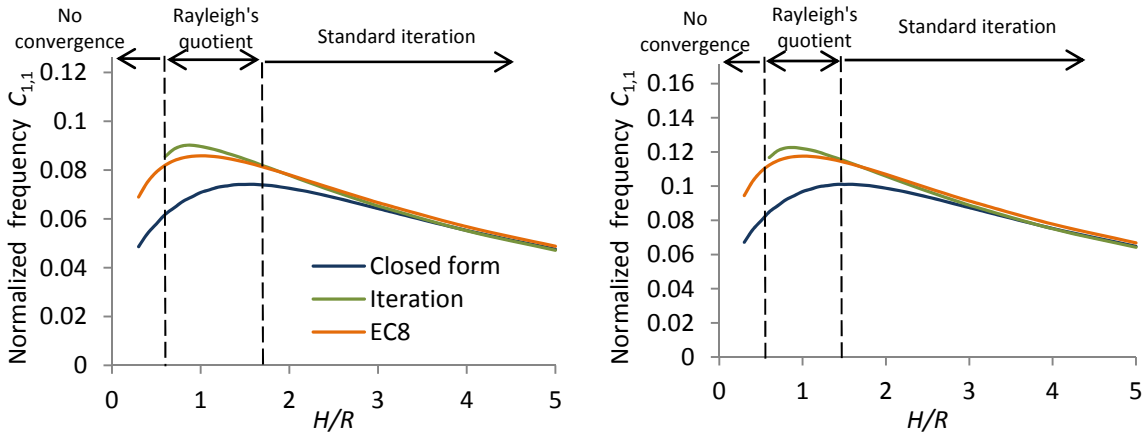

Figure 2.29: Dimensionless frequency factor $C_{1,1}$ for $R/h = 1500$ (left) and $R/h = 800$ (right).

The reason for the overestimation of the fundamental eigenfrequency by the iteration process lies in the basis on which the method is grounded: the kinetic energy of the fluid is treated analogously to the kinetic energy of the shell. This manipulation results in a fluid mass matrix which is banded whereas the fluid mass matrix $\mathbf{M}_A$ as obtained in section 2.1 possesses non-zero entries which are not confined in a diagonal (Figure 2.30). In order to gain an insight of the influence of the fluid's mass matrix non-diagonal coefficients on the eigenvalue problem, the percentage ratios of the non-diagonal to the diagonal coefficients of the fluid mass matrix corresponding to the radial nodal displacements, as calculated in section 2.1, are presented in Figure 2.31. Two steel tanks discretized with 40 elements, which differ only in the slenderness ratio, are investigated and the results are evaluated at three different heights: $z = 0.25\,H$, $z = 0.50\,H$ and $z = 0.75\,H$. Examination of the figures manifests that

the contribution of the non-diagonal entries is comparatively greater for broad tanks especially in the lower part of the model. Consequently, the ‘‘suppression’’ of those coefficients, inherent in the iteration scheme, distorts the dynamic system and leads to inaccurate eigenvectors and eigenfrequencies for broad tanks. On the contrary, the impulsive hydrodynamic pressure and moreover the modal mass and height as products of integration over the liquid-covered surface are closer to the corresponding values obtained by the closed-form method (Figure 2.32 and Figure 2.33).

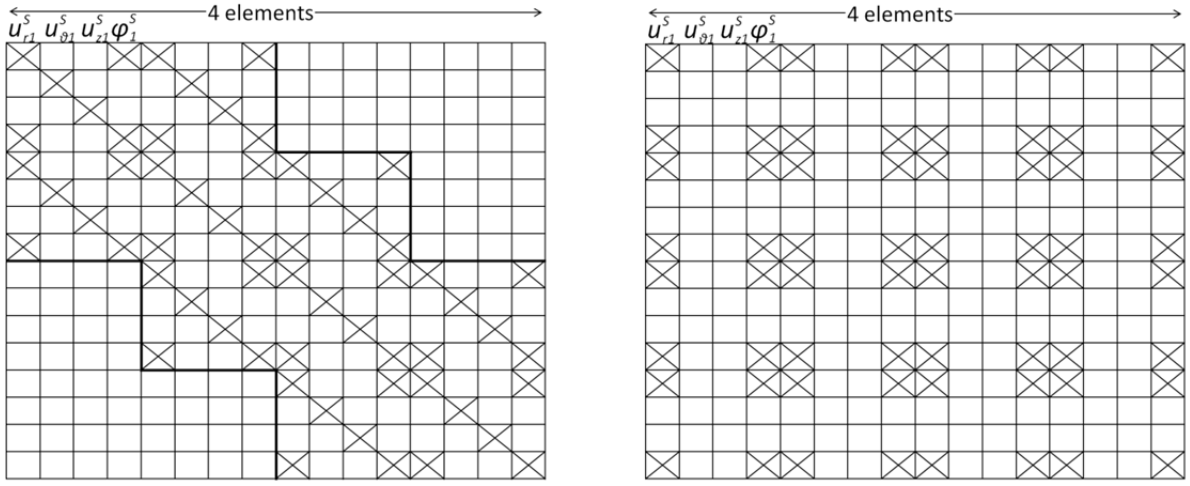

Figure 2.30: Fluid mass matrix $\mathbf{M}_A$ form of the iterative procedure (left) and according to the closed-form derivation (right).

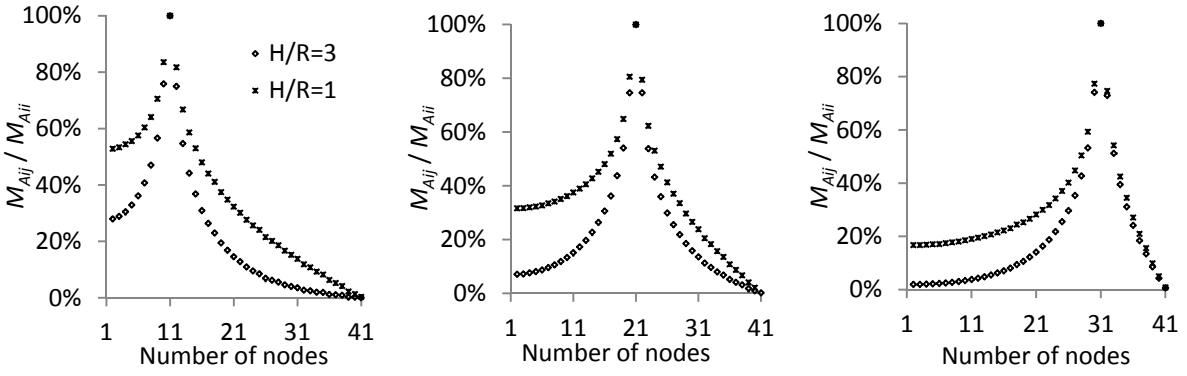

Figure 2.31: Percentage ratio of the non-diagonal to the diagonal entries of the fluid mass matrix corresponding to the radial nodal displacements evaluated at height: (a) $z = 0.25H$, (b) $z = 0.50H$, (c) $z = 0.75\,H$.

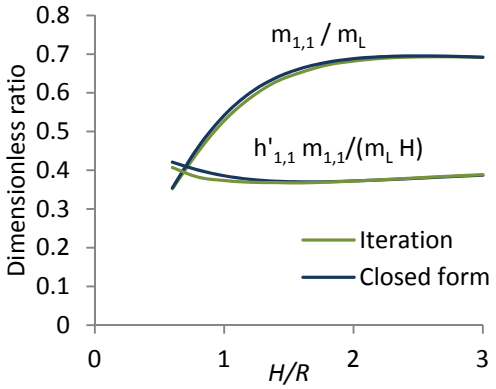

Figure 2.32: Normalized modal masses and equivalent heights, 1st circumferential and axial mode, $R/h = 1500$.

In summary, the method proposed in EC8 (2006) for the calculation of the hydrodynamic pressures and eigenvalues corresponding to the fundamental impulsive mode of antisymmetric vibration implicates the following drawbacks that should be taken into account:

a) The iteration scheme can be carried out and leads to precise results only for slender liquid-storage tanks.

b) The estimation of dynamic characteristics of broad containers requires the elimination of the density singularity on the tank bottom.

c) For small slenderness ratios the method furnishes inaccurate results since it intrinsically misrepresents the form of the fluid mass matrix. The deviations are more pronounced for the fundamental eigenfrequency, a fact which could possibly lead to erroneous spectral amplitudes in a response spectrum analysis.

d) Higher eigenmodes and eigenfrequencies can not be computed. A trial to assess even the second axial mode of the system crushes immediately, since negative values of the additional virtual density appear as a consequence of the -locally along the wall- opposite signs of the eigenform and pressure.

2.2.5 Combination of the impulsive pressure terms due to horizontal excitation

The solution of the modal equations Eq. (2.115) provides the response obtained by Eq. (2.118) as a function of time. The total wall pressure is given by:

$$p_H(R,z,\theta,t) = \rho_L\, R\, \cos(\theta) \left[\sum_{n=1}^{N} \bar{p}_{1,n}(R,z)\, \bar{S}_{a,x,n}^{rel.}(t) + \bar{p}_{HR}(R,z)\ddot{X}_g(t)\right] \tag{2.147}$$

or equivalently expressed as a function of the absolute pseudoacceleration functions:

$$p_H(R,z,\theta,t) = \rho_L\, R\cos(\theta)\left[\sum_{n=1}^{N} \bar{p}_{1,n}(R,z)\,\bar{S}^{abs.}_{a,x,n}(t)\right] \tag{2.148}$$

However, structural design is based on the peak values of stresses and deformations over the duration of the seismic motion. Accordingly, a response spectrum analysis is essential for the determination of the dynamically activated pressures in tanks, as long as nonlinearities do not occur. The current standard provisions do not provide guidelines for an appropriate combination of the maximum wall pressures due to the horizontal component of the ground motion, which is needed for a detailed stress analysis. To the author's knowledge, the only work which dealt with this problem was carried out by Rammerstorfer & al. (1989).

They proposed a square-root-of-sum-of-squares (SRSS) rule for the combination of the dynamically activated impulsive pressure due to the interaction of the liquid and the shell with the dynamically activated impulsive pressure due to the horizontal rigid tank motion (p_{HR}), by taking into account for simplicity only the fundamental natural vibration mode ($p_{1,1}$). However, as it can be observed in Figure 2.21, the influence of the pressure induced against the tank wall associated with higher modes may be significant for slender tanks for a certain frequency content of the earthquake record. Besides, consideration of the first eigenmode only, implies the necessity to acquire a relative pesudoacceleration response spectrum which, in contrast to the absolute pseudoacceleration response spectrum, is not derivable from a displacement spectrum or a relative pseudovelocity spectrum. Thus, an efficient procedure for a proper superposition of the individual modal contributions must be established. For this purpose, fifteen artificial accelerograms are in total generated, five for each of three selected shapes of the target horizontal elastic response spectra of EC8 (2011) corresponding to different ground types (Figure 2.34). Linear base line corrections are carried out by the program BASKOR provided by Meskouris (2000). The design ground acceleration is chosen $a_g = 0.72\ m/s^2$ corresponding to seismic zone 2 and importance factor $\gamma_I = 1.2$. The produced time histories have 16 sec duration, match the spectrum for 5% viscous damping and fulfill the requirements described in EC8 (2004), paragraph 3.2.3.1.2. Six steel tanks with different proportions regarding their slenderness and thickness are investigated. The properties of the examined tanks are summarized in Table 2.3.

The selection of different elastic spectrum characteristics in combination with various examined tanks geometries aims at covering an extended range of possible responses due to excitation of different eigenmodes and the inherent probabilistic differences that exist among ground motions. The purpose of generating multiple synthetic records is to manifest the efficiency of SRSS modal combination rule at estimating the mean of the peak pressure values to an ensemble of earthquake excitations. For each of the examined tanks and artificial records, the pseudoacceleration response of the nth mode is computed by solving Eq. (2.115) using the numerical time-stepping Newmark's method.

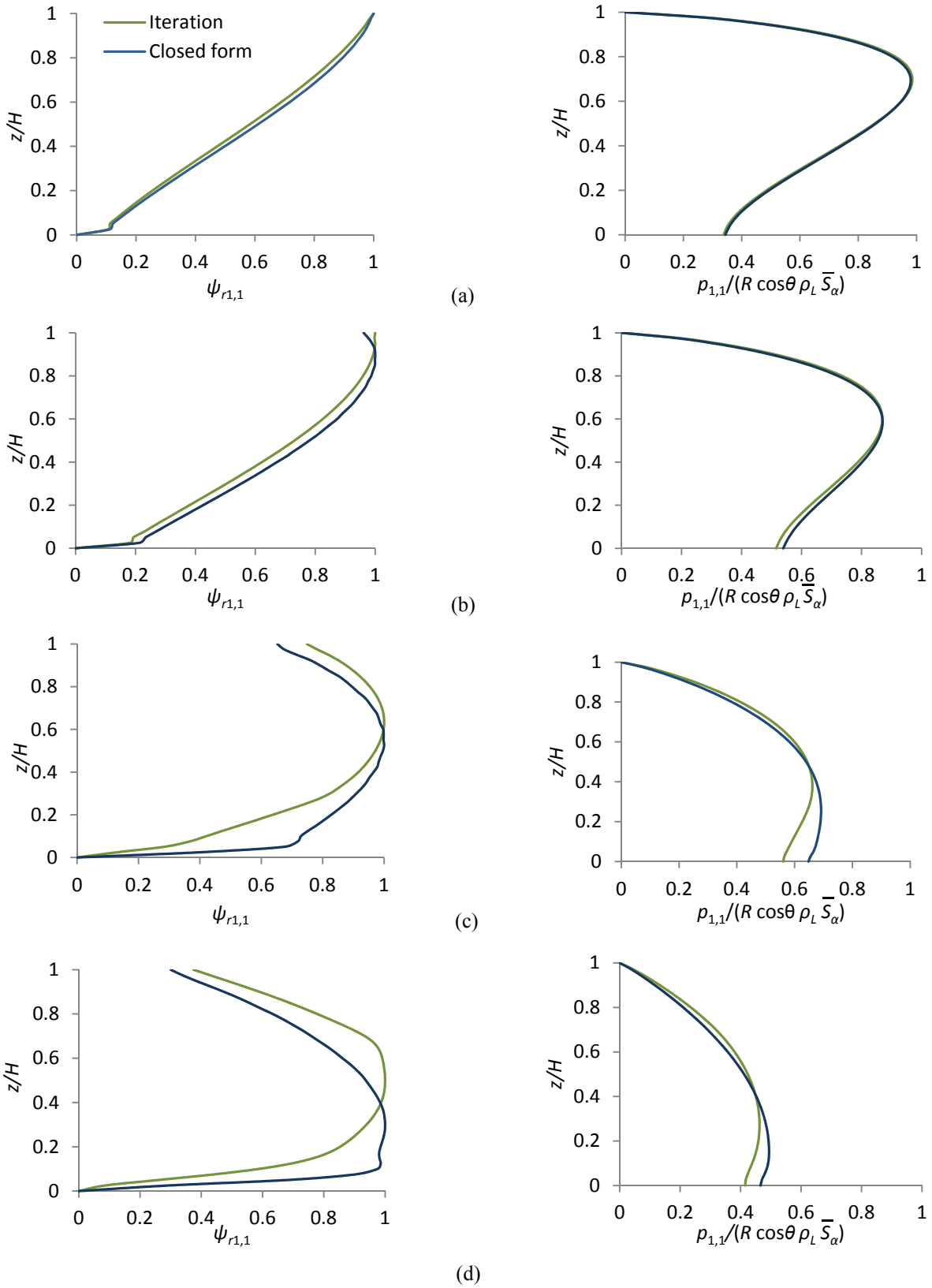

Figure 2.33: Radial eigenmodes (left) and corresponding pressures (right) of steel tanks, $R/h = 1500$, obtained by iterative procedure (a) $H/R = 3$, (b) $H/R = 2$, (c) $H/R = 1$, (d) $H/R = 0.6$.

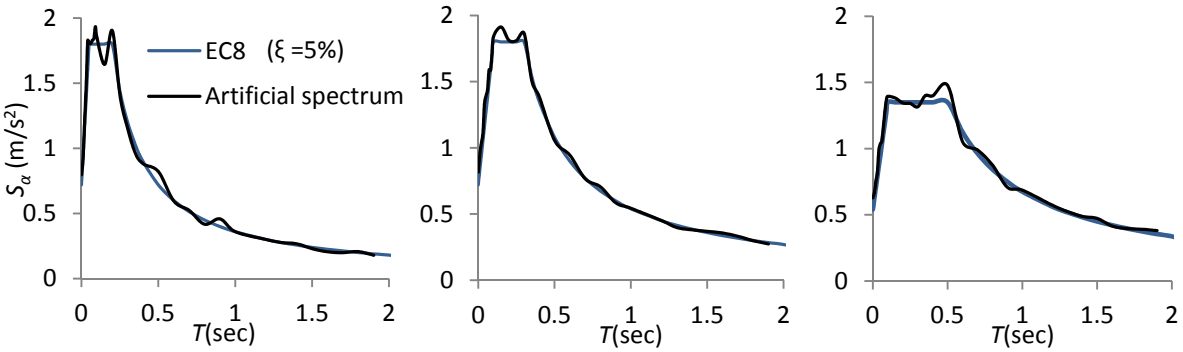

Figure 2.34: Horizontal elastic pseudoacceleration spectrum EC8 and mean matched artificial spectrum for ground type (a) A-R, (b) B-T, (c) C-S.

Table 2.3: Geometry and material data for the numerical investigations.

Uniform parameters		Tank type	H_L/R	R/h
H_L(m)	10	Tank T1	3	1000
H(m)	11	Tank T2	2	1000
E(MN/m²)	210000	Tank T3	1.5	1000
v	0.3	Tank T4	3	3000
ρ_L(t/m³)	1.0	Tank T5	2	3000
ρ(t/m³)	7.85	Tank T6	1.5	3000

The wall pressure distributions for the fundamental mode is evaluated by use of Eq. (2.147) for $N = 1$. The total response is obtained by using Eq. (2.148) for $N = 3$, since for the tanks analysed inclusion of higher modal responses does not alter the results independent of the ground motion. A uniform damping value $\xi_{1,1} = \xi_{1,2} = \xi_{1,3} = 0.02$ is chosen. As it can be seen in Figure 2.36, the pressure modal responses $p_{1,n}$ for a specific height of the liquid-covered wall attain their peaks at different time instants and the combined response p_H attains its peak at yet a different instant. In addition, the total maximum positive or negative pressure at a wall point does not generally coincide with the total maximum positive or negative pressure at another wall point (Figure 2.35). Thus, the design wall pressure distribution should be considered as an envelope of amplitudes defined by individual maximum peaks occurring at different time instants.

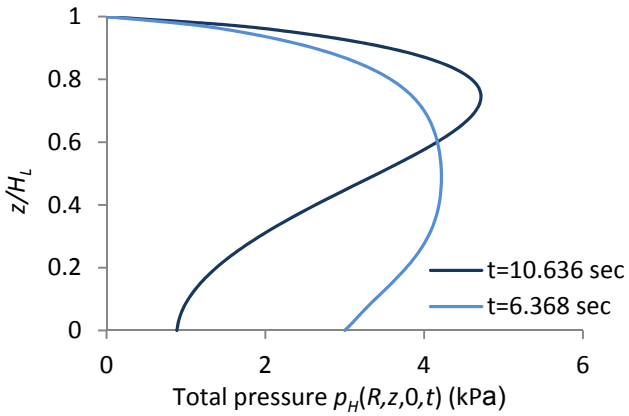

Figure 2.35: Wall pressure distributions when p_H reaches the maximum absolute value at height $z = 0$ ($t = 6.368$ sec) and $z = 0.8H_L$ ($t = 10.636$ sec) for tank type T1 induced by an artificial ground motion corresponding to ground type C-S of EC8.

In Figure 2.37 and 2.38, the mean maximum wall pressure distributions of the peak values of response to the individual excitations are presented for $N = 1$ and $N = 3$ and compared with the SRSS modal combination of the wall pressures computed according to following expression:

$$p_H(R,z,\theta) = \rho_L\, R\cos(\theta)\sqrt{\sum_{n=1}^{3}\left(\bar{p}_{1,n}(R,z)S_{a,x,n}^{abs.}\right)^2} \tag{2.149}$$

where $S_{a,x,n}^{abs.} = S_{a,x,n}^{abs.}(\omega_{1,n},\xi_{1,n}) = \max\left|\bar{S}_{a,x,n}^{abs.}(t,\omega_{1,n},\xi_{1,n})\right|$. The results indicate that the solution that includes only the fundamental mode is in good agreement with the pressure distribution obtained by taking into account 3 modes for a slenderness ratio $H_L/R = 1.5$. This trend is apparent for all induced ground motions even if they excite the second and/or the third mode. By contrast, for tanks with heights significantly larger than the radius the higher-mode response cannot be neglected. For $H_L/R = 3$, the deviations between the one and three-mode solution are more pronounced for the motion corresponding to ground type AR. For this case, the response is controlled by the second eigenmode as displayed in Table 2.4, where the mean maximum absolute pseudoaccelerations for each mode are presented. Although the SRSS modal combination rule is based on random vibration theory, generation of five synthetic records for each ground type suffices to provide an estimate of the peak pressure values obtained by response history analyses. Nevertheless, for the cases examined the SRSS rule generally underestimates the pressure amplitudes in the lower wall part. It should be noted that the frequencies of the lightly damped coupled shell-liquid vibrations of anchored steel tanks, which contribute significantly to the response, are well-separated. Thus, there is practically no correlation between the corresponding modes, and application of the complete quadratic combination (CQC) can be avoided. On the other hand, an absolute sum (ABSSUM) modal combination is not always conservative in contrast to conventional structural design, since it omits the algebraic sign of the normalized modal pressures.

Table 2.4: Mean spectral absolute pseudoaccelerations (m/s^2) for each ground type.

Tank type	A-R			B-T			C-S		
	$S_{a,x,1}^{abs.}$	$S_{a,x,2}^{abs.}$	$S_{a,x,3}^{abs.}$	$S_{a,x,1}^{abs.}$	$S_{a,x,2}^{abs.}$	$S_{a,x,3}^{abs.}$	$S_{a,x,1}^{abs.}$	$S_{a,x,2}^{abs.}$	$S_{a,x,3}^{abs.}$
Tank T1	2.17	2.60	1.88	2.77	1.61	1.29	1.88	1.27	0.97
Tank T2	2.60	2.48	1.74	2.43	1.79	1.39	1.64	1.29	1.05
Tank T3	2.67	2.44	1.83	2.32	1.77	1.51	1.70	1.33	1.24
Tank T4	1.81	2.62	2.44	2.78	2.26	1.80	1.92	1.77	1.28
Tank T5	2.10	2.11	2.25	2.38	2.52	1.95	1.78	1.95	1.43
Tank T6	2.32	2.48	2.65	2.54	2.44	2.05	1.77	1.71	1.46

2.2.6 Proposal for earthquake resistant design of anchored tanks

A simplified seismic design procedure for calculating the maximum dynamic pressures exerted on cylindrical steel tanks in fixed-base conditions can be followed on the basis of site response spectra and few simple calculations. The seismic responses due to the horizontal component of ground motion, regarding shear forces, overturning moments and sloshing wave height can be obtained according to a procedure proposed by Malhotra & al. (2000) which was adopted in EC8 (2006). The seismic responses, due to the vertical component of ground motion, regarding shear forces, can be obtained by use of Eq. (2.135) and the values $m_{0,n}$ provided from Figure 2.23b.

Horizontal excitation

Use of design response spectra requires the knowledge of the natural frequencies for sloshing and impulsive actions of the liquid. By carrying out standard regression analysis for fully filled tanks, the first three natural circular frequencies of the wall-liquid vibration can be calculated as a function of the slenderness ratio H/R and thickness ratio h/R according to the expression:

$$\omega_{1,n} = \frac{C_{1,n}}{H}\sqrt{\frac{E\,\rho_L}{\rho\,\rho_W}},\ \ n = 1,2,3 \tag{2.150}$$

where ρ_W is the mass density of water and the coefficients $C_{1,n}$ for each mode are given by:

$$C_{1,1} = 0.14\left(\frac{h}{R}\right)^{0.48}\left(\frac{H}{R}\right)^{3} - \left(\frac{h}{R}\right)^{0.48}\left(\frac{H}{R}\right)^{2} + 1.93\left(\frac{h}{R}\right)^{0.47}\frac{H}{R} + 1.76\left(\frac{h}{R}\right)^{0.54} \tag{2.151}$$

$$C_{1,2} = \left[1.85\ \ln\left(\frac{H}{R}\right) + 5.25\right]\left(\frac{h}{R}\right)^{0.5} \tag{2.152}$$

$$C_{1,3} = \left[2.75\ \ln\left(\frac{H}{R}\right) + 7.35\right]\left(\frac{h}{R}\right)^{0.5} \tag{2.153}$$

The above expressions are, strictly speaking, applicable for thin tanks $R/h \geq 200$ without roof and uniform wall thickness. The normalized wall pressure distributions $\bar{p}_{1,n}$ of fully filled tanks with slenderness ratios $0.3 \leq H/R \leq 3$ are given in Appendix B. The values presented correspond to steel tanks of uniform thickness ratio $h/R = 1000$. Nevertheless, there are also valid for other thickness ratios, since the pressure distribution is practically independent of the wall thickness apart from concrete tanks (Figure 2.20). For tanks with non-uniform thickness of the tank wall, h can be calculated by taking a weighted average over the height assigning the highest weight near the base of the tank (Malhotra et al., 2000). The total maximum dynamic wall pressure can be computed by use of Eq. (2.77), (2.93), (2.150) and the values provided in Tables B.1-B.3 (Appendix B) as:

$$p_H^{total}(R,z,\theta) = \rho_L\, R \cos(\theta) \sqrt{\left[\bar{p}_{SL,1}(R,z) S_{a,SL,1}\right]^2 + \sum_{n=1}^{3} \left[\bar{p}_{1,n}(R,z) S_{a,x,n}^{abs.}\right]^2} \tag{2.154}$$

Clearly, the contribution of the normalized pressure distributions $\bar{p}_{1,2}$ and moreover $\bar{p}_{1,3}$ is minor for broad tanks. However, it should be kept in the calculation for the sake of consistency and possible response amplifications due to excitation of higher eigenmodes.

Vertical excitation

For tanks with walls free to move in the radial direction at the bottom and top edges, the deformation figure is described by a cosine curve:

$$\psi_{r0,n} = cos\left(\frac{n\,\pi\,z}{2\,H}\right) \tag{2.155}$$

In this case and by neglecting the wall mass, the fundamental natural frequency can be obtained in closed form (Luft, 1984):

$$\omega_{0,1} = \frac{1}{R}\sqrt{\frac{\pi\, E\, h\, I_1(a_1 R)}{H\, \rho_L\, (1-\nu^2)\, I_0(a_1 R)}} \tag{2.156}$$

This expression was also adopted in EC8 and yields accurate results also for tank walls clamped at their base as it is depicted in Figure 2.17 for various thicknesses corresponding to steel tanks. Tang (1986) also manifested that the hydrodynamic effects of vertically excited tanks are insensitive to the condition of the support at the tank base. The exact total wall pressure is given by:

$$p_V^{total}(R,z,t) = \rho_L\, H \left[\sum_{n=1}^{N} \bar{p}_{0,n}(R,z)\, \bar{S}_{a,z,n}^{rel.}(t) + \left(1 - \frac{z}{H}\right)\ddot{Z}_g(t)\right] \tag{2.157}$$

For design purposes, the total maximum dynamic wall pressure can be computed by the following expression:

$$p_V^{total}(R,z) = \rho_L (H-z) S_{a,z,1}^{abs.} \tag{2.158}$$

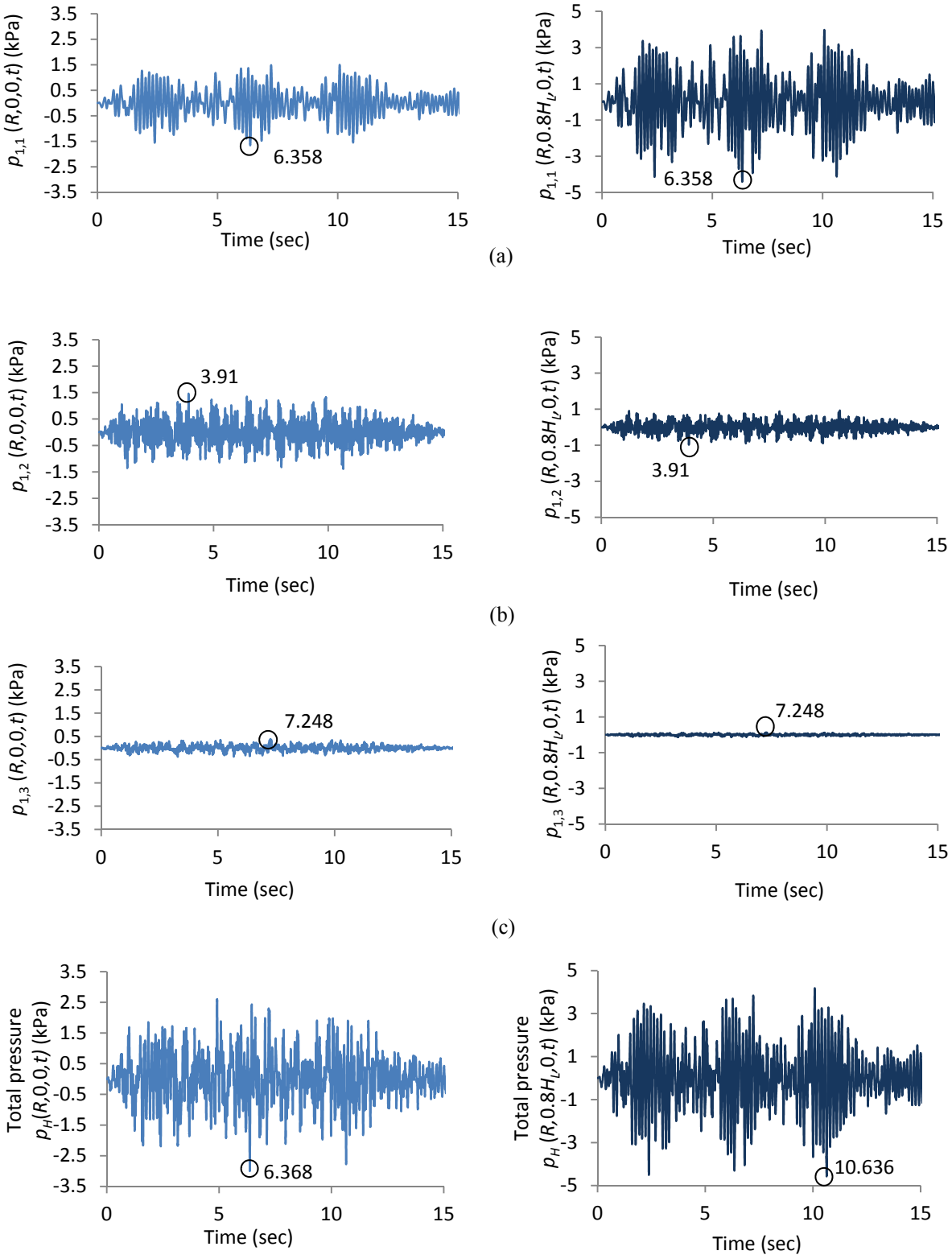

Figure 2.36: Pressure modal contributions (a) $p_{1,1}$, (b) $p_{1,2}$, (c) $p_{1,3}$ and total responses (d) p_H at height $z = 0$ (left) and $z = 0.8H_L$ (right) for tank type T1 induced by an artificial ground motion corresponding to ground type C-S of EC8.

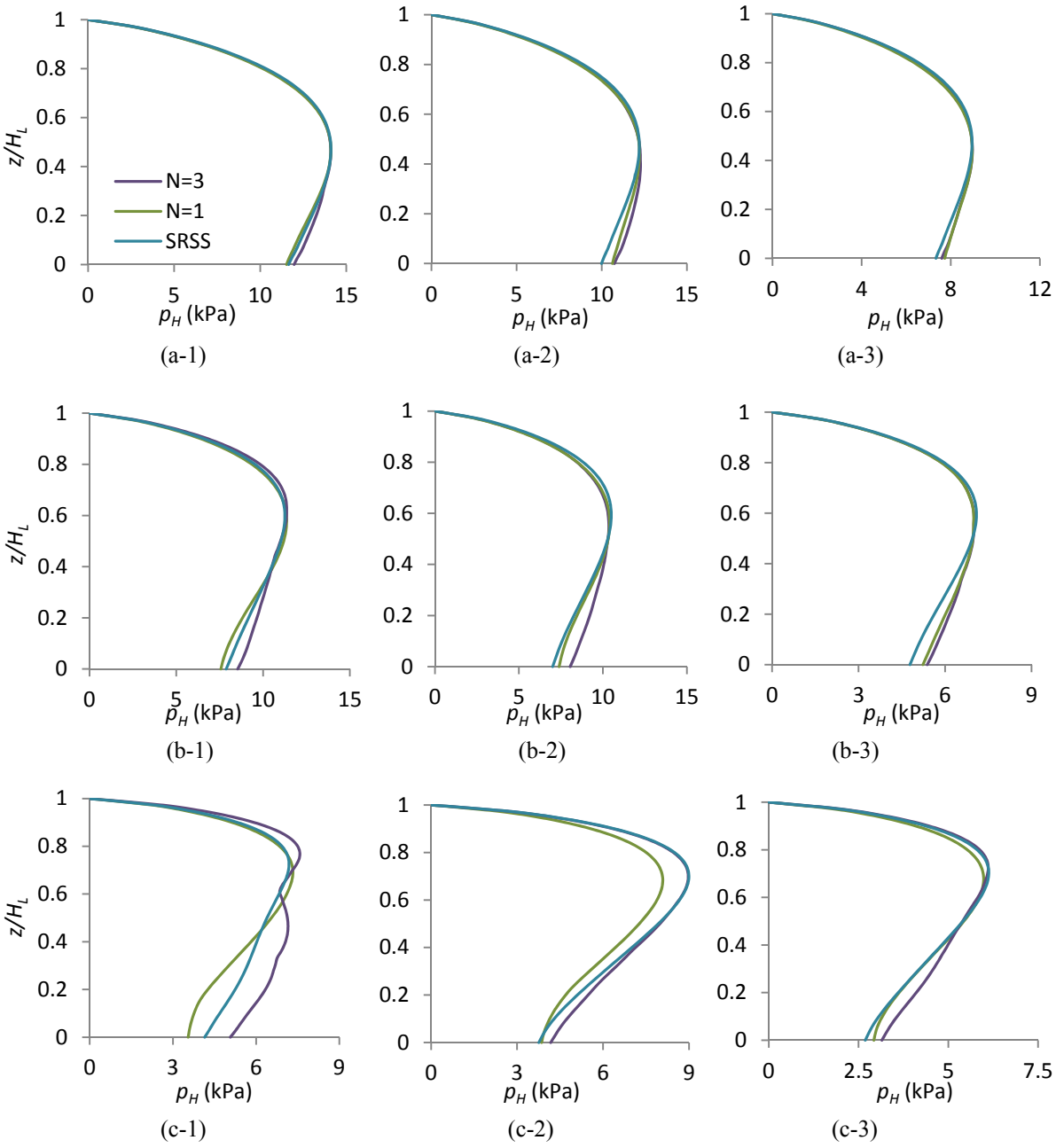

Figure 2.37: Mean maximum pressure wall distributions for tank types a) T3, b) T2, c) T1 caused by ground motion corresponding to ground types 1) A-R, 2) B-T, 3) C-S.

where $S_{a,z,n}^{abs.} = S_{a,z,n}^{abs.}(\omega_{0,n}, \xi_{0,n}) = \max\left|\bar{S}_{a,z,n}^{abs.}(t, \omega_{0,n}, \xi_{0,n})\right|$. It is important to note that, although the higher modes of vibration do not appear explicitly in Eq. (2.158), the contributions of them are accounted by approximately using the distribution function corresponding to a rigid tank and the absolute spectral acceleration of the fundamental mode. This is believed to be admissible, since in case of massless tanks, the pressure distribution functions of rigid and flexible tanks are interrelated by:

$$\sum_{n=1}^{N} \bar{p}_{0,n}(R,z) = (1 - \frac{z}{H}) \tag{2.159}$$

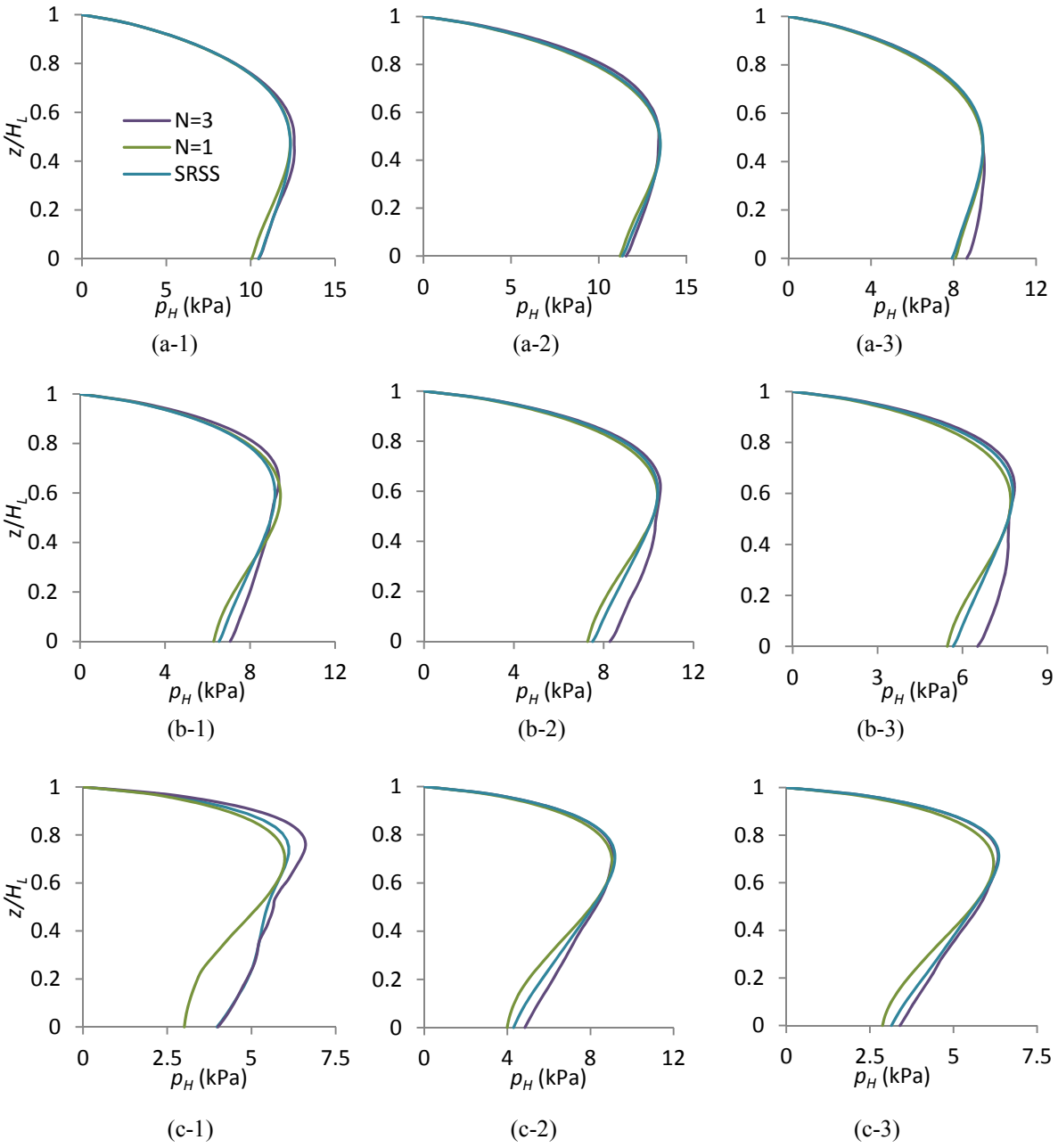

Figure 2.38: Mean maximum pressure wall distributions for tank types a) T6, b) T5, c) T4 caused by ground motion corresponding to ground types 1) A-R, 2) B-T, 3) C-S

In effect, Eq. (2.158) provides for all the modes the assumption that the pseudoacceleration responses for the higher modes are identical to that for the fundamental mode. Since the dimensionless functions $\bar{p}_{0,n}$ in which $n = 2,3 \ldots N$ are relatively small in comparison with $\bar{p}_{0,1}$, Eq. (2.158) furnishes sufficiently accurate results for steel tanks. It should be mentioned that the formula adopted in EC8 (2006) for the calculation of the maximum pressure due to vertical excitation:

$$p_V^{total}(R,z) = \rho_L \, H \sqrt{\left[(1-\frac{z}{H})\ddot{Z}_g\right]^2 + \left[\bar{p}_{0,1}(R,z) S_{a,z,1}^{abs.}\right]^2} \tag{2.160}$$

is inconsistent, due to the fact that the absolute and not the relative pseudoacceleration corresponding to the first eigenmode is superimposed with the vertical peak ground acceleration.

Two-dimensional horizontal excitation

The maximum dynamically activated pressures caused by a N-S excitation and the corresponding one caused by an E-W excitation may be superimposed according to SRSS rule (Rammerstorfer et al., 1989). Nevertheless, it should be mentioned that the individual components of the earthquake excitations are correlated and generally the maximum wall pressures do not occur at the angle where the maximum free field acceleration occurs. A more precise analysis demands the simultaneous excitation of the tank's mathematical model with the two horizontal earthquake components.

Superposition of dynamic pressures due to horizontal and vertical excitation

According to Rammerstorfer et al. (1988), a linear addition or subtraction of the individual pressure contributions has to be considered with respect to different types of damage during earthquake. Specifically, three different possibilities of superposition have to be analyzed as critical extreme cases that lead to discrete buckling modes:

Case 1: $p = p_H^{total,2D} + p_V^{total} + p_{stat.}$

Case 2: $p = p_H^{total,2D} - p_V^{total} + p_{stat.}$

Case 3: $p = -p_H^{total,2D} - p_V^{total} + p_{stat.}$

where $p_{stat.}$ stands for the static pressure.

2.3 Summary

The first part of this chapter deals with the free vibration characteristics of partially liquid-filled circular cylinders. A semi-analytical approach is refined, by considering both the sloshing condition and compressibility of the enclosed liquid. According to the proposed technique, the liquid velocity potential is expressed as a sum of two partial solutions which satisfy the Helmholtz equation and the relevant boundary conditions. The development of the shell model is based on classical thin shell theory. The boundary value problem is transformed into two differential equations in variational form, which contain two unknown field functions. In order to compensate with frequency-dependent matrices, an iterative incremental root-searching scheme is employed for the eigenvalue problem. Cases, for which the surface effects are significant and so far reported in the literature in a dispersive way, are addressed in a consistent manner. The results indicate that the effects of liquid's compressibility and free surface are pronounced in the same high frequency range. Thus, a significant reduction of the impulsive natural frequencies should be anticipated for lower circumferential wavenumbers and higher axial modes if the liquid's sound velocity is considered finite.

On the basis of this method, the response of liquid-storage tanks in fixed-base conditions to seismic loads is assessed in the second section of the chapter. For the vertical and horizontal components of ground motion, the differential equations of motions are derived in modal coordinates. The results are used to set up the tank-liquid model for the subsequent analysis in Chapter 4 and examine the adequacy of the procedure proposed by the European current standard provisions for the calculation of the impulsive hydrodynamic pressures. It is revealed that the iterative method proposed in EC8 imposes a considerable degree of inaccuracy, especially for broad tanks. Eventually, a simplified design process for the determination of the pressures exerted on flexible tank walls is introduced. This procedure can be promptly followed in practice since it involves only site response spectra and few elementary calculations.

.

3 Foundation-soil-foundation interaction

3.1 Introduction

In a soil-structure interaction (SSI) problem, external loads may correspond to forces and moments that the vibrating superstructure exerts on the soil-foundation interface. Inertia developed in a vibrating liquid-storage-tank gives rise to hydrodynamic pressures and consequently to shear forces and moments at the interface of the tank base and supporting foundation. In case of closely spaced -liquid containing- tanks founded on flexible soil, an external excitation of one tank generates a wavefield, which imposes vibration of the others; the latter subsequently produce a perturbed wavefield that affects the initial excited tank. Therefore, the problem of assessing the -through the soil- coupling effects on the response of closely spaced tank-liquid systems is directly associated with the determination of force-displacement relationships for the supporting foundations, defined as impedance functions (or by inversion compliance functions), which by definition do not possess mass. Once the harmonic response of the massless foundations has been determined, the response of adjacent tanks subjected to ground shaking, or of any structure supported on them, can be readily evaluated by an essential adjustment of the standard procedures to comprise multiple tank-liquid systems. The following literature review is restricted to cross-interaction studies associated with external dynamic forces only. The case of seismic waves impinging on foundations is discussed in the work of Tham et al. (1998).

3.1.1 State of the art report

Numerous studies have addressed the problem of the dynamic response of closely spaced foundations to external harmonic forces. Wong and Luko (1986) calculated the dynamic response of a group of rigid surface foundations bonded to a layered viscoelastic halfspace and subjected to external forces by means of a boundary integral equation technique and the Green's functions for the layered halfspace. Chouw and Schmid (1990) presented the results of the dynamic interaction of two square rigid foundations resting on a halfspace and on a soil layer over a rigid bedrock by using the BEM. Likewise, Karabalis and Mohammadi (1991) proposed a BEM formulation for the investigation of the interaction of surface massive footings, which resembled railway ties over homogeneous halfspace. The boundary integral equation in conjuction with the full-space fundamental solution was derived and extented to include the rigid foundation degrees of freedom, which finally resulted to a force-

displacement relationship in terms of a compliance matrix. A modification of the above procedure in order to take into account layered soil medium facilitated Karabalis and Mohammadi (1998) to study the dynamic response of adjacent rigid square foundations resting on a soil stratum over rigid bedrock. This approach demands discretization of the soil-foundation interface, part of the surrounding free surface and the soil layers interfaces. In all the aforementioned studies, the contact stresses were assumed uniform within each element. Qian and Beskos (1995) used quadratic boundary elements in order to investigate the cross-interaction effects between rigid foundations welded on the surface of a halfspace. The Finite Element Method (FEM) has been employed by Lin et al. (1987) to examine the dynamic interaction between adjacent rigid square foundations embedded in a homogeneous stratum and on its surface. A representation of the motion with finite elements was adopted in the near field whereas the waves in the far field were expressed in terms of semi-discrete modes of vibrations and particular solutions.

Efforts to solve analytically the problem of the subsoil coupling of adjacent foundations have also been reported. Triantafyllidis and Prange (1989) assessed the impedance functions of adjacent rigid foundations by transforming the integral equation system, which defines a mixed-boundary value prolem, to an algebraic one that incorporated approximately the unknown stress distributions at the interface foundation-subsoil as polynomial series expansions. Liou (1994) presented a procedure to generate the dynamic stiffness matrices for two adjacent circular foundations resting on an elastic halfspace. The use of an analytic solution of the wave equations, which satisfied the prescribed traction due to the vibration of one foundation, the superposition principle for the two foundations, and finally the equation of the work done by the contact tractions of the halfspace medium and the two foundations resulted to the generalized force-displacement relationships.

A few available direct time domain numerical solutions of foundation-soil-foundations interaction problems (FSFI) under external loads have to be mentioned. Karabalis and Huang (1994) utilized the space- and time-discretized fundamental solutions to establish the boundary integral equation, which combined with compatibility equations for a set of rigid surface square foundations over homogeneous halfspace, led to a equation for the unknown structural displacements. The results of these analyses motivated Mulliken and Karabalis (1998) to present a discrete model for the cases studied. The interaction of each foundation and the soil was realized through frequency independent lumped parameter models, the interaction between the foundations was realized by coupled springs and dashpots, and time lagging effects of the coupled dynamic input due to wave propagation were taken into acount by a modification of the Wilson-θ method. Guan and Novak (1994) utilized the Green's functions for a homogeneous halfspace, as developed by them, in order to investigate the transient response of multiple rigid foundations by means of a BEM formulation.

Although the aforementioned works manifested the significance of the FSFI effects, limited conclusions have been deduced, with regard to a quantitative assessment of the involved parameters

relative influence on the problem, due primarily to the fact that unique case studies were mainly investigated. Furthermore, little effort has been made to systematically inspect the FSFI phenomena from the standpoint of a comparison between the case of an isolated foundation and the case of multiple interacting foundations in view of different soil conditions. Even though an exhaustive study of all possible cases to be in reality encountered is not feasible, the present study intends to present a survey of the factors that control the impedance functions of adjacent (circular) rigid, surface foundations and provide a guideline for practical purposes. Two idealized soil profiles are examined and the results are illustrated in a comparative manner, which permits a clear conception of the relative impact of each participating parameter on the cross-interaction problem.

In the majority of the conducted research work and likewise in this study, the Boundary Element Method (BEM) is employed, which facilitates the dynamic modeling of the unbounded medium. Kernel of the method is the fundamental solutions of the corresponding partial differential equations. These solutions are addressed in the next section.

3.2 Green's functions

The fundamental solutions or so called Green's functions are expressions for the response anywhere in a solid elicited by a static or dynamic point source at some arbitrary distance. The utility of their knowledge lies in the potential to transform the governing differential equation of the problem at hand into an equivalent boundary integral equation and solve it in terms of boundary values only, avoiding any domain integration. In wave propagation problems for unbounded media, such as those that concern SSSI analysis, the solutions must not only satisfy the governing differential equations of elastodynamics and the free surface condition, if present, but also must be unique. In the frequency domain, the requirement for uniqueness, called the radiation condition, states that the displacement amplitude vanishes at infinity and no energy is transmitted from infinity towards the structures-medium interface. Since first Lamb (1904) addressed the problem of a dynamic source applied at the surface of an elastic halfspace, considerable work has been carried out for the purpose of obtaining exact formulas for the response of infinite bodies to dynamic loads. Nevertheless, closed-form solutions are available only for certain limited cases, such as those provided by Pekeris (1955) and Chao (1960) for a homogeneous elastic halfspace subjected to point load at its surface. Thus, complex configurations of the unbounded medium can be only treated numerically. In this study, the Green's functions for a homogeneous halfspace are obtained with the aid of the Stiffness Matrix Method (SMM), whereas the Green's functions for layered strata are obtained by using the discrete version of SMM, which is known as Thin Layer Method (TLM).

3.2.1 Homogeneous halfspace via the Stiffness Matrix Method

The dynamic behavior of a homogeneous halfspace represents an essential element in the SSI analysis. When a deep and relatively uniform soil deposit is encountered, it is desirable from an engineering perspective to model it as homogeneous semi-infinite medium. The Stiffness Matrix Method, conceived by Kausel and Roesset (1981) for the general case of laterally infinite, layered strata and/or halfspace, can be employed for the solution of a wave propagation problem in isotropic, homogeneous semi-infinite media. The method is exact, since the mathematical derivation does not contain approximations for the displacement field. Nevertheless, the resulting expressions must commonly be evaluated numerically, since only a limited number of simple cases can be handled analytically. The method is based on the calculation of the stiffness (impedance matrix) of a homogeneous, horizontal, elastic and laterally infinite layer of arbitrary thickness. It can be shown that the dynamic equilibrium of this layer in the frequency-wavenumber domain $\Omega, \kappa,$ in the absense of external sources, is expressed in cylindrical coordinates by (Kausel, 2011):

$$\begin{Bmatrix} \tilde{\mathbf{p}}_1 \\ \tilde{\mathbf{p}}_2 \end{Bmatrix} = \begin{bmatrix} \tilde{\mathbf{G}}_{11} & \tilde{\mathbf{G}}_{12} \\ \tilde{\mathbf{G}}_{21} & \tilde{\mathbf{G}}_{22} \end{bmatrix} \begin{Bmatrix} \tilde{\mathbf{w}}_1 \\ \tilde{\mathbf{w}}_2 \end{Bmatrix} \tag{3.1}$$

where $\tilde{\mathbf{p}}_1, \tilde{\mathbf{p}}_2$ are upper and lower external interface tractions and $\tilde{\mathbf{w}}_1, \tilde{\mathbf{w}}_2$ are upper and lower interface displacements. Due to the fact that the SH components are uncoupled from the SV-P wave components, Eq. (3.1) can be splitted into two separate matrix equations: an in-plane (4x4) and an anti-plane (2x2), which correspond to the P-SV and SH waves respectively. Closed form expressions for the elements of $\tilde{\mathbf{G}}$ are given by Kausel (2011). Material damping is modeled by means of complex moduli. The general case of a layered system characterized by discontinuities in material properties in the vertical direction and consisted of *N*-1 layers and *N* interfaces can be handled by an appropriate overlap of the matrices for the neighboring matrices. The result is a block-tridiagonal matrix of the form:

$$\begin{Bmatrix} \tilde{\mathbf{p}}_1 \\ \tilde{\mathbf{p}}_2 \\ \tilde{\mathbf{p}}_3 \\ \vdots \\ \tilde{\mathbf{p}}_N \end{Bmatrix} = \begin{bmatrix} \tilde{\mathbf{G}}_{11} & \tilde{\mathbf{G}}_{12} & \mathbf{0} & \dots & \mathbf{0} \\ \tilde{\mathbf{G}}_{21} & \tilde{\mathbf{G}}_{22} & \tilde{\mathbf{G}}_{23} & \dots & \mathbf{0} \\ \mathbf{0} & \tilde{\mathbf{G}}_{32} & \tilde{\mathbf{G}}_{33} & \ddots & \vdots \\ \vdots & \vdots & \ddots & \ddots & \tilde{\mathbf{G}}_{N-1,1} \\ \mathbf{0} & \mathbf{0} & \dots & \tilde{\mathbf{G}}_{N,N-1} & \tilde{\mathbf{G}}_{NN} \end{bmatrix} \begin{Bmatrix} \tilde{\mathbf{w}}_1 \\ \tilde{\mathbf{w}}_2 \\ \tilde{\mathbf{w}}_3 \\ \vdots \\ \tilde{\mathbf{w}}_N \end{Bmatrix} \tag{3.2}$$

The submatrices of the special case of a homogeneous elastic halfspace are herein presented, which are obtained by deleting the terms of the solution associated with upward propagating waves. For SH waves the impedance of the halfspace is given by:

$$\tilde{\mathbf{G}}_{SH}^{H} = \mu\sqrt{\kappa^2 - (\Omega/V_s)^2}\ , \qquad \kappa \neq 0 \tag{3.3}$$

where μ stands for the shear modulus of the soil and V_s is the S-wave velocity. For SV-P waves and generalized Rayleigh waves the impedance of halfspace is given by:

$$\widetilde{\mathbf{G}}_{SVP}^{H} = 2\,\kappa\,\mu\left[\frac{1-s^2}{2(1-p\,s)}\begin{Bmatrix} p & -1 \\ -1 & s \end{Bmatrix} + \begin{Bmatrix} 0 & 1 \\ 1 & 0 \end{Bmatrix}\right], \quad \kappa \neq 0 \tag{3.4}$$

where:

$$p = \sqrt{1 - S_p^2}, \qquad S_p = \frac{\Omega}{\kappa\, V_p}, \qquad V_p = \sqrt{\frac{\lambda + 2\mu}{\rho_s}} \tag{3.5}$$

$$s = \sqrt{1 - S_s^2}, \qquad S_s = \frac{\Omega}{\kappa\, V_s} \qquad V_s = \sqrt{\frac{\mu}{\rho_s}} \tag{3.6}$$

The expressions for the S and P waves (V_p) velocities are given in Eq. (3.5) and (3.6). The quantities λ and ρ_s stand for the Lamé constant and density of the medium respectively. Having obtained the stiffness matrix $\widetilde{\mathbf{G}}$ of the halfspace, the solution consists of the following steps (Kausel, 2011): The frequency-dependent surface point load is expressed in the wavenumber domain by carrying out a Hankel transformation. Subsequently, the surface displacements in the frequency-wavenumber domain are obtained by solving the following equation for the SV-P and SH waves:

$$\widetilde{\mathbf{w}} = \widetilde{\mathbf{G}}^{-1}\,\widetilde{\mathbf{p}} \tag{3.7}$$

Finally, the desired response in the spatial domain $\mathbf{w}$ is computed by an inverse Hankel transformation. The solution has the following form:

$$\begin{Bmatrix} w_r \\ w_\theta \\ w_z \end{Bmatrix} = \begin{bmatrix} G_{rr} & 0 & G_{rz} \\ 0 & G_{\theta\theta} & 0 \\ G_{zr} & 0 & G_{zz} \end{bmatrix} \begin{Bmatrix} p_r \\ p_\theta \\ p_z \end{Bmatrix} \tag{3.8}$$

or in compact vector-tensor notation:

$$\mathbf{w} = \mathbf{G}\,\mathbf{p} \tag{3.9}$$

The relationship between point loads and displacements on the free surface that Eq. (3.8) establishes is depicted in Figure 3.1. Due to the fact that the displacement vector $\mathbf{w}$ and the load vector $\mathbf{p}$ are located on the surface of the halfspace, $G_{rz} = -G_{zr}$ according to the reciprocal theorem and the response is fully described by four independent Green's functions. The matrix of the Green's functions is calculated in the following dimensionless form:

$$\begin{bmatrix} g_{rr} & 0 & g_{rz} \\ 0 & g_{\theta\theta} & 0 \\ -g_{rz} & 0 & g_{zz} \end{bmatrix} = \mu\, r \begin{bmatrix} G_{rr} & 0 & G_{rz} \\ 0 & G_{\theta\theta} & 0 \\ -G_{rz} & 0 & G_{zz} \end{bmatrix} \tag{3.10}$$

where r represents the distance of source and receiver in the cylindrical coordinate system. By using Eq. (3.10) each of the four independent Greens's functions for a specific level of material damping can be presented for different Poisson's ratio values ν_s as a function solely of the dimensionless frequency:

$$r_o = \frac{r\,\Omega}{V_s} \tag{3.11}$$

The normalized Green's functions are shown in Figure 3.2. It is interesting to note that the component $g_{\theta\theta}$ is practically independent from the values of Poisson's ratio and the oscillations have constant amplitudes as r_o increases. The latter is attributed to the fact that Rayleigh waves are absent in the out-of-plane motion, thus the behavior of $g_{\theta\theta}$ is controlled only by body waves, which attenuate with distance from point of application as r^{-1}. Since the components depicted in Figure 3.2 are normalized with r, the amplitudes remain constant for $r_o \to \infty$.

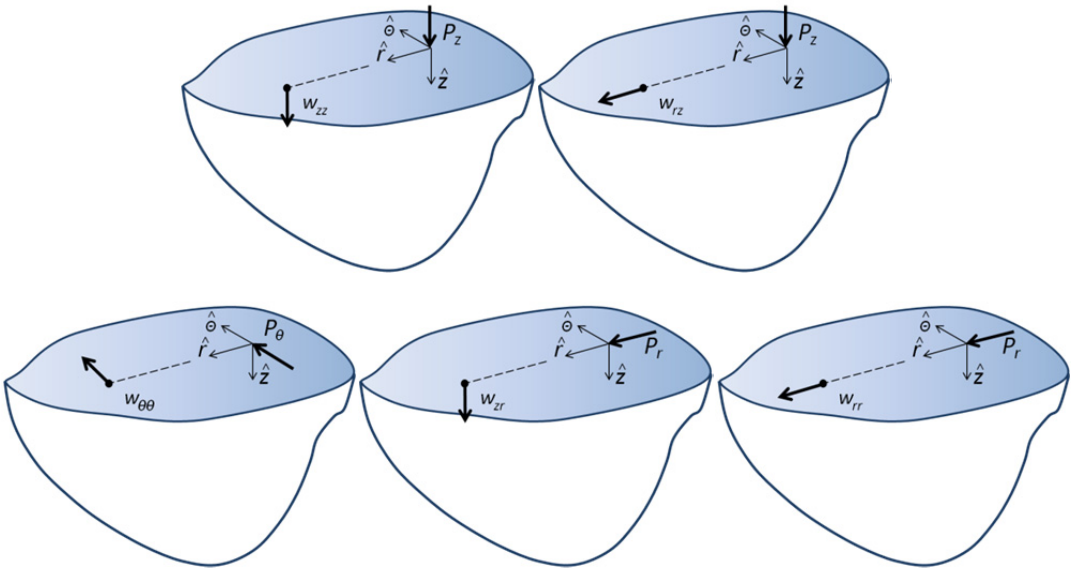

Figure 3.1: Relation between point loads applied on the halfspace's surface and the corresponding displacements, which define the Green's functions.

3.2.2 Layered halfspace via the Thin Layer Method

3.2.2.1 General formulation

Contrary to the homogeneous halfspace, analytic solutions for layered media with arbitrary boundary conditions do not exist. The closed-form evaluation of the integral transforms, which are used in SMM, is a formidable problem due to the transcendental functions which govern the displacements in the direction of layering. Therefore, for the calculation of the Green's functions for a horizontally stratified halfspace the Thin Layer Method (TLM) is preferable. The concept of this method is similar to the SSM; the principal difference lies in the employment of algebraic expressions in place of intricate transcendental functions in the direction in which material properties are heterogeneous. The solution in the remaining directions is derived analytically.

Starting point for the description of the method is the equation that governs the motion inside a horizontally stratified, locally homogneous and anisotropic medium of infinite lateral extent. Within

each layer the motion is described in cartesian coordinates by the following differential equation (Kausel, 1986):

$$\mathbf{L}^{\mathrm{T}}\,\mathbf{E}\,\mathbf{L}\,\mathbf{w}+\mathbf{b}=\rho_s\,\ddot{\mathbf{w}} \tag{3.12}$$

where:

$$\mathbf{w}=\mathbf{w}(x,y,z,t)=[w_x \quad w_y \quad w_z]^{\mathrm{T}} \tag{3.13}$$

$$\mathbf{b}=\mathbf{b}(x,y,z,t)=[b_x \quad b_y \quad b_z]^{\mathrm{T}} \tag{3.14}$$

stand for the displacement and body load vector respectively. $\mathbf{L}$ is a differential operator matrix given by:

$$\mathbf{L}^{\mathrm{T}}=\begin{bmatrix}\frac{\partial}{\partial \mathrm{x}} & 0 & 0 & 0 & \frac{\partial}{\partial \mathrm{z}} & \frac{\partial}{\partial \mathrm{y}}\\ 0 & \frac{\partial}{\partial \mathrm{y}} & 0 & \frac{\partial}{\partial \mathrm{z}} & 0 & \frac{\partial}{\partial \mathrm{x}}\\ 0 & 0 & \frac{\partial}{\partial \mathrm{z}} & \frac{\partial}{\partial \mathrm{y}} & \frac{\partial}{\partial \mathrm{x}} & 0\end{bmatrix}=\mathbf{L}_x\frac{\partial}{\partial \mathrm{x}}+\mathbf{L}_y\frac{\partial}{\partial \mathrm{y}}+\mathbf{L}_z\frac{\partial}{\partial \mathrm{z}} \tag{3.15}$$

and $\mathbf{E}$ is the constitutive matrix. The vector of internal stresses in a plane perpendicular to the z axis can be expressed as:

$$\mathbf{s}=[\tau_{zx} \quad \tau_{zy} \quad \sigma_z]^{\mathrm{T}}=\mathbf{L}_z^{\mathrm{T}}\,\mathbf{E}\,\mathbf{L}\,\mathbf{w} \tag{3.16}$$

where $\mathbf{L}_z^{\mathrm{T}}$ follows by inspection of Eq. (3.15). In order to solve the wave equation, the medium is divided into $M-1$ layers (z direction) that are thin in the finite element sense (Figure 3.3). The boundary conditions at the upper i and lower interfaces $i+1$ of an arbitrary thin layer where external tractions $\mathbf{t}$ are prescribed are:

$$\begin{Bmatrix}\mathbf{s}_{\mathrm{i}}\\ -\mathbf{s}_{\mathrm{i+1}}\end{Bmatrix}=\begin{Bmatrix}\mathbf{t}_{\mathrm{i}}\\ \mathbf{t}_{\mathrm{i+1}}\end{Bmatrix} \tag{3.17}$$

The displacements within one thin-layer of thickness *h* are interpolated as:

$$\mathbf{w}\cong\mathbf{N}\,\mathbf{U} \tag{3.18}$$

where $\mathbf{N}=\mathbf{N}(z)$ is the matrix that contains the interpolation polynomials and $\mathbf{U}=\mathbf{U}(x,y,t)$ a column vector which consists of the interface displacement vectors:

$$\mathbf{U}=\left[\mathbf{w}_i^{\mathrm{T}} \quad \mathbf{w}_{i+1}^{\mathrm{T}} \quad \ldots \quad \mathbf{w}_m^{\mathrm{T}}\right]^{\mathrm{T}} \tag{3.19}$$

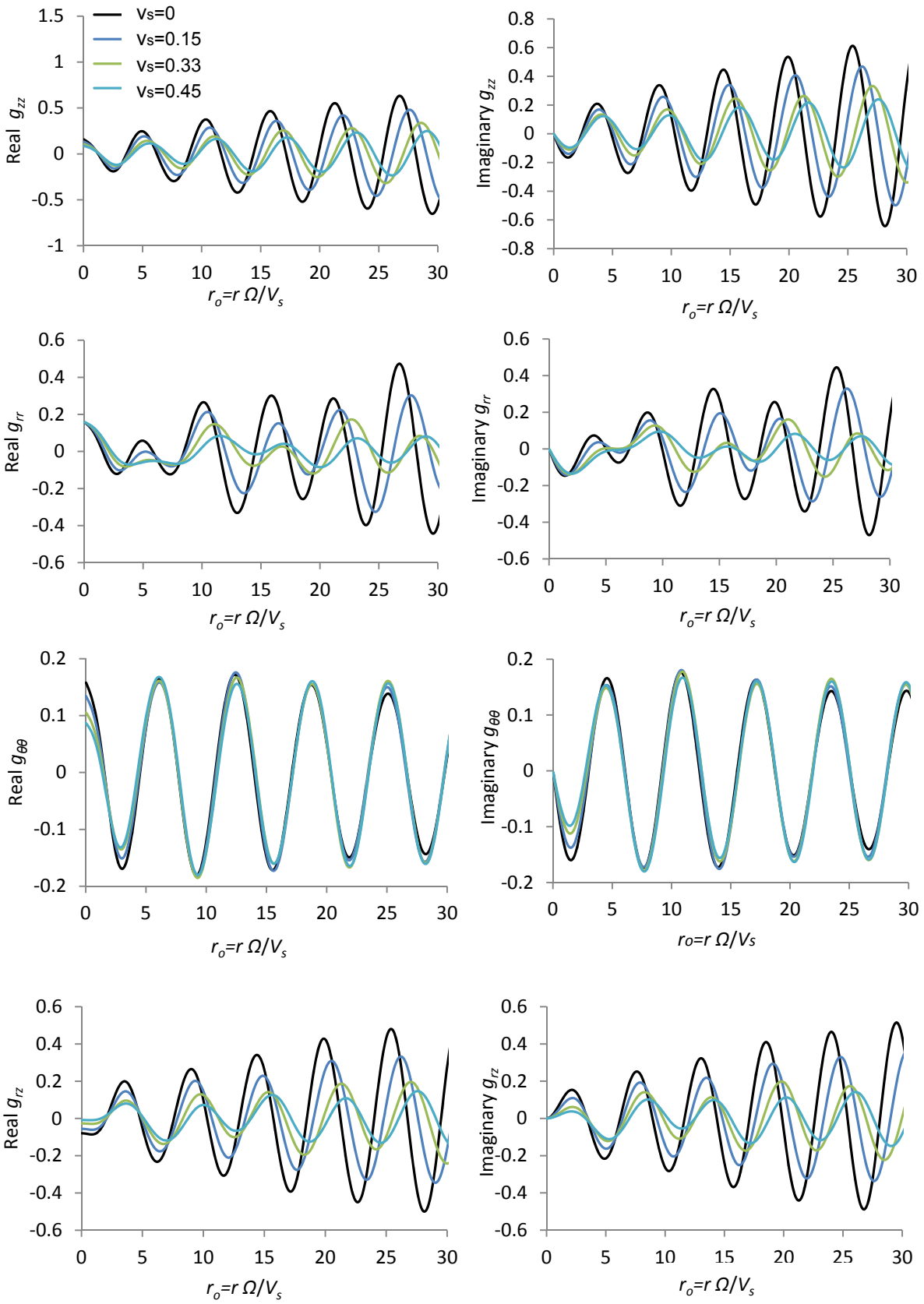

Figure 3.2: Real and imaginary part of Green's functions for homogeneous elastic halfspace and various Poisson's ratios (source and point load on the surface).

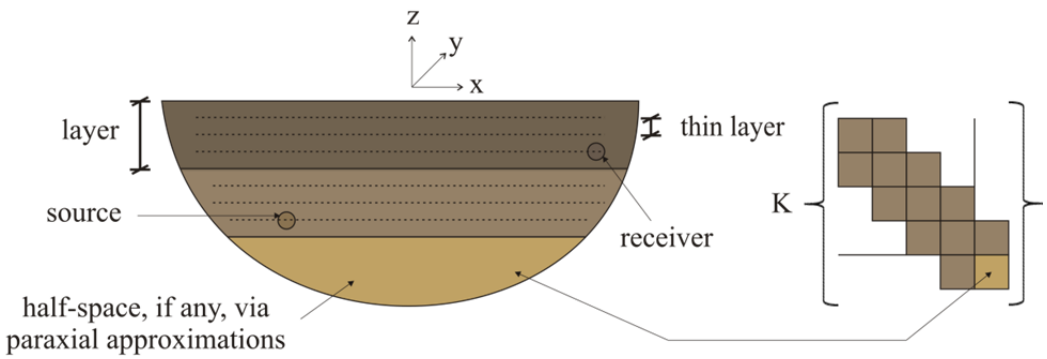

Figure 3.3: Discretization scheme in Thin Layer Method and stiffness matrix form.

Substitution of Eq. (3.18) into Eq. (3.12) and Eq. (3.17) yields two equations that are not satisfied exactly, since residual body forces $\mathbf{r} = \mathbf{r}(x, y, z, t)$ and residual boundary tractions $\mathbf{g} = \mathbf{g}(x, y, z, t)$ arise:

$$\mathbf{L}^{\mathrm{T}}\,\mathbf{D}\,\mathbf{L}\,\mathbf{w} + \mathbf{b} - \rho_s\,\ddot{\mathbf{w}} = \mathbf{r} \tag{3.20}$$

$$\mathbf{t} - \mathbf{s} = \mathbf{g} \tag{3.21}$$

Application of the method of weighted residuals to an arbitrary thin-layer furnishes the following equation:

$$\left[\delta\mathbf{w}_i^{\mathrm{T}}\mathbf{g}_i + \delta\mathbf{w}_{i+1}^{\mathrm{T}}\mathbf{g}_{i+1} + \int_{\mathbf{0}}^{\boldsymbol{h}} \delta\mathbf{w}^{\mathrm{T}}\,\mathbf{r}\,\mathrm{dz}\right]\mathrm{dx}\,\mathrm{dy} = 0 \tag{3.22}$$

The first two terms in Eq. (3.22) stand for the virtual work done by the residual tractions at the upper and lower boundaries respectively, whereas the third term represents the virtual work done by the residual body forces. After substituting Eq. (3.18), Eq. (3.20) and Eq. (3.21) into Eq. (3.22) and some algebra manipulation, we obtain a dynamic equilibrium equation for the thin-layer as (Park, 2002):

$$\mathbf{P} = \mathbf{X}\,\ddot{\mathbf{U}} - \mathbf{A}_{xx}\frac{\partial^2\mathbf{U}}{\partial \mathrm{x}^2} - \mathbf{A}_{xy}\frac{\partial^2\mathbf{U}}{\partial \mathrm{x}\,\partial \mathrm{y}} - \mathbf{A}_{yy}\frac{\partial^2\mathbf{U}}{\partial \mathrm{y}^2} - \mathbf{B}_x\frac{\partial\mathbf{U}}{\partial \mathrm{x}} - \mathbf{B}_y\frac{\partial\mathbf{U}}{\partial \mathrm{y}} + \mathbf{Z}\mathbf{U} \tag{3.23}$$

The left hand side in Eq. (3.23) is the vector of consistent external tractions acting on the interfaces. The matrices $\mathbf{X}$, $\mathbf{A}_{xx}$, $\mathbf{A}_{xy}$, $\mathbf{A}_{yy}$, $\mathbf{B}_x$, $\mathbf{B}_y$ and $\mathbf{Z}$ depend on the material properties of the layer, its thickness, and on the expansion order used for the discretization. The assemblage of all horizontal thin-layers, by overlapping the contribution of each layer's matrix at each node of the system, generates the system matrix (Figure 3.3). This matrix possesses $3M$ degrees of freedom, with M being the number of interfaces; the latter depends on the number of layers, the interpolation order and the boundary conditions at the top and bottom surfaces.

In order to solve Eq. (3.23) spatial and temporal transforms in each coordinate are necessary. In the transformed domain the discrete system displacement and traction fields can be written as $\widetilde{\mathbf{W}}$ and $\widetilde{\mathbf{P}}$

respectively. The transformed linear system of equation in the wavenumber-frequency domain $(\kappa_x, \kappa_y, \Omega)$ is expressed as:

$$\widetilde{\mathbf{P}} = \left(\widetilde{\mathbf{K}} - \Omega^2 \mathbf{X}\right) \widetilde{\mathbf{W}} \tag{3.24}$$

with:

$$\widetilde{\mathbf{K}} = \kappa_x^2 \mathbf{A}_{xx} + \kappa_x \kappa_y \mathbf{A}_{xy} + \kappa_y^2 \mathbf{A}_{yy} + \mathrm{i}\, \kappa_x \mathbf{B}_x + \mathrm{i}\, \kappa_y \mathbf{B}_y + \mathbf{Z} \tag{3.25}$$

The displacement vector $\widetilde{\mathbf{W}}$ can be calculated by inversion of the stiffness matrix $\widetilde{\mathbf{K}} - \Omega^2 \mathbf{X}$. Alternatively, the solution may be obtained by means of a spectral decomposition of the stiffness matrix, which is associated with the solution of the quadratic eigenvalue problem: $\left(\widetilde{\mathbf{K}} - \Omega^2 \mathbf{X}\right)\boldsymbol{\varphi} = \mathbf{0}$. The reader may refer to Kausel and Peek (1982) for a comprehensive presentation of the solution steps involved in this problem. The derivation of the inverse of the stiffness matrix in the frequency-wavenumber domain yields a flexibility matrix $\mathbf{f}^{pn}$, the components of which express the displacements at the *p*th interface due to unit harmonic loads applied at the *n*th interface. This matrix has the following form:

$$\mathbf{f}^{pn} = \begin{bmatrix} f_{xx}^{pn} & 0 & f_{xz}^{pn} \\ 0 & f_{yy}^{pn} & 0 \\ f_{zx}^{pn} & 0 & f_{zz}^{pn} \end{bmatrix} \tag{3.26}$$

The elements of the flexibility matrix depend on the propagation modes, the wavenumber κ and the Rayleigh or Love eigenvalues associated with the in plane or antiplane modes respectively. Subsequently the spatial domain displacements can be obtained analytically (due to the fact that the propagation modes $\boldsymbol{\varphi}$ are independent of the wavenumber κ) by well-known inverse integral transforms (Kausel and Peek, 1982). The Green's functions for point loads are derived by considering the limit of disk loads when the radius of the load approaches zero (Kausel, 1981).

3.2.2.2 Formulation for semi-infinite medium

The formulation of the TLM presented in the preceding section is applicable in the cases of media having finite depth, such as a layered stratum over rigid bedrock. However for media of infinite extent, such as a layered body with a flexible halfspace underneath, special care should be taken to prevent wave reflections at the boundary of the discrete model. This can be achieved by approximating the halfspace impedances with polynomial expressions, which match the structure of the stiffness matrices of the layers. Aim of this manipulation is to keep the method capable of solving the eigenvalue problem. One of the available approximation is the paraxial, which can be realized by expanding the exact impedances given by Eq. (3.3) and (3.4) in Taylor series in the wavenumber κ, and retaining only this number of terms, which convert the true halfspace stiffnesses to a similar form with the layer stiffness matrices in the TLM. Since the eigenvalue problem solved by the TLM is linear and

quadratic for SH and SV-P waves respectively, the paraxial approximation is essentially obtained in the form (Maeda and Kausel, 1991) :

$$\mathbf{K}_{SH} = \mathrm{i}\,\Omega\,\rho_s\;V_s\left(1-\frac{0.5}{S_s^2}\right) \tag{3.27}$$

$$\mathbf{K}_{SVP} = \Omega\,\rho_s\left[\mathrm{i}\begin{Bmatrix}V_s & 0\\ 0 & V_p\end{Bmatrix}+\begin{Bmatrix}0 & V_p-2V_s\\ V_p-2V_s & 0\end{Bmatrix}\frac{1}{S_s} + \begin{Bmatrix}V_s-2V_p & 0\\ 0 & \left(V_p-2V_s\right)\left(V_p/V_s\right)^2\end{Bmatrix}\frac{\mathrm{i}}{2S_s^2}\right] \tag{3.28}$$

For values of Poisson's ratio greater than $1/3$, the term $V_p - 2V_s$ on the diagonal of the third matrix changes sign, at which point the paraxial approximation turns unphysical (Maeda and Kausel, 1991). Numerical investigations suggest that this problem can be overcome by setting this term to zero. The expressions in Eq. (3.27) and (3.28) are incorporated into the global stiffness matrix and the eigenvalue problem can be readily solved. However a paraxial approximation alone is not sufficient to represent a halfspace. Spurious reflections take place at the paraxial boundary, which can lead to unstable reverberation phenomena, if no remedies are employed. It has been proved, that results are substantially improved if the approximate halfspace stiffnesses are used with a buffer layer that has the same material properties as the halfspace and is subdivided into an appropriate number of thin layers (Park, 2002). The theoretical documentation of TLM in the preceding section underlies the program PUNCH, which is used for the computation of the Green's functions presented in the next section.

3.2.2.3 Soil deposit underlain by rigid rock

Natural soil deposits are frequently underlain by very stiff material or bedrock at shallow depth, rather than extending to practically infinite depth as the homogeneous halfspace implies. The dimensionless Green's functions for a soil deposit underlain by rigid bedrock at shallow depth are calculated by using the TLM. Contrary to the case of a homogeneous halfspace, the dimensionless Green's functions depend not only on the Poisson's ratio but also on the ratio d/r, where d is the thickness of the stratum.

Perfectly elastic medium - Viscoelastic medium

The real and imaginary part of the vertical g_{zz} and radial g_{rr} Green's functions for sources and point load on the surface of a perfectly elastic layer and a viscoelastic layer over rigid bedrock for two levels of hysteretic material damping ξ_s and $d/r = 3$ are presented in Figure 3.4. For the medium without any internal dissipation, resonance phenomena (straight lines in Figure) appear associated with amplitudes, which diverge when a certain relation is satisfied between the depth of the stratum and the frequency exciting force. The resonant frequencies of the vertical and radial Green's functions of a perfectly elastic stratum coincide with the natural frequencies of the longitudinal and lateral vibration

respectively of a one-dimensional rod with one end fixed and the other free and ascribed the same rigidity and thickness of the stratum (Kobori et al., 1971):

$$\omega_H = \frac{2\,l+1}{2\,d}\pi\,V_s \tag{3.29}$$

$$\omega_V = \sqrt{\frac{2(1-v_s)}{1-2\,v_s}}\omega_H \tag{3.30}$$

where l is an integer. Another source of resonance is the vanishment of the group velocity of a mode or the agreement of the phase velocity between two modes, which corresponds to roots of the frequency equation for Rayleigh waves (Kobori et al., 1971). As it can observed in Figure 3.4, the imaginary part of the Green's functions, which represents the energy dissipation by waves propagating away from the source load, is exact zero below the first resonance frequencies of the stratum. In this range, any propagation of surface waves is impossible and therefore, no attenuation takes place since downward wave radiations of body waves do not occur because of the absolute wave reflections at the boundary surface of the rigid halfspace.

For the viscoleastic stratum the resonant amplitudes are finite and the variations of the Green's functions with the parameter r_o become smoother as the damping increases. The amount of energy attenuation owing to internal dissipation is added to that owing to wave radiation. This is clearly demonstrated in the frequency range below the lowest resonant frequency, where the dissipative attenuation prevails over the radiative one.

Effects of the ratio of stratum thickness to the distance of the Green's functions calculation point

The real and imaginary part of the azimuthial Green's functions $g_{\theta\theta}$ for a viscoelastic layer of various ratios d/r and the corresponding ones of a viscoelastic halfspace with the same material properties are presented in Figure 3.5. The results indicate that an increase of the ratio d/r is associated with a decrease of the amplitudes and a shift of the resonance peaks to the left of the normalized frequencies due to the reduction of the resonance frequency. For adequate large values of the ratio d/r, the stratum shows a close resemblance to the case of a halfspace in the entire low-frequency range and the differences between the two mediums become almost undistinguishable as the dimensionless frequency increases. The convergence of the dynamic response of the stratum to the halfspace solution is more notable in the high frequency range as Figure 3.5 demonstrates. Even for small values of the ratio such as $d/r = 2$, the two solutions are similar, since at high frequencies waves of short wavelength produced at the source on the surface of a stratum attenuate rapidly before they reach the boundary of the rigid bedrock and therefore the receiver ‘‘perceives’’ the supporting boundary as a halfspace.

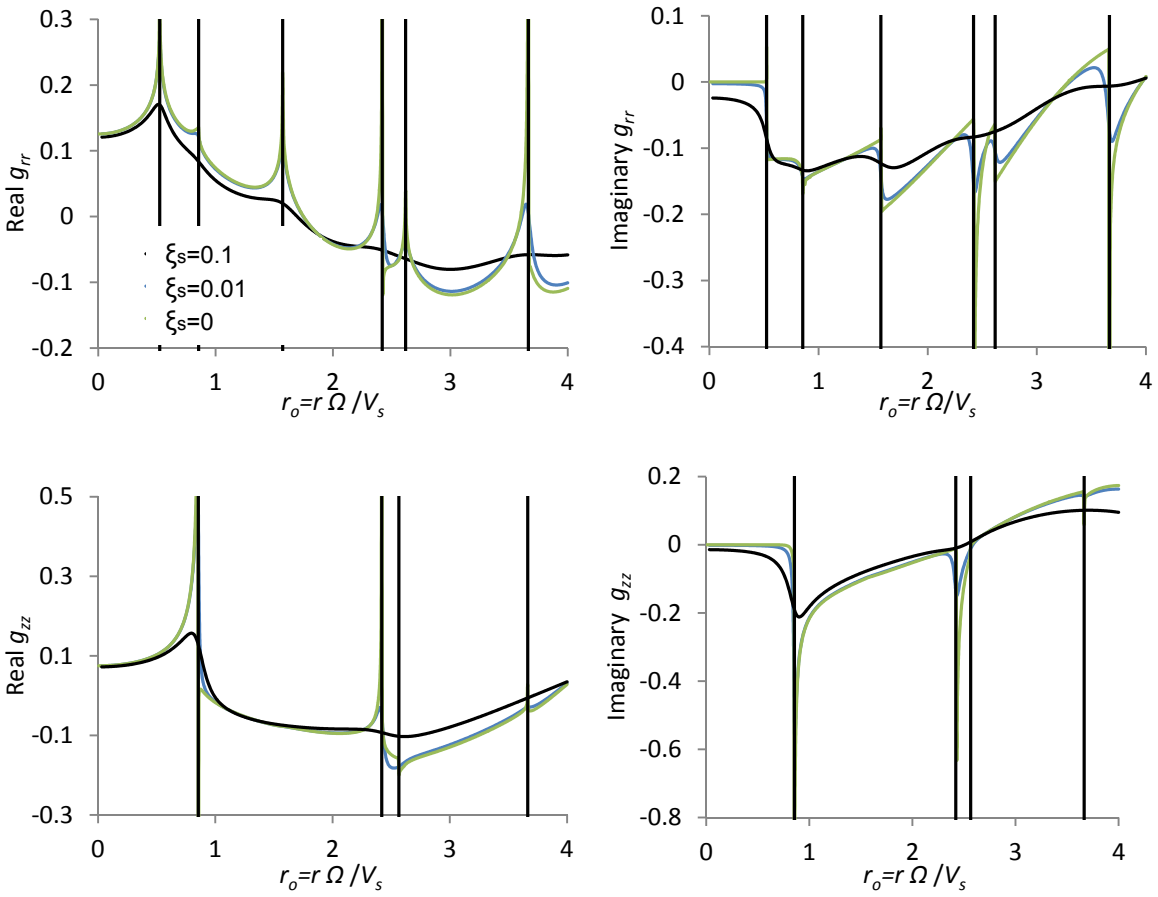

Figure 3.4: Real and imaginary part of the normalized Green's functions g_{rr} and g_{zz} for a layer over rigid bedrock for various damping ratios, $d/r = 3$, $\nu_s = 0.2$ (source and point load on the surface).

Layered medium

The real and imaginary part of the coupled Green's functions g_{rz} for two layers of equal thickness and stratum's total thickness ratio $d/r = 3$ are calculated. The cases investigated are chosen to represent different levels of contrast between the stiffness of the two layers, expressed in terms of the ratio of the shear modulus $B = \mu^{bottom}/\mu^{top}$. The results are normalized with the shear modulus of the top layer and are depicted in Figure 3.6. It is observed that as the ratio B decreases, the system becomes more flexible and the first resonance frequency shifts to lower values of the parameter r_o. This phenomenon may be readily perceived if the system is considered as a massive body of fixed stiffness (top layer) that is attached to a spring with gradually reduced stiffness. Turning point for the dynamic response is the value $B = 1$, which represents the case of one layer with the material properties of the top layer. For adequate large values of B, the solution converges to that of one layer with half thickness of the initial system, since the bottom layer acts as a supporting rigid halfspace.

As might be expected, a multi-layered deposit over rigid bedrock or over a halfspace of finite stiffness exhibits a more complex dynamic response due to the repeated reflection and refraction of traveling waves at the interfaces of the layers. In that case, the values of the Green's functions over the

frequency depend largely on the sharpness of the ratios of the material properties between the layers and their thickness.

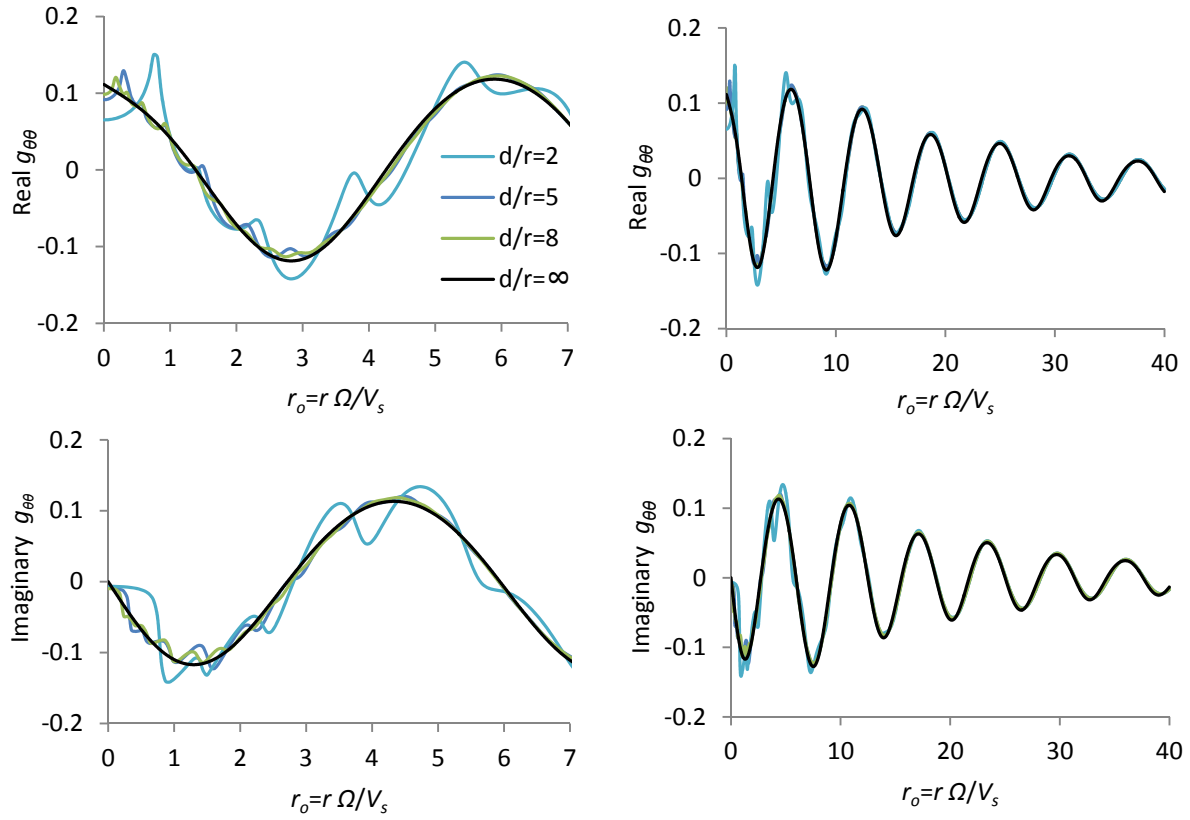

Figure 3.5: Normalized azimuthial Green's functions $g_{\theta\theta}$ for a layer over rigid bedrock for various ratios d/r, $\xi_s = 0.05$, $\nu_s = 0.3$ (source and point load on the surface).

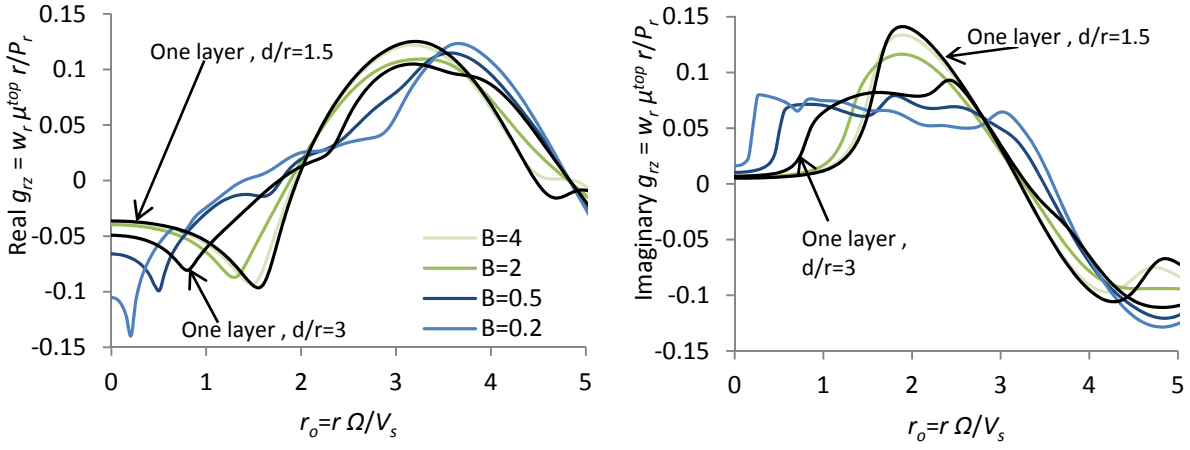

Figure 3.6: Normalized Green's functions g_{rz} for two layers over rigid bedrock for various ratios of shear modulus $B = \mu^{bottom}/\mu^{top}$, $\nu_s^{top} = 0.15$, $\nu_s^{bottom} = 0.30$, $\xi_s^{top} = 0.07$, $\xi_s^{bottom} = 0.1$ (source and point load on the surface).

3.3 Coupled FEM-BEM for multiple surface foundations

The coupling of the soil medium with multiple structures requires solution of a mixed-boundary value problem, involving vanishing tractions on the free surface beyond the foundation of each structure and prescribed displacements at the foundations interfaces with the underlying soil medium. Halfspace[1)] fundamental solutions take intrinsically into account the conditions of zero normal and shear stresses that characterize the free surface. Thus, we do not need to consider the halfspace as half of an infinite domain and discretization beyond the soil-foundations interfaces is avoided. On the contrary, use of full-space fundamental solutions imposes discretization of a limited portion of the infinite halfspace's surface, which leads to spurious artificial wave reflection on the interface between the discretized and undiscretized region (Tosecký, 2005). Additional grid around the foundations can be bypassed only by approximate formulations, which introduce an incomplete bonding between the soil halfspace and the foundations (Mohammadi and Karabalis, 1995).

The analyses conducted for the calculation of the impedance matrices of adjacent circular foundations are carried out by means of a substructure technique, which couples the BEM and FEM in the frequency domain. The surface halfspace Green's functions are used to formulate the boundary integral equation of the foundations. The method was first developed by Savidis and his co-workers (Hirschauer et al., 1999; Hirschauer, 2001); in what follows, the fundamental equations which describe the mixed boundary value problem are derived appropriately to account for the existence of more than one foundation.

3.3.1 BEM formulation

In elastodynamics starting point of the derivation of a boundary integral formulation in the frequency domain is the Lamé-Navier's equation given by Eq. (3.12). This is the governing differential equation for an elastic, isotropic and homogeneous solid of volume such as a halfspace. Elimination of the time variable in order to transform the problem into a static-like form is the next step. Well-established procedures such as those related with the dynamic reciprocal theorem or variatonal principles (Manolis and Beskos, 1988) furnish subsequently an expression for the displacements v_i $(i = x, y, z)$ on the surface Γ of a halfspace medium assuming zero body forces at any point **x** according to:

$$v_i(\mathbf{x}) = \int_{\Gamma} U_{ij}(\mathbf{x}\,;\mathbf{x}')\; q_j(\mathbf{x}')\mathrm{d}\Gamma \tag{3.31}$$

where $U_{ij}(\mathbf{x};\mathbf{x}')$ is the halfspace Green's function for surface displacements in the *i*th direction at $(x, y, 0)$ due to unit harmonic load acting in the *j*th direction at $(x', y', 0)$ and q_j represents the stress acting on the surface Γ. The free traction condition at the surface of the soil is intrinsically fulfilled;

1) To avoid confusion, the term ''halfspace'' herein refers to an unbounded free surface whether the soil medium extends downwards to infinite or not.

thus, the discretization is confined to the foundation-soil interface and the halfspace Green's functions for surface tractions are not part of the solution. The integral equation is discretized into *N* elements of uniform rectangular shape, within each of them the contact stresses are assumed to be constant. By doing so, the soil displacements will be transformed to a finite number of displacement degrees of freedom in the centre of the $k = 1,2..N$ contact elements:

$$v_i(\mathbf{x}^l) = \sum_{k=1}^{\mathrm{N}} \int_{\Delta \mathrm{A}^k} U_{ij}(\mathbf{x}^l; \mathbf{x}^k) q_j(\mathbf{x}^k) \mathrm{dA}^k \tag{3.32}$$

In case of more than one structure, the boundary integral Eq. (3.32) is expressed in the form:

$$v_i(\mathbf{x}^{lm}) = \sum_{p=1}^{R} \sum_{k=1}^{N_p} \int_{\Delta \mathrm{A}^{lm}} \int_{\Delta \mathrm{A}^{kp}} U_{ij}^{mp}(\mathbf{x}^l; \mathbf{x}^k)\, q_j(\mathbf{x}^{kp}) \mathrm{dA}^{lm}\, \mathrm{dA}^{kp} \tag{3.33}$$

where $v_i(\mathbf{x}^{lm})$ represents the displacement vector at the *l*th interaction point of the *m*th foundation, $q_j(\mathbf{x}^{kp})$ corresponds to the traction vector over the *k*th subregion of the *p*th foundation, *R* is the total number of the surfaces, N_p is the number of subdivisions of the *p*th foundation and $\Delta \mathrm{A}^{lm}$ corresponds to the area of the *l*th region of the *m*th foundation (Figure 3.7). The combined effect of all contact stresses acting on the soil-interface on the soil displacements at all interaction points for the *R* foundations can be expressed in matrix notation as follows:

$$\begin{Bmatrix} \mathbf{v}^1 \\ \vdots \\ \mathbf{v}^m \\ \vdots \\ \mathbf{v}^p \\ \vdots \\ \mathbf{v}^R \end{Bmatrix} = \begin{bmatrix} \mathbf{F}^{11} & \dots & \mathbf{F}^{1m} & \dots & \mathbf{F}^{1p} & \dots & \mathbf{F}^{1R} \\ \vdots & \ddots & \vdots & \ddots & \vdots & \ddots & \vdots \\ \mathbf{F}^{m1} & \dots & \mathbf{F}^{mm} & \dots & \mathbf{F}^{mp} & \dots & \mathbf{F}^{mR} \\ \vdots & \ddots & \vdots & \ddots & \vdots & \ddots & \vdots \\ \mathbf{F}^{p1} & \dots & \mathbf{F}^{pm} & \dots & \mathbf{F}^{pp} & \dots & \mathbf{F}^{pR} \\ \vdots & \ddots & \vdots & \ddots & \vdots & \ddots & \vdots \\ \mathbf{F}^{R1} & \dots & \mathbf{F}^{Rm} & \dots & \mathbf{F}^{Rp} & \dots & \mathbf{F}^{RR} \end{bmatrix} \begin{Bmatrix} \mathbf{q}^1 \\ \vdots \\ \mathbf{q}^m \\ \vdots \\ \mathbf{q}^p \\ \vdots \\ \mathbf{q}^R \end{Bmatrix} \tag{3.34}$$

in which:

$$\mathbf{F}^{mp} = \sum_{p=1}^{R} \sum_{k=1}^{N_p} \int_{\Delta \mathrm{A}^{lm}} \int_{\Delta \mathrm{A}^{kp}} U_{ij}^{mp}(\mathbf{x}^l; \mathbf{x}^k)\ \mathrm{dA}^{lm}\, \mathrm{dA}^{kp} \tag{3.35}$$

By omitting the superscripts equation can be written in inversed form as:

$$\mathbf{q} = \mathbf{F}^{-1}\, \mathbf{v} \tag{3.36}$$

All quantities in Eq. (3.36) are complex and frequency dependent. The displacement boundary conditions, necessary to solve the mixed boundary problem, are imposed through the coupling of soil and each foundation (compatibility condition). The latter is modeled in a finite element conception.

3.3.2 FEM formulation

In matrix notation, the FE-discretized equation of motion of R independent structures built on a compliant soil can be expressed in the frequency domain in terms of the nodal displacements $\mathbf{u}$ as:

$$\begin{bmatrix} \mathbf{S}_1 & 0 & 0 & 0 & 0 \\ 0 & \ddots & 0 & 0 & 0 \\ 0 & 0 & \mathbf{S}_m & 0 & 0 \\ 0 & 0 & 0 & \ddots & 0 \\ 0 & 0 & 0 & 0 & \mathbf{S}_R \end{bmatrix} \begin{Bmatrix} \mathbf{u}^1 \\ \vdots \\ \mathbf{u}^m \\ \vdots \\ \mathbf{u}^R \end{Bmatrix} = \begin{Bmatrix} \mathbf{V}^1 \\ \vdots \\ \mathbf{V}^m \\ \vdots \\ \mathbf{V}^R \end{Bmatrix} - \begin{Bmatrix} \mathbf{Q}^1 \\ \vdots \\ \mathbf{Q}^m \\ \vdots \\ \mathbf{Q}^R \end{Bmatrix} \tag{3.37}$$

where $\mathbf{S}^m$ represents the complex dynamic stiffness matrix of the mth structure, while $\mathbf{Q}^m$ and $\mathbf{V}^m$ are the vectors of the fequency dependent interaction and external forces respectively. The matrix $\mathbf{S}^m$ is specified as:

$$\mathbf{S}^m = -\omega^2 \mathbf{M}^m + \mathrm{i}\omega \mathbf{D}^m + \mathbf{R}^m \tag{3.38}$$

where ω, $\mathbf{M}^m$, $\mathbf{D}^m$, $\mathbf{R}^m$ stand for the natural frequencies, mass matrix, damping matrix and static stiffness matrix of the mth structure. Eq. (3.37) can be decomposed into the displacements $\mathbf{u}_I^m$ that correspond to the interaction surface and the rest displacements $\mathbf{u}_T^m$. Subsequently, the matrix equation of motion for the mth structure is given by:

$$\begin{bmatrix} \mathbf{S}_{TT}^m & \mathbf{S}_{TI}^m \\ \mathbf{S}_{IT}^m & \mathbf{S}_{II}^m \end{bmatrix} \begin{Bmatrix} \mathbf{u}_T^m \\ \mathbf{u}_I^m \end{Bmatrix} = \begin{Bmatrix} \mathbf{V}_T^m \\ \mathbf{V}_I^m \end{Bmatrix} - \begin{Bmatrix} \mathbf{0} \\ \mathbf{Q}^m \end{Bmatrix} \tag{3.39}$$

Accordingly, for the R structures Eq. (3.37) is written by use of Eq. (3.39) in vector-tensor notation:

$$\mathbf{S}\,\mathbf{u} = \mathbf{V} - \mathbf{Q} \tag{3.40}$$

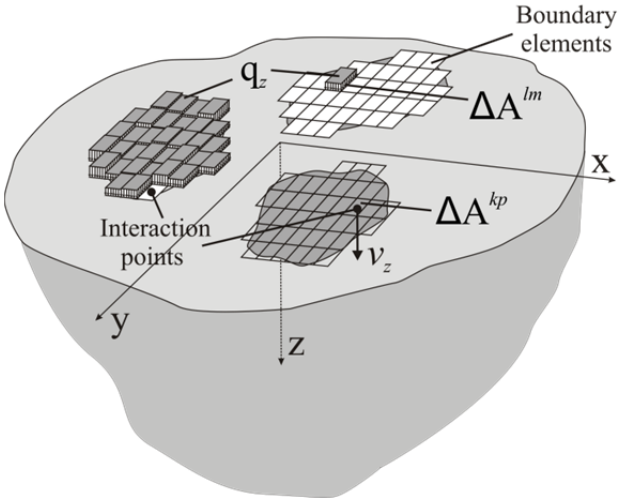

Figure 3.7: Spatial discretization of the contact areas between foundations and soil with constant contact stresses within each element.

The diagonal matrix $\mathbf{S}$ is evaluated with aid of the commercial Finite Element Software ©ANSYS (2013b). The determination of the still unknown vector of interaction forces $\mathbf{Q}$ is accomplished through the coupling of the two substructures. This procedure is described in the next section.

3.3.3 Coupling FEM and BEM

The contact stresses $\mathbf{q}$ can be transformed, on an energy equivalent basis, to the interaction forces $\mathbf{Q}$ with the aim of the matrix $\mathbf{T}_q$ as follows:

$$\mathbf{Q} = \mathbf{T}_q \, \mathbf{q} \tag{3.41}$$

The structural nodes along the soil-foundations interface do not generally coincide with the interaction points, thus the compatibility condition for the R foundations is satisfied by use of a transformation matrix $\mathbf{T}_u$ as follows:

$$\mathbf{v} = \mathbf{T}_u \, \mathbf{u} \tag{3.42}$$

The matrices $\mathbf{T}_\mathrm{u}$ and $\mathbf{T}_\mathrm{q}$ contain the shape functions- evaluated at the interaction points- of the finite elements used to model the foundations. In the context of this work, 8-nodes solid elements (SOLID45) are employed. Substitution of Eq. (3.42) into (3.36) and Eq. (3.36) into Eq. (3.41) yields:

$$\mathbf{Q} = \mathbf{T}_q \, \mathbf{F^{-1}} \, \mathbf{T}_\mathrm{u} \, \mathbf{u} = \mathbf{S}_\mathrm{soil} \, \mathbf{u} \tag{3.43}$$

where $\mathbf{S}_\mathrm{soil}$ stands for the subgrade stiffness with respect to the finite element nodes at the interface of the foundations. Finally, substitution of Eq. (3.43) into Eq. (3.40) furnishes the equation of motion of the total system:

$$[\mathbf{S} + \mathbf{S}_\mathrm{soil}] \, \mathbf{u} = \mathbf{K} \, \mathbf{u} = \mathbf{V} \tag{3.44}$$

Alternatively, we can write:

$$\mathbf{u} = \mathbf{C} \, \mathbf{V} \tag{3.45}$$

Eq. (3.45) is a linear system with only unknowns the displacements $\mathbf{u}$ and can be solved by standard methods for harmonic loads $\mathbf{V} = \mathbf{V}\, \mathrm{e}^{\mathrm{i}\Omega t}$ and a sequence of frequencies Ω. Due to the fact that the above formulation makes use of rectangular volume elements for the structure lying on the interaction horizon, the calculation of the impedance functions for circular foundations, presented in the next sections, is accomplished by approximating the soil-foundations interfaces as dentiform areas consisting of equal square sub-regions, in a manner that the total areas size equals that of a corresponding circle. A similar procedure was followed by Wong and Luco (1976). In all succeeding calculations, a perfect bonding between foundations and the underlying soil is considered. Thus,

rocking and vertical translations are associated with shear apart from normal stresses and horizontal translation and torsion are related with normal apart from shear stresses.

3.4 Impedance functions for single circular foundations

For an isolated rigid massless circular foundation (and without including structural damping) on the free surface (corresponds to zero values for the off-diagonal elements of matrix **F**) and subjected to harmonic external forces P_i $(i = 1,2,3)$ and moments M_i $(i = 4,5,6)$ according to Figure 3.8, the matrix **K** in Eq. (3.44) becomes the foundation impedance matrix and is obtained by inversion of **C** in Eq. (3.45). In this case, Eq. (3.44) can be written in matrix notation and normalized form as:

$$\begin{Bmatrix} P_1/\mu R^2 \\ P_2/\mu R^2 \\ P_3/\mu R^2 \\ M_4/\mu R^3 \\ M_5/\mu R^3 \\ M_6/\mu R^3 \end{Bmatrix} = \begin{bmatrix} K_{11} & 0 & 0 & 0 & K_{15} & 0 \\ 0 & K_{22} & 0 & K_{24} & 0 & 0 \\ 0 & 0 & K_{33} & 0 & 0 & 0 \\ 0 & K_{42} & 0 & K_{44} & 0 & 0 \\ K_{51} & 0 & 0 & 0 & K_{55} & 0 \\ 0 & 0 & 0 & 0 & 0 & K_{66} \end{bmatrix} \begin{Bmatrix} u_1/R \\ u_2/R \\ u_3/R \\ \varphi_1 \\ \varphi_2 \\ \varphi_3 \end{Bmatrix} \tag{3.46}$$

The components of matrix **K** are the impedance functions for each particular harmonic excitation of the active degrees of freedom. In soil dynamics, it is convenient to express the impedance functions in the following complex form:

$$K_{ij} = k_{ij} + \mathrm{i}\, a_o\, c_{ij} = k_{ij} + \mathrm{i}\, C_{ij} \tag{3.47}$$

where the first index i indicates the direction of the resultant forces along or the resultant moments about the principal axes, whereas the second index j indicates the direction of the displacements along or the rotations about the principal axes. The dimensionless frequency factor is given by:

$$a_o = \frac{\Omega\, R}{V_s} \tag{3.48}$$

The real part k_{ij} of Eq. (3.47) reflects the stiffness and inertia of the supporting medium; the imaginary component c_{ij} reflects the radiation and material damping of the system. The former is the result of energy dissipation of the waves propagating away from the foundation, whereas the latter is related to the hysteric cyclic behavior of the soil. Both real and imaginary part are frequency-dependent and thus, can be presented as functions of the normalized frequency a_o for different Poisson's ratios ν_s. Regarding the coupling terms, because of the symmetry in Eq. (3.46) $K_{42} = K_{24}$ and $K_{51} = K_{15}$. Due to the axis of symmetry of the foundation $K_{51} = -K_{42}$.

3.4.1 Homogeneous halfspace

Although the problem of circular plates underlain by homogeneous halfspace has been exhaustively investigated in the past (Luco and Westman, 1971; Veletsos and Wei, 1971; Luco and Mita, 1987; Triantafyllidis and Prange, 1998) it is deemed necessary to provide results obtained by the FEM-BEM formulation for verification purposes and moreover, aiming to supply the succeeding foundation-soil-foundation analyses with a benchmark solution. The dimensionless impedance functions for all modes of vibration of a circular rigid foundation on a homogeneous elastic halfspace are presented in Figure 3.9 and Figure 3.10 as a function of the frequency parameter a_o. The corresponding results obtained with the aid of the Precise Integration Method (PIM) (Mykoniou et al., 2012) are also provided. The natural phenomena associated with the response are well known and need not be further elaborated herein. Nevertheless, the following main trends are worthy of note: The dynamic stiffness coefficients with the exception of the swaying mode exhibit a strong sensitivity to variations in the frequency parameter for large values of the Poisson's ratio. Regarding the damping coefficients, smaller amount of wave energy is radiated during rocking and torsional oscillations in comparison with vertical and horizontal oscillations independent of the Poisson's ratio. Incorporation of material (hysteretic) damping into the soil yields merely realistic results of the system's response in the low frequency range.

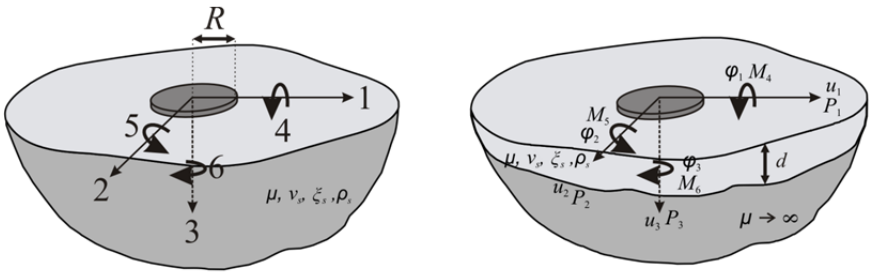

Figure 3.8: Single foundation models and coordinate system for a single foundation on halfspace (left) and on stratum (right).

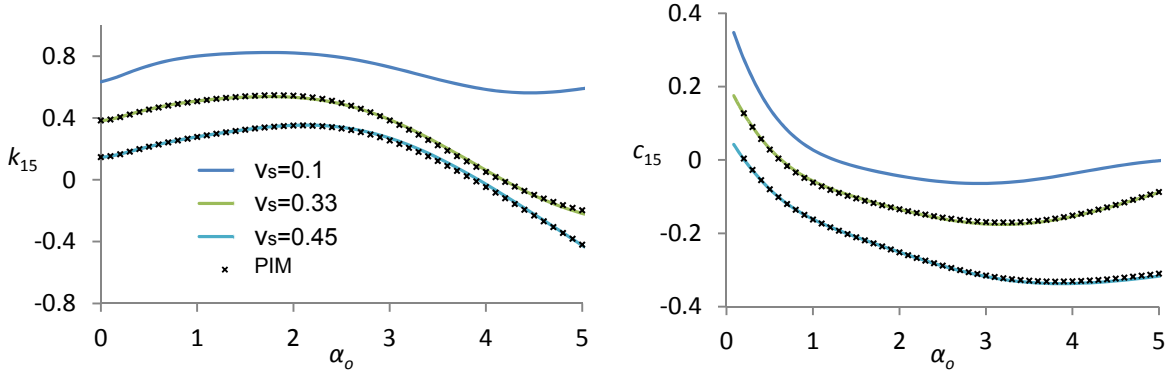

Figure 3.9: Real (left) and imaginary (right) part of the impedance matrix coupled term for a circular foundation on elastic homogeneous halfspace (horizontal-rocking mode).

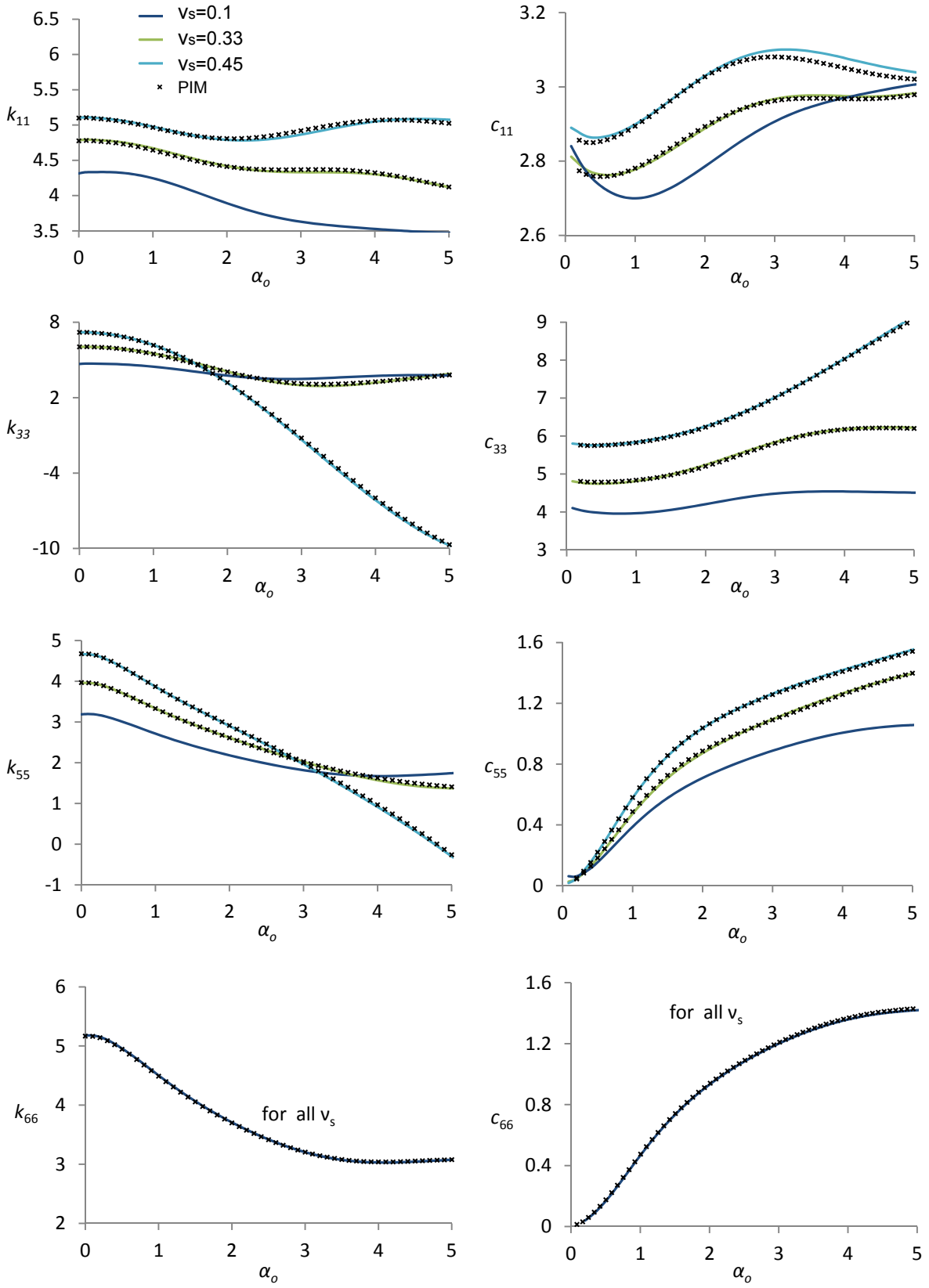

Figure 3.10: Real (left) and imaginary (right) part of the impedance matrix diagonal terms for a circular foundation on elastic homogeneous halfspace (horizontal, vertical, rocking, torsional modes).

3.4.2 Bedrock at shallow depth

The dimensionless impedance functions for all modes of vibration of a circular rigid foundation on a layer over rigid bedrock (Figure 3.8) are presented in Figure 3.11 and Figure 3.12 as a function of the frequency parameter a_o. The thickness of the stratum is expressed by means of the ratio d/R. Observation of the real part of the impedance functions reveals that the depth of the layer affects strongly the rigidity of the system since the bedrock imposes another boundary condition which is absent in a semi-infinite medium. The frequency spring parameter exhibits undulations associated with the resonance phenomena discussed in 3.2.2.3. For rocking modes (torsional and rocking), the variation with the frequency is relatively smooth and similar to the halfspace solution, due to the cancelling effect of the exciting force distribution. In addition, the system's overall stiffness is shifted to different magnitudes in comparison with an unbounded medium as indicated by the stiffness values for $a_o = 0$. Mylonakis et al. (2006) provide formulas for the calculation of the surface circular rigid footings static stiffness as a function of the ratio d/R and the static stiffness of a homogeneous halfspace with the same material properties for the corresponding mode. For all possible modes, but for the coupling rocking-swaying, approximating expressions presented in Table 3.1 are given. In order to determine the static stiffness for the coupled mode, the amplitudes of the corresponding impedance function's real part for $a_o = 0$ are calculated for various ratios R/d and $\nu_s = 0.33$. The results are presented in Figure 3.13. It should be noted that the effects of layer's depth and Poisson's ratio are practically uncoupled. Thus, the tendency shown is common for all Poisson's ratios. As opposed to other modes, the coupling static stiffness does not increase monotonically with an increase of R/d; systems consisting of surface foundations over shallow deposits are more flexible in this mode compared with an unbounded medium. Extrapolation of the values shown in Figure 3.13 leads to the expression proposed in Table 3.1.

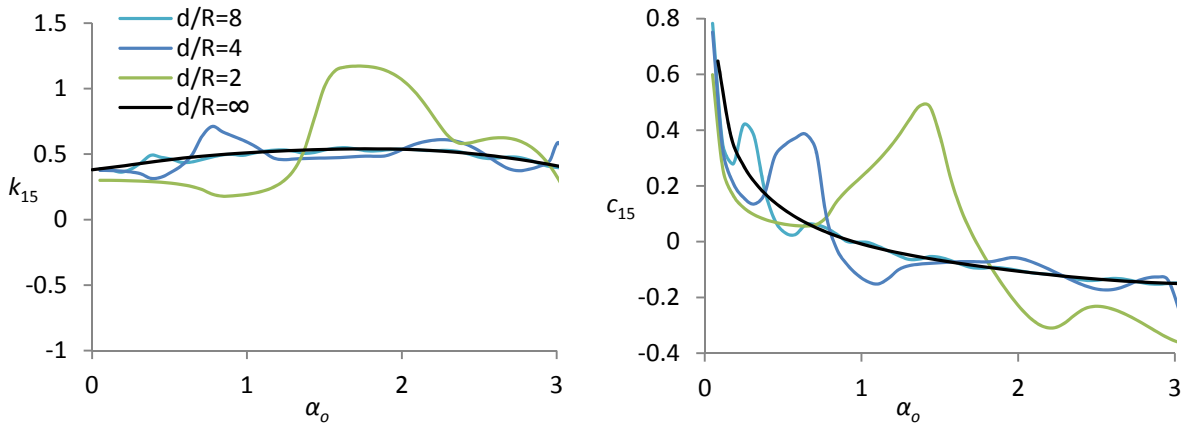

Figure 3.11: Real (left) and imaginary (right) part of the impedance matrix coupled term for a circular foundation on stratum over rigid bedrock, $\xi_s = 0.05$, $\nu_s = 0.33$ (horizontal-rocking mode).

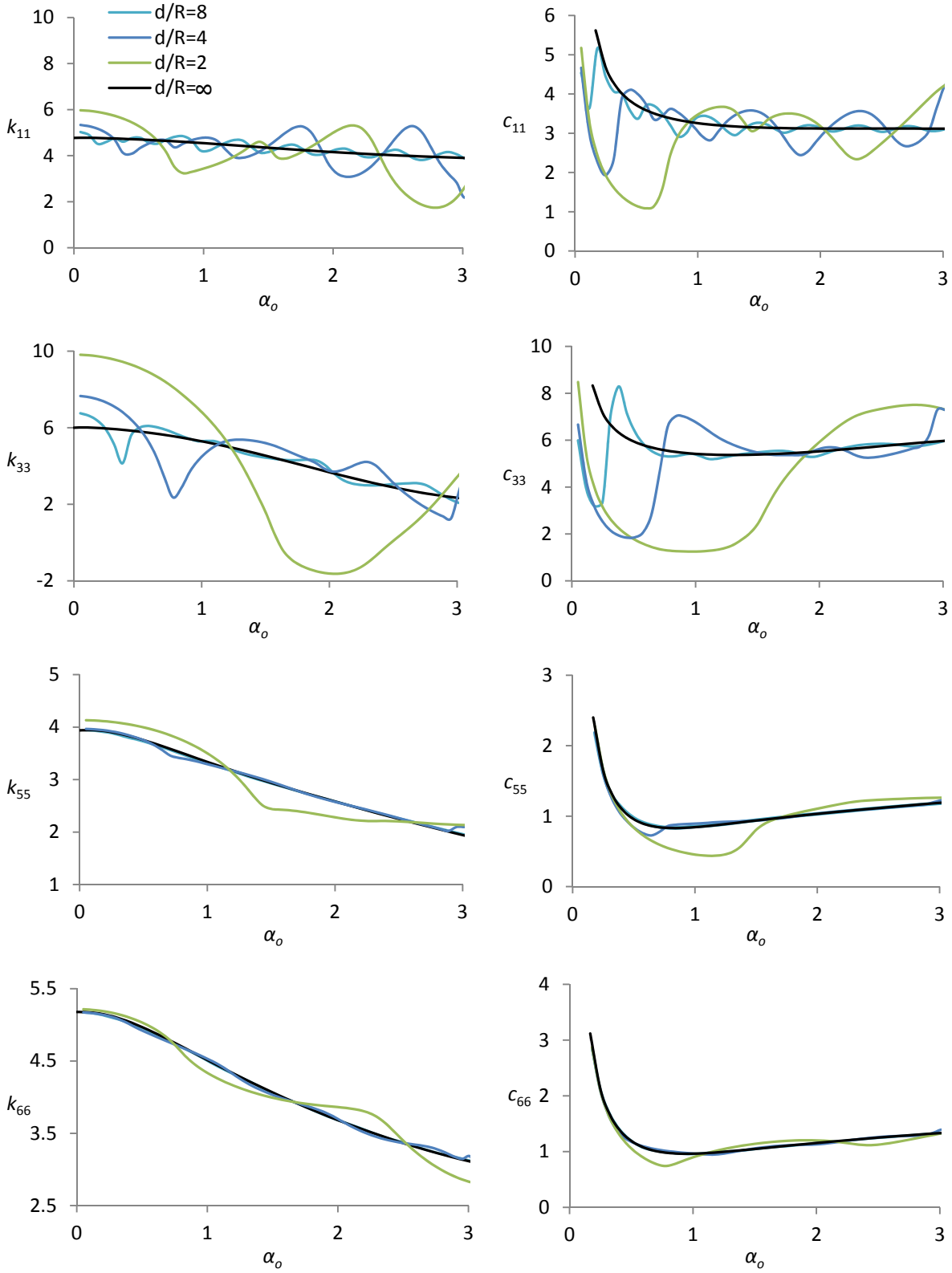

Figure 3.12: Real (left) and imaginary (right) part of the impedance matrix diagonal terms for a circular foundation on stratum over rigid bedrock, $\xi_s = 0.05$, $\nu_s = 0.33$ (horizontal, vertical, rocking, torsional modes).

The waviness of the response is also noticeable for the dashpot coefficient. From a practical viewpoint, it is more significant that below the first resonance frequency of each mode, the radiation damping is negligible (and would be exact zero if no internal damping is considered as explained in

3.2.2.3). This phenomenon could have a great impact on liquid-storage tanks with natural frequencies in this range, regarding their response under horizontal and vertical ground excitation. For rocking modes (torsional and rocking), the amount of wave radiation energy in a soil deposit is practically the same with that of halfspace.

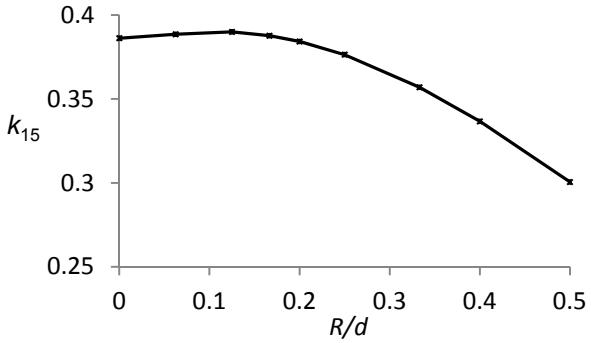

Figure 3.13: Extrapolation of the values for the coupled static spring constant $k_{15}(a_o = 0)$ corresponding to circular foundation on stratum over rigid bedrock, $\nu_s = 0.33$.

Table 3.1: Approximating expressions for the static stiffness of circular rigid foundations on stratum over bedrock (Mylonakis et al., 2006).

Response mode	Static stiffness
Vertical	$\frac{4\,\mu\,R}{1-\nu_s}\left(1+1.3\frac{R}{d}\right)$
Horizontal	$\frac{8\,\mu\,R}{2-\nu_s}\left(1+0.5\frac{R}{d}\right)$
Rocking	$\frac{8\,\mu\,R^3}{3(1-\nu_s)}\left(1+0.17\frac{R}{d}\right)$
Torsional	$\frac{16\,\mu\,R^3}{3}\left(1+0.10\frac{R}{d}\right)$
Coupling Horizontal-Rocking (Present study)	$\frac{16\,\pi\,\mu\,R^2}{3(1-2\nu_s)}\left[-0.53\left(\frac{R}{d}\right)^2+0.10\frac{R}{d}+0.39\right]$

3.5 Impedance functions for multiple circular foundations

Having determined the response of single foundations to external loads, the attention is turned to the dynamic behavior of adjacent surface rigid circular foundations. A set of parametric analyses is conducted, with respect to the distance, the number and the spatial arrangement of the foundations as well as the soil conditions. Regarding the latter, homogeneous halfspace and uniform stratum over

rigid base are examined, which are undoubtedly two idealizations of soil profiles. More complex soil conditions, such as media consisting of multiple layers over halfspace, bedrock with certain flexibility, or other kind of soil heterogeneities are frequently more realistic cases to be encountered. Nevertheless, regarding the inherent uncertainties of the complex field under study, the soil variables at play are limited in order to facilitate the survey of the relative influence of the soil conditions on the dynamic subsoil coupling of adjacent foundations. Additionally, it is known from the analysis of single surface foundations on stratum that the solution converges to the halfspace for special limiting cases. Therefore, the two extreme cases investigated should be understood as benchmarks, which bound to some extent other soil profiles.

The matrix $\mathbf{K}$ in case of one circular footing contains only one coupled term, namely the swaying-rocking component. On the contrary, in a general foundation-soil-foundation problem (by arbitrary arrangement of the circular foundations in space) it becomes a fully populated matrix, that is to say, any mode of vibration is related with responses in all directions. Furthermore, each of the non-zero components of the impedance matrix of a single-independent foundation is different to the corresponding components of the impedance matrix of the same foundation when adjacent foundations exist. Besides, it is necessary to determine the coupled -between the foundations- force-displacement relationships, since excitation of one footing causes responses in the nearby footings, which in return produce a secondary wavefield which influences the former one; the foundations are dynamically coupled through the soil due to the scattered wavefields between them.

The frequency dependent dimensionless stiffness matrix of an assembly of R foundations can be defined as follows:

$$\mathbf{K}_{group} = \begin{bmatrix} \mathbf{K}^{11} & \dots & \mathbf{K}^{1m} & \dots & \mathbf{K}^{1p} & \dots & \mathbf{K}^{1R} \\ \vdots & \ddots & \vdots & \ddots & \vdots & \ddots & \vdots \\ \mathbf{K}^{m1} & \dots & \mathbf{K}^{mm} & \dots & \mathbf{K}^{mp} & \dots & \mathbf{K}^{mR} \\ \vdots & \ddots & \vdots & \ddots & \vdots & \ddots & \vdots \\ \mathbf{K}^{p1} & \dots & \mathbf{K}^{pm} & \dots & \mathbf{K}^{pp} & \dots & \mathbf{K}^{pR} \\ \vdots & \ddots & \vdots & \ddots & \vdots & \ddots & \vdots \\ \mathbf{K}^{R1} & \dots & \mathbf{K}^{Rm} & \dots & \mathbf{K}^{Rp} & \dots & \mathbf{K}^{RR} \end{bmatrix} \tag{3.49}$$

where:

$$\mathbf{K}^{mp} = \frac{\mathbf{F}^m}{\mathbf{u}^p} \tag{3.50}$$

expresses the ratio between the generalized forces $\mathbf{F}^m(t) = \mathbf{F}^m \exp(\mathrm{i}\Omega t)$ applied at the base of the mth foundation and the harmonic generalized displacements $\mathbf{u}^p(t) = \mathbf{u}^p \exp(\mathrm{i}\Omega t)$ along the principal axes of the base of the pth foundation. For a group of circular foundations arranged in a row, an arbitrary submatrix of $\mathbf{K}_{group}$ has the following form:

$$\mathbf{K}^{mp} = \begin{bmatrix} K_{11}^{mp} & 0 & K_{13}^{mp} & 0 & K_{15}^{mp} & 0 \\ 0 & K_{22}^{mp} & 0 & K_{24}^{mp} & 0 & K_{26}^{mp} \\ K_{31}^{mp} & 0 & K_{33}^{mp} & 0 & K_{35}^{mp} & 0 \\ 0 & K_{42}^{mp} & 0 & K_{44}^{mp} & 0 & K_{46}^{mp} \\ K_{51}^{mp} & 0 & K_{53}^{mp} & 0 & K_{55}^{mp} & 0 \\ 0 & K_{62}^{mp} & 0 & K_{64}^{mp} & 0 & K_{66}^{mp} \end{bmatrix} \tag{3.51}$$

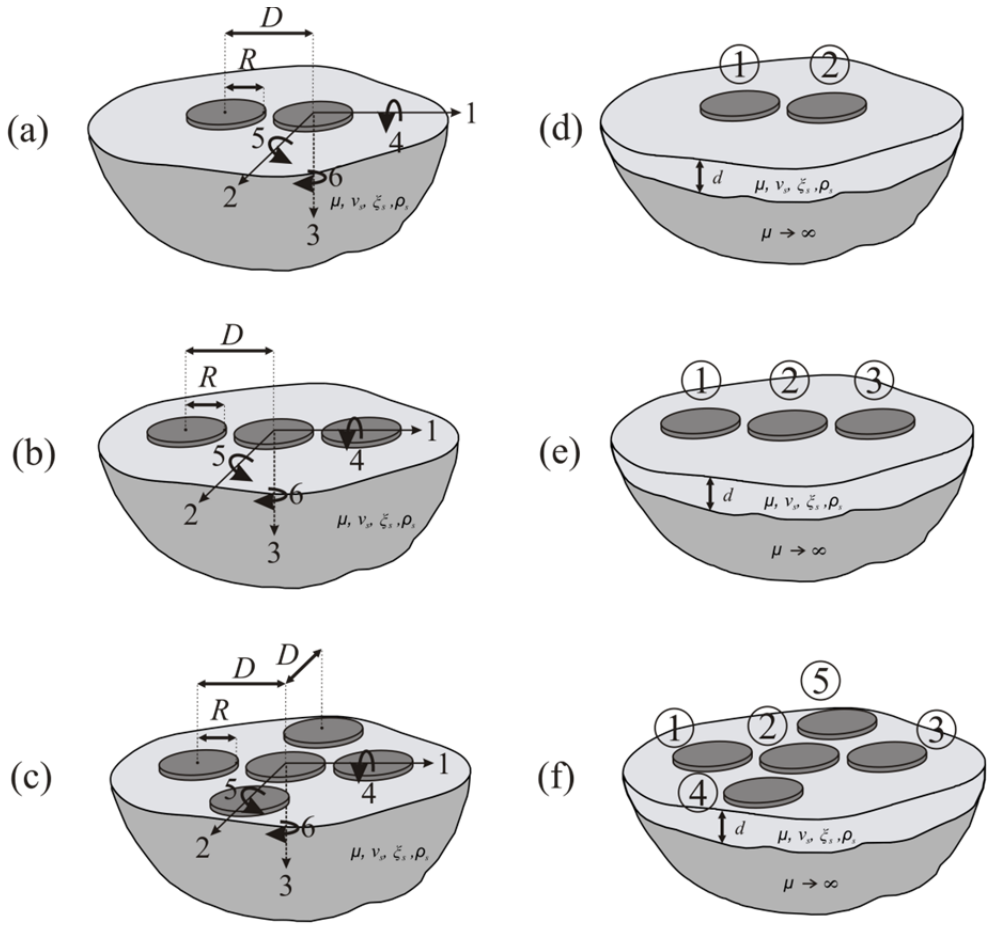

Figure 3.14: Multiple foundations models and coordinate system.

3.5.1 Homogeneous halfspace

The cases investigated regarding the dynamic response under external loads of adjacent circular rigid footings on homogeneous halfspace are depicted in Figure 3.14a-c. Among the plethora of obtained results, only representative, to the greatest extent possible, of the system's behavior are presented.

The diagonal terms of the matrix $\mathbf{K}^{11}$ (= $\mathbf{K}^{22}$) of two circular foundations (Figure 3.14a) are evaluated for normalized distances D/R from 2.2 to 14 and values of a_o from 0 to 4. The homogeneous, isotropic halfspace is characterized by Poisson's ratio $\nu_s = 0.33$ and material damping $\xi_s = 0$. The

real and imaginary part of the impedance functions K_{11}^{11}, K_{22}^{11} and K_{33}^{11} are presented in Figure 3.15; the real and imaginary part of the impedance functions K_{44}^{11}, K_{55}^{11} and K_{66}^{11} are presented in Figure 3.16. The values of K_{11}^{11} corresponding to the horizontal mode indicate that for small separation distances subsoil coupling is prominent, especially in the low frequency range. For higher frequencies and given distance, the solution converges rapidly to response of a single foundation. This is attributed to the decaying coupling effect emanated by a greater number of wavelengths in the high frequency range (Triantafyllidis and Prange, 1989). The function K_{22}^{11} is comparatively less affected by the presence of the second foundation, since it acts perpendicular to the axis between the centers of the foundations. The interaction effects are also noticeable in the low frequency range and for small distances for the vertical mode associated with K_{33}^{11}. On the contrary, the diagonal impedance functions for the rocking modes K_{55}^{11}, and in particular for K_{44}^{11}, are almost identical even for small separations to the corresponding functions of a single foundation. Similarly, minor influence of coupling between the foundations is observed for the torsional impedance function K_{66}^{11}. The destructive interference of waves emitted by footings that exhibit rotating (rocking and torsion) oscillations diminishes the impact of cross-interaction. The imaginary coefficient c_{ii}^{11} generally decreases as the ratio D/R decreases. The trend is reversed for the real part, since the dynamic stiffness of the system k_{ii}^{11} increases with decrease of the normalized distance in the low frequency range. The horizontal-vertical coupling term K_{13}^{11} is shown in Figure 3.17. This function exists merely due to the subsoil coupling of the foundations, since the vertical excitation of a single surface foundation produces only vertical vibration response. Nevertheless, this term and the rest of the impedance functions K_{ij}^{11}, $i \neq j$ are rather small for all distances in comparison with the diagonal terms K_{ii}^{11} of the impedance matrix.

The real k^{12} and imaginary parts C^{12} of the impedance functions, corresponding to the displacements induced to foundation 1 due to an external harmonic load applied on foundation 2, are presented in Figure 3.19 for the horizontal, vertical and coupled horizontal-vertical modes. Common feature of these functions is that for small distances the solution exhibits long-period oscillations with considerable magnitudes. As the distance increases remarkable fluctuations with respect to the frequency parameter are observed, however the steep, especially for K_{33}^{12}, oscillatory behavior of the functions is related with values around zero.

As discussed in 3.4.1, the impedance functions of single foundations on halfspace are very sensitive to the values of Poisson's ratio, especially for the vibration modes associated with pressure waves. Investigation of the influence of this parameter on the dynamic response of two adjacent foundations indicates (not shown herein) that an increase of Poisson's ratio results to an amplified cross-interaction, especially for rocking (and vertical) and less for swaying vibrations. However, the trend regarding the frequency band affected by FSFI, described so far for $\nu_s = 0.33$, is reserved for all Poisson's ratios.

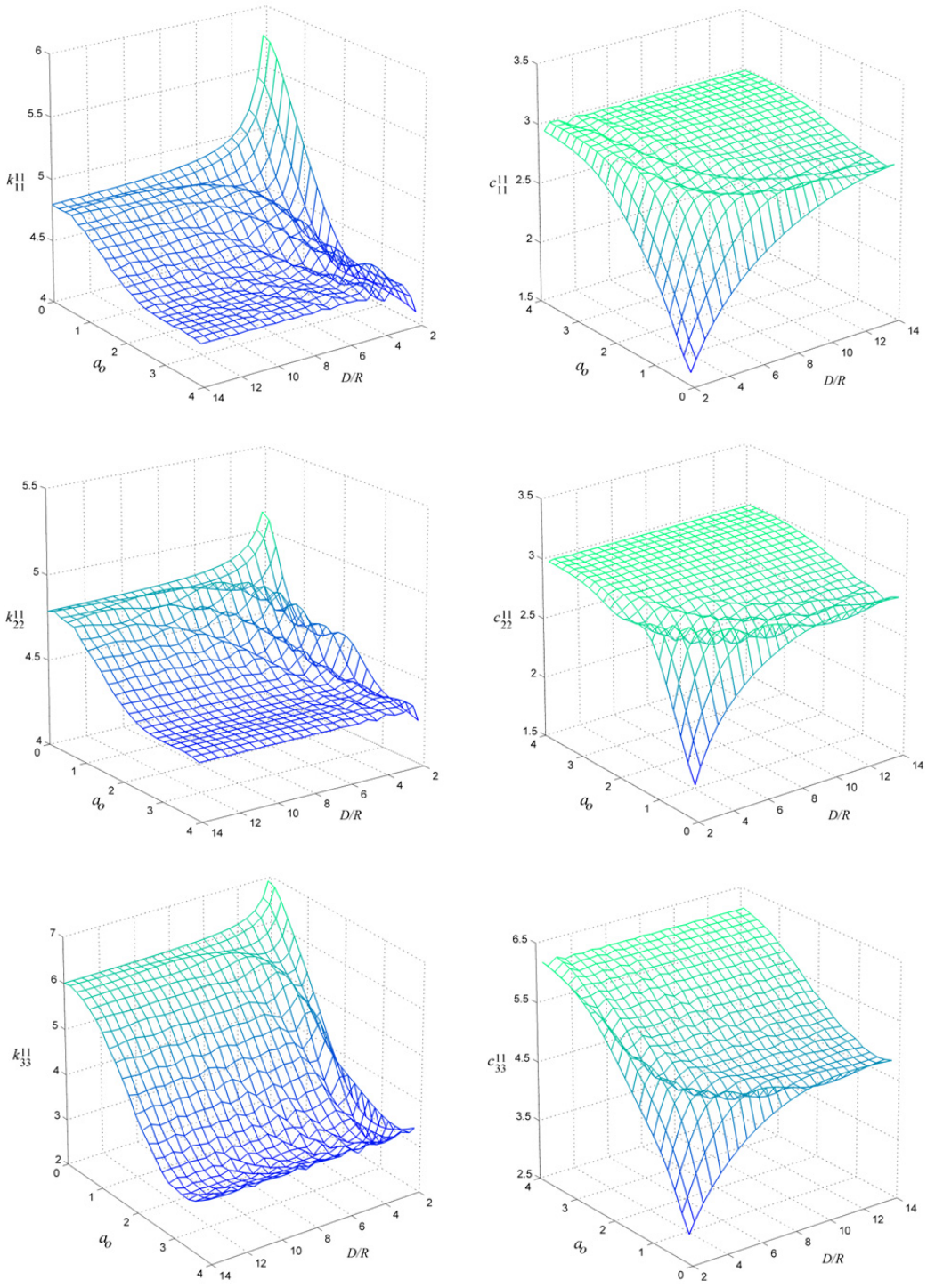

Figure 3.15: Real (left) and imaginary (right) part of the impedance matrix $\mathbf{K}^{11}$ diagonal terms for two circular foundations on elastic homogeneous halfspace, $\nu_s = 0.33$ (horizontal, horizontal, vertical modes).

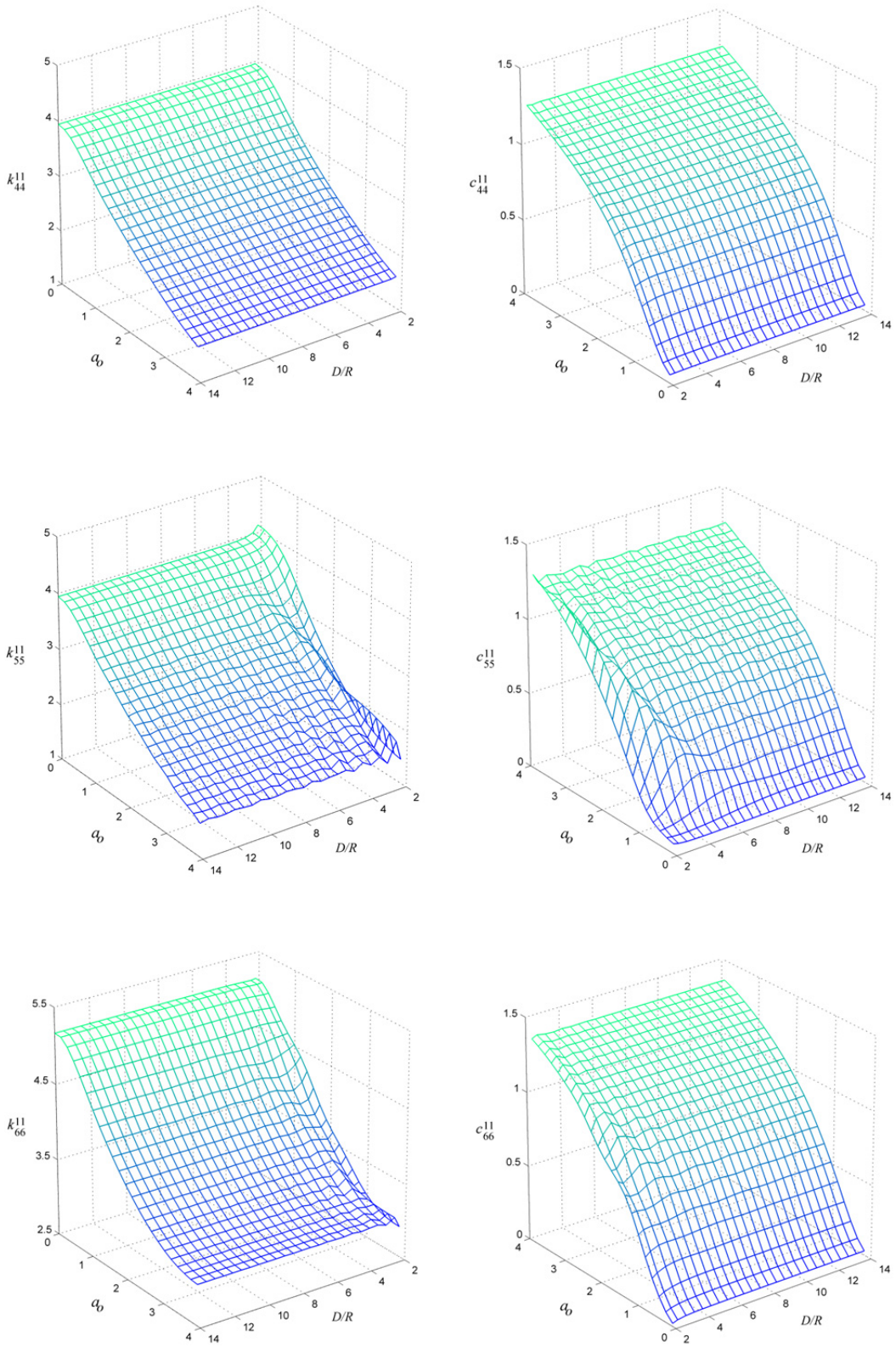

Figure 3.16: Real (left) and imaginary (right) part of the impedance matrix $\mathbf{K}^{11}$ diagonal terms for two circular foundations on elastic homogeneous halfspace, $\nu_s = 0.33$ (rocking, rocking, torsional modes).

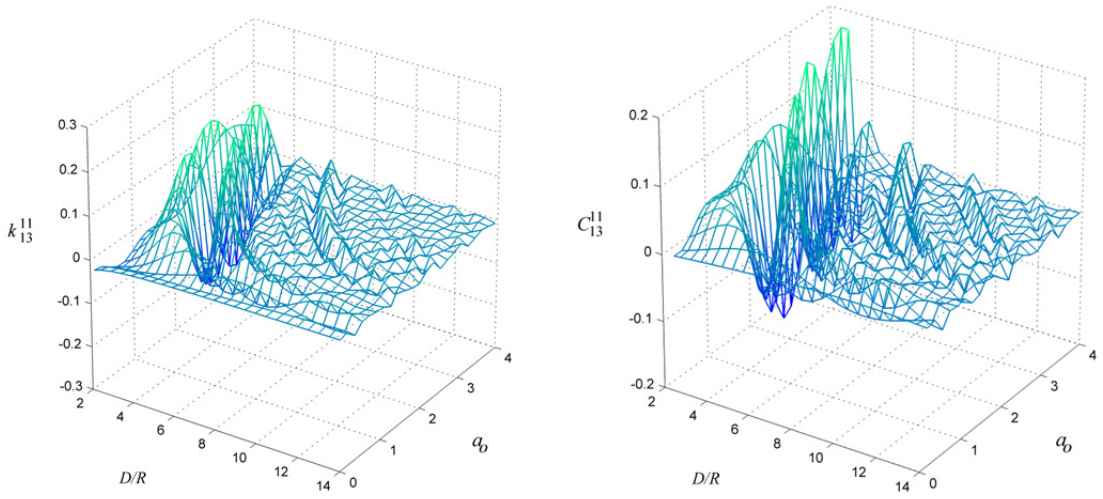

Figure 3.17: Real (left) and imaginary (right) part of the impedance matrix $\mathbf{K}^{11}$ off-diagonal term for two circular foundations on elastic homogeneous halfspace, $\nu_s = 0.33$ (horizontal-vertical mode).

The set of two foundations is supplemented with a third foundation in the row identical to the other two and in equal distance (Figure 3.14b). A visualization of the generated system by means of dynamic springs and dashpots is given in Figure 3.18. Figure 3.20 shows the spring and damping coefficients of the impedance function K_{11}^{11} (= K_{11}^{22}) for the -two foundations- system and K_{11}^{11} (= K_{11}^{33}) as well as K_{11}^{22} for the -three foundations- system. It can be observed that foundations 1 and 3 on the borders do not appreciably interact even for small distances. Other modes of vibration reveal similar trend. Thus, the functions $K_{ii}^{11}(= K_{ii}^{22})$ for two foundations and the corresponding $K_{ii}^{11}(= K_{ii}^{33})$ for three foundations configuration in the row are practically equal for all frequencies. On the other hand, the middle foundation, as a receiver of waves emitted by both adjacent foundations, evidences a strong coupling with them. Specifically, the real part of the impedance function k_{11}^{22} is significantly greater than k_{11}^{11} for the three foundations system in the low frequency range and for small separations, whereas the imaginary part c_{11}^{22} remains smaller than c_{11}^{11} for the lowest frequencies even for a distance $D = 8\,R$.

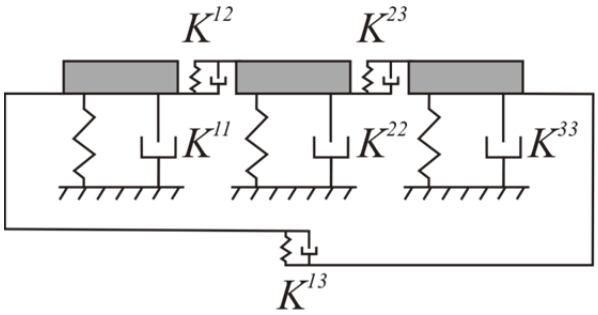

Figure 3.18: Dynamic springs and dashpots for a -three foundations- set.

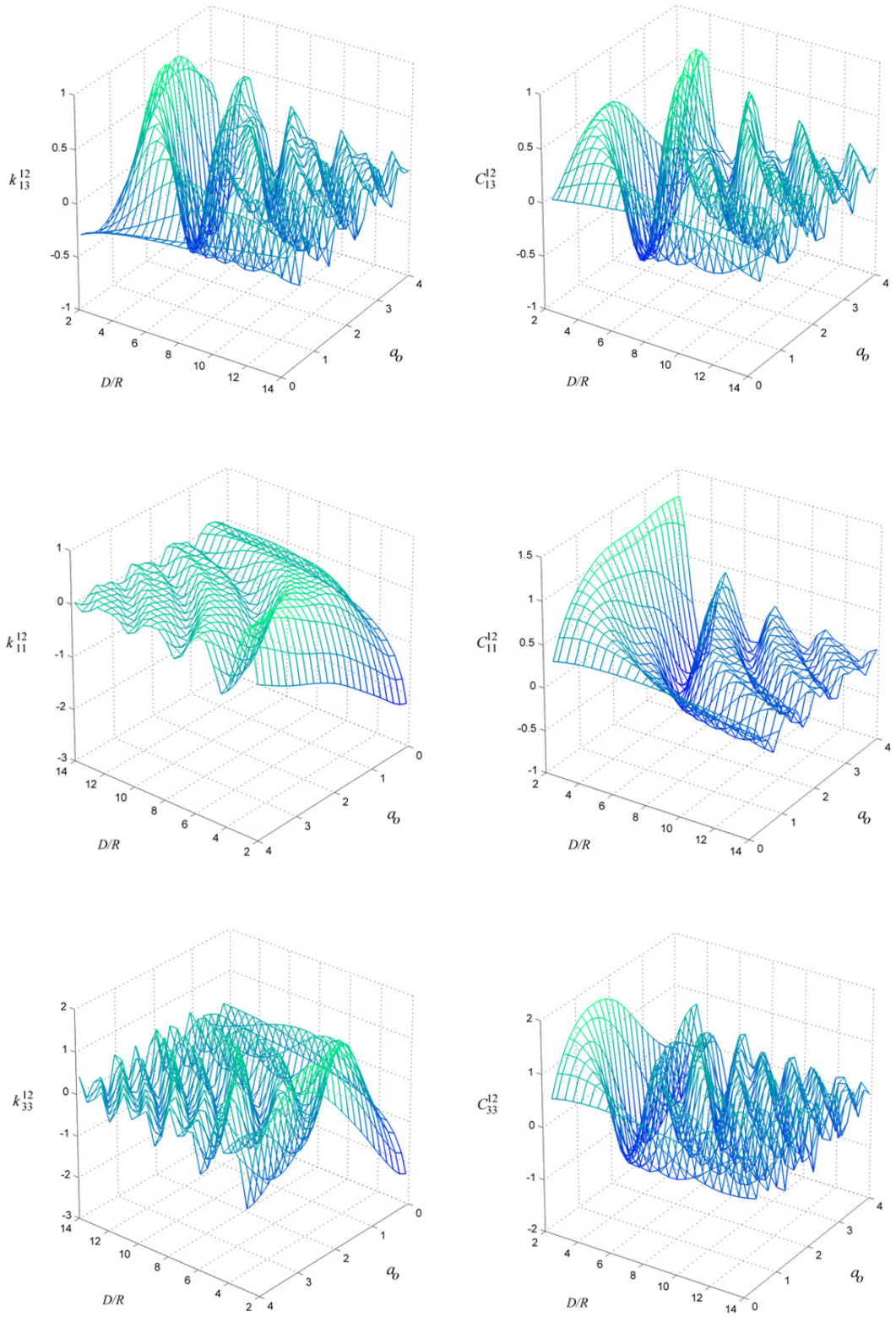

Figure 3.19: Real (left) and imaginary (right) part of the coupled impedance matrix $\mathbf{K}^{12}$ diagonal and off-diagonal terms for two circular foundations on elastic homogeneous halfspace, $\nu_s = 0.33$ (horizontal-vertical, horizontal, vertical modes).

Figure 3.21 shows the real k_{55}^{12} and imaginary part C_{55}^{12} of the impedance function for two and three foundations vibrating in a rocking mode. The results between the two systems are indistinguishable, manifesting that the response of a rigid foundation when a harmonic load is applied to an adjacent one

is independent of the number of foundations in the row; in this case, the number of foundations in the immediate neighborhood governs the coupled -between the foundations- response.

The influence of the spatial arrangement of adjacent circular foundations on their cross-interaction is examined by placing two identical foundations perpendicular to the middle foundation of the previous three foundations system (Figure 3.14c). The distance along the axes between all five footings is kept equal. In this case, all elements of the matrix $\mathbf{K}^{mp}$ in Eq. (3.49) possess non-zero values. Figure 3.22 displays the diagonal spring and damping coefficients of the impedance function K^{22} associated with horizontal and rocking modes with respect to the frequency parameter a_o for two, three and five foundations system and normalized distance $D/R = 2.2$. The corresponding coefficients for a single foundation are also presented for comparison purposes. As may be anticipated, for the functions K_{22}^{11} and K_{44}^{11} associated with modes acting previously out of plane, the three-dimensional space effects become apparent. On the contrary, the functions K_{11}^{11} and moreover K_{55}^{11} are less affected by the addition of two foundations in the -three foundation- set. The imaginary part of the presented stiffness functions for all vibration modes decreases monotonically with the increase of foundations number for the frequency range investigated. The overall radiation of wave energy from the central foundation 2 for this -five foundations- configuration is negligible or nonexistent for all modes.

The dynamic stiffness of foundation 2 increases significantly at low frequencies with inclusion of foundations in closed-space, whereas reduces in the high frequency range. In Figure 3.23 the coupled -between foundations 1 and 2– impedance functions for the horizontal mode 1 is presented with respect to the frequency parameter a_o and normalized distance $D/R = 2.2$. As it can be observed, the transition from the three foundations solution to the five alters the response in a distinct way in contrast to the imperceptible changes between the two -and three- foundations solution. Obviously, the response of each foundation in a group is controlled primarily from the number of foundations that lie in its immediate neighborhood.

3.5.2 Bedrock at shallow depth

The cases investigated regarding the dynamic response under external loads of adjacent circular rigid surface footings on a deposit over rigid bedrock are shown in Figure 3.14d-f. The diagonal terms of the matrix $\mathbf{K}^{11}$ (= $\mathbf{K}^{22}$) of two circular foundations (Figure 3.14d) are evaluated for normalized distances D/R from 2.2 to 8 and values of a_o from 0 to 3. The viscolelastic stratum is characterized by normalized thickness $d/R = 2$, Poisson's ratio $\nu_s = 0.33$ and material damping $\xi_s = 0.05$. The real and imaginary part of the impedance functions K_{11}^{11} and K_{33}^{11} are presented in Figure 3.24. The rotating (rocking and torsional) diagonal terms are not herein presented, since they show a close resemblance with the case of halfspace, as discussed for a single foundation case in section 3.4.

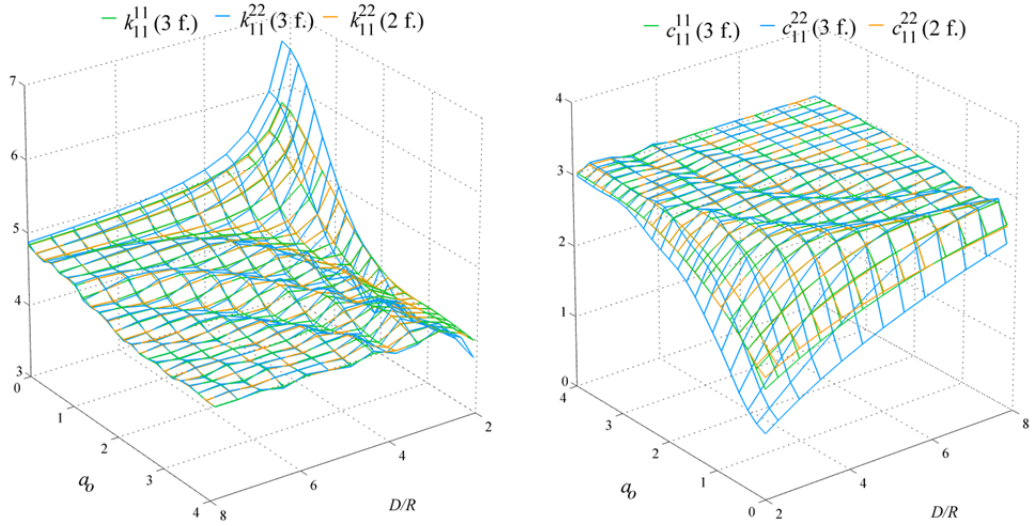

Figure 3.20: Real (left) and imaginary (right) part of the impedance matrices $\mathbf{K}^{11}$ and $\mathbf{K}^{22}$ diagonal terms for two and three circular foundations on elastic homogeneous halfspace, $\nu_s = 0.33$ (horizontal mode).

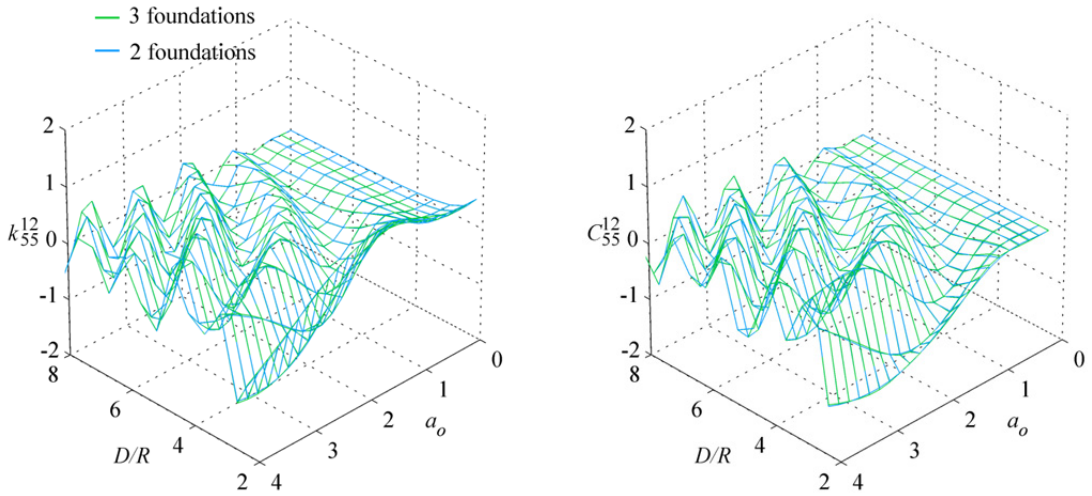

Figure 3.21: Real (left) and imaginary (right) part of the coupled impedance matrix $\mathbf{K}^{12}$ diagonal term for two and three circular foundations on elastic homogeneous halfspace, $\nu_s = 0.33$ (rocking mode).

The values of K_{11}^{11} corresponding to the horizontal mode indicate that even for small separation distances subsoil coupling is of minor importance and the solution converges rapidly to that of a single foundation. The same trend is also observed for K_{33}^{11} especially in the low frequency range. The cause for this system's response must be sought in the fact that at low frequencies, below the first resonant frequency radiation damping is negligible due to the absence of propagating surface waves. Thus, the evident FSFI phenomena for the case of the halfspace in the low frequency range are ''suppressed'' in the case of a soil deposit.

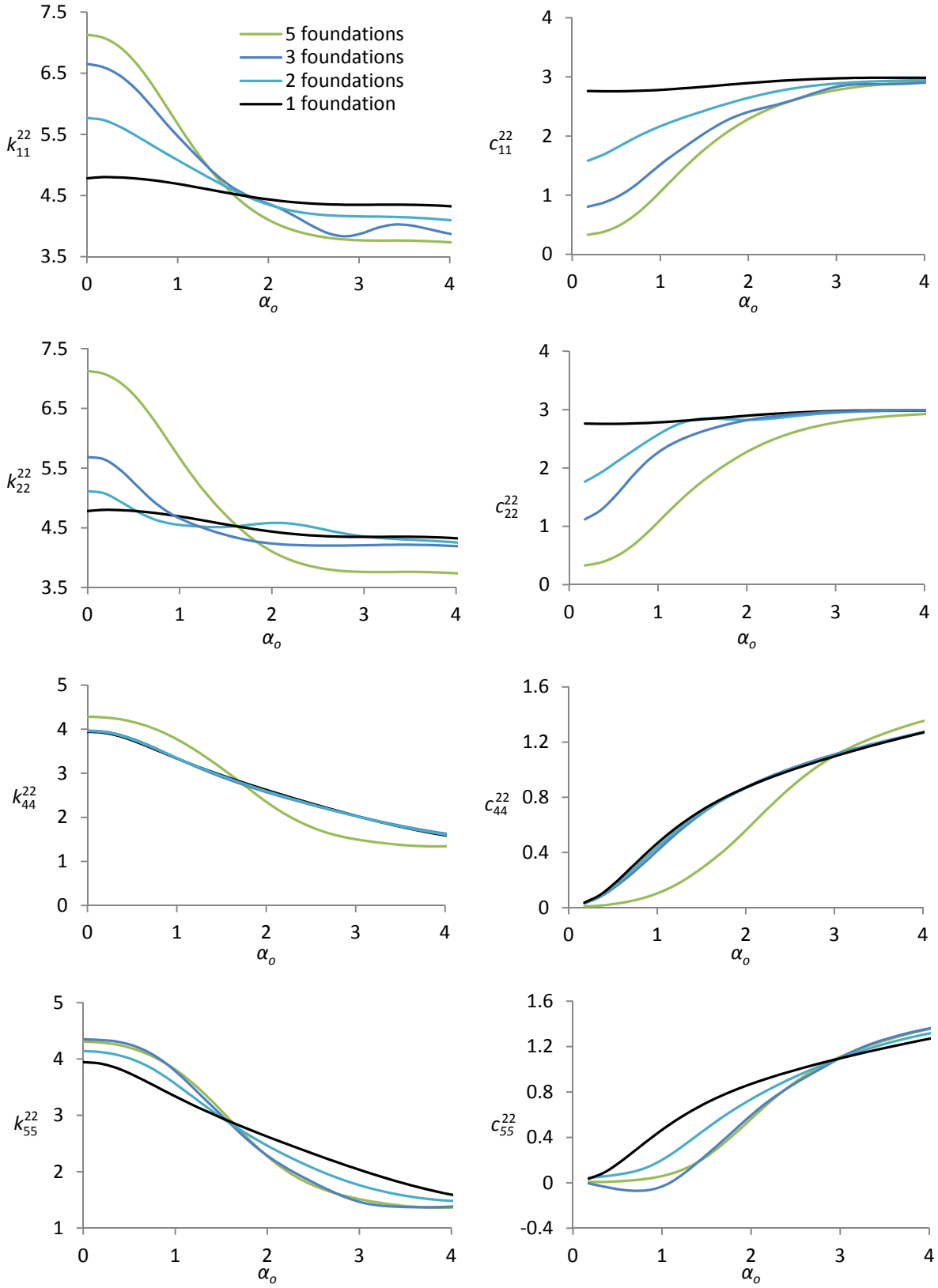

Figure 3.22: Real (left) and imaginary (right) part of the impedance matrix $\mathbf{K}^{22}$ diagonal terms for different number of circular foundations on elastic homogeneous halfspace, $\nu_s = 0.33$, $D/R = 2.2$ (horizontal, horizontal, rocking, rocking modes).

The real part of the diagonal impedance function K_{11}^{11} slightly increases for small distances in the low frequency range. The above remarks are emphasized by inspecting the terms k_{33}^{12} and c_{33}^{12} corresponding to vertical displacements induced to foundation 1 due to an external harmonic load applied on foundation 2 in the same direction (Figure 3.25). The response is practically nonexistent in the low frequency range, whereas oscillations around zero above the "cut-off" frequency take place.

Analogously to the procedure followed for the halfspace, the set of two foundations is supplemented with a third foundation in the row identical to the other two (Figure 3.14e). The influence of the spatial arrangement of adjacent circular foundations on their cross-interaction is investigated by setting two identical foundations perpendicular to the middle foundation of the three foundations system (Figure 3.14f). The distance along the axes between all five footings is kept equal.

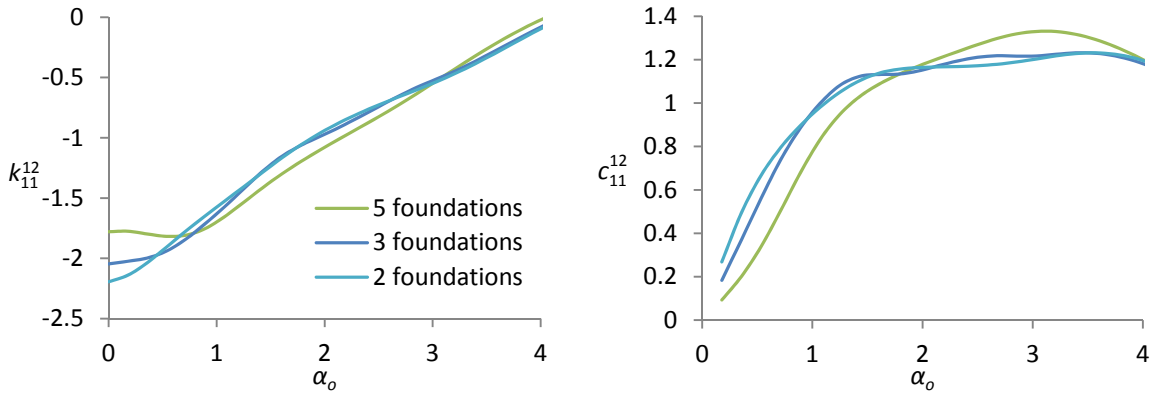

Figure 3.23: Real (left) and imaginary (right) part of the coupled impedance matrix $\mathbf{K}^{12}$diagonal term for different number of circular foundations on elastic homogeneous halfspace, $\nu_s = 0.33$, $D/R = 2.2$ (horizontal mode).

Figure 3.26 displays the diagonal spring and damping coefficients of the impedance function K^{22} associated with horizontal and vertical modes with respect to the frequency parameter a_o for two, three and five foundations system and normalized distance $D/R = 2.2$. It can be readily observed that the inclusion of more foundations in the system alters the response only locally in the frequency range as opposed to the halfspace case. The peaks and valleys associated with resonance frequencies of the stratum become more pronounced for the vertical vibration and smoother for the horizontal vibration. In Figure 3.27, the coupled -between foundations 1 and 2- complex stiffness term for the horizontal mode 1 is presented with respect to the frequency parameter a_o and normalized distance $D/R = 2.2$. An antisymmetric addition of two foundations in the -three footings- arrangement affects noticeably only the real part of the impedance.

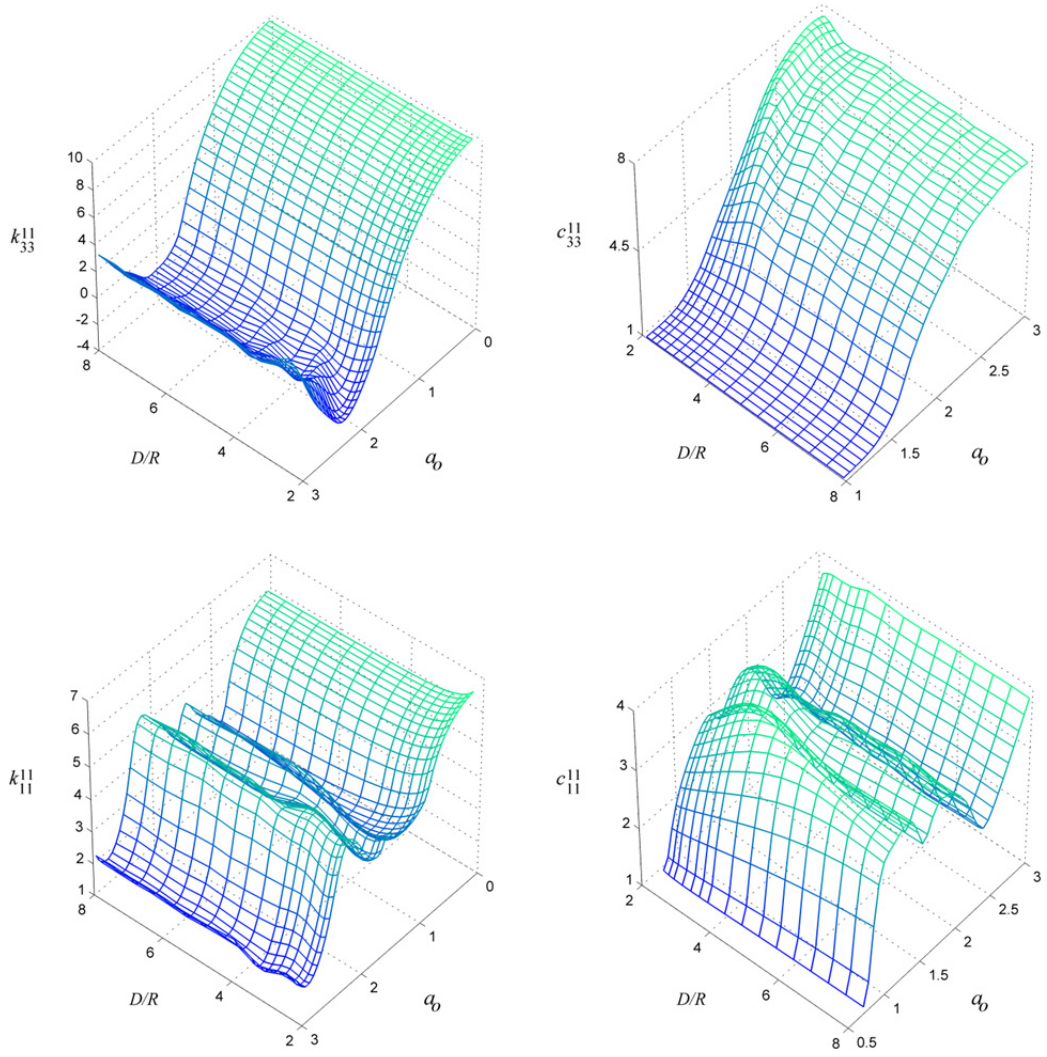

Figure 3.24: Real (left) and imaginary (right) part of the impedance matrix $\mathbf{K}^{11}$ diagonal terms for two circular foundations on viscoelastic stratum, $\nu_s = 0.33$, $d/R = 2$, $\xi_s = 0.05$ (vertical, horizontal modes).

In section 3.2.2.3, the effect of hysteric damping on the amplitudes of Green's functions obtained for a soil deposit has been found to be significant. The existence of energy dissipation produced by internal friction softens the resonant divergence; hence it must be anticipated that the stiffness functions of a single foundation over stratum do not exhibit sharp peaks and valleys (Kausel, 1974). Aiming to assess the influence of internal damping on the dynamic FSFI, the impedance functions of two adjacent foundations on viscoelastic layer of depth $d/R = 2$ over rigid bedrock and separation distance $D/R = 3$ are calculated for three different values of the damping ratio ξ_s. As reference point, the corresponding solutions of a single foundation are used. Figure 3.28 shows the imaginary part of the impedance function K_{11}^{11}. It is obvious that a reduction of the material damping results to amplified responses, in particular for the resonant frequencies; the same tendency is detected for other modes of vibration. Nevertheless, as far as internal friction is always present in soils, the relative importance of

this parameter in a FSFI analysis is minor, since its impact on the overall response is practically of the same degree as for a FSI analysis.

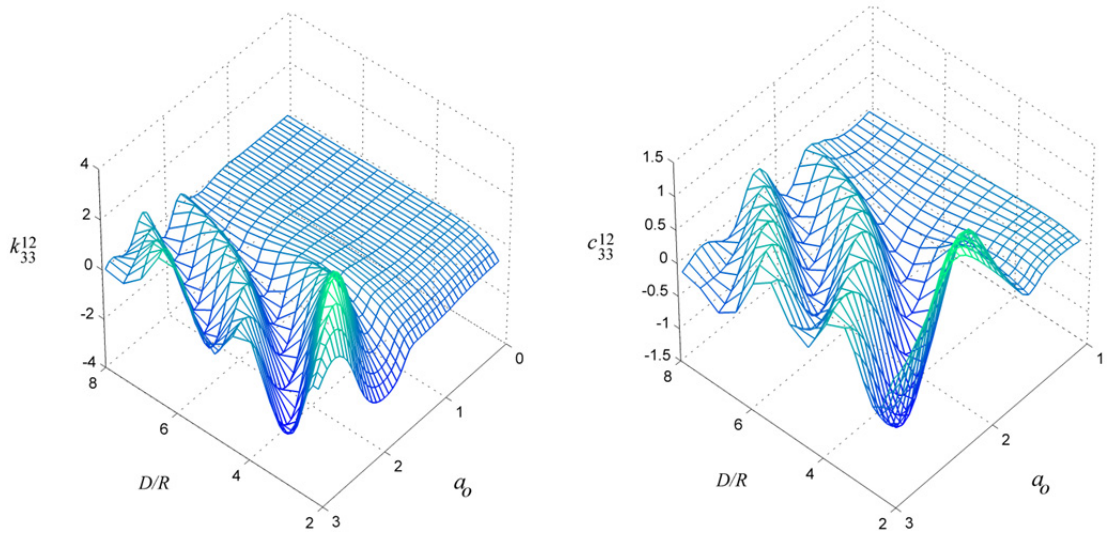

Figure 3.25: Real (left) and imaginary (right) part of the coupled impedance matrix $\mathbf{K}^{12}$ diagonal term for two circular foundations on viscoelastic stratum, $\nu_s = 0.33$, $d/R = 2$, $\xi_s = 0.05$ (vertical mode).

3.6 Guideline for preliminary estimation of structure-soil-structure interaction

The presented results indicate that: a) The separation of the foundations and the excitation frequency should be interrelated, since the assessment of the foundations response in a group requires knowledge of both parameters. Obviously, the number of transmitted wavelengths for a certain distance can elevate or degrade the cross-interaction effects. b) The dynamic behavior of each foundation is appreciably affected only by the number of the foundations that lie in its immediate circumference and this fact holds true independent from the distance. c) Existence of a shallow deposit beneath the foundations diminishes the group effects in the frequency range below the fundamental natural frequency of the stratum for the associated vibrational mode of the foundations.

Taking into consideration these findings, it is expedient for practical purposes to establish a criterion for a preliminary estimation of the cross-interaction effects for nearby identical structures founded on a deformable ground and subjected to seismic motion. This can be achieved by comparing the distances between each structure in a group with the wavelengths corresponding to the predominant natural frequencies of the structure-soil system. In the vicinity of the latter, the structures exhibit large responses. By doing so, the separation between the components in a group is straightforwardly related with a structural parameter. Strictly speaking, the natural frequencies of the structures in the presence of the other ones are needed. However, in a preliminary stage, it suffices to calculate them by

considering only the interaction with the soil. This can be done with the aid of structural models possessing few dynamic degrees of freedom (Wolf, 1985).

Since the swaying mode of vibration is most sensible to the presence of nearby foundations, it is appropriate to consider wavelengths corresponding to S waves. Consequently, the following dimensionless ratio is introduced for each structure in a group:

$$\mathrm{DR}^{ij} = \frac{V_s\, T_i}{D_j}, i = 1..K, j = 1..R_{\mathrm{adj.}} \tag{3.52}$$

where T_i is the ith natural period of the structure-soil system that contributes significantly to the response, D_j corresponds to the distance between the structure and the jth adjacent one and $R_{\mathrm{adj.}}$ represents the total number of structures lying in its immediate neighborhood. For a prescribed finite value of the medium's shear wave velocity, if this ratio is significantly greater than unity for a great number of i and j, it should be expected that the dynamic response of the structure is strongly influenced by the group effects. On the contrary, if the ratio is less than unity for a great number of i and j, the structure can be analyzed individually by neglecting the presence of others. The cross-interaction effects can be also disregarded in case of a shallow stratum ($d/R < 2$), if the dominant natural frequencies of the structure-soil system fall in the range below the fundamental natural frequency of the layer for the related mode of vibration. Of course, necessity of structure-soil-structure interaction analysis postulates in the first place interaction of each structure with the supporting soil. In other words, the ratio of the stiffness of the structure to that of the soil should be in that range of values, for which soil-structure interaction is apparent. Results of analytic studies on simplified structural models are available for an initial evaluation of the importance of soil-structure effects (Jennings and Bielak, 1973; Wolf, 1985; Stewart et al., 1999). The fact that soil shear modulus varies in most cases with depth and the presence of additional weight from the structure, complicates the selection of an appropriate shear wave velocity. Guidance on calculating average effective profile velocities is provided in NEHRP (2012).

Due to the fact that the proposed approach is based on the swaying mode of vibration, it may overestimate the cross-interactions effects in some cases. Just to mention one of these: slender structures vibrate predominantly in rocking and hence, are comparatively less affected by the presence of other similar structures. It must be also noted, that despite the practicality of the rule given by Eq. (3.52), awareness of the complications arising from the inertia of the structures, foundations flexibility, soil inhomogeneity, magnitude and above all, frequency content of the ground motion, is essential for the determination of the overall response in the group.

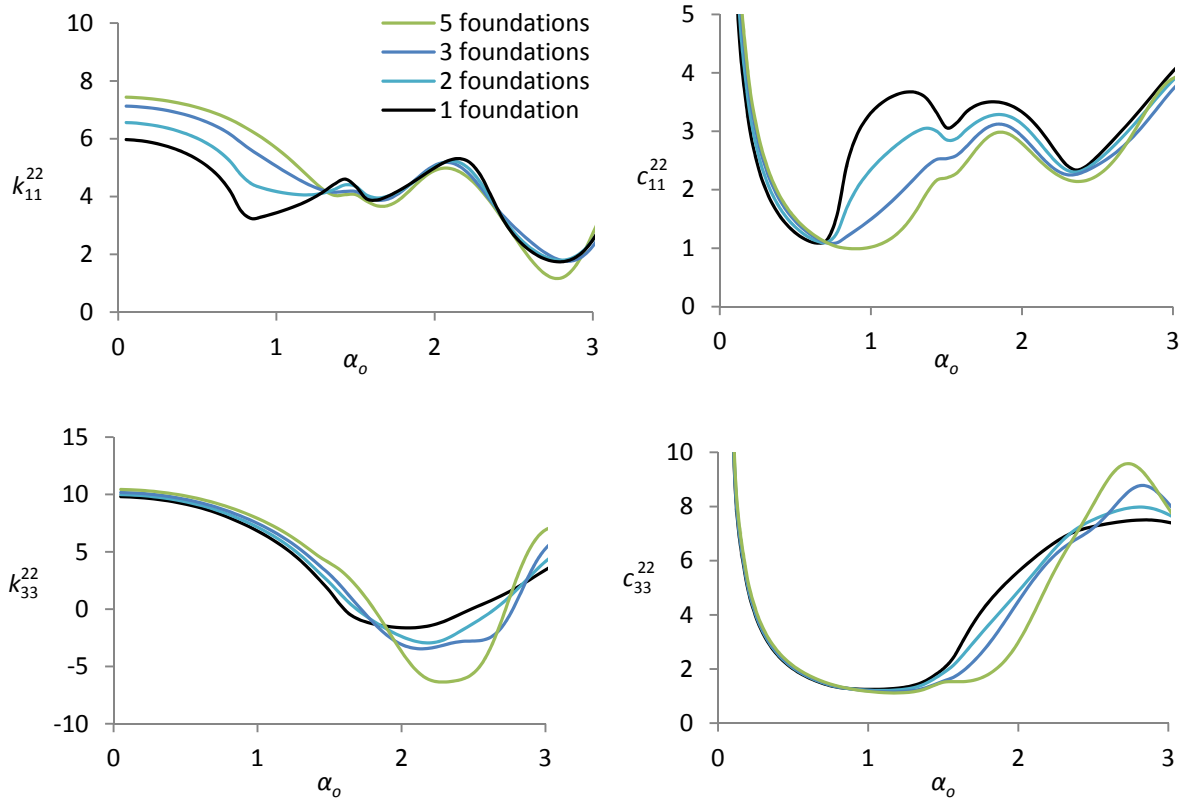

Figure 3.26: Real (left) and imaginary (right) part of the impedance matrix $\mathbf{K}^{22}$ diagonal terms for different number of circular foundations on viscoelastic stratum,$\nu_s = 0.33$, $d/R = 2$, $D/R = 2.2$, $\xi_s = 0.05$ (horizontal, vertical modes).

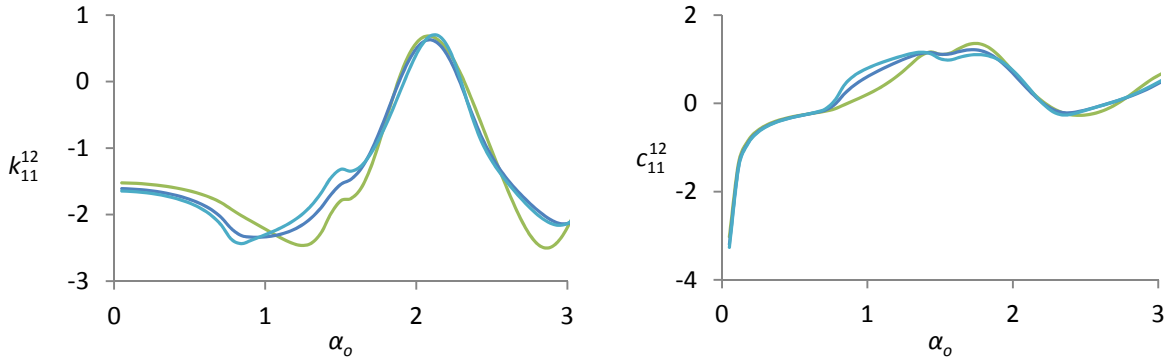

Figure 3.27: Real (left) and imaginary (right) part of the impedance matrix $\mathbf{K}^{12}$ diagonal term for different number of circular foundations on viscoelastic stratum,$\nu_s = 0.33$, $d/R = 2$, $D/R = 2.2$, $\xi_s = 0.05$ (horizontal mode).

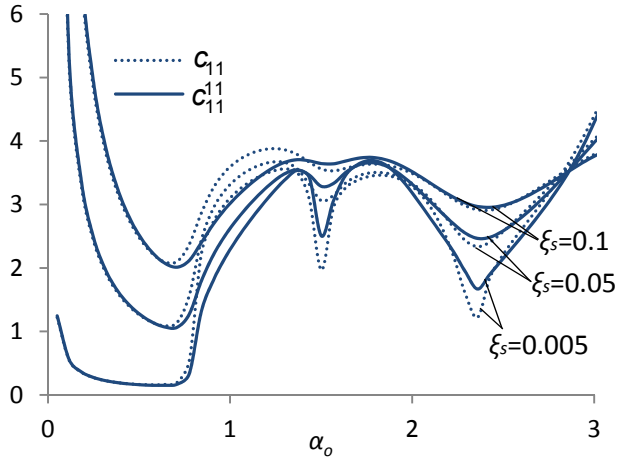

Figure 3.28: Imaginary part of the impedance matrix $\mathbf{K}^{11}$ diagonal term for two circulars foundations on viscoelastic stratum for various values of internal damping, $\nu_s = 0.33$, $d/R = 2$, $D/R = 3$ (horizontal mode).

3.7 Summary

This chapter deals with the response of multiple identical rigid circular foundations on deformable soil medium under external harmonic loads. Initially, the solution of a three-dimensional wave propagation problem for a bounded and unbounded soil medium is introduced with the aid of Green's functions. Afterwards, a coupled FEM-BEM formulation is employed for the foundations-soil system and impedance functions are determined over wide ranges of frequencies and distances between the foundations. The results constitute elementary part of the analyses conducted in the next chapter. A series of numerical investigations with respect to the number, arrangement of the foundations in space and two idealized soil profiles indicate the following principal trends:

- For a given distance, the coupling effects between foundations on semi-infinite soil medium are greater in the low frequency range. For higher frequencies a larger number of wavelengths is transmitted and the group effects are comparatively of lower degree.
- The swaying modes of vibration are most affected by the presence of nearby foundations, followed by the vertical and lastly rotational modes (rocking and torsion).
- The dynamic behavior of each foundation is considerably affected only by the number of the foundations that lie in its immediate neighborhood and this fact holds true independent from the distance.
- Existence of a shallow deposit beneath the foundations diminishes the cross-interaction effects in the frequency range below the fundamental natural frequency of the stratum for the associated vibrational modes of the foundations.

On the basis of these conclusions, a guideline for a preliminary estimation of the degree of dynamic structure-soil-structure interaction is proposed for engineering practice.

4 Dynamic interaction of adjacent liquid-storage tanks

In this study, the problem of assessing the dynamic response of multiple liquid-storage tanks subjected to ground motion is solved by means of the substructure method. This approach is well established for single structures; namely for the case in which other structures are assumed to be located in infinite distance. Scope of this chapter is the refinement of the method in order to take into account the dynamic subsoil coupling of multiple tanks. For the sake of a better comprehension of the solution scheme of this chapter, the basic steps involved in the conventional substructure method are firstly outlined.

4.1 Substructure method for single structures

4.1.1 Free field response of site

Prior to a soil-structure interaction analysis emerges the determination of the spatial and temporal variation of the seismic motion induced in the structure before excavating the soil and establishing the structure, known as the free-field response. Since modeling of the total seismic environment is a laborious task, a control point at a distance from the source is commonly defined and the free-field motion is subsequently calculated. At this stage, certain judgments on the location of the control point and the wave pattern that produces a prescribed control motion (consistent to the seismic hazard of the region) must be made. The selection of those two interdependent factors is crucial for the structural final response.

Regarding the location of the control point, three main different possibilities among others exist: a) The motion is specified at the free surface of the soil deposit without any structure. b) The motion is specified at the hypothetical outcropping of rock in absence of structure. c) The motion is specified at bedrock. Choosing a) necessitates deconvolution of the design motion from the surface to bedrock. Options b) and c) are not equivalent unless the soil properties are greatly different from those of the underlying rock or if there is a considerable amount of internal damping in the soil. Generally, the control point should be located on the surface; otherwise the control strong motion will spuriously comprise the characteristics of the soil at the chosen depth. With respect to the assumed wave pattern, vertically incident or inclined body waves or surface waves may be considered in a three dimensional

analysis. However, current microzonation practice has widely adopted the one-dimensional amplification theory to predict surface motions at a site. This is briefly presented along the following lines.

We consider a general case of $N-1$ horizontal layers of constant material properties that overlie a homogeneous viscoelastic halfspace (Figure 4.2a). Cartesian coordinate system $\mathbf{x}=\{x_1, x_2, x_3\}^{\mathrm{T}}$ is defined. The control point is chosen at a fictitious stress-free rock outcrop, which has the same properties with the halfspace below the layers. The system is subjected to vertically propagating SH waves (out-of-plane) that are characterized by harmonic motion $w'_{2,N} \equiv w'_{2,b}$ along the x_2 axis. An arbitrary individual layer of thickness d is examined as a free body in space, which is equilibrated by appropriate external harmonic shearing traction at the upper and lower interfaces $P_1 = -\tau_{x_2x_3}\big|_{x_3=0}$ and $P_2 = \tau_{x_2x_3}\big|_{x_3=d}$ respectively, where the displacement field is regarded. The impedance matrix of the layer is given in matrix form with the aid of the Stiffness Matrix Method by:

$$\mathbf{p} = \mathbf{K}_{SH}^{L}\mathbf{w} \tag{4.1}$$

where:

$$\mathbf{K}_{SH}^{L} = \rho_s^L\, V_s^{L*}\, \Omega \begin{bmatrix} \cot(\kappa_s d) & -\dfrac{1}{\sin(\kappa_s d)} \\ -\dfrac{1}{\sin(\kappa_s d)} & \cot(\kappa_s d) \end{bmatrix} \tag{4.2}$$

In the above expression, V_s^{L*} stands for the complex shear wave velocity given by: $V_s^{L*} = V_s^L\sqrt{1+2\xi_s^L}$, Ω is the excitation frequency, $\kappa_s = \Omega/V_s^{L*}$, ρ_s^L is the mass density of the layer and ξ_s^L is the layer's ratio of linear hysteretic damping for S waves.

The impedance of the elastic halfspace is given by Eq. (3.3) for $\kappa = 0$:

$$K_{SH}^{H} = \mathrm{i}\,\Omega\,\rho_s^H\,V_s^{H*} \tag{4.3}$$

where $V_s^{H*} = V_s^H\sqrt{1+2\xi_s^H}$ and ξ_s^H is the halfspace's ratio of linear hysteretic damping for S waves. By applying the unknown internal stress τ_N as external traction at the interaction horizon of halfspace and bottom layer and assembling the matrices of each layer and halfspace, we obtain the following equation for the system's dynamic equilibrium:

$$\begin{bmatrix} K_{11} & K_{12} & 0 & \dots & 0 \\ K_{21} & K_{22} & K_{23} & \dots & 0 \\ 0 & K_{32} & K_{33} & \ddots & \vdots \\ \vdots & \vdots & \ddots & \ddots & K_{N-1,1} \\ 0 & 0 & \dots & K_{N,N-1} & K_{NN} \end{bmatrix} \begin{Bmatrix} w_{2,1} \\ w_{2,2} \\ w_{2,3} \\ \vdots \\ w_{2,N} \end{Bmatrix} = \begin{Bmatrix} 0 \\ 0 \\ 0 \\ \vdots \\ -\tau_N \end{Bmatrix} = \begin{Bmatrix} 0 \\ 0 \\ 0 \\ \vdots \\ -K^H w_{2,N} + K^H w'_{2,N} \end{Bmatrix} \tag{4.4}$$

The dynamic equation for a single layer over halfspace is accordingly:

$$\rho_s^L\, V_s^{L*}\, \Omega \begin{bmatrix} \cot(\kappa_s d) & -\dfrac{1}{\sin(\kappa_s d)} \\ -\dfrac{1}{\sin(\kappa_s d)} & \cot(\kappa_s d) + \dfrac{K_{SH}^H}{\rho^L\, V_s^{L*}\, \Omega} \end{bmatrix} \begin{Bmatrix} w_{2,ff} \\ w_{2,b} \end{Bmatrix} = \begin{Bmatrix} 0 \\ K^H w'_{2,b} \end{Bmatrix} \tag{4.5}$$

with $w_{2,ff} \equiv w_{2,1}$ representing the free field displacement. If we introduce the complex impedance ratio a_s^* as:

$$a_s^* = \frac{\rho_s^H\, V_s^{H*}}{\rho_s^L\, V_s^{L*}} \tag{4.6}$$

Eq. (4.5) can be written as:

$$\begin{bmatrix} \cos(\kappa_s d) & -1 \\ -1 & \cos(\kappa_s d) + \mathrm{i} a_s^* \sin(\kappa_s d) \end{bmatrix} \begin{Bmatrix} w_{2,ff} \\ w_{2,b} \end{Bmatrix} = \begin{Bmatrix} 0 \\ \mathrm{i} a_s^* \sin(\kappa_s d) \end{Bmatrix} w'_{2,b} \tag{4.7}$$

The solution is given by the following expression:

$$\begin{Bmatrix} w_{2,ff} \\ w_{2,b} \end{Bmatrix} = \frac{1}{\cos(\kappa_s d) + \dfrac{\mathrm{i}}{a_s^*} \sin(\kappa_s d)} \begin{Bmatrix} 1 \\ \cos(\kappa_s d) \end{Bmatrix} w'_{2,b} \tag{4.8}$$

The ratio of the soil surface amplitude to the rock outcrop amplitude in terms of absolute values is:

$$FS_2 = \frac{1}{\sqrt{\cos^2(\kappa_s d) + \dfrac{1}{a_s^{*2}} \sin^2(\kappa_s d)}} = \begin{Bmatrix} |w_{2,ff}| \\ |w'_{2,b}| \end{Bmatrix} \tag{4.9}$$

Apparently, the denominator in Eq. (4.9) does not become zero for finite values of the stiffness for the halfspace even if the layer is considered undamped. The ratio $|w_{2,ff}|/|w'_{2,b}|$ is always smaller than or equal to $|w_{2,ff}|/|w_{2,b}|$ due to the reflected waves that propagate towards infinity (radiation damping). In the case of out-of-plane motion the lth natural frequency of an undamped layer over rigid bedrock can be found as:

$$\omega_s = \frac{2\,l + 1}{2\,d} \pi\, V_s \tag{4.10}$$

The above resonant frequencies of a perfectly elastic stratum coincide with the natural frequencies of the lateral vibration of a one-dimensional rod with one end fixed and the other free and ascribed the same rigidity and thickness of the stratum as explained in section 3.2.2.3. Regarding vertical incidence, the amplification of SV waves and the frequencies determined by Eq. (4.10) are identical to that of SH waves, thus $FS_2 = FS_1$. For P waves, the ratio of the soil surface amplitude to the rock outcrop amplitude in terms of absolute values is calculated by:

$$FS_3 = \frac{1}{\sqrt{\cos^2\left(\kappa_p d\right) + \dfrac{1}{a_p^{*2}} \sin^2\left(\kappa_p d\right)}} = \begin{Bmatrix} |w_{3,ff}| \\ |w'_{3,b}| \end{Bmatrix} \tag{4.11}$$

where $V_p^{L*} = V_p^L \sqrt{1 + 2\xi_p^L}$, $\kappa_p = \Omega / V_p^{L*}$ and ξ_p^L is the layer's ratio of linear hysteretic damping for P waves and a_p^* is given by:

$$a_p^* = \frac{\rho_s^H V_p^{H*}}{\rho_s^L V_p^{L*}} \tag{4.12}$$

where $V_p^{H*} = V_p^H \sqrt{1 + 2\xi_p^H}$ and ξ_p^H is the halfspace's ratio of linear hysteretic damping for P waves. In this case, the lth natural frequencies of an undamped layer over rigid bedrock can be found as:

$$\omega_p = \sqrt{\frac{2(1 - v_s)}{1 - 2\,v_s}}\,\omega_s \tag{4.13}$$

where v_s is Poisson's ratio. The ratios FS_2 and FS_3 are shown in Figure 4.1 as a function of the dimensionless frequency for impedance ratios a_s and a_p respectively.

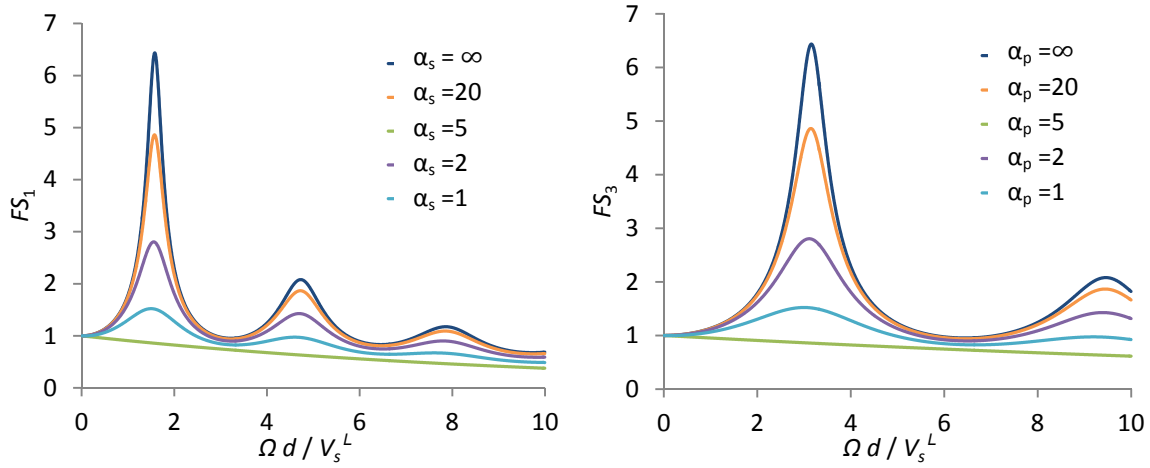

Figure 4.1: Amplification of vertically incident SH/SV waves (left) and P waves (right) for a single layer over halfspace, $\rho_s^H = \rho_s^L$, $\xi^H = \xi^L$, $v_s = 0.33$.

The one-dimensional theory, although provides a valuable physical insight into the basic principles of wave amplification, is not reliable in all circumstances. Local site conditions, such as lateral discontinuities, inclined soil layers and irregular surface topography may generate amplifications on soft soils significantly larger than those produced by plane soil layers of infinite lateral extent overlaying a homogeneous halfspace (Makra et al., 2001; Ktenidou et al., 2007). Moreover, soil exhibits nonlinear behavior even at small strains, whereas the ratios in Eq. (4.9) and (4.13) are unique irrespective of the magnitude of earthquake. Customarily, in order to compensate for the inelastic behavior, approximate linear solutions are obtained iteratively by adjusting the frequency- and depth-dependent material parameters to the levels of strain computed (Kausel and Asimaki, 2002). In cases of high seismic intensities at rock base and/or high strains levels in the soil layers, a nonlinear time-domain solution is recommended (Phillips and Hashash, 2009).

4.1.2 Seismic response of single structures

The matrix equation of motion of a two-dimensional single structure-foundation system such as that depicted in Figure 4.2a is given by:

$$\mathbf{M}\,\ddot{\mathbf{w}} + \mathbf{C}\,\dot{\mathbf{v}} + \mathbf{K}\,\mathbf{v} = \mathbf{0} \tag{4.14}$$

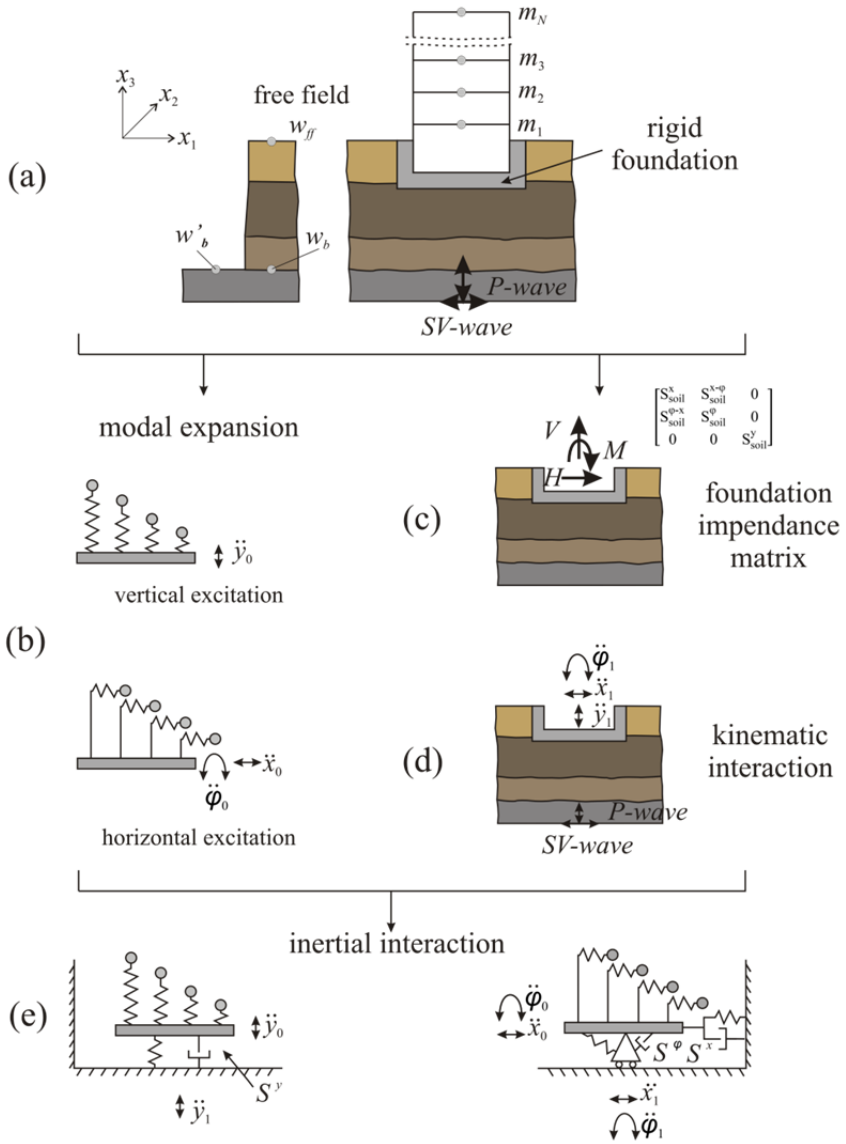

Figure 4.2: Substructure-based solution scheme of a two-dimensional soil-structure interaction problem for seismic excitation.

The solution of Eq. (4.14) is equivalent to the solution of two matrix equations (Kausel et al., 1978):

$$\mathbf{M}_1\,\ddot{\mathbf{w}}_1 + \mathbf{C}\,\dot{\mathbf{v}}_1 + \mathbf{K}\,\mathbf{v}_1 = \mathbf{0} \tag{4.15}$$

$$\mathbf{M}\,\ddot{\mathbf{v}}_2 + \mathbf{C}\,\dot{\mathbf{v}}_2 + \mathbf{K}\,\mathbf{v}_2 = -\mathbf{M}_2\,\ddot{\mathbf{w}}_1 \tag{4.16}$$

where $\mathbf{w_1} = \mathbf{v_1} + \mathbf{w}_{ff}$, $\mathbf{w} = \mathbf{w_1} + \mathbf{v_2}$, $\mathbf{v} = \mathbf{v_1} + \mathbf{v_2}$ and $\mathbf{M} = \mathbf{M_1} + \mathbf{M_2}$. $\mathbf{M_1}$ stands for the mass of the system excluding the mass of the structure, whereas $\mathbf{M_2}$ represents exclusively the mass of the structure. In Eq. (4.15) the response of the massless structure is obtained first and is referred as kinematic motion. The latter determines the fictitious load to be applied in the actual dynamic analysis, the inertial interaction part, as expressed in Eq. (4.16). The kinematic interaction imposes a motion which is generally different from the free-field motion and in addition contains a rotational component (Qian and Beskos, 1996). These effects are significant for embedded foundations. Only for the special case of structures with no embedment under the assumption of vertically propagating seismic waves, the kinematic interaction vanishes (Mylonakis et al., 2006). Provided that the foundation is rigid, the solution breaks then in the following three steps:

a) Determination of the motion of the massless rigid foundation when subjected to the same input motion as the total solution (Figure 4.2d).
b) Calculation of the subgrade impedance functions corresponding to each mode of vibration; the soil medium is replaced by dynamic springs and dashpots, which represent the soil's dynamic stiffness and energy dissipation in the medium respectively (Figure 4.2c).
c) Computation of the response of the structure supported on the springs and dashpots and subjected to the motion computed in step a) (Figure 4.2e).

Generally, it is suitable to carry out the analysis in the frequency domain, since the impedance functions are frequency-dependent. For structures of multiple degrees of freedom such as multistory buildings the total response can be expressed as a superposition of modal contributions (Figure 4.2b) (Meek and Veletsos, 1972). Regarding step c), the solution cannot be obtained straightforwardly since the foundation motion is different from the motion in the absence of the superstructure. Indeed, the method requires, due to the decoupled response in horizontal and vertical direction, solution of two simultaneous equations for the horizontal and rotational footing motion and one equation for the vertical footing motion. The structural response follows by back substitution in horizontal and vertical direction. Specifically, formulation of the dynamic equilibrium equations of the total system for the active degrees of freedom combined with the dynamic equilibrium of each modal mass and elimination of the superstructure's degrees of freedom yields:

$$\begin{bmatrix} S_{str.}^{x} & S_{str.}^{x-\varphi} & 0 \\ S_{str.}^{\varphi-x} & S_{str.}^{\varphi} & 0 \\ 0 & 0 & S_{str.}^{y} \end{bmatrix} \begin{bmatrix} x_0 \\ \varphi_0 \\ y_0 \end{bmatrix} = \begin{bmatrix} H \\ M \\ V \end{bmatrix} \tag{4.17}$$

where $S_{str.}$ are complex, frequency dependent coefficients of the superstructure's dynamic stiffness expressed as sum of all modal contributions, x_0, y_0 and φ_0 stand for the foundation horizontal, vertical displacement and rotation respectively and H, M and V represent the interface shear, moment and vertical reaction respectively. All response quantities are complex-valued and frequency

dependent. A free body cut the through the soil-structure interface yields a dynamic generalized force-deformation relationship in matrix form as:

$$\begin{bmatrix} S_{soil.}^{x} & S_{soil.}^{x-\varphi} & 0 \\ S_{soil.}^{\varphi-x} & S_{soil.}^{\varphi} & 0 \\ 0 & 0 & S_{soil.}^{y} \end{bmatrix} \begin{bmatrix} x_0 - x_1 \\ \varphi_0 - \varphi_1 \\ y_0 - y_1 \end{bmatrix} = \begin{bmatrix} H \\ M \\ V \end{bmatrix} \tag{4.18}$$

where $S_{soil.}$ are complex, frequency dependent coefficients of the soil's dynamic stiffness (springs and dashpots), x_1, y_1 and φ_1 are the horizontal, vertical and rotational components of the foundation input motion ($\mathbf{w_1}$). Due to the embedment: $\mathbf{w}_1 \neq \mathbf{w}_{ff}$. The expressions in Eq. (4.17) and Eq. (4.18) are equated and the steady state footing motion can be solved in terms of x_1, y_1 and φ_1. The response of the superstructure for each mode is then determined by means of transfer functions for the modal contributions and the total response is obtained by superimposing all responses of the modes.

4.2 Substructure method for multiple liquid-storage tanks

This section is concerned with the development of a refined procedure for the seismic analysis of multiple liquid-storage tanks. Inclusion of the subsoil cross-interaction effects in the analysis necessitates revision of the formulations described in section 4.1.2. In particular, the determination of the base motion for every tank requires in the most general case solution of a $5J$x$5J$ linear system, where J is the number of tanks, as will be demonstrated successively, since the wavefields propagating between the structures produce coupled modes of vibration for the foundations-soil substructure which in turn generate coupled responses for the tank-liquid substructures.

Since in this work the dynamic response of tanks lying on surface foundations under vertically incident waves is examined, the solution step a) in section 4.1.2 is omitted and the input motion includes only translational components corresponding to the free-field motion. Regarding step b), the impedance functions for multiple rigid circular foundations have been computed in section 3.5. The tank-liquid systems modeled by means of effective masses and equivalent heights as developed in section 2.2 constitute the structural part for the step c).

4.2.1 System considered and assumptions

The system under investigation is composed of J circular, cylindrical liquid-storage tanks distributed in three dimensional space. A general illustration is given in Figure 4.3. Interconnecting pipings or other transmission equipment between the tanks are not taken into account. Each of the tanks is supported through rigid circular mat at the surface of an elastic or viscoelastic, isotropic, homogeneous stratum over rigid bedrock. The rigid substratum may be at shallow depth d or in the limiting case at infinite distance from the surface, a state which is equivalent with a semi-infinite soil medium. The

identical radii R of the foundations are considered to be equal to the radii of the roofless containers. Each tank is assumed to be completely filled ($H = H_L$) with an incompressible, inviscid liquid. The thickness h of the –clamped to their base- tanks walls is regarded as uniform. Torsional effects due to the subsoil coupling of the tanks response are not considered.

It is worth mentioning that the proposed computational procedure maintains its generality even if other soil conditions or tank properties are considered. The restrictions involved in the approach concern the potential nonlinear behavior of the tanks, foundations and soil region and the deformability of the foundations. The effects of primary nonlinearities for the soil medium can be estimated by a standard repetitive method in which the shear moduli and damping are modified in each iteration so as to be consistent with the levels of strain of the previous iteration in the free field (Kausel and Asimaki, 2002). The results can be used as estimates of the soil properties in the total solution. The response of superstructures must be strictly considered linear-elastic due to the applicability of the principle of superposition. With respect to the foundations rigidity, the substructure method is incompetent to reproduce flexible mats, unless series of distributed springs and dashpots acting around each foundation are used.

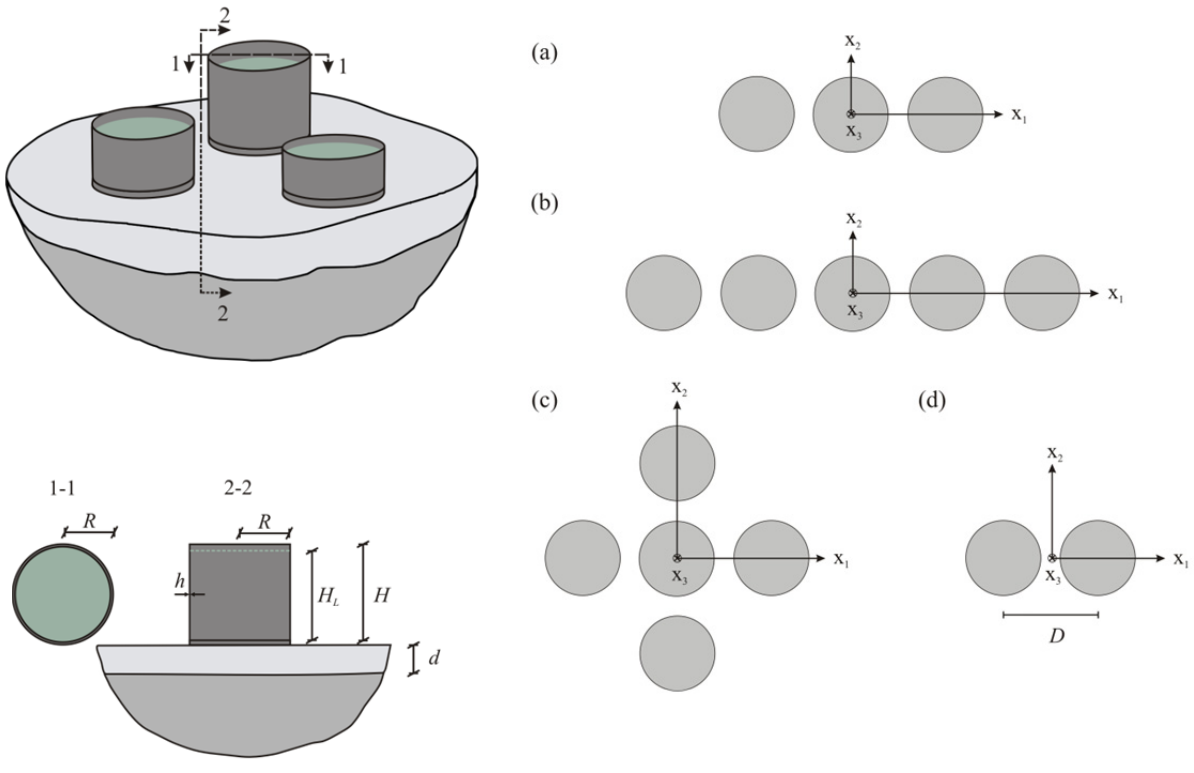

Figure 4.3: Group of adjacent liquid-storage tanks (left) and layout of examined spatial arrangements (right).

The examined spatial arrangements for the tanks are depicted in Figure 4.3. Spatial variations of the seismic motions are ignored and all tanks are subjected to the same ground motion. The seismic

excitation is represented by vertically incident plane SH, SV and P waves. The particle motion of the SH waves is polarized along the x_2-axis, whereas the particle motion of SV and P waves is polarized in the plane defined by the axes x_1 and x_3. The center-to-center distance D between the tanks is measured in parallel to x_1 and x_2 axes and is the same between all tanks for every configuration.

4.2.2 Response of superstructures to prescribed base motion

The models for the tanks and the foundations-soil developed in the previous chapters, which are depicted in Figures 2.24 and 3.18 respectively, are interrelated in order to establish the equations of dynamic equilibrium at the interfaces of the tank bases and foundations. By doing so, the model shown in Figure 4.4 is set up.

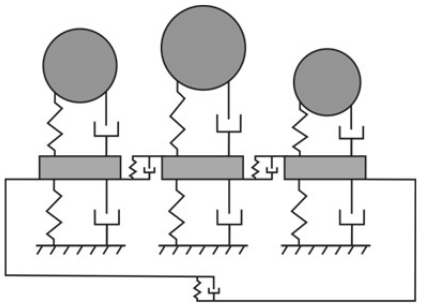

Figure 4.4: Illustrative model for multiple liquid-storage tanks on deformable soil.

The response of each tank-liquid system to a prescribed vertical and combined horizontal-rocking excitation is evaluated by superimposing the natural modes of vibration associated with a non-deformable medium.

Impulsive effects: Vertical component

The component of the instantaneous value of base shear for the *n*th mode is:

$$Q_3^{IMP\cdot}(t) = m_{VR}\ddot{w}_{3,ff}(t) + \sum_{n=1}^{N1} m_{0,n}\,\ddot{w}_{3,n}^{IMP\cdot}(t) \tag{4.19}$$

where $\ddot{w}_{3,n}^{IMP\cdot}(t)$ represents the vertical absolute pseudoacceleration response associated with the *n*th fixed-base mode of the liquid-tank system subjected to a prescribed vertical base excitation $\ddot{w}_3^b$ acting along the x_3 axis and $m_{VR} = m_L - \sum_{n=1}^{N} m_{0,n}$.

Impulsive effects: Horizontal components

The component of the instantaneous value of base shear for the *n*th mode is:

$$Q_k^{H\cdot}(t) = \sum_{n=1}^{N2} m_{1,n}\, \ddot{w}_{k,n}^{H\cdot}(t) \tag{4.20}$$

where $\ddot{w}_{k,n}^{H\cdot}(t)$ represents the horizontal absolute pseudoacceleration response associated with the nth fixed-base mode of the liquid-tank system subjected to a prescribed horizontal base excitation $\ddot{w}_k^b$ along the horizontal x_k axis ($k = 1,2$). The corresponding value of bending moment at a section of the tank immediately above the base is:

$$M_k^{H\cdot}(t) = \sum_{n=1}^{N2} m_{1,n}\, h_{1,n}\, \ddot{w}_{k,n}^{H\cdot}(t) \tag{4.21}$$

The moment induced by the pressure on the tank base can be written as:

$$\Delta M_k^{H\cdot}(t) = \sum_{n=1}^{N2} m_{1,n}\, \Delta h_{1,n}\, \ddot{w}_{k,n}^{H\cdot}(t) \tag{4.22}$$

The total moment carried from the foundation is:

$$MM_k^{H\cdot}(t) = \sum_{n=1}^{N2} m_{1,n}\, h'_{1,n}\, \ddot{w}_{k,n}^{H\cdot}(t) \tag{4.23}$$

where: $h'_{1,n} = h_{1,n} + \Delta h_{1,n}$

Impulsive effects: Rocking components

Because of the soil's flexibility, the tank base experiences a rocking base motion $\ddot{\varphi}_\kappa,\ k = 1,2$ about the horizontal axes. This motion causes an angular vibration of the flexible wall and the rigid base itself. Regarding the former, an interrelationship of a tank responses to rocking and lateral motions of assumed same temporal variation can be established according to the generalization of Betti's principle (Veletsos and Tang, 1990): the work done by the base shear for a tank in rocking acting through the base displacement for the laterally excited tank is equal to the work done by the foundation moment for the laterally excited tank through the base rotation of the tank in rocking. Accordingly, we can write:

$$m_{R,n} = \frac{h'_{1,n}}{H}\ m_{1,n} \tag{4.24}$$

Regarding the rotation of the rigid base, additional moments at base of the tank about each horizontal axis should be considered. These moments are proportional to the base motion $\ddot{\varphi}_\kappa,\ k = 1,2$ and can be determined by solving Laplace equation given by (2.79) with the following boundary conditions:

$$\varphi_R: \qquad \left.\frac{\partial \varphi_R}{\partial z}\right|_{z=0} = -\dot{\varphi}(t)\, r\cos(\theta)\ , \quad \left.\frac{\partial \varphi_R}{\partial r}\right|_{r=R} = 0, \qquad \rho_L \left.\frac{\partial \varphi_R}{\partial t}\right|_{z=H_L} = 0 \tag{4.25}$$

The solution can be obtained by separation of variables and expressed in the form (Veletsos and Tang, 1987):

$$\varphi_R(r,\theta,t) = \left\{\sum_{i=1}^{\infty} \frac{2}{{a_i}^2}\left[(-1)^{i+1} - \frac{2}{H_L\, a_i}\right]\frac{I_1(a_i\, r)}{{I_1}'(a_i\, R)} + H_L r\right\}\cos(\theta)\,\dot{\varphi}(t) \tag{4.26}$$

where $a_i = \pi(2\,i-1)/(2\,H_L)$. The hydrodynamic pressure corresponding to the solution of Eq. (4.26) is given by:

$$p_R(r,\theta,t) = \bar{p}_R(r) R\,\rho_L\,\cos(\theta)\,H_L\,\dot{\varphi}(t) \tag{4.27}$$

where:

$$\bar{p}_R(r) = \sum_{i=1}^{\infty} \frac{2}{R\,H_L\,{a_i}^2}\left[(-1)^{i+1} - \frac{2}{H_L\,a_i}\right]\frac{I_1(a_i\, r)}{{I_1}'(a_i\, R)} + \frac{r}{R} \tag{4.28}$$

The mass moment of inertia I_0^B about a horizontal centroidal axis for the part of the liquid that is considered to move together with the rocking base is determined by integration of the pressure, given by Eq. (4.28), over the tank base. Accordingly, the moment induced by the pressure on the tank base is given by:

$$\Delta M_0^R(t) = \int_0^{2\pi}\int_0^{R} p_R(r,\theta,t)\, r^2\cos(\theta)\,\mathrm{d}r\mathrm{d}\theta = I_0^B\,\ddot{\varphi}(t) \tag{4.29}$$

where:

$$I_0^B = \left\{\frac{1}{4} + \sum_{i=1}^{\infty}\frac{2}{H_L\,R^2\,{a_i}^3}\left[(-1)^{i+1} - \frac{2}{H_L\,a_i}\right]\frac{I_2(a_i\,R)}{{I_1}'(a_i\,R)}\right\} m_L R^2 \tag{4.30}$$

Analogously to the horizontal component the base shear and base moments induced by the rocking excitation are:

$$Q_k^R(t) = \sum_{n=1}^{N2} m_{R,n}\,\ddot{w}_{k,n}^{R.}(t) \tag{4.31}$$

$$M_k^R(t) = \sum_{n=1}^{N2} m_{R,n}\,h_{1,n}\,\ddot{w}_{k,n}^{R.}(t) \tag{4.32}$$

$$\Delta M_k^R(t) = \sum_{n=1}^{N2} m_{R,n}\,\Delta h_{1,n}\,\ddot{w}_{k,n}^{R.}(t) + I_0^B\,\ddot{\varphi}_k(t) \tag{4.33}$$

$$MM_k^R(t) = \sum_{n=1}^{N2} m_{R,n}\,h'_{1,n}\,\ddot{w}_{k,n}^{R.}(t) + I_0^B\,\ddot{\varphi}_k(t) \tag{4.34}$$

where $\ddot{w}_{k,n}^{R.}(t)$ represents the horizontal absolute pseudoacceleration response associated with the *n*th fixed-base mode of the liquid-tank system subjected to a prescribed horizontal base excitation $H\ddot{\varphi}_k$.

Impulsive effects: Combined horizontal and rocking components

After plugging Eq. (4.24) into Eq. (4.31)-(4.34), the total impulsive effects for laterally excited tanks can be determined by superposition:

$$Q_k^{IMP\cdot}(t) = \sum_{n=1}^{N2} m_{1,n}\, \ddot{w}_{k,n}^{IMP\cdot}(t) \tag{4.35}$$

$$M_k^{IMP\cdot}(t) = \sum_{n=1}^{N2} m_{1,n}\, h_{1,n}\, \ddot{w}_{k,n}^{IMP}\,(t) \tag{4.36}$$

$$\Delta M_k^{IMP\cdot}(t) = \sum_{n=1}^{N2} m_{1,n}\, \Delta h_{1,n}\, \ddot{w}_{k,n}^{IMP\cdot}(t) + I_0^b \ddot{\varphi}_k(t) \tag{4.37}$$

$$MM_k^{IMP\cdot}(t) = \sum_{n=1}^{N2} m_{1,n}\, h'_{1,n}\, \ddot{w}'_{k,n}\,(t) \tag{4.38}$$

where:

$$\ddot{w}_{k,n}^{IMP\cdot}(t) = \ddot{w}_{k,n}^{H\cdot}(t) + \frac{h'_{1,n}}{H} \ddot{w}_{k,n}^{R\cdot}(t) \tag{4.39}$$

$$\ddot{w}'_{k,n}(t) = \ddot{w}_{k,n}^{IMP\cdot}(t) + \frac{I_0^b \ddot{\varphi}_k(t)}{\sum_{n=1}^{N2} m_{1,n}\, h'_{1,n}} \tag{4.40}$$

Convective effects

The convective effects of rigidly supported flexible tanks can be evaluated considering the tank wall to be rigid as explained in section 2.2. Thus, impulsive and convective actions are assumed to be uncoupled. Veletsos and Tang (1990) confirmed the validity of this assumption also for the case of tanks founded on soft soils; soil-structure interaction effects have a negligible influence on the convective components of the response, therefore it is admissible to evaluate them for the free-field ground motion considering both the tank and the supporting medium as rigid. The adequacy of this conclusion for the case of multiple tanks is examined in section 4.3.3. The base shear and moments induced by the convective action are given by:

$$Q_k^{SL}(t) = \sum_{n=1}^{N3} m_{SL,n}\, \ddot{w}_{k,n}^{SL\cdot}(t) \tag{4.41}$$

$$M_k^{SL}(t) = \sum_{n=1}^{N3} m_{SL,n}\, h_{SL,n}\, \ddot{w}_{k,n}^{SL\cdot}\,(t) \tag{4.42}$$

$$\Delta M_k^{SL}(t) = \sum_{n=1}^{N3} m_{SLk,n}\, \Delta h_{SL,n}\, \ddot{w}_{k,n}^{SL\cdot}(t) \tag{4.43}$$

$$MM_k^{SL}(t) = \sum_{n=1}^{N3} m_{SLk,n}\, h'_{SL,n}\, \ddot{w}_{k,n}^{SL\cdot}\,(t) \tag{4.44}$$

where: $h'_{SL,n} = h_{SL,n} + \Delta h_{SL,n}$ and:

$$\ddot{w}_{k,n}^{SL\cdot}(t) = \ddot{w}_{k,n}^{SLH\cdot}(t) + \frac{h'_{SL,n}}{H}\ddot{w}_{k,n}^{SLR\cdot}(t) \tag{4.45}$$

4.2.3 Steady state analysis of tank-liquid systems

Impulsive effects

If each modal mass $m_{0,n}$ is isolated, the vertical force equilibrium is obtained:

$$m_{0,n}\ddot{w}_{3,n}^{IMP\cdot}(t) + c_{0,n}\dot{w}_{3,n}^{IMP\cdot}(t) + k_{0,n}w_{3,n}^{IMP\cdot}(t) = -m_{0,n}\ddot{w}_3^b(t) \tag{4.46}$$

The quantities $\ddot{w}_{3,n}^{IMP\cdot}$, $\dot{w}_{3,n}^{IMP\cdot}$ and $w_{3,n}^{IMP\cdot}$ refer to relative responses. For a steady state case in which: $w_3^b(t) = w_3^b e^{\mathrm{i}\Omega t}$, Eq. (4.46) can be transformed into the following expression for $w_{3,n}^{IMP\cdot}$ in terms of the unknown vertical footing motion:

$$\ddot{w}_{3,n}^{IMP\cdot}(t) = -\Omega^2\, T_{0,n}\, w_3^b\, e^{\mathrm{i}\Omega t} \tag{4.47}$$

where:

$$T_{0,n} = \frac{1 + 2\,\mathrm{i}\,\xi_{0,n}\dfrac{\Omega}{\omega_{0,n}}}{1 - \left(\dfrac{\Omega}{\omega_{0,n}}\right)^2 + 2\,\mathrm{i}\,\xi_{0,n}\dfrac{\Omega}{\omega_{0,n}}} \tag{4.48}$$

The equation, which expresses the dynamic equilibrium of each modal mass $m_{1,n}$ concentrated at distance $h'_{1,n}$ from the ground surface in each horizontal direction, follows as:

$$m_{1,n}\ddot{w}_{k,n}^{IMP\cdot}(t) + c_{1,n}\dot{w}_{k,n}^{IMP\cdot}(t) + k_{1,n}w_{k,n}^{IMP\cdot}(t) = -m_{1,n}\ddot{w}_k^b(t) - m_{1,n}h'_{1,n}\,\ddot{\varphi}_k(t) \tag{4.49}$$

For a steady state case in which: $w_k^b(t) = w_k^b e^{\mathrm{i}\Omega t}$, $\varphi_k(t) = \varphi_k e^{\mathrm{i}\Omega t}$, Eq. (4.49) can be transformed into the following expression for $w_{k,n}^{IMP}$ in terms of the unknown horizontal and rocking footing motion:

$$\ddot{w}_{k,n}^{IMP\cdot}(t) = -\Omega^2\, T_{1,n}\left(w_k^b + h'_{1,n}\,\varphi_k\right) e^{\mathrm{i}\Omega t} \tag{4.50}$$

where $T_{1,n}$ is a transfer function for the superstructure:

$$T_{1,n} = \frac{1 + 2\,\mathrm{i}\,\xi_{1,n}\dfrac{\Omega}{\omega_{1,n}}}{1 - \left(\dfrac{\Omega}{\omega_{1,n}}\right)^2 + 2\,\mathrm{i}\,\xi_{1,n}\dfrac{\Omega}{\omega_{1,n}}} \tag{4.51}$$

Convective effects

Analogously to the case of the impulsive modal masses the response for every sloshing mode is given by:

$$\ddot{w}_{k,n}^{SL.}(t) = -\Omega^2\, T_{SL,n}\left(w_k^b + h'_{SL,n}\,\varphi_k\right) e^{\mathrm{i}\Omega t} \tag{4.52}$$

where:

$$T_{SL,n} = \frac{1 + 2\,\mathrm{i}\,\xi_{SL,n}\dfrac{\Omega}{\omega_{SL,n}}}{1 - \left(\dfrac{\Omega}{\omega_{SL,n}}\right)^2 + 2\,\mathrm{i}\,\xi_{SL,n}\dfrac{\Omega}{\omega_{SL,n}}} \tag{4.53}$$

Next, the equations for the dynamic equilibrium of the mth tank, $m = 1..J$ as a whole are established:

$$m'_0\,\ddot{w}_3^b(t) + \sum_{n=1}^{N1} m_{0,n}\,\ddot{w}_{3,n}^{IMP.}(t) + V_3(t) = 0 \tag{4.54}$$

$$\left(I_F + I_0^b\right)\ddot{\varphi}_k(t) + \sum_{n=1}^{N2} m_{1,n}\,h'_{1,n}\,\ddot{w}'_{k,n}(t)\,(t) + \sum_{n=1}^{N3} m_{SL,n}\,h'_{SL,n}\,\ddot{w}_{k,n}^{SL.}\,(t) + M_k(t) = 0 \tag{4.55}$$

$$m_F\,\ddot{w}_k^b(t) + \sum_{n=1}^{N2} m_{1,n}\,\ddot{w}_{k,n}^{IMP.}(t) + \sum_{n=1}^{N3} m_{SL,n}\,\ddot{w}_{k,n}^{SL.}(t) + V_k(t) = 0 \tag{4.56}$$

where $m'_0 = m_F + m_{VR}$, m_F and I_F represent the mass and mass moment of inertia of the footing respectively. V_3, V_k and M_k are the forces and moments at the foundation-soil interface. Elimination of the degrees of freedom associated with the superstructure requires substitution of Eq. (4.50), (4.47) and (4.52) into Eq. (4.54)-(4.56). Accordingly, the matrix steady-state version of Eq. (4.54)-(4.56) for the mth tank is obtained as:

$$\begin{bmatrix} S_{11} & 0 & 0 & 0 & S_{15} \\ 0 & S_{22} & 0 & S_{24} & 0 \\ 0 & 0 & S_{33} & 0 & 0 \\ 0 & S_{42} & 0 & S_{44} & 0 \\ S_{51} & 0 & 0 & 0 & S_{55} \end{bmatrix}_m \begin{Bmatrix} w_1^b \\ w_2^b \\ w_3^b \\ \varphi_1 \\ \varphi_2 \end{Bmatrix}_m = \begin{Bmatrix} V_1 \\ V_2 \\ V_3 \\ M_1 \\ M_2 \end{Bmatrix}_m \tag{4.57}$$

where:

$$S_{11} = m_F\Omega^2 + \sum_{n=1}^{N2} m_{1,n}\,\Omega^2\,T_{1,n} + \sum_{n=1}^{N3} m_{SL,n}\,\Omega^2\,T_{SL,n} \tag{4.58}$$

$$S_{33} = m'_0\,\Omega^2 + \sum_{n=1}^{N1} m_{0,n}\,\Omega^2\,T_{0,n} \tag{4.59}$$

$$S_{24} = \sum_{n=1}^{N2} m_{1,n}\,\Omega^2\,h'_{1,n}\,T_{1,n} + \sum_{n=1}^{N3} m_{SL,n}\,\Omega^2 h'_{SL,n}\,T_{SL,n} \tag{4.60}$$

$$S_{44} = I_F\,\Omega^2 + I_0^b\,\Omega^2 + \sum_{n=1}^{N2} m_{1,n}\,\Omega^2\left(h'_{1,n}\right)^2 T_{1,n} + \sum_{n=1}^{N3} m_{SL,n}\,\Omega^2\left(h'_{SL,n}\right)^2 T_{SL,n} \tag{4.61}$$

and $S_{22} = S_{11}$, $S_{55} = S_{44}$, $S_{15} = S_{51} = S_{24} = S_{42}$. Alternatively, Eq. (4.57) can be written in vector-tensor notation:

$$\mathbf{S}_m \, \mathbf{X}_m = \mathbf{F}_m \tag{4.62}$$

where:

$$\boldsymbol{X}_m = \{w_1^b \quad w_2^b \quad w_3^b \quad \varphi_1 \quad \varphi_2\}^{\mathrm{T}} \tag{4.63}$$

$$\boldsymbol{F_m} = \{V_1 \quad V_2 \quad V_3 \quad M_1 \quad M_{\mathbf{2}}\}^{\mathrm{T}} \tag{4.64}$$

The above procedure can be followed similarly for $J-1$ tanks, yielding the following equation:

$$\begin{bmatrix} \mathbf{S}_1 & 0 & 0 & 0 & 0 \\ 0 & \ddots & 0 & 0 & 0 \\ 0 & 0 & \mathbf{S}_m & 0 & 0 \\ 0 & 0 & 0 & \ddots & 0 \\ 0 & 0 & 0 & 0 & \mathbf{S}_J \end{bmatrix} \begin{Bmatrix} \mathbf{X}^1 \\ \vdots \\ \mathbf{X}^m \\ \vdots \\ \mathbf{X}^J \end{Bmatrix} = \begin{Bmatrix} \mathbf{F}^1 \\ \vdots \\ \mathbf{F}^m \\ \vdots \\ \mathbf{F}^J \end{Bmatrix} \tag{4.65}$$

By omitting the indices, Eq. (4.65) can be written in the form:

$$\mathbf{S} \, \mathbf{X} = \mathbf{F} \tag{4.66}$$

4.2.4 Steady state analysis of soil

The generalized reactions forces $\mathbf{F}_m$ of the mth foundation in a group of J tanks can be determined by passing a free a body cut through the soil-foundations interfaces. The dynamic force-deformation relationship for the subgrade is written in matrix form as:

$$\mathbf{F}_m = \mathbf{K}^{m1}(\mathbf{X}_1 - \mathbf{X}_{ff}) + .. + \mathbf{K}^{mm}(\mathbf{X}_m - \mathbf{X}_{ff}) + .. + \mathbf{K}^{mp}(\mathbf{X}_p - \mathbf{X}_{ff}) + .. + \mathbf{K}^{mJ}(\mathbf{X}_J - \mathbf{X}_{ff}) \tag{4.67}$$

where $\mathbf{K}^{mp}$ is a complex, frequency-dependent matrix which contains the impedance functions given by:

$$\mathbf{K}^{mp} = \begin{bmatrix} K_{11}^{mp} & K_{12}^{mp} & K_{13}^{mp} & K_{14}^{mp} & K_{15}^{mp} \\ K_{21}^{mp} & K_{22}^{mp} & K_{23}^{mp} & K_{24}^{mp} & K_{25}^{mp} \\ K_{31}^{mp} & K_{32}^{mp} & K_{33}^{mp} & K_{34}^{mp} & K_{35}^{mp} \\ K_{41}^{mp} & K_{42}^{mp} & K_{43}^{mp} & K_{44}^{mp} & K_{45}^{mp} \\ K_{51}^{mp} & K_{52}^{mp} & K_{53}^{mp} & K_{54}^{mp} & K_{55}^{mp} \end{bmatrix} \tag{4.68}$$

and $\mathbf{X}_{ff}$ the vector of the free field ground motion defined as:

$$\mathbf{X}_{ff} = \{w_{1,ff} \quad w_{2,ff} \quad w_{3,ff} \quad 0 \quad 0\}^{\mathrm{T}} \tag{4.69}$$

in which the index $k = 1,2,3$ stands for the axis x_k along the motion is produced. The dynamic equilibrium for the J foundations is subsequently obtained by inspection in the following form:

$$\begin{Bmatrix} \mathbf{F}_1 \\ \vdots \\ \mathbf{F}_m \\ \vdots \\ \mathbf{F}_p \\ \vdots \\ \mathbf{F}_J \end{Bmatrix} = \begin{bmatrix} \mathbf{K}^{11} & \dots & \mathbf{K}^{1m} & \dots & \mathbf{K}^{1p} & \dots & \mathbf{K}^{1J} \\ \vdots & \ddots & \vdots & \ddots & \vdots & \ddots & \vdots \\ \mathbf{K}^{m1} & \dots & \mathbf{K}^{mm} & \dots & \mathbf{K}^{mp} & \dots & \mathbf{K}^{mJ} \\ \vdots & \ddots & \vdots & \ddots & \vdots & \ddots & \vdots \\ \mathbf{K}^{p1} & \dots & \mathbf{K}^{pm} & \dots & \mathbf{K}^{pp} & \dots & \mathbf{K}^{pJ} \\ \vdots & \ddots & \vdots & \ddots & \vdots & \ddots & \vdots \\ \mathbf{K}^{J1} & \dots & \mathbf{K}^{Jm} & \dots & \mathbf{K}^{Jp} & \dots & \mathbf{K}^{JJ} \end{bmatrix} \begin{Bmatrix} \boldsymbol{X}_1 - \boldsymbol{X}_{ff} \\ \vdots \\ \boldsymbol{X}_m - \boldsymbol{X}_{ff} \\ \vdots \\ \boldsymbol{X}_p - \boldsymbol{X}_{ff} \\ \vdots \\ \boldsymbol{X}_J - \boldsymbol{X}_{ff} \end{Bmatrix} \tag{4.70}$$

By omitting the indices, Eq. (4.70) can be written in the form:

$$\mathbf{F} = \mathbf{K}\ \{\boldsymbol{X} - \boldsymbol{X}_{ff}\} \tag{4.71}$$

4.2.5 Subsoil coupling of tank-liquid systems

Eq. (4.66) expresses the generalized interface forces in terms of the dynamic stiffness of the tank-liquid systems, whereas Eq. (4.71) gives a complementary expression relating the same forces with the dynamic stiffness of the soil. It is expedient to equate these relations to obtain a $5J$x$5J$ linear system, which may be solved for the $5J$ steady state footings motions:

$$\mathbf{X} = [\mathbf{K} - \mathbf{S}]^{-1}\ \mathbf{K}\ \mathbf{X}_{ff} \tag{4.72}$$

The procedure to be followed for the assessment of the system's harmonic response is summarized in the following steps:

a) Calculation of the complex-valued amplitudes of the displacements and rotations of each foundation from Eq. (4.72).

b) Evaluation of the tank-liquid pseudoaccelerations by recurrent application of Eq. (4.47), (4.50) and (4.52) for every element in the group.

c) Computation of the responses from Eq. (4.19), (4.35)-(4.38) and (4.41)-(4.44).

The ratios of the absolute displacements of each modal mass to the sinusoidal displacements at the free surface, known as system's transfer functions (or transmissibility ratios), are introduced for the sloshing and impulsive modes:

$$AF_{k,n}^{SL.} = \left|\frac{w_{k,n}^{SL.}}{w_{k,ff}}\right|, n = 1..N_3, k = 1{,}2 \tag{4.73}$$

$$AF_{k,n}^{IMP.} = \left|\frac{w_{k,n}^{IMP.}}{w_{k,ff}}\right|, n = 1..N_2, k = 1{,}2 \qquad AF_{3,n}^{IMP.} = \left|\frac{w_{3,n}^{IMP.}}{w_{3,ff}}\right|, n = 1..N_1 \tag{4.74}$$

The overall transfer functions of the response for each component of the group are expressed as:

$$AS_{k,n}^{SL.} = AF_{k,n}^{SL.}\ FS_k\ , \qquad AS_{k,n}^{IMP.} = AF_{k,n}^{IMP.} FS_k, \qquad AS_{3,n}^{IMP.} = AF_{3,n}^{IMP.} FS_3 \tag{4.75}$$

where $FS_k, k = 1{,}2$ and FS_3 are the displacements transfer functions of the free surface to the excitation at the soil-rock interface. The developed formulations have been implemented in a computer program with the aid of the commercial mathematical software ©MAPLE.

4.3 Dynamic response of adjacent liquid-storage tanks

4.3.1 Dimensionless parameters

The interpretation of the interaction effects on the dynamic response of adjacent liquid-storage tanks is facilitated by introducing dimensionless parameters. For a specific excitation, the system's response depends on the relative stiffness of the tank-liquid systems and the soil, which can be expressed by the ratio: $H\omega_{m,1}/V_s, m = 0{,}1$. Since the numerator is almost constant for the systems under investigation, the problem is controlled by the shear wave velocity of the supporting medium. In this study, the analyses for multiple tanks are carried out for $V_s = 304.8\,\mathrm{m/s}$ and $\rho_s = 2\,t/m^3$. The distance between the tanks is expressed by the ratio D/R and the thickness of the soft layer by the ratio d/R. Theslenderness ratio H/R is the main parameter with regard to the superstructures. A normalized wall thickness $h/R = 0.001$ is chosen for all tanks. However, one may safely anticipate that the trends associated with the presented results apply also for other values of this ratio insofar as the thin shell theory is applicable, since the impulsive modal masses and heights are practically independent from this parameter. The tanks are considered to be filled with liquid of relative mass density $\rho_L/\ \rho = 0.127$. Hysteretic-damping ratio of the tank-liquid system in its fixed-base condition is chosen $\xi_{m,n} = 0.02, m = 0{,}1$ and for the sloshing modes $\xi_{SL,n} = 0.005$. For the viscoelastic soil medium, the soil damping coefficient is taken as $\xi_s = 0.05$. Poisson's ratios for the tank material and soil are 0.3 and 0.33 respectively. The frequency ratio $\Omega/\omega_{m,n}$ is used for the presentation of the results.

4.3.2 Validation of the model

The response of single circular cylindrical tanks on s homogeneous halfspace subjected to harmonic ground motion is firstly examined. The solution to this problem is compared with the corresponding results obtained by Habenberger (2001), who used the mechanical model introduced by Tang (1986) for vertical excitation and refined the mechanical model developed by Veletsos and Tang (1990,1992) by considering the horizontal-rocking coupled response under horizontal excitation. This comparison serves as verification of the implemented formulation, if the matrix in Eq. (4.68) is evaluated for infinite distances between tanks in a group. In addition, investigation of the response of single tanks supplies the succeeding analyses of multiple containers with benchmark solutions. The results are presented for tanks with $H/R = 2$. The foundation mass is not taken into account. Preliminary analyses indicated that consideration of foundation's inertia does not affect significantly the response and can be neglected. Two values of shear wave velocity for the soil are considered: $V_s = 250\,\mathrm{m/s}$ and $V_s = \infty$. The latter corresponds to the solution in absence of SSI effects. From Figure 4.5, it can be

observed that the agreement between the two models is generally satisfactory and slight discrepancies appear only in the high frequency range for the horizontal excitation.

4.3.3 Response to harmonic surface ground excitation

To begin with, two identical containers lying on a semi-infinite, homogeneous medium at a distance $D/R = 2.2$ and subjected to harmonic excitation corresponding to SV and P waves are considered as the simplest cross-interaction system (Figure 4.3d). Initially, the soil medium is considered as perfectly elastic in order to clarify the cross-interaction characteristics.

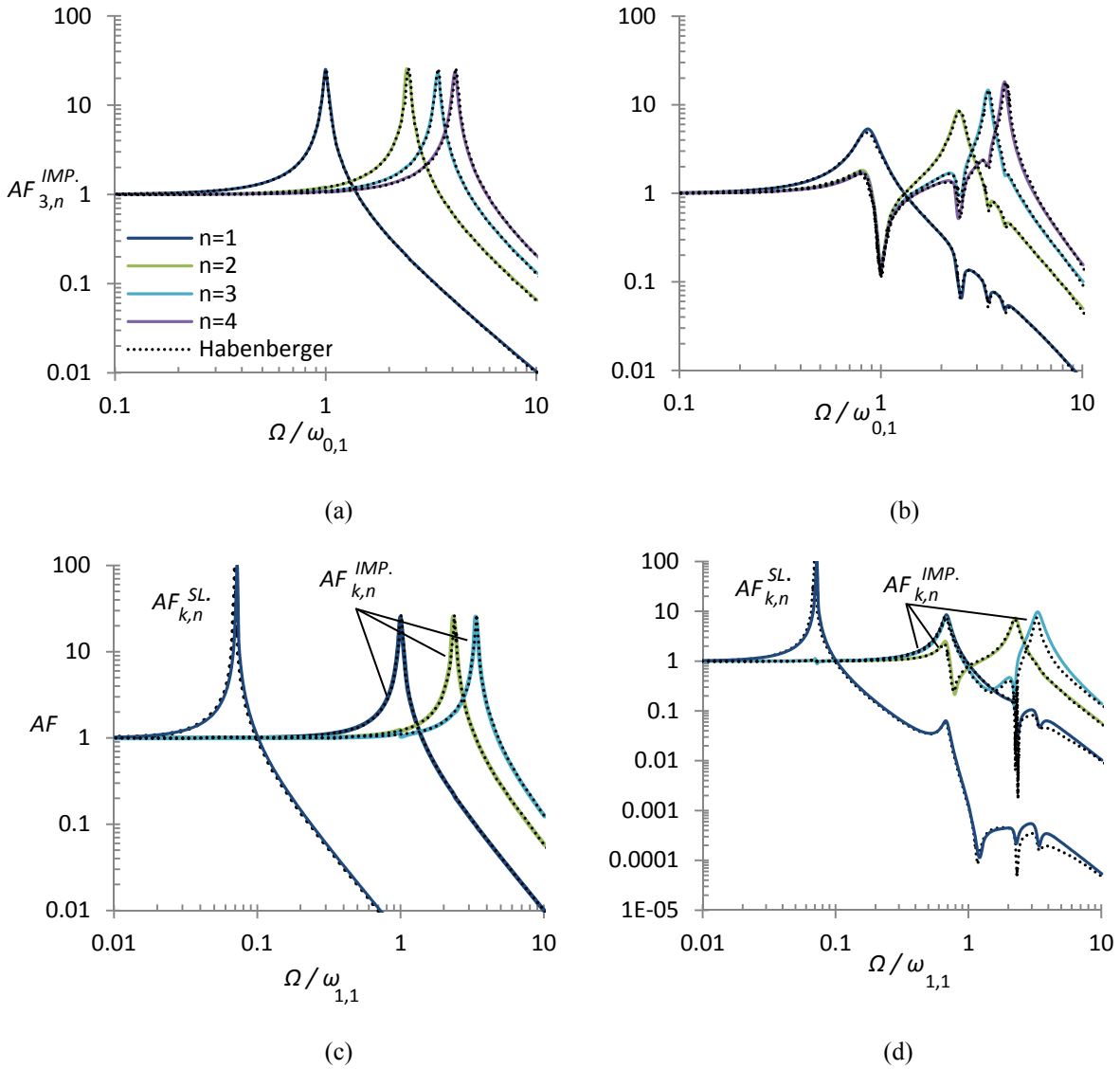

Figure 4.5: Dynamic response of single tanks on elastic semi-infinite medium under a) P waves, $V_s = \infty$, b) P waves, $V_s = 250$ m/s, c) S waves, $V_s = \infty$, d) S waves, $V_s = 250$ m/s.

Figure 4.6 shows the dynamic response in terms of transfer functions for the impulsive and sloshing modes of vibration. The results elucidate two consequences of the cross-interaction between tanks. First, vertical excitation of the system imposes antisymmetric impulsive vibrational modes and vice versa, horizontal excitation imposes axisymmetric impulsive vibrational modes. In addition, nearby tanks subjected to vertical motion sustain sloshing oscillations; these effects are absent in case of single containers and result from the wave energy emitted from one tank to another. Nevertheless, the free surface amplitudes and the lateral/vertical response produced by the vertical/horizontal component of seismic motion are generally small and may be neglected. Second, the interaction between the tanks can alter the impulsive components response in comparison with the corresponding response of a single tank interacting only with the soil underneath, whereas the convective components remain practically insensitive to the presence of adjacent structures. For the frequency range, in which the tank-liquid and sloshing motions appear as coupled, the free surface amplitudes are minor. Thus, it is admissible to evaluate the convective components response considering both tank walls and supporting soil to be rigid. The soil medium, together with the adjacent containers, is ‘‘conceived’’ as rigid by the long-period action of the liquid’s free surface. Due to the fact that for prescribed soil flexibility the presence of nearby tanks does not alter considerably the system’s overall stiffness, at least for a semi-infinite medium, the solution for the convective component is practically the same with that corresponding to single tanks. This fact has been confirmed for all analyses conducted in this study and therefore the sloshing motion is herein not further addressed.

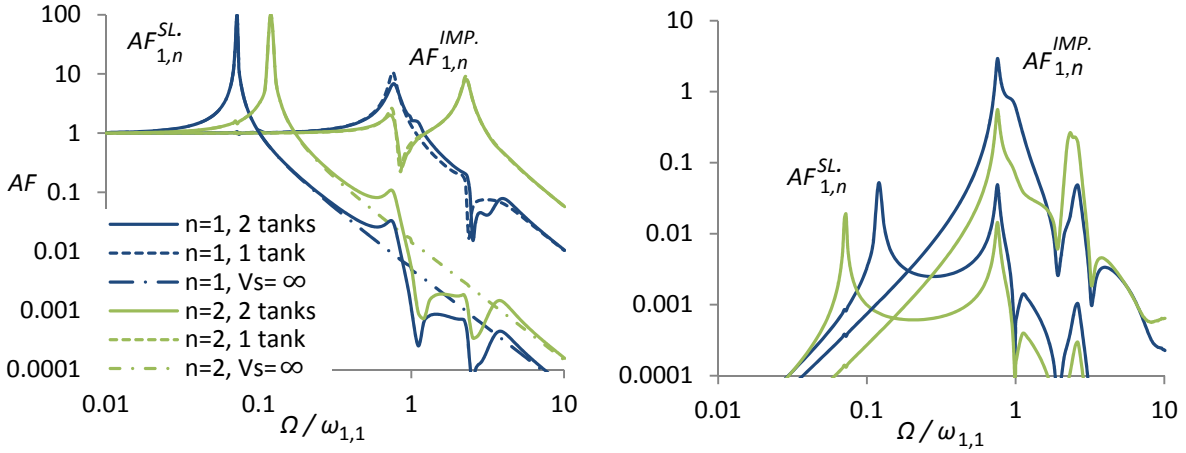

Figure 4.6: Dynamic response of tanks on elastic homogeneous halfspace under SV (left) and P (right) waves, $H/R = 2$.

In Figures 4.7-4.9 the dynamic response of three identical tanks in a row (Figure 4.3d) founded on an elastic semi-infinite medium and subjected to SV waves is presented, regarding their first antisymmetric impulsive natural mode of vibration. Due to the symmetric configuration, the response of the lateral tanks is identical. Three different ratios are examined: $H/R = 0.4$, 1.6 and 2.5. By comparing the three figures, it turns out that the slenderness ratio has a strong influence on tanks

cross-interaction. For small values of the containers height to radius, the transfer functions, with respect to the distance between the tanks, exhibit a wavy behavior with peaks and valleys appearing at regular intervals. In particular, it can be detected that the lowest resonant amplifications occur at frequencies given by:

$$\frac{\Omega}{V_s} = \frac{2\,\pi\,l}{D}, l = 1,2.. \tag{4.76}$$

This feature with regard to the so-called ‘‘Rayleigh’’ frequencies obtained by Eq. (4.76) was also reported by Murakami and Luco (1977) at their study on the dynamic interaction of an infinite number of identical infinitely long elastic shear walls equally spaced. Eq. (4.76) indicates that the amplitudes associated with the resonant frequencies of the total system depend straightforward on the relationship between the corresponding wavelength and the distance between the superstructures. Due to the fact that the fundamental mode of the impulsive component for broad tanks is comparatively excited by waves having short wavelength, the response with respect to the distance oscillates around the solution of a single tank. The impedance functions of multiple foundations calculated in section 3.5.1 provide an insight into these phenomena. As a matter of fact, the amplitudes of the dynamic response observed in Figure 4.7 are controlled by the imaginary part of the translational impedance functions K_{11}^{12} (=K_{11}^{23}) and K_{11}^{ii}, $i = 1,2,3$. For increasing distance, the former oscillate around the impedance of a single foundation in the higher frequency range, whereas the latter in the same range approach zero. From the standpoint of the cross interaction effects relative impact, the steady-state foundations interacting behavior dominates over the inertia effects, the latter are anyhow strongly damped in case of a single tank. As the slenderness of the adjacent tanks increases, the displacement transfer functions are steeper in the vicinity of the first impulsive natural frequency of the tank-liquid-soil system. The effects are more pronounced due to the fact that hysteretic type of damping, which is always present in nature, is not considered in these examples. In case of containers with $H/R = 2.5$, the amplifications functions decrease monotonous for small distances, whereas for an intermediate slenderness $H/R = 1.6$ the displacement amplitudes exhibit a transition state between the other two slenderness ratios. The fundamental antisymmetric impulsive mode of slender tanks is excited by waves having relatively large wavelength, hence one may anticipate that the response is characterized by small overall radiation of wave energy. However, as it was demonstrated in section 3.5, the presence of adjacent tanks does not significantly alter the rocking mode of vibration, which governs the behavior of slender tanks. Therefore, the relative difference of the maximum response that can be recorded between a single tank and a similar one in a group generally decreases as the slenderness increases. From the remarkable reduction of the peak values at small distances for the central tanks with $H/R = 1.6$ and 2.5, one concludes that the vibrational mode of the central tank is out-of-phase with the mode of the lateral containers. It appears that the lateral tanks act like a tuned mass damper for the central tank.

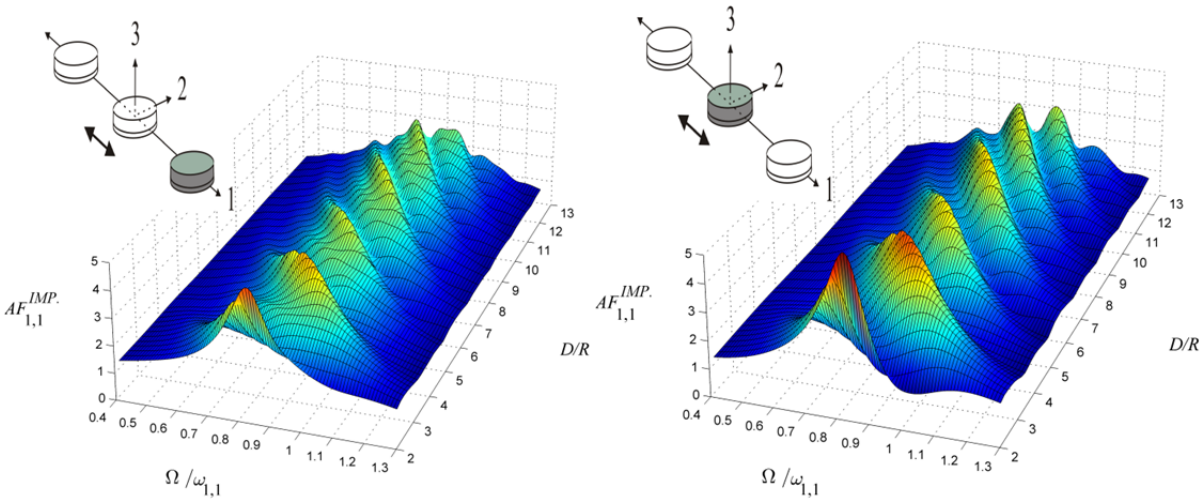

Figure 4.7: Interaction between three identical tanks on elastic homogeneous halfspace under SV waves, $H/R = 0.4$, 1st antisymmetric mode.

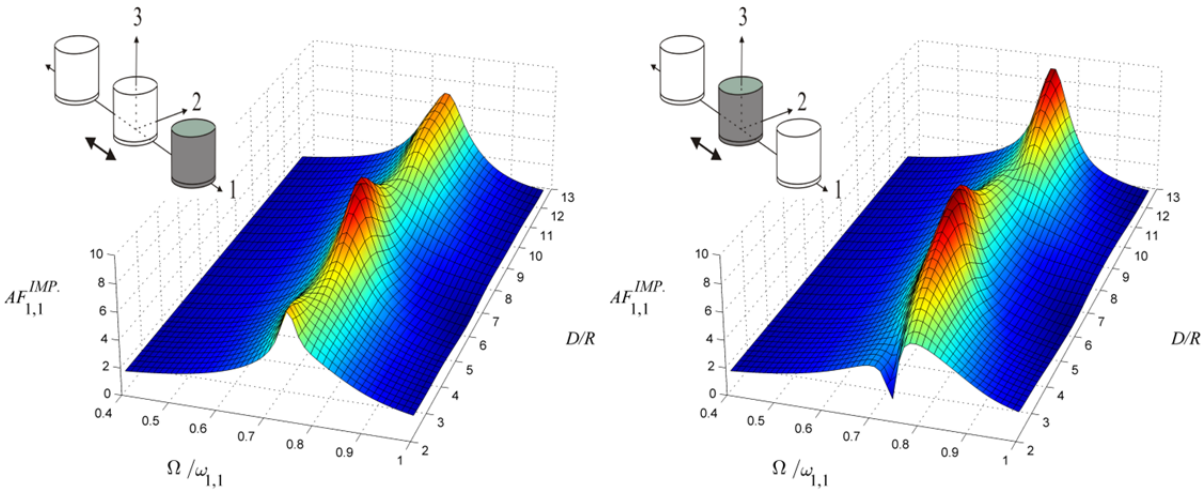

Figure 4.8: Interaction between three identical tanks on elastic homogeneous halfspace under SV waves, $H/R = 1.6$, 1st antisymmetric mode.

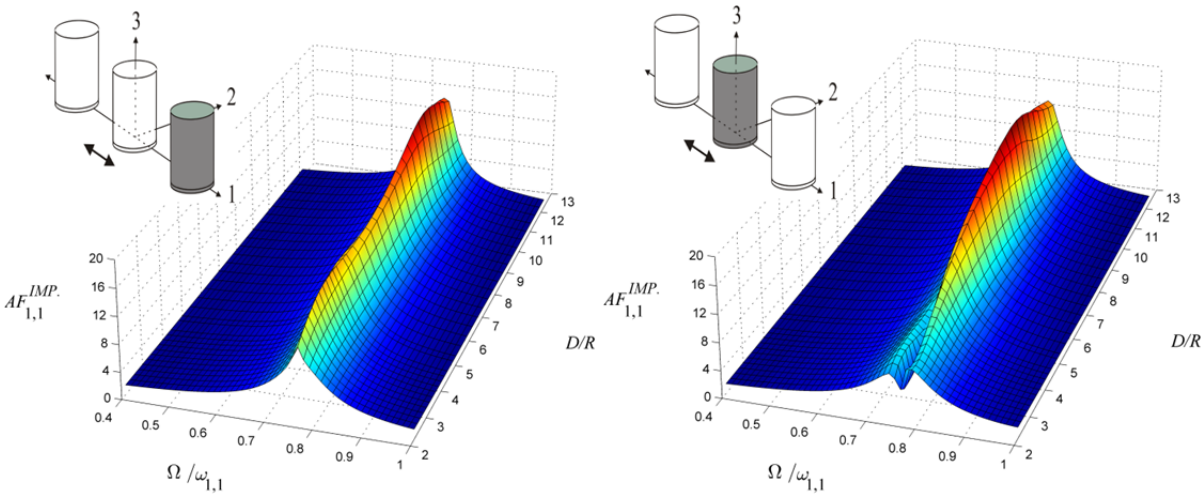

Figure 4.9: Interaction between three identical tanks on elastic homogeneous halfspace under SV waves, $H/R = 2.5$, 1st antisymmetric mode.

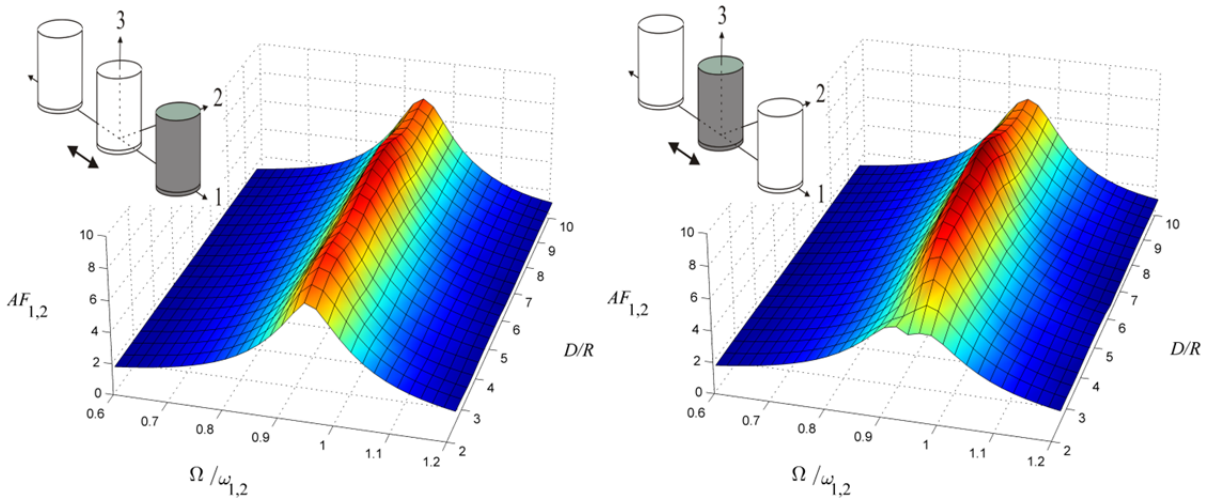

Figure 4.10: Interaction between three identical tanks on elastic homogeneous halfspace under SV waves, $H/R = 2.5$, 2nd antisymmetric mode.

Similar observations have been made for adjacent buildings by using discrete models (Padrón et al., 2009, Alexander et al., 2013). However, it should be expected that inclusion of material damping for the soil in the analysis diminishes to some extent this ‘‘destructive’’ interference of the modes.

By comparing the dynamic response of the lateral and central tanks in Figures 4.7-4.9, it appears that the cross-interaction effects are more distinct for the central containers for all slenderness ratios. As it may be anticipated, the transfer functions of the latter display sharp variations with respect to the distance, whereas the dispersion for the lateral tanks about the average is relatively small. The tank in the middle is the receiver of energy transmitted by two ‘‘sources’’ at distance D, while the lateral tanks receive the energy produced by two ‘‘sources’’ at distance D and $2D$. Thus, the preliminary filtering action of the unbounded soil medium smoothens in effect their transfer functions shape.

The dynamic response for tanks with $H/R = 2.5$ is presented in Figure 4.10 with respect to the second antisymmetric impulsive natural frequency. It can be readily observed that the degree of the -through the soil- interaction of the tanks is inferior to that corresponding to the first natural frequency and same slenderness. Only for sufficient small distances the response of the central tank displays the favorable effects implicated in the cross-interaction. Due to the fact that the resonances associated with higher eigenmodes occur in a frequency-range for which the energy of the waves decay rapidly with the distance, the separation of the modes remains incomplete.

The transfer functions in the vicinity of the first asymmetric natural frequency for three tanks in a row subjected to P waves are shown in Figure 4.11 for $H/R = 0.4$ and 2.5. Comparison of these figures with the corresponding figures for horizontal excitation reveals that dynamic interaction between tanks lying on a semi-infinite soil due to vertical seismic loads is clearly weaker. This fact was also manifested in the analysis of multiple foundations and should be attributed to the primary participation of vertical dilatational waves to the response, which do not ‘‘perceive’’ the existence of nearby tanks in the horizontal plane. Nevertheless, likewise for the horizontal excitation, at small distances the

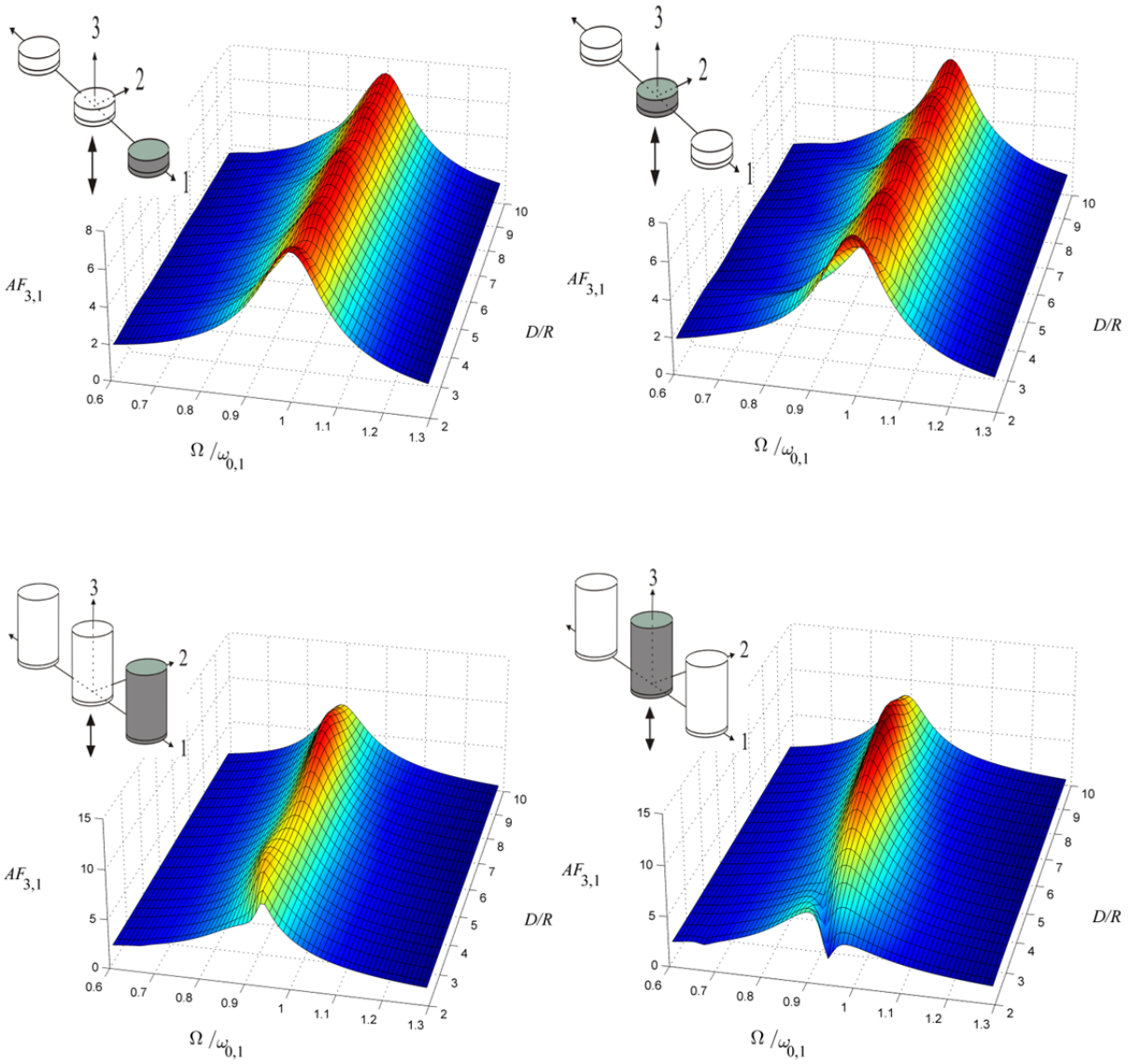

Figure 4.11: Interaction between three identical tanks on elastic homogeneous halfspace under P waves, $H/R = 0.4$ (top), $H/R = 2.5$ (bottom), 1st axisymmetric mode.

amplitudes of the slender lateral tanks are rather smaller in comparison with the single tank solution, whereas for the central tank, the destructive interference of the waves reduces drastically the peak values. For the broad tanks, an oscillatory behavior of the coupled system's solution around the solution of a single tank takes place.

The influence of the ground motion's directionality, with respect to the horizontal component, on the tanks antisymmetric vibration for the first impulsive mode is shown in Figures 4.12 and 4.13 for $H/R = 0.7$ and 2.2 respectively. An elastic semi-infinite soil medium is considered. For $H/R = 0.7$, when the tanks are placed perpendicular to the shaking direction, the cross-interaction effects are minor and become evident only for small separations, since the solution converges rapidly to that of a single tank even for perfectly elastic subsoil. This trend applies with almost imperceptible variations for both lateral and central tanks. On the contrary, the interaction between the tanks subjected to

vertically incident S waves producing motion parallel to the direction of alignment of the tanks is apparent in greater distances. The dynamic response of tanks with $H/R = 2.2$ is not analogously sensible to the direction of ground motion horizontal component. Nevertheless, it may be observed that an excitation perpendicular to the line connecting the containers emphasizes in a stronger manner the interaction between the tanks with regard to the distance. For instance, the response for the middle tank subjected to SH waves exhibits a sharper abruptness at the system's resonance frequency for small separations compared to that produced by SV waves. For the lateral tanks, the interference of the impulsive modes is only evident for SH waves.

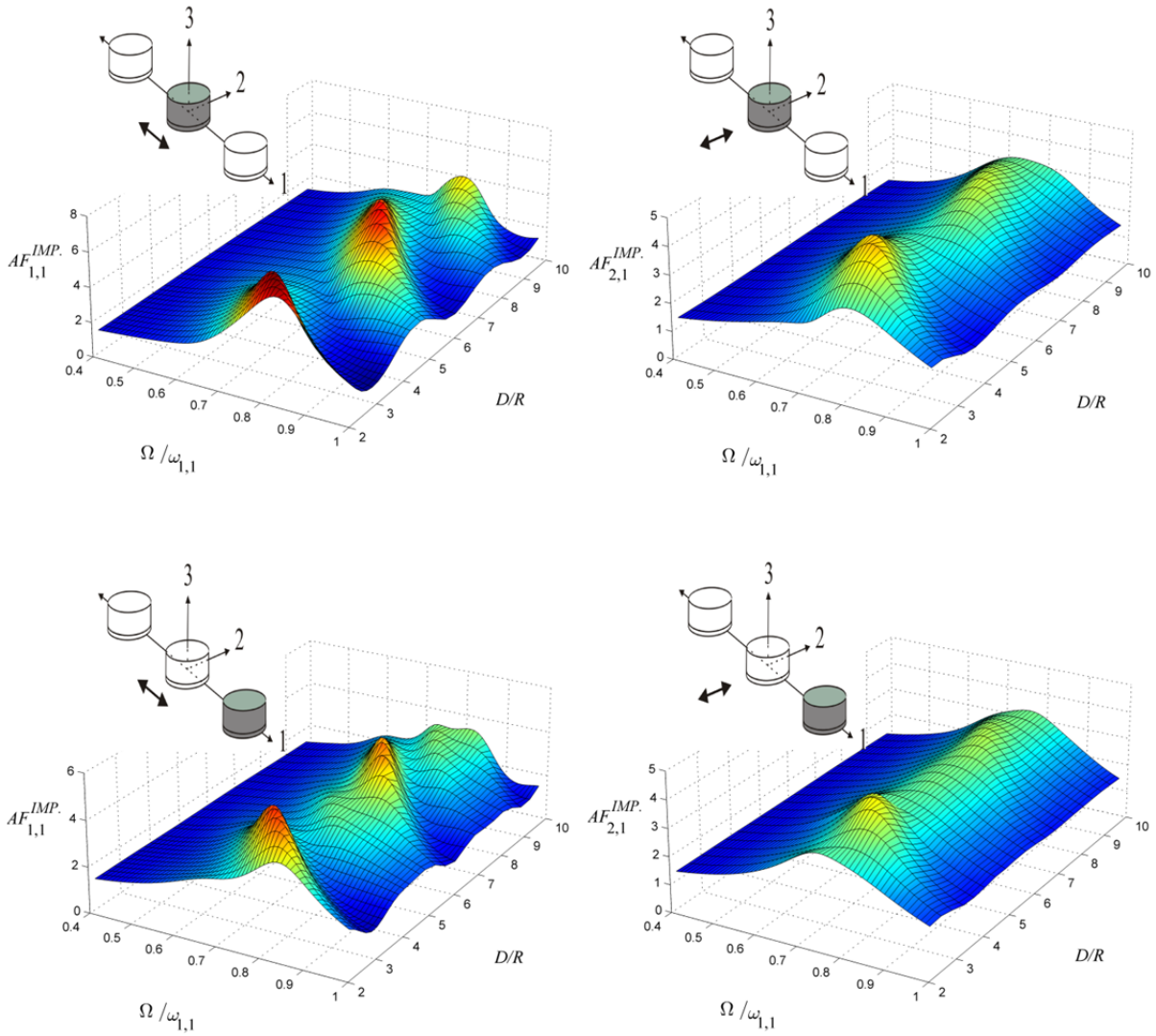

Figure 4.12: Interaction between three identical tanks on elastic homogeneous halfspace under SV (left) and SH waves (right), $H/R = 0.7$, 1st antisymmetric mode.

Figures 4.14 and 4.15 show the transfer functions of three tanks for mixed configurations regarding the ratios $H/R = 1$ and 1.3. The containers, excited by SV waves, are placed on elastic semi-infinite medium and the results refer to the first antisymmetric impulsive mode. From these figures, it is generally indicated that the peak responses of dissimilar tanks follow on average a turbulent, wide

distribution with respect to both frequency and distance. This fact reflects ‘‘superposition’’ of waves with different, yet close wavelengths that contribute to the maximum displacements. In addition, it appears that the waves interference decrease the peak responses compared to the case of similar tanks for the distances at which the latter attain their maximum, whereas increase the amplitudes for the rest separations. Specifically, the dynamic coupled-liquid response of tanks with $H/R = 1$ is more affected by the presence of neighbored tanks with $H/R = 1.3$ in comparison to the opposite state, since for equal radii, higher containers filter the contribution of narrow tanks to the total response. Representative example for this occurrence is the response of a tank with $H/R = 1.3$ bounded by two tanks with $H/R = 1.0$. In this case, the solution shows a close resemblance to that of a single tank even for small distances.

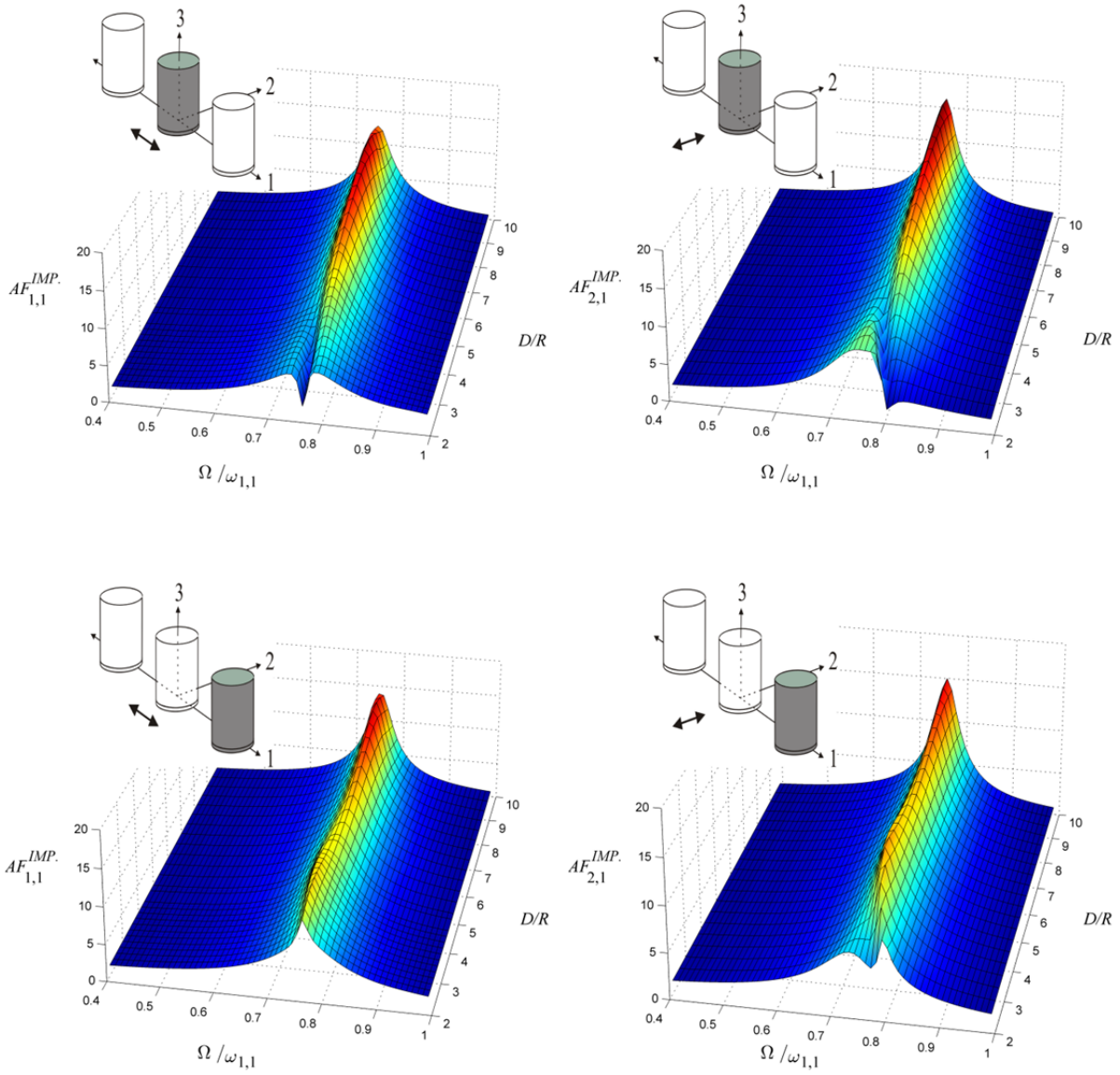

Figure 4.13: Interaction between three identical tanks on elastic homogeneous halfspace under SV (left) and SH waves (right), $H/R = 2.2$, 1st antisymmetric mode.

Figure 4.16 shows the dynamic response of five identical tanks having $H/R = 1.9$ with regard to their first antisymmetric natural mode of vibration. Two configurations are considered, one concerns containers constructed in a row and the other a cross arrangement on an elastic semi-infinite medium (Figure 4.3b-c). In both cases, only SV waves are taken into account. Independent of each container's position in the group, the general trend observed in the previous cases, regarding the decrease of slender tanks peak responses at small distances, is reserved. However, the arrangement of the tanks in space affects noticeably the response of each individual superstructure. The largest deviations from a single tank solution emerge in average for the central tank in a cross configuration, followed by the inner tanks and subsequently the outer tanks placed in a row. Eventually, the response of the peripheral components in the cross arrangement converge most rapidly to the single tank solution.

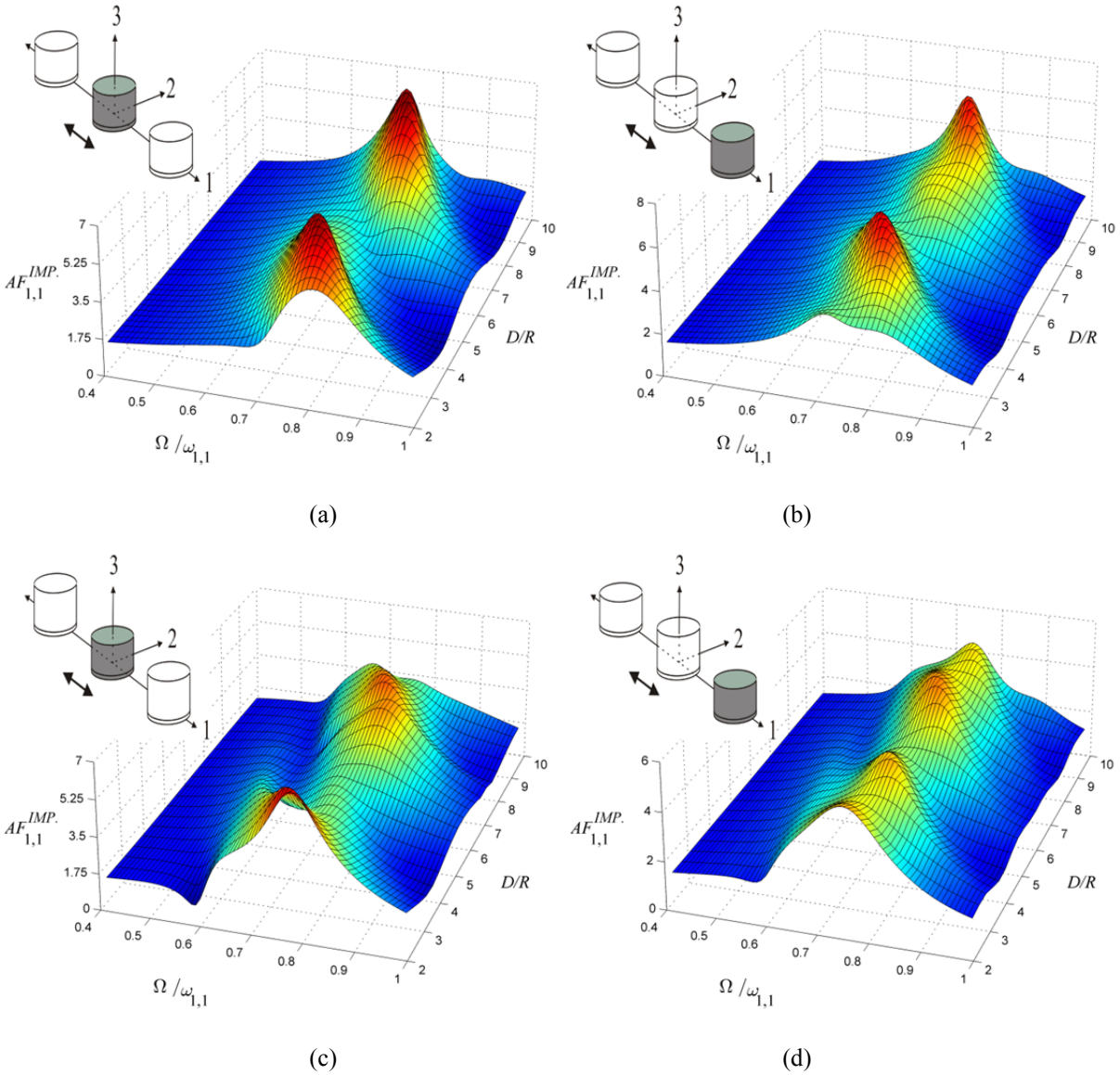

Figure 4.14: Interaction between three tanks on elastic homogeneous halfspace under SV waves, 1st antisymmetric mode, (a) (b) identical $H/R = 1$, (c) lateral $H/R = 1.3$, central $H/R = 1$, (d) lateral $H/R = 1$, central $H/R = 1.3$.

Generally, as the number of identical tanks increases, the maximum value of the response that can recorded in the group increases independent from the arrangement. It is also interesting to notice the similarities of the transfer functions for the outer tanks in a group of three (Figure 4.17) and five in the row, which gradually diminish for interior tanks. This pairwise agreement between the solutions was also remarked by Padrón et al. (2009) for nearby piled buildings. The reason for this occurrence lies in a fact that was stressed in the analysis of multiple foundations under external loads in section 3.6. The amplitude characteristics of each component in a group depend primarily on the number of adjacent components that lie inside in its immediate neighborhood.

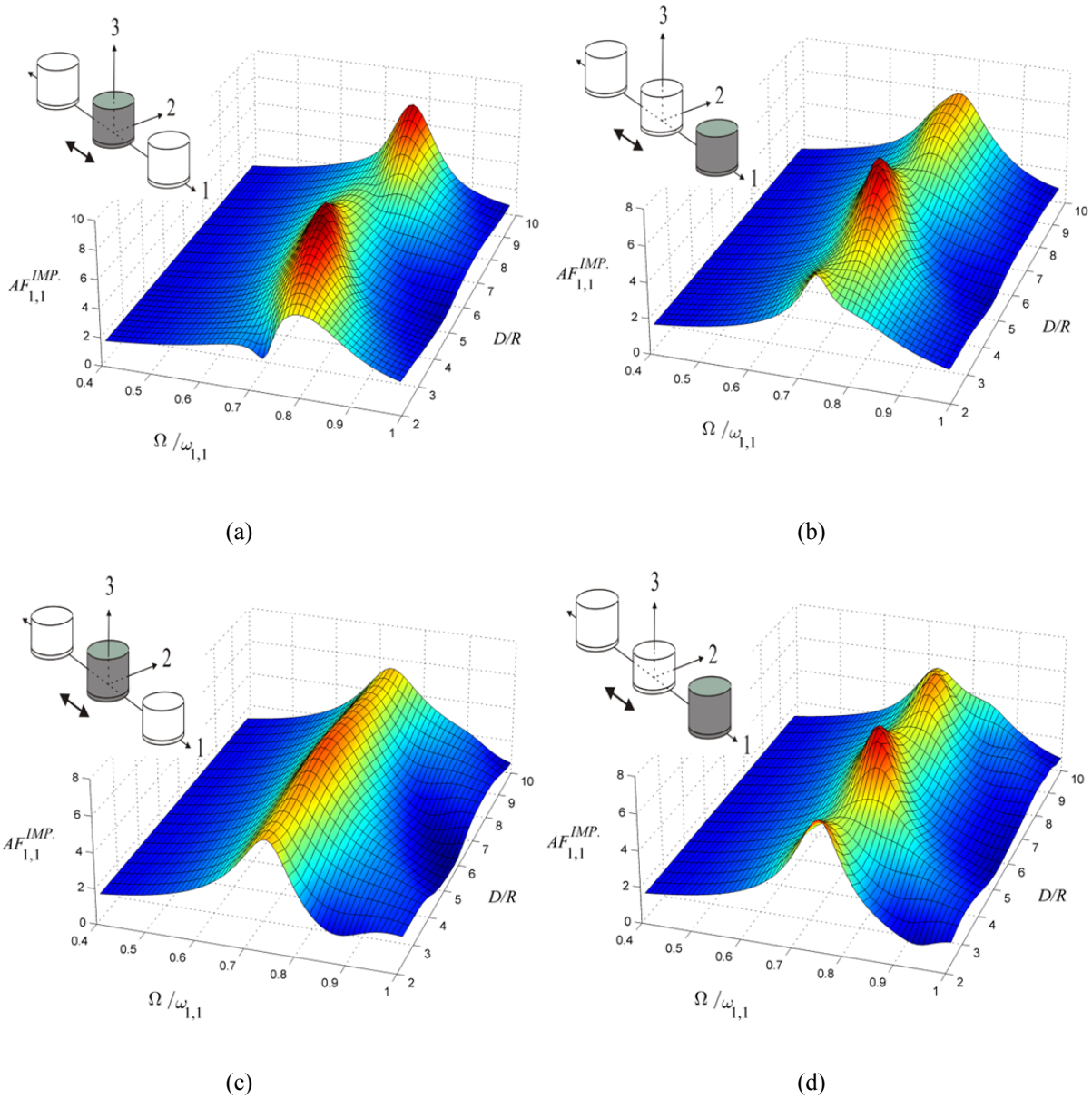

Figure 4.15: Interaction between three tanks on elastic homogeneous halfspace under SV waves, 1st antisymmetric mode, (a) (b) identical $H/R = 1.3$, (c) lateral $H/R = 1$, central $H/R = 1.3$, (d) lateral $H/R = 1.3$, central $H/R = 1$.

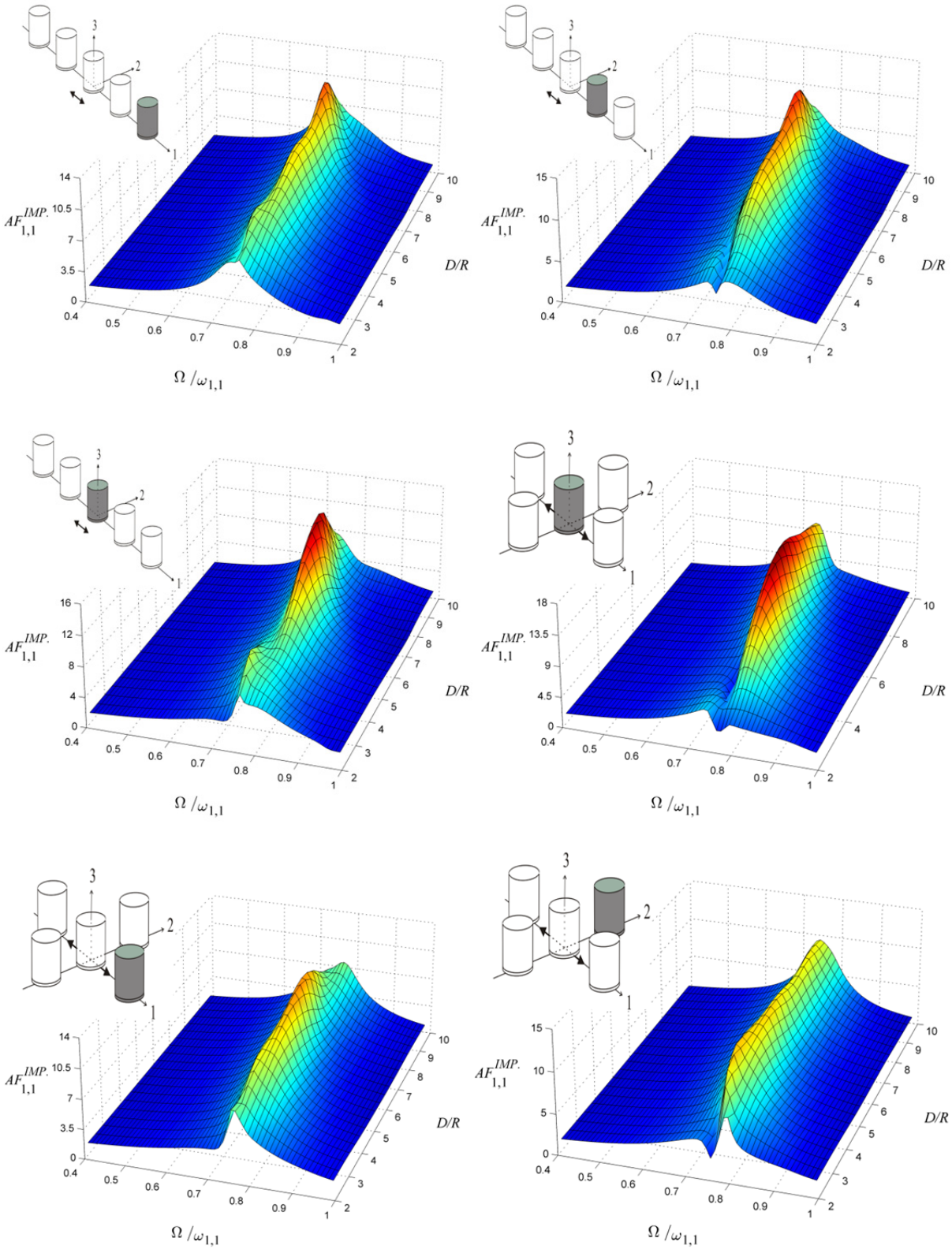

Figure 4.16: Interaction between five tanks on elastic homogeneous halfspace under SV waves, $H/R = 1.9$, 1st antisymmetric mode.

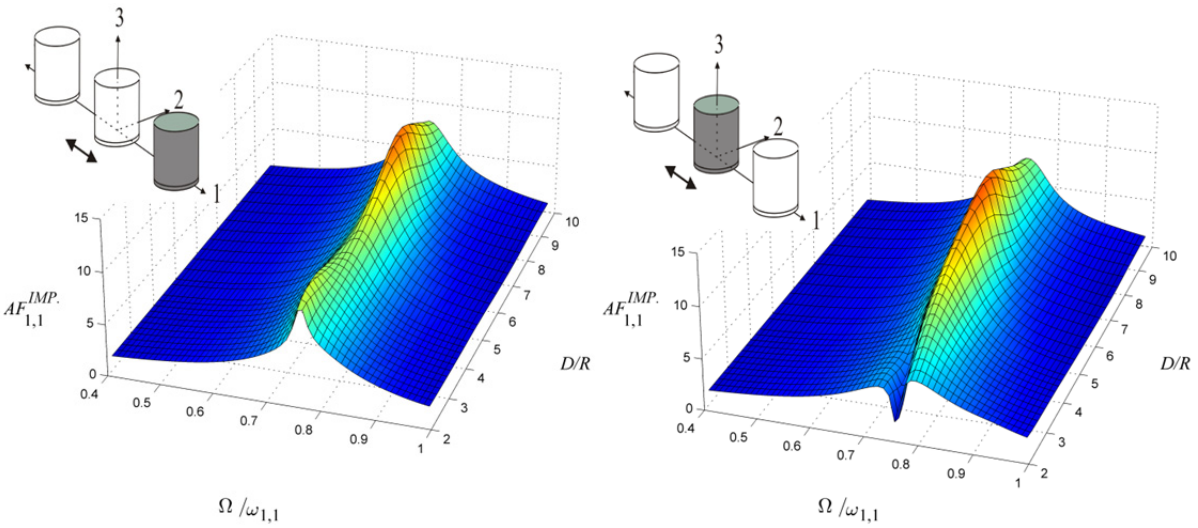

Figure 4.17: Interaction between three tanks on elastic homogeneous halfspace under SV waves, $H/R = 1.9$, 1st antisymmetric mode (to be compared with Figure 4.16).

Finally, the interaction of tank groups lying on viscoelastic stratum is addressed. Three cases are examined with regard to its thickness expressed by the ratios $d/R = 2{,}4$ and ∞. The latter case corresponds to an isotropic, homogeneous semi-infinite medium. Figures 4.18 and 4.19 depict the transfer functions with respect to the first antisymmetric natural mode of vibration for three identical tanks with $H/R = 0.9$ and 3 respectively subjected to SV waves. It can be readily observed that the cross-interaction effects vary significantly with respect to the thickness of the stratum. Crucial factor for assessing the system's response is the relationship between the fundamental natural frequencies of the stratum and the first antisymmetric tank-liquid-soil natural frequency in presence of adjacent containers. Referring to shallow strata, if the latter is smaller than the former, the solution is close to the corresponding one for a single tank, since the energy transmitted between the superstructures is trivial owing to the immediate attenuation of the surface waves. In this case, the transfer functions at the resonance frequency appear sharp with relatively large values. The only dissipative mechanisms involved in the system are the damping of the impulsive mode for the coupled liquid-tank vibration and the internal damping of the soil. On the contrary, if the first antisymmetric tank-liquid-soil natural frequency is larger than the fundamental natural frequencies of the stratum, the displacement amplitudes characteristics become relatively broad and exhibit peaks with comparatively reduced values. In this case, the interaction between the tanks is evident for greater distances. Due to the fact that the horizontal component of seismic motion induces primarily horizontal and rocking oscillations at the superstructures, the horizontal and vertical fundamental natural frequencies of the stratum are relevant. It should be reminded that the rocking impedance functions, given in section 3.4.2, have slight critical points at the vertical natural frequency of the soil. Concretely, for the ratio $H/R = 0.9$, the fundamental horizontal natural frequencies of the stratum are $0.49\,\omega_{1,1}$ and $0.24\,\omega_{1,1}$ approximately, while the vertical natural frequencies are close to $0.98\,\omega_{1,1}$ and $0.49\,\omega_{1,1}$ for the depths $d/R = 2$ and 4 respectively.

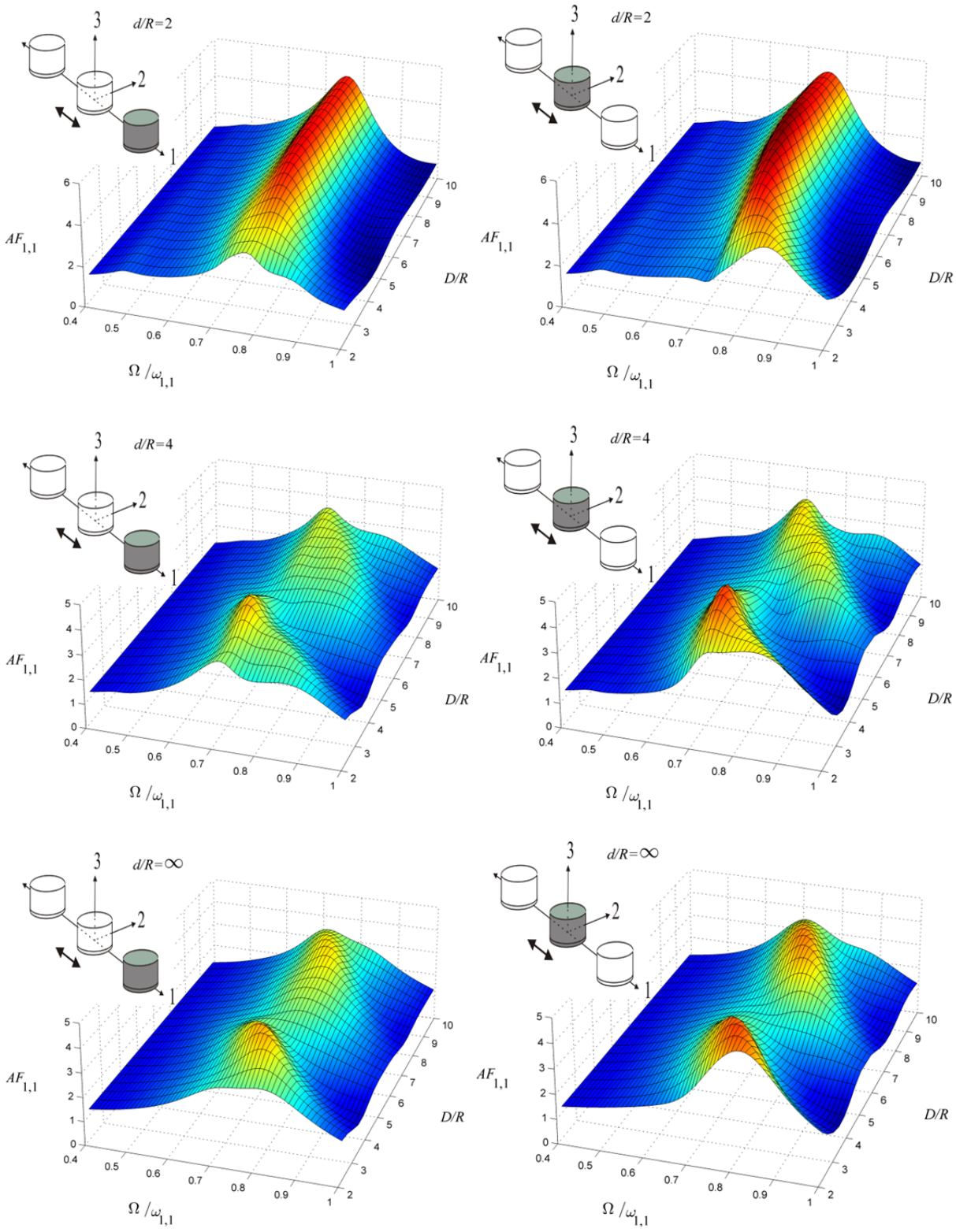

Figure 4.18: Interaction between three tanks on viscoelastic stratum under SV waves, $H/R = 0.9$, 1st antisymmetric mode.

Regarding the shallow deposit, the system's resonance frequencies for all distances fall into the frequency range between the first horizontal and vertical natural frequency of the soil. Because of the elimination of damping for the rocking mode of vibration, the amplitude characteristics, especially for large distances, are sharp and their values are larger compared to those corresponding to a semi-infinite medium. For the deeper deposit, the system's resonance frequencies are larger than its natural frequencies and the response shows a close resemblance to that of a semi-infinite medium due to the high frequency range within the resonance occurs. On the other hand, the dynamic response of tanks having $H/R = 3$ is rather distinct. In this case, the fundamental horizontal natural frequencies of the stratum are $1.76\ \omega_{1,1}$ and $0.88\ \omega_{1,1}$ approximately, while the vertical natural frequencies are close to $3.51\ \omega_{1,1}$ and $1.76\ \omega_{1,1}$ for the depths $d/R = 2$ and 4 respectively. Practically, the nearby tanks do not interact with each other since the resonance frequencies for a certain separation are much smaller than the natural frequencies of the stratum. However, the peak amplitudes for the shallow are slightly larger compared to those of the deeper stratum due to the degradation of damping characteristics as the height of the deposit decreases for the same frequency in the lower range. The increased system's stiffness of the shallow deposit does not suffice to alter this trend, since the resonance frequencies for the two cases are almost the same. The cross-interaction effects become apparent if the bottom rigid boundary is set to infinite distance from the surface. For instance, the maximum displacement amplification of the central tank with $H/R = 3$ on semi-infinite medium at distance $D/R = 2.6$ is 50 percent lower than the corresponding amplification of an identical tank on stratum with $d/R = 2$ at the same distance. In reality, the rigidity of a subgrade has a finite stiffness and therefore the wave reflections of the body waves at the boundary are not perfect, allowing for wave energy penetration into bedrock. Consequently, the overall response is also affected by the contrast between the layer's and underlying halfspace's stiffness.

Figures 4.20 and 4.21 depict the transfer functions with respect to the first axisymmetric natural mode of vibration for three identical tanks with $H/R = 0.9$ and 3 respectively, lying on a viscoelastic stratum and subjected to P waves. Under vertical seismic loads the first vertical natural frequency of the stratum becomes decisive for the tanks behavior. Regarding the ratio $H/R = 0.9$, the fundamental vertical natural frequencies of the soil are $0.95\ \omega_{0,1}$ and $0.48\ \omega_{0,1}$ approximately for the depths $d/R = 2$ and 4 respectively. For the shallow deposit, the first axisymmetric tank-liquid frequency in presence of nearby containers is smaller than the resonance frequency of the deposit for all examined distances, thus the response appears enlarged compared to that associated with a semi-infinite medium, especially for distant tanks. A local minimum of the amplitudes appears at the resonance frequency of the stratum. The displacement amplitude characteristics corresponding to $d/R = 4$ deviate remarkably from those of the shallow deposit. In this case, the peak response occurs for a frequency greater than the resonance frequency of the stratum and the solution is similar to that of a semi-infinite medium.

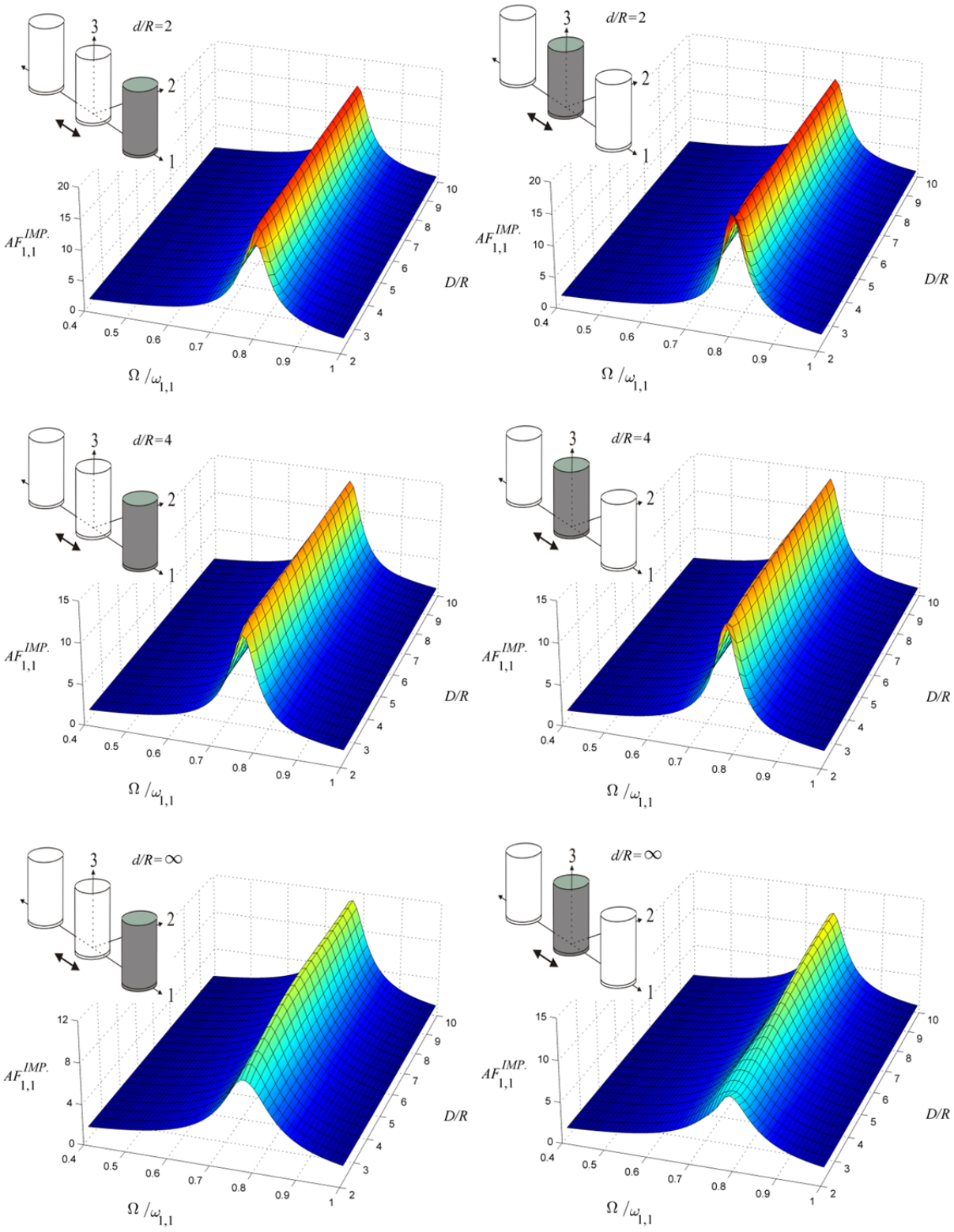

Figure 4.19: Interaction between three tanks on viscoelastic stratum under SV waves, $H/R = 3.0$, 1st antisymmetric mode.

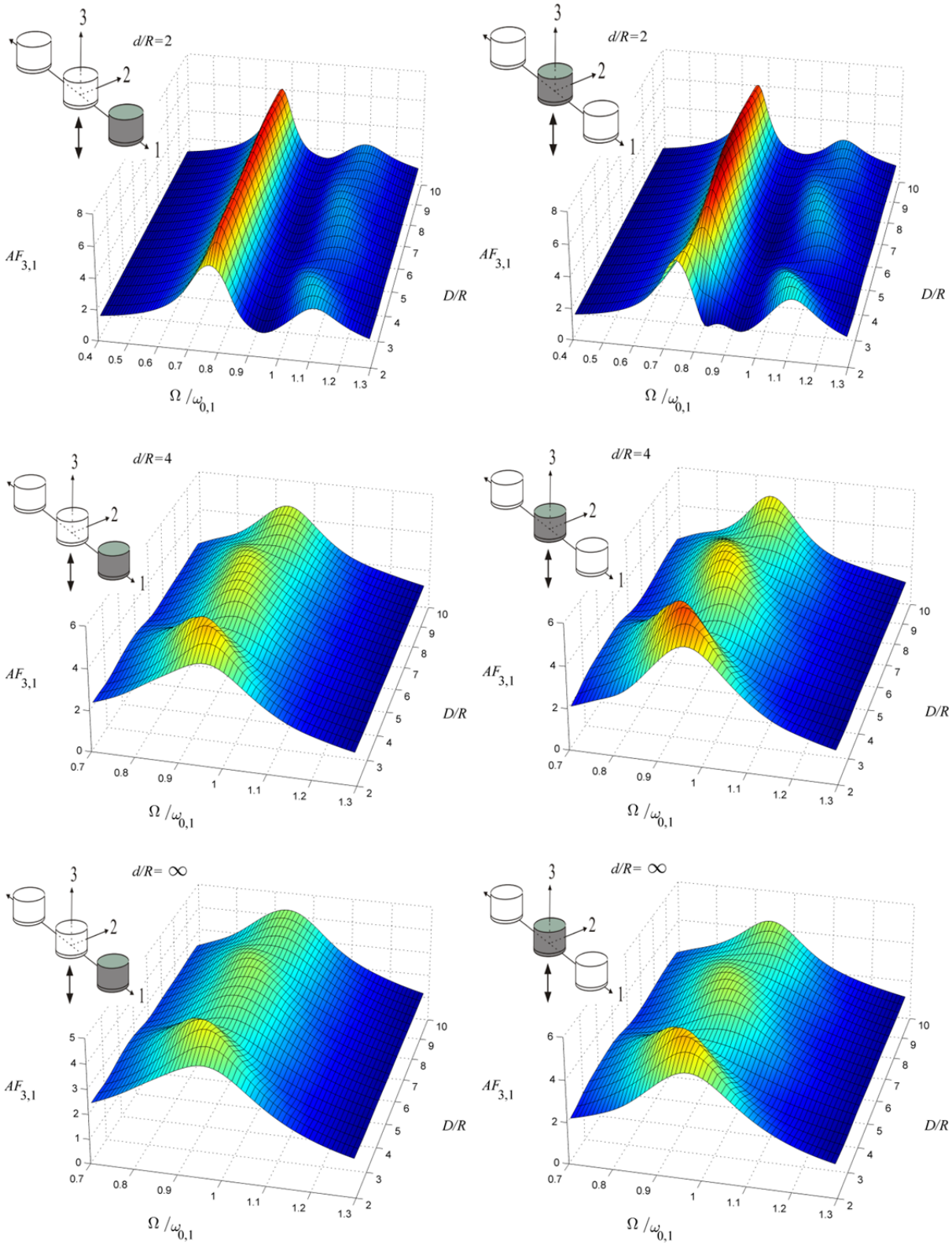

Figure 4.20: Interaction between three tanks on viscoelastic stratum under P waves, $H/R = 0.9$, 1st axisymmetric mode.

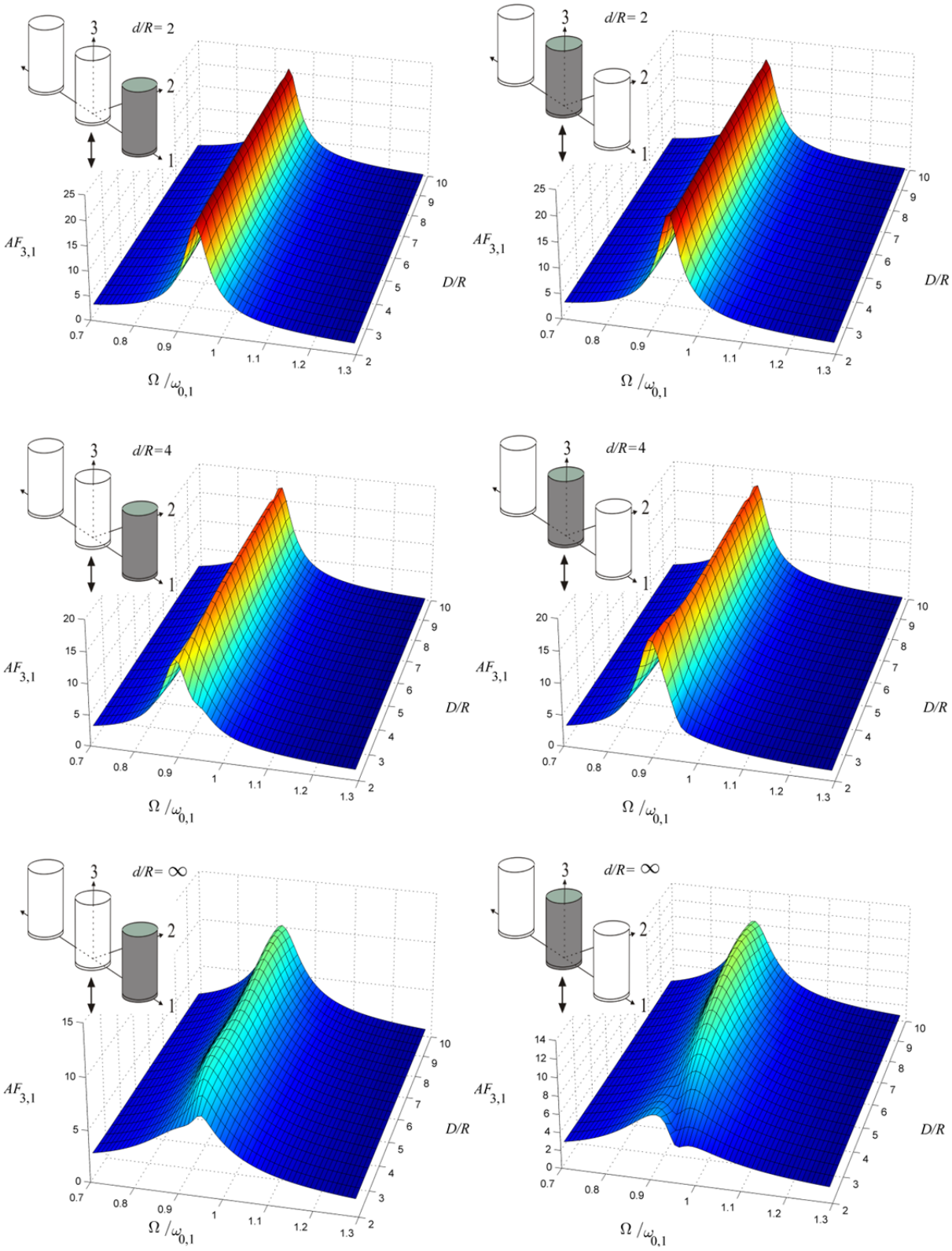

Figure 4.21: Interaction between three tanks on viscoelastic stratum under P waves, $H/R = 3.0$, 1st axisymmetric mode.

However, the undulations that exhibit the foundations dynamic impedance coefficients, resulting from the presence of the bedrock, elevate the narrow valleys and abrupt hillsides that characterize the dynamic response of relatively broad tanks with respect to the distance. Referring to the ratio $H/R = 3.0$, the fundamental vertical natural frequencies of the soil are $0.35\ \omega_{0,1}$ and $0.7\omega_{0,1}$ approximately for the depths $d/R = 2$ and 4 respectively. Likewise for the horizontal excitation, the presence of bedrock diminishes the cross-interaction effects concerning the slender tanks, since the system's peak amplitudes occur at frequencies substantially smaller than the first resonance frequencies of the soil. Setting again the bedrock at infinite distance from the surface reveals the favorable effects emanated by the waves emitted between the containers. For example, the maximum displacement amplification of the central tank with $H/R = 3$ on semi-infinite medium at distance $D/R = 2.6$ is 30 percent lower than the corresponding amplification of an identical tank on stratum with $d/R = 2$ at the same distance.

4.3.4 Response to seismic excitation

Having obtained the response to harmonic loads, the response to an arbitrary transient excitation can be determined with the aid of Fourier analysis. In this section, results are obtained for the horizontal component of Pacoima downstream motion, recorded on stiff rock outcrop ($V_s = 2016.1$ m/s) during the Northridge earthquake in 1994. Control point for the seismic input is selected the soil-bedrock interface of a homogeneous viscoelastic deposit. The acceleration time history and its five and ten percent damped spectra are shown in Figure 4.22. The Fourier transform of the acceleration is obtained with the aid of a FFT algorithm. The product of the transfer function, which relates the ground surface to the bedrock motion as calculated in section 4.1.1, and the Fourier series of the bedrock motion represents the free-field surface motion. The latter is multiplied with the transmissibility ratios for the superstructures to determine the response of the tanks in the frequency-domain. The time-domain response is finally computed with the aid of an IFFT algorithm.

Time histories for the total impulsive, overturning moments transmitted to the foundation are presented for the central tank of a group consisting of three identical tanks in a row. It is assumed that the motion acts parallel or perpendicular to the direction of alignment of the tanks, producing responses along the axes x_1 and x_2 respectively as depicted in Figure 4.3a. The properties of the tanks and the soil are those given in section 4.3.1. The thickness of the homogeneous deposit over rigid bedrock varies. Apart from the value $V_s = 304.8$ m/s, the soil is also ascribed with $V_s = 457.2$ m/s for the analyses. The first three modes of vibration for the tank-liquid systems are considered for the solution. The fixed-base natural circular frequencies of the tanks are $\omega_{1,1} = 28.27$ rad/sec corresponding to slenderness ratios $H/R = 0.4$ and $H/R = 2.5$. Results are presented for distances $D/R = 2.2$ and ∞. The latter case corresponds to the solution of a single tank.

Figures 4.23 and 4.24 show the responses of the central tank with $H/R = 0.4$ for a stratum of thickness $d = 67.5$ m and 12.4 m. The results demonstrate that the properties of the soil can remarkably affect the response of the tanks in view of the cross-interaction effects. For the deep stratum, the moments induced to the central foundation are greater than those corresponding to the solution of a single tank when the impinging waves produce motions in the direction of tanks alignment. However, the subsoil coupling appears stronger for the case of $V_s = 304.8$ m/s due to the fact that the system's response is controlled by the second resonance frequency of the soil, which falls in the vicinity of the tank-liquid-soil resonant frequency, whereas the response related to $V_s = 457.2$ m/s is governed by the first resonance frequency of the soil leading, however, to greater values for the moments. These incidents become clearer by inspecting the Fourier amplitude spectrum of the motion on the free surface depicted in Figure 4.25. As already demonstrated for harmonic excitation (Figure 4.7), the interaction among adjacent broad, identical containers affects a wide range of frequencies in the neighborhood of the tank-liquid-soil resonant frequency (ω_{SSI}). Thus, the second peak of the spectrum corresponding to $V_s = 304.8$ m/s intensifies the influence of the adjacent tanks in a more distinct way. On the other hand, the tanks on the shallow stratum behave almost independently since the tank-liquid-soil resonant frequency is much smaller than the fundamental frequency of the deposit in its horizontal and vertical vibrational mode, as explained in section 4.3.3. The values of the recorded overturning moments can be, though, substantially larger compared to those corresponding to a deeper stratum (Figure 4.23) because of the small amount of energy radiating in the frequency range below the ‘‘cut-off’’ frequency of the soil, but also smaller (Figure 4.24) depending on the predominant frequencies of the signal at the soil-bedrock interface and the characteristics of the deposit.

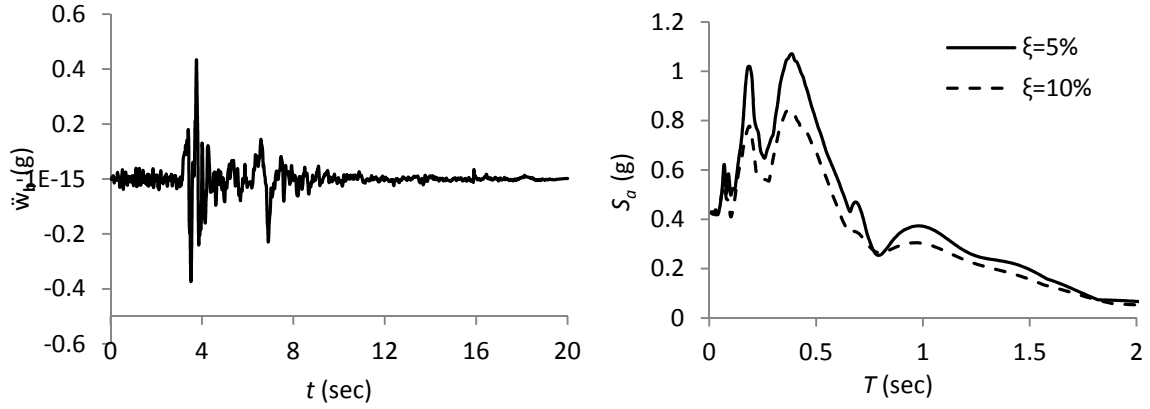

Figure 4.22: Pacoima motion (left) and corresponding response spectra (right) for 5% and 10% damping.

Figures 4.26 and 4.27 show the responses of the central tank with $H/R = 2.5$ for a deep and shallow stratum of thickness $d = 67.5$ m and 12.4 m respectively. For the deep stratum and $V_s = 304.8$ m/s, the moments induced to the central foundation are much smaller than those corresponding to the solution of a single tank independent of the direction of shaking. Specifically, the maximum value that experiences the foundation in the direction of tanks alignment ($k = 1$) is 24 percent smaller than that of an isolated tank. The favorable effects of the interaction between identical slender tanks in small distances have been manifested for the case of harmonic excitation. The reduction's degree of the forces that the adjacent slender tanks experience depends mainly on the relationship of the impulsive fundamental natural frequency of the tank-liquid-soil system and the predominant frequencies of the excitation on the surface. The reader may observe the minor differences in the response of the single tank and the central tank in a group on the deep stratum for $V_s = 457.2$ m/s. For a constant depth of the deposit, variation of the shear wave velocity leads to amplifications of the motion in different frequencies and subsequently to an elevation or degradation of the dynamic interactions. This fact can be clearly recognized in Figure 4.28, which shows the Fourier amplitude spectrum of the motion on the free surface for the values of the shear wave velocity under examination. The natural frequency of the tank-liquid-soil system corresponding to $V_s = 304.8$ m/s is close to the second natural frequency of the stratum associated with considerable amplitudes, whereas the natural frequency of the stiffer system falls into a range, where the amplitudes are rather small. Since the presence of other tanks does not alter significantly the frequencies at which resonance occurs and the interaction between the tanks is evident only at the resonant frequencies, the effects of cross-interaction are apparent only for the comparatively softer soil. Regarding the shallow stratum, the dynamic interaction is of minor importance due to the negligible radiation of wave energy from the tanks, the first natural frequency of which is much smaller than the ''cut-off'' frequency of the soil for the vertical mode of vibration as explained in section 4.3.3.

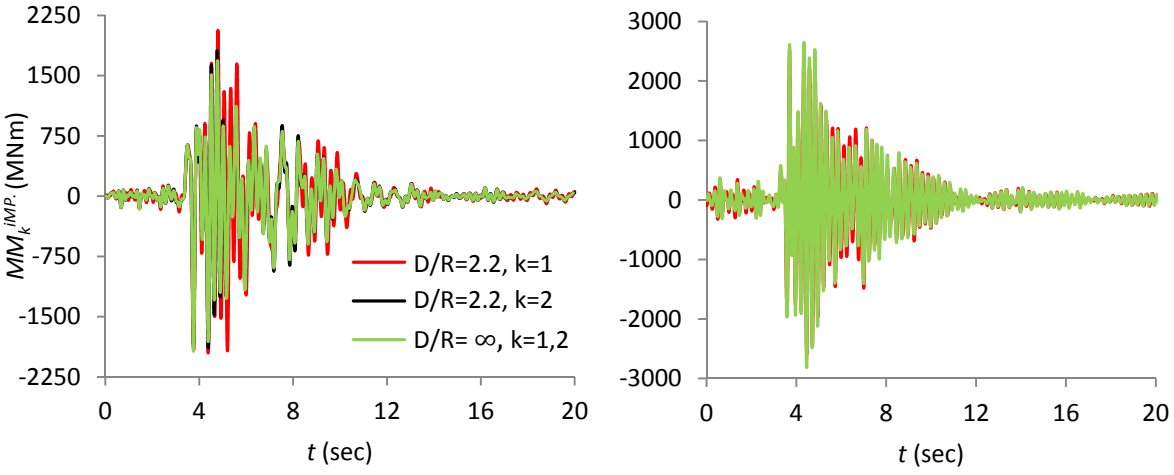

Figure 4.23: Total impulsive moments transmitted to the foundation of the central tank in a -three tanks- group for $d = 60.28$ m (left) and $d = 12.4$ m (right), H/R=0.4, $\omega_{1,1} = 28.27$ rad/sec, $V_s = 304.8$ m/s.

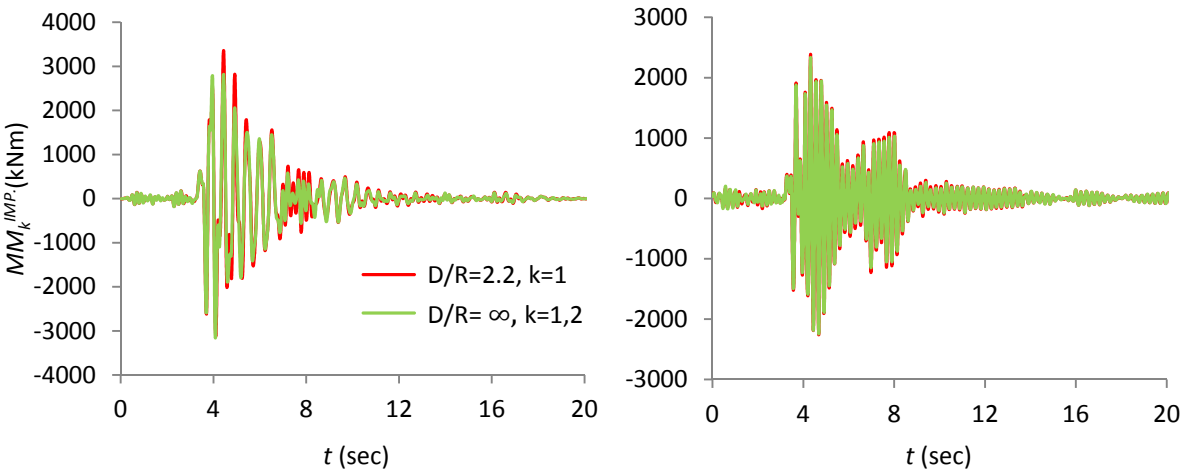

Figure 4.24: Total impulsive moments transmitted to the foundation of the central tank in a -three tanks- group for $d = 60.28$ m (left) and $d = 12.4$ m (right), H/R=0.4, $\omega_{1,1} = 28.27$ rad/sec, $V_s = 457.2$ m/s.

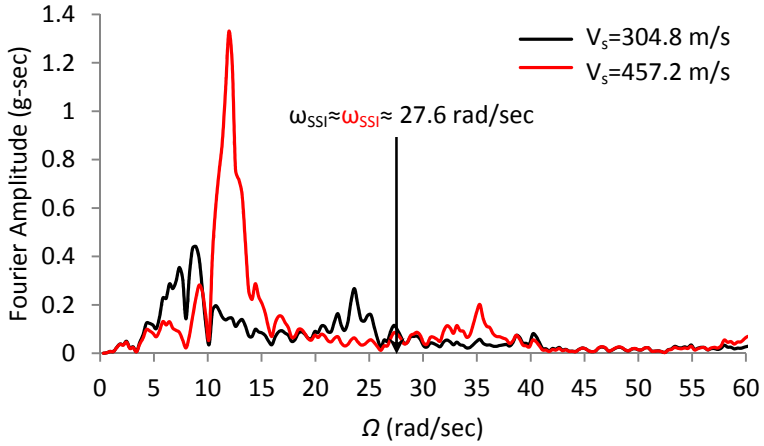

Figure 4.25: Fourier amplitude spectrum of the free-field surface motion for a stratum with $d = 60.28$ m, $\xi_s = 5\%$ and circular eigenfrequencies (ω_{SSI}) of single tanks with H/R=2.5, $\omega_{1,1} = 28.27$ rad/sec lying on it.

The obtained results manifest that, in the realm of linear analysis, the relationship between the predominant frequencies of the input seismic motion and the fundamental natural frequency of the tank-liquid-soil systems determines the degree of significance of the interaction between nearby liquid-storage tanks. Referring to broad containers of equal size on semi-infinite medium and arranged in small separations, it should be expected that a ground motion with large amplitudes in a frequency range close to the fundamental natural frequency of the tank-liquid-soil system will increase the values of shear forces and moments that the inner tanks in a group experience. This trend is reversed for slender tanks. It should be pointed out that a quantitative assessment of the detrimental or beneficial effects emanating from the cross-interaction demands knowledge of the nonlinear mechanisms associated with the response of the containers and the soil subjected to strong ground motion. This last point goes beyond the scope of the present study.

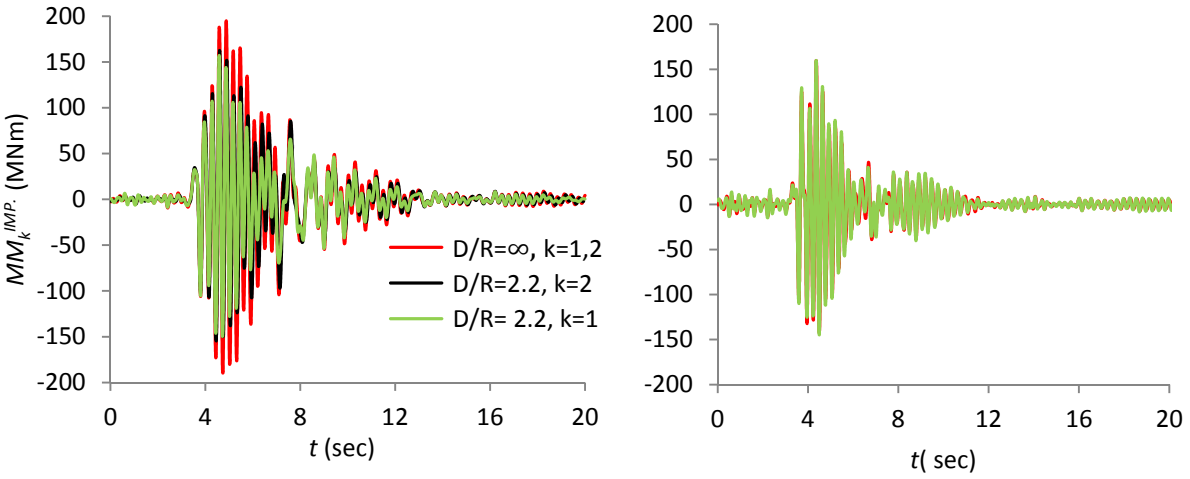

Figure 4.26: Total impulsive moments transmitted to the foundation of the central tank in a -three tanks- group for $d = 67.5$ m (left) and $d = 12.4$ m (right), H/R=2.5, $\omega_{1,1} = 28.27$ rad/sec, $V_s = 304.8$ m/s.

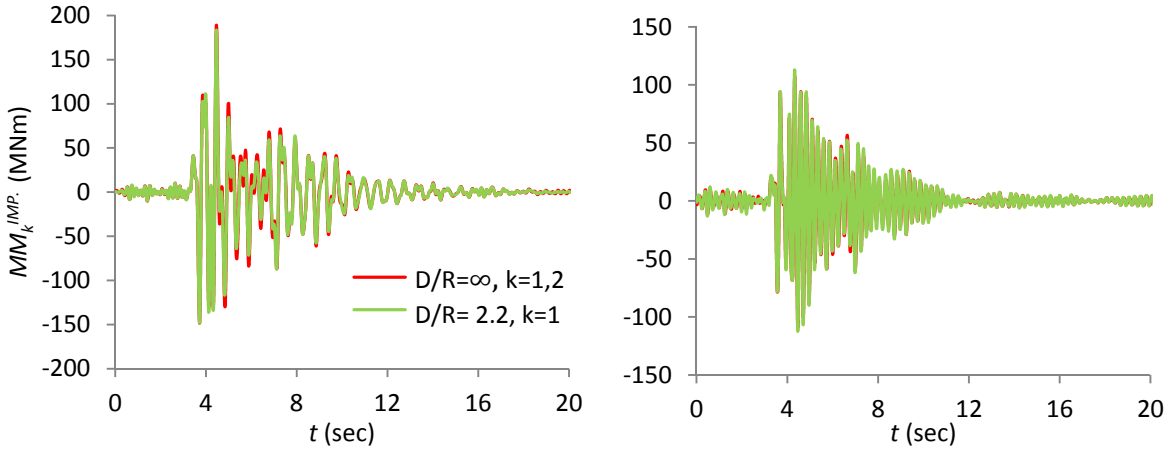

Figure 4.27: Total impulsive moments transmitted to the foundation of the central tank in a -three tanks- group for $d = 67.5$ m (left) and $d = 12.4$ m (right), H/R=2.5, $\omega_{1,1} = 28.27$ rad/sec, $V_s = 457.2$ m/s.

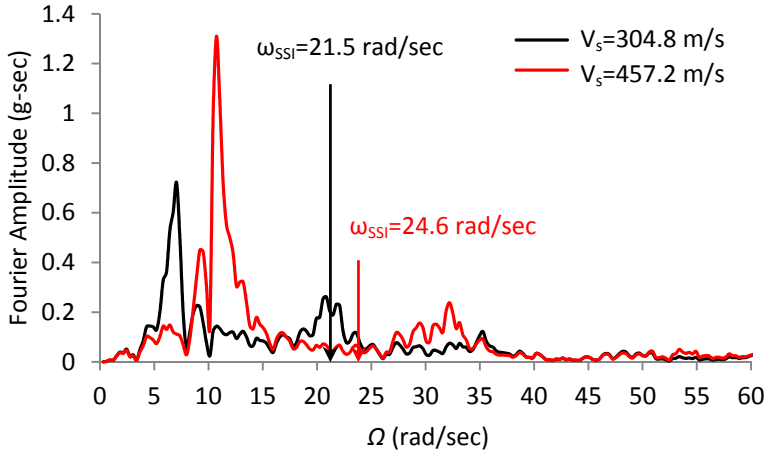

Figure 4.28: Fourier amplitude spectrum of the free-field surface motion for a stratum with $d = 67.5$ m, $\xi_s = 5\%$ and circular eigenfrequencies (ω_{SSI}) of single tanks with H/R=2.5, $\omega_{1,1} = 28.27$ rad/sec lying on it.

4.4 Summary

The assessment of the dynamic interaction of nearby liquid-storage tanks excited by ground motion is the primary scope of the present work. In this chapter, a model representing multiple tanks is realized by composing the constitutive elements built up in the previous chapters. After introducing the key aspects of the substructure approach for the dynamic analysis of single structures, the equations of motion for multiple liquid-storage tanks founded on a deformable soil are derived. A set of parametric analyses for harmonic and seismic excitations are conducted in order to elucidate the influence of the main parameters involved in the problem. Although far from being an exhaustive examination, some remarks arousing interest worth a mention:

- The cross-interaction effects have a trivial effect on the convective components of the response. Thus, the latter can be evaluated for the seismic motion considering both tank walls and subsoil as rigid. Vertical excitation of the group imposes antisymmetric impulsive vibrational modes and vice versa, horizontal excitation imposes axisymmetric impulsive vibrational modes. These responses are insignificant and can be neglected.
- The dynamic interaction between identical nearby tanks on semi-infinite soil medium causes different responses for the impulsive components with respect to the slenderness ratio. The amplifications for broad tanks, regarding the fundamental mode of vibration, are larger for small distances than the corresponding one for a single tank having the same dimensions and founded on the same soil. However, the response exhibits convergent oscillations around that of a single tank as the separation decreases. On the other hand, the interaction between similar slender tanks leads to considerable reduction of the peak responses for small distances. Soil's hysteretic damping diminishes in some extent this trend. Generally, the relative difference of the maximum response that can be recorded between a single tank and a similar one in a group decreases as the slenderness increases. Higher modes associated with the impulsive component of the response are less affected by the cross-interaction. The tank-liquid response for groups consisting of containers having equal radii and different, yet similar heights indicates destructive inference of comparable wavelengths associated by diminution of the peak responses undulations with respect to the distance.
- Horizontal excitation emphasizes more the coupled group response regarding the impulsive pressure components compared to vertical excitation. Referring to broad tanks, the cross-interaction effects appear degraded for vertical incident S waves that produce motion perpendicular to the line that connects tanks in a row, compared to the case of tanks aligned along the direction of shaking. The opposite trend applies for slender tanks.
- Considering identical tanks, the impulsive amplitude characteristics of each component in a group founded on semi-infinite soil medium depend primarily on the number of adjacent

elements that lie inside in its immediate circumference. However, increase of the number of tanks increases the transmitted energy and can result to amplified responses for the inner containers.

- Presence of bedrock at a shallow depth affects the dynamic characteristics for a group of identical tanks. The relationship between the lowest natural frequency of each tank-liquid system in presence of other containers and the fundamental natural frequency of the underlying stratum for the associated mode of vibration is the factor that governs the response. If the former is smaller than the latter, a large response should be anticipated for a seismic excitation with certain frequency content. In this case, however, the cross-interaction effects are minor. Depending on the slenderness of the tanks and the assumed wave pattern, deeper strata can intensify the dynamic interaction between containers compared to a semi-infinite medium.
- Knowledge of the relationship between the predominant frequencies of the input seismic motion and the fundamental natural frequencies of the tank-liquid-soil systems is essential for the evaluation of the significance of the dynamic interaction between tanks. Coincidence of the values of those two parameters elevates the cross-interaction phenomena for semi-infinite soil medium.

5 Conclusions and outlook

Liquid-storage tanks are frequently encountered in groups as components of complex systems, known as tank farms. At the very beginning of this work, a question is raised whether the dynamic response of liquid-storage tanks subjected to seismic motion is affected by the presence of others in the vicinity or they should be designed independently according to the current practice. An attempt to set up a scheme that could pave the way for an answer brings out two ticklish issues. The first concerns the major dimensions of the problem, since apart from the need to consider the supporting soil as an unbounded domain, finite element modeling of the tank-liquid system becomes inefficient when more than one container are examined. The second is related with the uncertainties involved in the problem, which regard, besides those emanating from the ground motion that includes knotty wave propagation and source effects, the soil conditions and the response of the tanks. Thus, the selection of those parameters that should be by all means considered and others that can be left out without distorting the nature of the problem seems a tricky task. In order to tackle with these issues, a refined substructure method is employed, which permits consideration of the -through the soil- coupling effects among the tanks. Accordingly, the system of multiple tanks is divided in the subsystems liquid-tank and foundations-soil. This approach enables a stepwise evaluation of the parameters relative importance and gives rise to a reduction of the domain's dimensions. Nevertheless, it imposes a severe restriction: nonlinear behavior of the tanks cannot be considered. Indisputably, this fact prohibits generalization of the results to unanchored tanks and strong ground shaking.

Initially, the eigenvalue problem for circular, liquid-filled cylinders is solved on the basis of an added-mass concept. It is demonstrated that the compressibility of the liquid can be included in the analysis by means of an an iterative incremental root-searching scheme. Free-surface effects and compressibility can affect the free vibrational characteristics of the shell-liquid system, however in a frequency range and for circumferential wavenumbers not practically relevant to liquid-storage tanks. The shift of attention to the seismic response of tanks in fixed-base conditions reveals that the European current standard provisions (EC8) for the calculation of the impulsive hydrodynamic pressures are not sufficiently accurate, especially for broad tanks. For engineering practice, an alternative procedure is recommended, which involves only site response spectra and few elementary calculations.

Having established a mechanical model for the superstructures, analyses of multiple, identical, circular foundations under external sinusoidal loads over wide ranges of frequencies and distances are carried out with the aid of a coupled FEM-BEM formulation. A set of numerical investigations with respect to

the number, spatial arrangement of rigid foundations and two idealized soil profiles indicate the following principal trends:

- For a given distance, the coupling effects between foundations on semi-infinite, homogeneous soil medium are greater in the low frequency range. For higher frequencies, a larger number of wavelengths is transmitted and the group effects are comparatively of lower degree.
- The swaying modes of vibration are most affected by the presence of nearby foundations, followed by the vertical and lastly rotational modes (rocking and torsion).
- The dynamic behavior of each foundation is considerably affected only by the number of the foundations that lie in its immediate neighborhood and this fact holds true independent from the distance.
- Existence of a shallow deposit beneath the foundations diminishes the cross-interaction effects in the frequency range below the fundamental natural frequency of the stratum for the associated vibrational mode of the foundations.

These distinct findings give us confidence to propose a guideline for a preliminary estimation of group effects for general structure-soil-structure interaction problems. Regarding identical structures, knowledge of the predominant natural frequencies of the soil-structure systems and the stiffness of the supporting medium in terms of shear wave velocity suffices for an initial evaluation of the cross-interaction effects.

The computation of the dynamic impedances for groups of foundations in conjunction with the model for the superstructures establishes finally the system of multiple liquid-storage tanks. The dynamic response of groups of adjacent tanks for harmonic and seismic excitations is evaluated. Even though the conducted analyses represent by no means a thorough investigation, the following principal conclusions are reached:

- The dynamic interaction between adjacent liquid-storage tanks subjected to ground motion can alter the impulsive components of response of each component in a group. The degree of this impact is mainly controlled by the tank proportions and the relationship between the predominant frequencies of the input seismic motion and the fundamental natural frequencies of the tank-liquid-soil systems. Coincidence of the values of the latter two parameters results to significant cross-interaction effects for close-spaced, identical tanks, unless the fundamental natural frequency of the soil is greater than the fundamental natural frequency of the tank-liquid-soil system for the corresponding mode of vibration.
- The group effects for tanks under seismic loading can be either beneficial or detrimental depending on the tank proportions, the type of excitation and the distance between them. The greatest differences between the responses of multiple and single tanks of the same characteristics are detected for identical, slender, nearby tanks on unbounded soil medium, subjected to vertically propagating horizontal ground motion. In this case, a favorable

influence of the cross-interaction is evident. Broad tanks of the same dimensions are adversely affected by the interactions, however practically only for small separations.

- The impulsive amplitude characteristics of each component in a group founded on semi-infinite soil medium depend primarily on the number of adjacent elements that lie inside in its immediate circumference. However, increase of the number of tanks increases the transmitted energy and can result to amplified responses for the inner containers.

After all, going back to the initial question, whether the cross-interaction effects between nearby liquid-storage tanks should be considered in the seismic design, the answer is…yes, especially for tank farms having high density of containers on a soft soil medium. A word of caution is in order here: SSI and even more SSSI analysis are meaningful as long as the uncertainties and complexities do not exceed the cognizability and measurability. The design procedure should be supplied with comprehensive information with respect to the seismic input, soil conditions and non-linear behavior of the supporting medium. Blind recourse to advanced computational models is inadequate to assess the seismic response. Use of average response spectra, ignorance of local soil heterogeneities beneath the neighboring structures and lack of field/laboratory testing results for the soil properties at small and large strain, may give precise answers, however to the wrong problem.

The methodology developed in this work is applied in the frequency domain. Towards future incorporation of the subsoil coupling effects into a design procedure, a general time domain formulation will have to be developed. To gain efficiency and practical benefits, frequency independent models for the foundation-soil-foundation analysis are particularly suitable for this purpose. Systematic lumped-parameters models, realized as several SDOF oscillators in series, should be constructed, which will consider the interconnection between the degrees of freedom of adjacent foundations. In this regard, parametric studies based on rigorous methods should be performed in order to determine the constitutive frequency-independent coefficients of the models for varying parameters such as the distance between the foundations and their spatial arrangement. The results of such an effort for a limited number of configurations for the foundations and the soil have been proven so far encouraging; see e.g. the work of Mulliken and Karabalis (1998). The angle and direction of incident wavefields, as well the case of multilayered subgrade must be further investigated.

The time-domain concept serves in addition one principal purpose of earthquake-engineering analysis: the prediction of the structural damage, which necessitates nonlinear analysis. In practice, many unanchored liquid-storage tanks are supported directly on flexible foundations. When subjected to strong ground motion, these tanks exhibit strong nonlinear behavior due to the uplift of their base plate. From the viewpoint of engineering practice, it is crucial to examine whether refinement of simple mechanical models suffices to replicate accurately the uplifting resistance, energy dissipation capacity and pressure distribution of unanchored tanks. This query can find its ultimate answer only by means of experimental evidence.

References

Abramowitz M., Stegun I. A. (1972). *Handbook of mathematical functions with formulas, graphs and mathematical tables*. National Bureau of Standards, Washington.

Achenbach J. D. (1984). *Wave propagation in elastic solids*. North-Holland, Amsterdam.

Alexander N. A., Ibraim E., Aldaikh H. (2013). A simple discrete model for interaction of adjacent buildings during earthquakes. *Computer and Structures*, 124:1-10.

Amabili M. (1996). Horizontal vibration of partially filled horizontal cylindrical shells. *Journal of Sound and Vibration*, 191:757-780.

Amabili M., Paidoussis M. P., Lakis A. A. (1996). Vibrations of partially filled cylindrical tanks with ring-stiffeners and flexible bottom. *Journal of Sound and Vibration*, 213:259-299.

Amabili M. (2000). Eigenvalue problem for vibrating structures coupled with quiescent fluids with free surface. *Journal of Sound and Vibration*, 231:79-97.

Amabili M. (2003). Theory and experiments for large-amplitude vibrations of empty and fluid-filled circular cylindrical shells with imperfections. *Journal of Sound and Vibration,* 262:921-975.

ANSYS Inc (2013a). ANSYS Academic Teaching Mechanical, Release 12.1.

ANSYS Inc. (2013b). ANSYS University Advanced, Release 8.1.

Beer G., Watson J. O. (1989). Infinite boundary elements. *International Journal for Numerical Methods in Engineering*, 28:1233-1247.

Beskos D. E., Maier G.(2003). *Boundary Element Advances in Solid Mechanics*. Springer, Wien.

Brüggemann M. (2002). *Zur nichtlinearen Zeitbereichsimulation flüssigkeitsgefüllter Tankbauwerke unter Erdbebebenanregung*. Dissertation, Universität Wuppertal.

Chao C. (1960). Dynamic response of an elastic halfspace to tangential surface loadings. *Journal of Applied Mechanics* 27 (1960) 559-567.

Cho J. R., Song J. M. (2001). Assessment of classical numerical models for the separate fluid-structure modal analysis. *Journal of Sound and Vibration*, 239:995-1012.

Cho J. R., Song J. M., Lee J. K. (2001). Finite element techniques for the free-vibration and seismic analysis of liquid-storage tanks. *Finite elements in Analysis and Design*, 37:467-483.

Cho J. R., Kim K. W., Lee J. K., Park T. H., Lee W. Y. (2002). Axisymmetric modal analysis of liquid-storage tanks considering compressibility effects. *International Journal for Numerical Methods in Engineering*, 55:733-752.

Chouw N., Schmid G (1990). Influence of the geometrical effects of the soil on the structure-soil-structure interaction. *Proc.of the first European Conference on Structural Dynamics*, pp. 667-674, Ruhr-University Bochum.

Eurocode 8 (2004). European Committee for Standardization, Brussels, Belgium. Design of structures for earthquake resistance-Part 1: General rules, seismic actions and rules for buildings.

Eurocode 8 (2006). European Committee for Standardization, Brussels, Belgium. Design of structures for earthquake resistance-Part 4: Silos, tanks and pipelines.

Eurocode 8 (2011). European Committee for Standardization, Brussels, Belgium. Design of structures for earthquake resistance-Part 1: General rules, seismic actions and rules for buildings, German National Annex.

Fischer F. D. (1979). Dynamic fluid effects in liquid-filled flexible cylindrical tanks. *Earthquake Engineering and Structural Dynamics*, 7:587-601.

Fisher F. D., Rammerstorfer F. G. (1982). The stability of liquid-filled cylindrical shells under dynamic loading. *Proc. of a State-of-the-Art Colloquium*, pp. 569-597, Stuttgart.

Fischer F. D., Seeber R. (1988). Dynamic response of vertically excited liquid storage tanks considering liquid-soil interaction. *Earthquake Engineering and Structural Dynamics*, 16: 329-342.

Gonçalves P. B., Ramos N. R. S. S. (1996). Free vibration analysis of cylindrical tanks partially filled with liquid. *Journal of Sound and Vibration*, 195:429-444.

Guan F., Novak M. (1994). Transient response of multiple rigid foundations on an elastic, homogeneous halfspace. *Journal of Applied Mechanics*, 61:656-663.

Habenberger J. (2001). *Contribution to the analysis of flexibly supported liquid storage tanks under earthquake excitation*. Ph.D. Thesis, Weimar University (in german).

Haroun M. A. (1980). *Dynamic analysis of liquid storage tanks*. Ph.D. Thesis, California Institute of Technology.

Haroun M. A., Housner G. W. (1981). Seismic design of liquid storage tanks. *Journal of the Technical Council of ASCE*, 107:191-207.

Haroun M. A., Tayel M. A. (1985). Axisymmetrical vibrations of tanks-numerical. *Journal of Engineering Mechanics*, 111:329-345.

Hildebrand F. B. (1962). *Advanced Calculus for Applications*. Prentice-Hall, New Jersey.

Hirschauer R., Bode R., Savidis S. A. (1999). Berechnung der dynamischen Baugrund-Bauwerk Wechselwirkung mit ANSYS bei vollständiger Berücksichtigung der Wellenabstrahlung. *Beiträge zum 17. CAD-FEM ANSYS Users Meeting*, München.

Hirschauer R. (2001). *Kopplung von Finiten Elementen mit Rand-Elementen zur Berechnung der dynamischen Baugrund-Bauwerk-Interaktion*. Dissertation, Veröffentlichungen des Grundbauinstitutes der Technischen Universität Berlin.

Housner G. W. (1957). Dynamic pressures on accelerated fluid containers. *Bulletin of the Seismological Society of America*, 47:15-37.

Jennings P. C., Bielak J. (1973). Dynamics of building-soil interaction. *Bulletin of the Seismological Society of America*, 63:9-48.

Jeong K. H., Kim K. J. (1998). Free vibration of a cylindrical shell filled with bounded compressible fluid. *Journal of Sound and Vibration*, 217:197-221.

Karabalis D. L., Mohammadi M. (1991). Foundation-soil-foundation dynamics using a 3-D frequency domain BEM. In C. A. Brebbia and G. S. Gipson (eds), *Boundary Elements XIII*, Computational Mechanics Publications, pp. 447-456, Southampton.

Karabalis D. L., Mohammadi M. (1998). 3-D dynamic foundation-soil-foundation interaction on layered soil. *Soil Dynamics and Earthquake Engineering*, 17:139-152.

Karabalis D. L, Huang. C. –F. D. (1994). 3-D foundation-soil-foundation interaction. In C. A. Brebbia and A. J. Kassab (eds), *Boundary Element Technology IX*, Computational Mechanics Publications, pp. 197-209, Southampton.

Kausel E. (1974). *Forced vibrations of circular foundations on layered media*. Research Report R74-11, Massachusetts Institute of Technology.

Kausel E., Roësset J. M., Christian J. T. (1976). Nonlinear behavior in soil-structure interaction. *Journal of the Geotechnical Engineering Division*, 102:1159-1170.

Kausel E., Whitman R. V., Morray J. P., Elsabee F. (1978). The spring method for embedded foundations. *Nuclear Engineering and Design*, 48:377-392.

Kausel E. (1981). *An explicit solution for the Green functions for dynamic loads in layered media*. Research Report R81-13, No 699, Massachusetts Institute of Technology.

Kausel E., Roësset J. M. (1981). Stiffness matrices for layered soils. *Bulletin of Seismological Society of America*, 71:1743-1761.

Kausel E., Peek R. (1982). Dynamic loads in the interior of a layered stratum: An explicit solution. *Bulletin of Seismological Society of America*, 72:1459-1481.

Kausel E. (1986). Wave propagation in anisotropic layered media. *International Journal for Numerical Methods in Engineering*, 23:1567-1578.

Kausel E. (1988). Local transmitting boundaries. *Journal of Engineering Mechanics*, 114: 1011-1027.

Kausel E. (1992). Physical interpretation and stability of paraxial boundary conditions. *Bulletin of the Seismological Society of America*, 82:898-913.

Kausel E., Assimaki D. (2002). Seismic simulation of inelastic soils via frequency-dependent moduli and damping. *Journal of Engineering Mechanics*, 128:34-47.

Kausel E. (2011). *Fundamental solutions in elastodynamics*. Cambridge University Press, New York.

Kham M., Semblat J.-F., Bard P.-Y., Dangla P. (2006). Seismic Site-City Interaction: Main governing phenomena through simplified numerical models. *Bulletin of the Seismological Society of America*, 96:1934-1951.

Kobori T., Minai R., Suzuki T. (1971). The dynamical ground compliance of a rectangular foundation on a viscoelastic stratum. *Bull. Disas. Prev. Res. Inst*., 289-329, Kyoto Univ.

Ktenidou O. –J., Pitilakis D., Apostolidis P., Pitilakis K. (2007). Aspects of surface topography and site effects-experimental and numerical studies at Aegion, Greece. *4th International Conference on Earthquake Geotechnical Engineering*, Thessaloniki.

Kumar A. (1981). *Studies of dynamic and static response of cylindrical liquid-storage tanks*. Ph.D. Thesis, Rice University.

Lakis A. A., Sinno M. (1992). Free vibration of axisymmetric and beam-like cylindrical shells, partially filled with liquid. *International Journal for Numerical Methods in Engineering*, 33:235-268.

Lakis A. A., Neagu S. (1997). Free surface effects on the dynamics of cylindrical shells partially filled with liquid. *Journal of Sound and Vibration*, 207:175-205.

Lamb H. (1904). On the propagation of tremors over the surface of an elastic solid. *Philosophical Transactions of the Royal Society of London*, 203:1-42.

Lay K. (1993). Seismic coupled modeling of axisymmetric tanks containing liquids. *Journal of Engineering Mechanics*, 119:1747-1761.

Lin H. –T., Roësset J. M., Tassoulas J. L. (1987). Dynamic interaction between adjacent foundations. *Earthquake Engineering and Structural Dynamics*, 15:323-343.

Liou G. –S. (1994). Dynamic stiffness matrices for two circular foundations. *Earthquake Engineering and Structural Dynamics*, 23:193-210.

Luco J. E., Westman R. A. (1971). Dynamic response of circular footings. *Journal of the Engineering Mechanics Division ASCE*, 97:1381-1395.

Luco J. E., Mita A. (1987). Response of a circular foundation on a uniform halfspace to elastic waves. *Earthquake Engineering and Structural Dynamics*, 15:105-118.

Luft R. W. (1984). Vertical accelerations in prestressed concrete tanks. *Journal of Structural Engineering*, 110:706-714.

Lysmer J., Kuhlemeyer R. L. (1969). Finite-dynamic model for infinite media. *Journal of the Engineering Mechanics Division*, 95: 859-877.

Maeda T., Kausel E. (1991). On the accuracy of some approximate antiplane halfspace stiffnesses. *Bulletin of Seismological Society of America*, 81:1340-1359.

Maekawa A. (2012). Recent advances in seismic response analysis of cylindrical liquid storage tanks. *Earthquake-Resistant Structures-Design, Assessment and Rehabilitation*, Abbas Moustafa (ed.).

Makra K., Raptakis D., Chavez-Garcia F. J., Pitilakis K. (2001). Site Effects and Design Provisions: The case of Euroseistest. *Journal of Pure and Applied Geophysic*s, 158:2349-2367.

Malhotra P. K. (1997). Seismic response of soil-supported unanchored liquid-storage tanks. *Journal of Structural Engineering*, 123:440-450.

Malhotra P. K., Wenk T., Wieland M. (2000). Simple procedure for seismic analysis of liquid-storage tanks. *Structural Engineering International*, 3:197-201.

Manolis G. D., Beskos D. E. (1988). *Boundary Element Methods in Elastodynamics*. Unwin-Hyman, London.

MAPLE (2013). Waterloo Maple Inc., Release 17.

Meek J. W., Veletsos A. S. (1972). *Dynamic analysis and behavior of structure-foundation systems*. Research Report No. 13, Rice University.

Menglin L., Huaifeng W., Xi C., Yongmei Z. (2011). Structure-soil-structure interaction: Literature review. *Soil Dynamics and Earthquake Engineering*, 31:1724-1731.

Meskouris K. (2000). *Structural Dynamics*. Ernst & Sohn, Berlin.

Mohammadi M., Karabalis D. L. (1995). Dynamic 3-D soil-railway track interaction by BEM-FEM. *Earthquake Engineering and Structural Dynamics*, 24:1177-1193.

Moslemi M., Kianoush M. R. (2012). Parametric study on dynamic behavior of cylindrical ground-supported tanks. *Journal of Engineering Structures*, 42:214-230.

Mulliken J. S., Karabalis D. L. (1998). Discrete model for dynamic through-the-soil coupling of 3-D foundations and structures. *Earthquake Engineering and Structural Dynamics*, 27 :687-710.

Murakami H., Luco J. E. (1977). Seismic response of a periodic array of structures. *Journal of the Engineering Mechanics Division ASCE*, 103:965-977.

Mykoniou K., Holtschoppen B. (2013). Lateral free vibration of liquid-storage tanks. *Proc. of the International Conference on Seismic Design of Industrial Facilities*, pp. 403-416, Aachen.

Mykoniou K., Taddei F., Han Z. (2012). Dynamic foundation-soil interaction: A comparative study. *Bauingenieur D-A-CH-Mitteilungsblatt*, 87:9-13.

Mylonakis G., Nikolaou S., Gazetas G. (2006). Footings under seismic loading: Analysis and design issues with emphasis on bridge foundations. *Soil Dynamics and Earthquake Engineering*, 26:824-853.

NEHRP Consultants Joint Venture (2012). *Soil-structure interaction for building structures*. Report NIST GCR 12-917-21, National Institute of Standards and Technology.

Novozhilov V. V. (1964). *Thin Shell Theory*. P. Noordhoff Ltd., Groningen.

Ozdemir Z., Souli M., Fahjan Y. M. (2010). Application of nonlinear fluid-structure interaction methods to seismic analysis of anchored und unanchored tanks. *Journal of Engineering Structures*, 32:409-423.

Padrón L. A., Aznárez J. J., Maeso O. (2009). Dynamic structure-soil-structure interaction between nearby piled buildings under seismic excitation by BEM-FEM model. *Soil Dynamics and Earthquake Engineering*, 29:1084-1996.

Park J. (2002). *Wave motion in finite and infinite media using the Thin-Layer Method*. Ph.D. Thesis, Massachusetts Institute of Technology.

Peek R. (1986). *Analysis of unanchored liquid storage tanks under seismic loads*. Ph.D. Thesis, California Institute of Technology.

Pekeris C. L. (1955). The seismic surface pulse. *Proceedings of the National Academy of Sciences*, 41:469-480.

Phillips C., Hashash Y. M. A. (2009). Damping formulation for nonlinear 1D site response analyses. *Soil Dynamics and Earthquake Engineering*, 29:1143-1158.

PUNCH. A computer program for the determination of the Green's functions in layered media, by E. Kausel.

Qian J., Beskos D. E. (1995). Dynamic interaction between 3-D rigid surface foundations and comparison with the ATC-3 provisions. *Earthquake Engineering and Structural Dynamics*, 24:419-437.

Qian J., Beskos D. E. (1996). Harmonic wave response of two 3-D rigid surface foundations. *Soil Dynamics and Earthquake Engineering*, 15:95-110.

Rammerstorfer F. G., Scharf K., Fischer F. D., Seeber R. (1988). Collapse of earthquake excited tanks. *Res Mechanica*, 25:129-143.

Rammerstorfer F. G., Scharf K., Fischer F. D. (1989). On problems in the use of earthquake response sprctrum methods for fluid-structure-soil interaction. *Proc. of ASME Pressure Vessels and Piping Conference*, pp. 61-68, Hawaii.

Sommerfeld A. (1994). *Vorlesungen über theoretische Physik*. Band 1,2,6, Harri Deutsch, Frankfurt/M.

Song C., Wolf J. P. (1997). The scaled boundary finite-element method-alias consistent infinitesimal finite-element cell method-for elastodynamics. *Computational Methods in Applied Mechanics and Engineering*, 147:329-355.

Stewart J. P., Fenves G. L., Seed R. B. (1999). Seismic soil-structure interaction in buildings. I: Analytical methods. *Journal of Geotechnical and Geoenvironmental Engineering*, 125:26-37.

Tang Y. (1986). *Studies of dynamic response of liquid storage tanks*. Ph.D. Thesis, Rice University.

Tham L. G., Qian J., Cheung Y. K. (1998). Dynamic response of a group of flexible foundations to incident seismic waves. *Soil Dynamics and Earthquake Engineering*, 17:127-137.

Tosecký A. (2005). *Wave propagation in homogeneous elastic halfspace using the Dual Reciprocity Boundary Element Method*. Ph.D. Thesis, Ruhr University Bochum.

Triantafyllidis T., Prange B. (1988). Rigid circular foundation: Dynamic effects of coupling to the halfspace. *Soil Dynamics and Earthquake Engineering*, 7:40-52.

Triantafyllidis T., Prange B. (1989). Dynamic subsoil-coupling between rigid, circular foundations on the halfspace. *Soil Dynamics and Earthquake Engineering*, 8:9-21.

U.S. Energy Information Administration, http://www.eia.gov.

Veletsos A. S., Wei Y. T. (1971). Lateral and rocking vibration of footings. *Journal of the Soil Mechanics and Foundation Division ASCE*, 97:1227-1248.

Veletsos A. S., Yang J. Y. (1977). Earthquake response of liquid-storage tanks. *Proc. of the Second Annual Engineering Mechanics Division Specialty Conference*, pp. 1-24, North Carolina.

Veletsos A. S. (1984). *Seismic response and design of liquid storage tanks, Guidelines for the seismic design of oil and gas pipeline systems*. American Society of Civil Engineers, New York.

Veletsos A. S., Tang Y. (1987). Rocking response of liquid storage tanks. *Journal of Engineering Mechanics*, 113:1774-1792.

Veletsos A. S., Tang Y (1990). Soil-structure interaction effects for laterally excited liquid storage tanks. *Earthquake Engineering and Structural Dynamics*, 19:473-496.

Veletsos A. S., Tang Y (1992). Dynamic response of flexibly supported liquid-storage tanks. *Journal of Structural Engineering*, 118:264-283.

Virella J. C., Godoy L. A., Suárez L. E. (2006). Fundamental modes of tank-liquid systems under horizontal motions. *Journal of Engineering Structures*, 28:1450-1461.

Wolf J. P. (1985). *Dynamic soil-structure interaction*. Prentice-Hall, New Jersey.

Wong H. L., Luco J. E. (1976). Dynamic response of rigid foundations of arbitrary shape. *Earthquake Engineering and Structural Dynamics*, 4:579-587.

Wong H. L., Luco J. E. (1986). Dynamic interaction between rigid foundations in a layered halfspace. *Soil Dynamics and Earthquake Engineering*, 5:149-158.

Yang J. Y. (1976*). Dynamic behavior of fluid-tank systems*. Ph.D. Thesis, Rice University.

Zhu F. (1991). Orthogonality of wet modes in coupled vibration. *Journal of Sound and Vibration*, 146:439-338.

Zhu F. (1994). Rayleigh quotients for coupled free vibrations. *Journal of Sound and Vibration*, 171:641-649.

Zienkiewicz O. C., Kelly D. W., Bettess P. (1977). The coupling of the finite element method and boundary solution procedures. *International Journal for Numerical Methods in Engineering*, 11:355-375.

Zienkiewicz O. C., Taylor R. L. (2000). *The Finite Element Method for Solid and Structural Mechanics* (Vol. 2), Butterworth-Heinemann, Oxford.

Appendix A

$$N_{ri}(\bar{z}) = 1 - 3\frac{\bar{z}^2}{L_e^2} + 2\frac{\bar{z}^3}{L_e^3} \qquad N_{rj}(\bar{z}) = 3\frac{\bar{z}^2}{L_e^2} - 2\frac{\bar{z}^3}{L_e^3} \tag{A.1}$$

$$N_{\varphi i}(\bar{z}) = \bar{z} - 2\frac{\bar{z}^2}{L_e} + \frac{\bar{z}^3}{L_e^2} \qquad N_{\varphi j}(\bar{z}) = -\frac{\bar{z}^2}{L_e} + \frac{\bar{z}^3}{L_e^2} \tag{A.2}$$

$$N_{\theta i}(\bar{z}) = N_{zi}(\bar{z}) = 1 - \frac{\bar{z}}{L_e} \qquad N_{\theta j}(\bar{z}) = N_{zj}(\bar{z}) = \frac{\bar{z}}{L_e} \tag{A.3}$$

$$N_i^f(\bar{r}) = 1 - \frac{\bar{r}}{R_e} \qquad N_j^f(\bar{r}) = \frac{\bar{r}}{R_e} \tag{A.4}$$

$$A_{im} = \frac{2\rho_L \pi R\, I_m(R\bar{a}_i)}{H\, I_m'(R\,\bar{a}_i)\,\bar{a}_i} \qquad A_{0m} = \frac{\rho_L \pi R\, I_m(R\bar{a}_0)}{H\, I_m'(R\bar{a}_0)\bar{a}_0} \tag{A.5}$$

$$B_{nm} = \frac{2\rho_L \pi\, \bar{\lambda}_n^2}{\left(\bar{\lambda}_n^2 - m^2\right) J_m(\bar{\lambda}_n)\sinh\left(\frac{\lambda_n H_L}{R}\right)\lambda_n} \tag{A.6}$$

$$C_{nm} = \frac{2\rho_L \pi\, \bar{\lambda}_n^2}{R\left(\bar{\lambda}_n^2 - m^2\right)\left[J_m(\bar{\lambda}_n)\right]^2 \tanh\left(\frac{\lambda_n H_L}{R}\right)\lambda_n} \tag{A.7}$$

$$D_{im} = \frac{2\rho_L \pi \cos(a_i H_L)}{H\, I_m'(R\bar{a}_i)\,\bar{a}_i} \qquad D_{0m} = \frac{\rho_L \pi}{H\, I_m'(R\bar{a}_0)\,\bar{a}_0} \tag{A.8}$$

$$E_{i1} = \frac{2\,\rho_L \pi\, R(-1)^{i+1}\, I_1(a_i\, R)}{H_L\, {a_i}^2\, {I_1}'(a_i\, R)} \tag{A.9}$$

$$\mathbf{T}_{ie} = \int_0^{L_e} \mathbf{N}_r(\bar{z}) \cos[a_i(\bar{z} + (e-1)L_e)]\mathrm{d}\bar{z} \tag{A.10}$$

$$\mathbf{Z}_{nme} = \int_0^{R_e} \mathbf{N}^f(\bar{r})\,(\bar{r} + (e-1)R_e)\, J_m\left[\frac{[\bar{r} + (e-1)R_e]\bar{\lambda}_n}{R}\right]\mathrm{d}\bar{r} \tag{A.11}$$

$$\mathbf{Y}_{nk} = \int_0^{L_k} \mathbf{N}_r(\bar{z}) \cosh\left[\frac{[\bar{z} + (e-1)L_k]\lambda_n}{R}\right]\mathrm{d}\bar{z} \tag{A.12}$$

$$\mathbf{L}_{imk} = \int_0^{R_e} \mathbf{N}^f(\bar{r})\,[\bar{r} + (e-1)R_e]\, I_m\left[[\bar{r} + (e-1)R_e]\bar{a}_i\right]\mathrm{d}\bar{r} \tag{A.13}$$

$$\mathbf{V}_e = \rho_L \pi\, g \int_0^{R_e} \left[\mathbf{N}^f(\bar{r})\right]^{\mathrm{T}} \mathbf{N}^f(\bar{r})\, [\bar{r} + (e-1)R_e]\, \mathrm{d}\bar{\mathrm{r}} \tag{A.14}$$

$$\mathbf{X}_e = \int_0^{L_e} \mathbf{N}_r(\bar{z}) - \mathbf{N}_\theta(\bar{z})\, \mathrm{d}\bar{z} \tag{A.15}$$

$$\mathbf{Q}_e = \int_0^{L_e} \mathbf{N}_z(\bar{z})\, \mathrm{d}\bar{z} \tag{A.16}$$

$$\mathbf{J}_e = \int_0^{L_e} \frac{\mathbf{N}_r(\bar{z})}{H_L} [(\bar{z} + (e-1)L_e) - 1]\, \mathrm{d}\bar{z} \tag{A.17}$$

Appendix B

Table B.1: Design normalized wall pressure distributions $\bar{p}_{1,1}(R, z)$.

	H/R									
z/H	0.3	0.6	0.9	1.2	1.5	1.8	2.1	2.4	2.7	3
0.000	0.214	0.458	0.613	0.659	0.634	0.577	0.512	0.449	0.392	0.342
0.050	0.218	0.470	0.629	0.678	0.653	0.596	0.531	0.468	0.411	0.361
0.100	0.227	0.485	0.644	0.694	0.672	0.620	0.558	0.498	0.443	0.394
0.150	0.235	0.491	0.651	0.707	0.694	0.648	0.592	0.537	0.485	0.439
0.200	0.240	0.490	0.654	0.719	0.715	0.679	0.632	0.582	0.535	0.492
0.250	0.241	0.486	0.654	0.728	0.737	0.712	0.673	0.631	0.589	0.550
0.300	0.239	0.478	0.651	0.735	0.757	0.744	0.716	0.682	0.647	0.613
0.350	0.233	0.467	0.643	0.738	0.773	0.774	0.757	0.733	0.705	0.677
0.400	0.225	0.453	0.631	0.736	0.785	0.800	0.796	0.782	0.762	0.740
0.450	0.215	0.435	0.614	0.729	0.792	0.820	0.829	0.826	0.815	0.801
0.500	0.203	0.413	0.592	0.716	0.791	0.834	0.856	0.864	0.863	0.857
0.550	0.189	0.388	0.565	0.696	0.783	0.839	0.873	0.893	0.902	0.905
0.600	0.174	0.359	0.532	0.668	0.766	0.833	0.880	0.911	0.931	0.944
0.650	0.156	0.328	0.494	0.632	0.738	0.816	0.873	0.916	0.946	0.969
0.700	0.138	0.292	0.450	0.587	0.697	0.784	0.851	0.903	0.944	0.976
0.750	0.118	0.254	0.399	0.532	0.644	0.735	0.809	0.869	0.919	0.960
0.800	0.096	0.212	0.341	0.465	0.574	0.666	0.743	0.809	0.865	0.913
0.850	0.074	0.167	0.276	0.385	0.485	0.572	0.648	0.715	0.774	0.826
0.900	0.051	0.118	0.201	0.288	0.372	0.448	0.515	0.576	0.631	0.682
0.950	0.026	0.064	0.114	0.170	0.225	0.277	0.326	0.370	0.412	0.450
1.000	0.000	0.000	0.000	0.000	0.000	0.000	0.000	0.000	0.000	0.000

Table B.2: Design normalized wall pressure distributions $\bar{p}_{1,2}(R, z)$.

	H/R									
z/H	0.3	0.6	0.9	1.2	1.5	1.8	2.1	2.4	2.7	3
0.000	0.008	0.012	0.021	0.091	0.178	0.259	0.320	0.358	0.374	0.373
0.050	0.009	0.012	0.022	0.096	0.188	0.272	0.337	0.377	0.396	0.397
0.100	0.010	0.013	0.022	0.096	0.187	0.272	0.340	0.386	0.410	0.418
0.150	0.010	0.013	0.021	0.091	0.179	0.263	0.333	0.385	0.417	0.435
0.200	0.010	0.011	0.019	0.082	0.164	0.246	0.317	0.373	0.414	0.441
0.250	0.009	0.009	0.016	0.071	0.144	0.220	0.291	0.350	0.398	0.434
0.300	0.007	0.007	0.012	0.057	0.119	0.188	0.255	0.315	0.368	0.410
0.350	0.005	0.004	0.008	0.041	0.091	0.150	0.211	0.269	0.324	0.371
0.400	0.002	0.001	0.004	0.024	0.060	0.108	0.160	0.214	0.267	0.316
0.450	-0.001	-0.002	-0.001	0.007	0.029	0.063	0.105	0.152	0.201	0.248
0.500	-0.004	-0.005	-0.005	-0.010	-0.002	0.018	0.048	0.085	0.127	0.170
0.550	-0.007	-0.007	-0.009	-0.025	-0.031	-0.024	-0.008	0.018	0.050	0.085
0.600	-0.009	-0.009	-0.012	-0.037	-0.056	-0.063	-0.060	-0.047	-0.026	0.000
0.650	-0.011	-0.011	-0.014	-0.047	-0.076	-0.095	-0.105	-0.105	-0.096	-0.082
0.700	-0.011	-0.011	-0.015	-0.054	-0.091	-0.119	-0.140	-0.152	-0.156	-0.154
0.750	-0.011	-0.011	-0.015	-0.056	-0.098	-0.134	-0.163	-0.185	-0.201	-0.211
0.800	-0.010	-0.010	-0.015	-0.055	-0.097	-0.137	-0.171	-0.201	-0.227	-0.247
0.850	-0.009	-0.009	-0.013	-0.049	-0.089	-0.127	-0.163	-0.197	-0.228	-0.256
0.900	-0.006	-0.007	-0.010	-0.038	-0.071	-0.104	-0.137	-0.169	-0.201	-0.231
0.950	-0.003	-0.004	-0.006	-0.023	-0.044	-0.066	-0.088	-0.112	-0.136	-0.161
1.000	0.000	0.000	0.000	0.000	0.000	0.000	0.000	0.000	0.000	0.000

Table B.3: Design normalized wall pressure distributions $\bar{p}_{1,3}(R, z)$.

	H/R									
z/H	0.3	0.6	0.9	1.2	1.5	1.8	2.1	2.4	2.7	3
0.000	0.009	0.013	0.017	0.020	0.025	0.034	0.050	0.074	0.104	0.138
0.050	0.009	0.015	0.019	0.022	0.027	0.037	0.053	0.078	0.111	0.147
0.100	0.011	0.016	0.018	0.020	0.024	0.033	0.048	0.071	0.103	0.138
0.150	0.011	0.013	0.014	0.015	0.018	0.024	0.037	0.056	0.083	0.116
0.200	0.009	0.008	0.007	0.007	0.009	0.013	0.021	0.035	0.056	0.082
0.250	0.005	0.000	-0.002	-0.002	-0.002	0.000	0.003	0.011	0.024	0.042
0.300	0.000	-0.007	-0.010	-0.011	-0.012	-0.013	-0.014	-0.014	-0.010	-0.001
0.350	-0.005	-0.013	-0.016	-0.018	-0.020	-0.024	-0.030	-0.036	-0.041	-0.042
0.400	-0.010	-0.018	-0.021	-0.023	-0.026	-0.032	-0.041	-0.053	-0.065	-0.075
0.450	-0.013	-0.019	-0.022	-0.024	-0.028	-0.035	-0.046	-0.062	-0.080	-0.097
0.500	-0.013	-0.017	-0.020	-0.022	-0.026	-0.033	-0.046	-0.063	-0.084	-0.106
0.550	-0.011	-0.013	-0.015	-0.017	-0.021	-0.027	-0.039	-0.056	-0.077	-0.100
0.600	-0.007	-0.007	-0.008	-0.010	-0.013	-0.018	-0.027	-0.041	-0.059	-0.081
0.650	-0.001	0.001	0.000	-0.002	-0.004	-0.007	-0.013	-0.022	-0.035	-0.051
0.700	0.004	0.008	0.008	0.007	0.006	0.005	0.003	-0.001	-0.007	-0.017
0.750	0.009	0.013	0.014	0.013	0.014	0.015	0.017	0.019	0.020	0.018
0.800	0.012	0.016	0.017	0.018	0.019	0.022	0.028	0.034	0.041	0.047
0.850	0.012	0.016	0.018	0.019	0.020	0.025	0.033	0.042	0.054	0.065
0.900	0.011	0.013	0.015	0.016	0.018	0.023	0.030	0.041	0.054	0.067
0.950	0.007	0.008	0.009	0.010	0.011	0.015	0.021	0.029	0.039	0.050
1.000	0.000	0.000	0.000	0.000	0.000	0.000	0.000	0.000	0.000	0.000

Schriftenreihe

des Lehrstuhls für Baustatik und Baudynamik

der RWTH Aachen

Verzeichnis der bisher erschienenen Dissertationen:

98/1: Ruth Feill, Zum Einfluss frequenzabhängiger aerodynamischer Beiwerte auf das Antwortverhalten schlanker Strukturen unter stochastischer Windbelastung, 1998.

00/1: Uwe Weitkemper, Zur numerischen Untersuchung seismisch erregter Hochbauten mit Aussteifungssystemen aus Stahlbetonwandscheiben, 2000.

00/2: Carsten Könke, Schädigungssimulationsverfahren zur Lebensdauerabschätzung von Tragwerken, 2000

01/1: Sam-Young Noh, Beitrag zur numerischen Analyse der Schädigungsmechanismen von Naturzugkühltürmen, 2001.

02/1: Hamid Sadegh-Azar, Schnellbewertung der Erdbebengefährdung von Gebäuden, 2002.

02/2: Falko Schube, Beitrag zur numerischen Simulation des Wirbelsäulenverhaltens eines Kraftfahrers infolge durch Straßenunebenheiten induzierter Ganzkörperschwingungen, 2002.

03/1: Jörg Rocco Wagner, Seismisch belastete Schüttgutsilos, 2003.

04/1: Arno Grunendahl, Beitrag zur numerischen Simulationen des sitzenden Menschen zur Beurteilung der Auswirkung von Ganzkörperschwingungen, 2004.

04/2: Wolfram Kuhlmann, Gesamtkonzept zur Ermittlung der seismischen Vulnerabilität von Bauwerken am Beispiel unterirdischer Rohrleitungen, 2004.

06/1: Iman Karimi, Risk Management of Natural Disasters: A Fuzzy-Probabilistic Methodology and its Application to Seismic Hazard, 2006.

06/2: Stefan Holler, Dynamisches Mehrphasenmodell mit hypoplastischer Materialformulierung der Feststoffphase, 2006.

06/3: Michael Mistler, Verformungsbasiertes seismisches Bemessungskonzept für Mauerwerksbauten, 2006.

07/1: Ines Kalker, Numerische Simulation von unbewehrten und textilverstärkten Mauerwerksscheiben unter zyklischer Belastung, 2007.

07/2: Philippe Renault, Bewertungsverfahren zur Beurteilung der Erdbebensicherheit von Brückenbauwerken, 2007.

08/1: Frank Peiffer, Framework for adaptive multi-scale simulation of textile reinforced concrete, 2008.

08/2: Martin Konrad, Effect of multifilament yarn crack bridging on uniaxial behavior of textile reinforced concrete, 2008.

09/1: Britta Holtschoppen, Beitrag zur Auslegung von Industrieanlagen auf seismische Belastungen, 2009.

10/1: Andreas Gömmel, Modellbildung und Fluid-Struktur-Interaktion in der Biomechanik am Beispiel der menschlichen Phonation, 2010.

10/2: Christoph Gellert, Nichtlinearer Nachweis von unbewehrten Mauerwerksbauten unter Erdbebeneinwirkung, 2010.

11/1: Jakub Jerabek, Numerical Framework for Modeling of Cementitious Composites at the Meso-Scale, 2011.

12/1: Timo Schmitt, Zusammenhänge zwischen makroseismischen Intensitäten und Antwortspektren, Erdbebendauer und Bauwerksvulnerabilität, 2012.

12/2: Jaime Campbell, Numerical Model of Nonlinear Analysis of Masonry Walls, 2012.

13/1: Jin Park, Makroelemente für unbewehrte Mauerwerkswandscheiben unter Erdbebeneinwirkung, 2013.

13/2: Hannah Norda, Beitrag zum statischen nichtlinearen Erdbebennachweis von unbewehrten Mauerwerksbauten unter Berücksichtigung einer und höherer Modalformen, 2013.

01(2013): Okyay Altay, Flüssigkeitsdämpfer zur Reduktion periodischer und stochastischer Schwingungen turmartiger Bauwerke, 2013, ISBN: 978-3-946090-01-4.

02(2015): Francesca Taddei, Numerical Investigation of Soil-Structure Interaction for Onshore Wind Turbines Grounded on a Layered Soil, 2015, ISBN: 978-3-946090-00-7.

03(2015): Wolfang Dornisch, Interpolation of Rotations and Coupling of Patches in Isogeometric Reissner-Mindlin Shell Analysis, 2015, ISBN: 978-3-946090-02-1.

Lebenslauf

Name	Konstantinos Mykoniou
Geboren am	22.06.1984 in Thessaloniki, Griechenland
Familienstand	Ledig
Kontakt	Email: myk22684@yahoo.gr

07/2002	Abschluss des einheitlichen Lyzeums von Kalamaria, Thessaloniki
2002-2009	Studium des Bauingenieurwesens
	Aristoteles Universität Thessaloniki
2006	Erasmus-Stipendium an der RWTH Aachen
04/2009	Diplom
2009-2010	Besuch des Postgraduirtenprogramms: Erdbebensicherer Entwurf von Technischen Werken
	Aristoteles Universität Thessaloniki
10/2010-06/2014	Wissenschaftlicher Mitarbeiter
	Lehrstuhl für Baustatik und Baudynamik, RWTH Aachen
2015	Wehrdienst